KU LEUVEN

ARENBERG DOCTORAL SCHOOL

FACULTY OF BIOSCIENCE ENGINEERING

Spatially distributed recharge and groundwater – surface water interactions in groundwater models: from the field to the catchment scale

Antoine Di Ciacca

Supervisors:

Prof. Dr. Jan Vanderborght

Dr. Bertrand Leterme

Dr. Eric Laloy

Dissertation presented in partial fulfilment of the requirements for the degree of Doctor of Bioscience Engineering

2020

SPATIALLY DISTRIBUTED RECHARGE AND GROUNDWATER – SURFACE WATER INTERACTIONS IN GROUNDWATER MODELS: FROM THE FIELD TO THE CATCHMENT SCALE

Antoine Di Ciacca

Supervisors:
Prof. Dr. Jan Vanderborght
Dr. Bertrand Leterme
Dr. Eric Laloy

Members of the Examination Committee:
Prof. Dr. Kevin Verstrepen (chairman)
Prof. Dr. Jan Diels
Prof. Dr. Guido Wyseure
Prof. Dr. Marijke Huysmans (Vrije Universiteit Brussel, Belgium)
Prof. Dr. Jirka Simunek (University of California Riverside, USA)
Prof. Dr. Zahra Thomas (AGROCAMPUS OUEST - Rennes, France)

Dissertation presented in partial fulfilment of the requirements for the degree of Doctor of Bioscience Engineering

2020

Doctoraatsproefschrift nr. 1676 aan de faculteit Bio-ingenieurswetenschappen van de KU Leuven

(Only for PhD in Bioscience Engineering, contact doctoraatbiw@biw.kuleuven.be)

© 2020 Antoine Di Ciacca

Uitgegeven in eigen beheer, Antoine Di Ciacca, Mol, Belgium

Alle rechten voorbehouden. Niets uit deze uitgave mag worden vermenigvuldigd en/of openbaar gemaakt worden door middel van druk, fotokopie, microfilm, elektronisch of op welke andere wijze ook zonder voorafgaandelijke schriftelijke toestemming van de uitgever.

All rights reserved. No part of the publication may be reproduced in any form by print, photoprint, microfilm, electronic or any other means without written permission from the publisher.

Picture on the cover page retrieved from https://www.natuurpunt.be/nieuws/rapport-levende-beken-vlaanderen-20160823, made by Wim Dirckx.

To my grandfather

Acknowledgements

This work is the outcome of four years (and a little more) of research full of intense experiences. I would like to thank all the people who have helped me over this long journey.

In the first place, I would like to thank my mentor at SCK CEN, Dr. Bertrand Leterme. Thanks for giving me the opportunity to be part of this project. You have been present through all the ups and downs of my PhD journey and I am deeply grateful for your availability and your support. I may not have exactly followed the initial plan, but I hope this work has been rewarding for you. It was a pleasure to work with you. I would like then to thank my co-mentor at SCK CEN, Dr. Eric Laloy. Thanks for the stimulating discussions, it helped me more than one time when the motivation was getting low. Thanks also for initiating me to the Bayesian inverse modeling world, although we had not much time to go deeply into this and it remains mysterious for me in many aspects. I feel lucky that I had the opportunity to learn that from you, with even some difficult explanations in French. I would also like to thank my supervisor at the KU Leuven, Prof. Jan Vanderborght. It was a very inspiring experience to work with you. Thanks for your great contribution to the work and your pertinent remarks. I learn a lot by working with you and it will definitely shape my way of doing science in the future. Finally, I would like to thank Dr. Diederik Jacques who welcomed me in his research team at SCK°CEN. Thank you for supporting the project and for the time you took to improve my work with your valuable comments.

Thanks to Prof. Jan Diels for being part of my supervisory committee and especially for the very useful comments on tree water storage.

I am grateful to Dr. Zahra Thomas, Prof. Marijke Huysmans, Prof. Jirka Simunek and Prof. Guido Wyseure for their useful comments, which helped improving the quality of this manuscript. I am thankful to Prof. Kevin Verstrepen for having chaired this committee.

I want to thank my colleagues of the Hydro team in SCK CEN for the interesting discussions we had about my work and other topics. A special thanks to Dr. Bart Rogiers for sharing his deep knowledge of R with me and to Dr. Matej Gedeon for helping me with the few Python lines I had to write and the MODFLOW model. Thanks to Min Lu and Alberto Casillas for the

collaborations we had, and I wish you the best with your PhD projects. Finally, thanks to Serge Labat for his valuable help on the field and his good mood.

I also want to thank all my PhD student colleagues at SCK CEN. Thank you for the nice time in and out of the office. I wish you a lot of success with your PhD projects and jobs for the ones who already graduated, keep it up!

Also, many thanks to my friends I met in Belgium. It was nice to spend time with you and escape a bit from the PhD work sometimes.

Lea, you deserve a special mention here, thanks for all the support in these difficult times and thanks for your corrections on the thesis. I did not use all your commas but definitely some improved the readability of this document.

Some special thanks to my friends in France. I was pleased to see that you believed in me, supported me when I was doubting and honestly wanted me to make it. It is nice to see that after all these years of friendship and all the distances that have separated us, we still remain united.

Finally, I would like to thank my family for all their support, for developing my curiosity in my childhood and for giving me the opportunity to find my own way. Zoé, you may start your own PhD research soon, I hope my experience can give you some inspiration.

Abstract

Flow and transport in lowland area aquifers are strongly influenced by recharge processes and interactions with the surface water network. In lowlands, the groundwater table is close to the topographic surface. Therefore, the interactions between groundwater, atmosphere, soil, vegetation and surface water take place over short distances, within the so-called critical zone. Because of these short distances and the non-linearity of flow processes in the critical zone, a correct representation of these processes in catchment/regional scale groundwater models remains a challenge. This thesis presents an attempt to improve the representation of critical zone water transfer processes in a temperate lowland area catchment scale groundwater model while maintaining computational costs reasonable. In particular, the representation of groundwater – surface water interactions and groundwater recharge were studied in depth. The general approach used in this work is a bottom-up upscaling. First, processes are mechanistically simulated at a smaller scale (point and field scales), considering the small scale spatio-temporal features of the system. These simulated processes are then averaged or aggregated to a larger scale (catchment scale) and functional relations between larger scale averaged processes and features of the smaller scale structure are derived. In this way, small scale process understanding is effectively used to constrain relations that emerge at larger scales.

In regional models, groundwater – surface water exchange fluxes are usually represented with a Cauchy boundary condition governed by a conductance parameter. To improve the representation of groundwater – surface water interactions in regional hydrogeological models, a new expression of the groundwater – surface water conductance was derived. Parameterization of the conductance parameter is currently problematic because it relies on the assumption that conductance is exclusively controlled by streambed properties. However, depending on the specific system and the spatial discretization of the hydrogeological model, aquifer conductance can be a limiting factor for groundwater – surface water interactions. The resulting scale dependency of this parameter is not considered in the current conceptualization. The new expression, derived using analytical equations and 2D vertical field scale simulations of a stream-aquifer cross section, links the conductance to aquifer hydraulic properties and thickness as well as the discretization of the groundwater model and the

surface water network density. The expression was evaluated using 3D hydrogeological simulation models at different spatial resolutions and compared against previously published parameterization approaches. The results show that the new expression captures accurately both the grid size and the surface water network density dependency of the conductance, without adding complexity to the numerical model.

The third chapter of the thesis presents a field scale modeling study investigating the link between diurnal groundwater level fluctuations and root water uptake from the groundwater. A 3D variably saturated model was set-up to simulate the observed diurnal groundwater fluctuations in a deciduous tree plot and in the adjacent grass plot. The model simulated the main features of the observed diurnal groundwater level fluctuations properly, though a more advanced vegetation compartment would be needed to better represent the timing of the diurnal fluctuations. Significant diurnal patterns were simulated in the fluxes time series between the tree plot, the neighboring grass plot and the adjacent river. Furthermore, excluding root water uptake from groundwater led to larger (10 to 30 %) groundwater – surface water fluxes during dry periods. This suggests that groundwater uptake by plants is potentially an important process to represent in a catchment scale model.

The last chapter of this thesis presents a steady-state groundwater model of the Kleine Nete catchment (northeastern Belgium). We considered different parameterizations of groundwater recharge and groundwater – surface water interactions and assessed their effects on simulated groundwater head and fluxes. Concerning groundwater – surface water interactions, we used the new groundwater – surface water conductance expression and compared this approach to the calibration of a uniform groundwater – surface water conductance value. Our groundwater recharge calculations relied on 1D variably saturated simulations, which were integrated to the groundwater model through a look-up table, summarizing the relationships between groundwater depth and groundwater recharge. The 1D variably saturated simulations considered variable groundwater depth, sub-grid variability and tree root water uptake from the saturated zone. The relative importance of considering these factors on simulated groundwater recharge and groundwater flow fields was evaluated. The results highlight the relevance of using our new groundwater – surface water conductance expression and the importance of considering the coupling between groundwater depth and groundwater recharge in shallow groundwater environments.

Samenvatting

Stroming en transport in watervoerende lagen in vlakke laag gelegen gebieden of laagland worden sterk beïnvloed door grondwatervoeding en interacties met het oppervlaktewaternetwerk. In laagland ligt de grondwaterspiegel dicht bij het topografische oppervlak. Daarom vinden de interacties tussen grondwater, atmosfeer, bodem, vegetatie en oppervlaktewater plaats over korte afstanden binnen de zogenaamde kritische zone. Vanwege deze korte afstanden en de niet-lineariteit van stromingsprocessen in de kritische zone blijft een correcte weergave van deze processen in catchment/regionale grondwatermodellen een uitdaging. Deze dissertatie onderzoekt hoe watertransfer in de kritische zone tussen grondwatervoerende lagen, het oppervlaktewater en het bodemoppervlak in laagland accuraat in grondwatermodellen beschreven kan worden tegen een aanvaardbare rekenkost. De algemene aanpak die in dit werk wordt gebruikt is een bottom-up opschaling. Eerst worden processen mechanistisch gesimuleerd op kleinere schaal (punt- en veldschaal), rekening houdend met de kleinschalige spatio-temporele kenmerken van het systeem. Deze gesimuleerde processen worden vervolgens gemiddeld of geaggregeerd tot een grotere schaal (catchment scale) en functionele relaties tussen gemiddelde processen op grotere schaal en kenmerken van de kleinere schaalstructuur worden afgeleid. Op deze manier worden het inzicht in en kennis van kleinschalige processen en strukturen effectief gebruikt om relaties die op grotere schaal ontstaan af te leiden.

In regionale modellen wordt watertransfer tussen grondwater en oppervlaktewater meestal voorgesteld met een Cauchy-randvoorwaarde die gebruik maakt van een geleidingsparameter. Om de representatie van grondwater - oppervlaktewater interacties in regionale hydrogeologische modellen te verbeteren, is in het tweede hoofdstuk een nieuwe uitdrukking voor deze geleidingsparameter afgeleid. Parametrisering van de geleidingsparameter is op dit moment problematisch omdat deze uitgaat van de veronderstelling dat de geleiding uitsluitend wordt bepaald door eigenschappen van de rivierbedding. Afhankelijk van het specifieke systeem en de ruimtelijke discretisatie van het hydrogeologische model kan de hydraulisch conductiviteit van de watervoerende laag echter een beperkende factor zijn voor de interacties tussen grond- en oppervlaktewater. De resulterende schaalafhankelijkheid van de geleidingsparameter wordt in de huidige

conceptualisering niet in aanmerking genomen. De nieuwe uitdrukking, die is afgeleid uit analytische vergelijkingen en 2D simulaties van een verticale beek-aquifer doorsnede, koppelt de geleiding aan de dikte en hydraulische conductiviteit van de aquifer, de discretisatie van het grondwatermodel en de dichtheid van het oppervlaktewaternetwerk. De expressie werd geëvalueerd met behulp van 3D hydrogeologische simulatiemodellen met verschillende ruimtelijke resoluties en vergeleken met eerder gepubliceerde parameterisatiemethoden. De resultaten laten zien dat de nieuwe expressie zowel het effect van de rastergrootte als de dichtheid van het oppervlaktewaternetwerk op de geleidingsparameter accuraat weergeeft, zonder dat dit het numerieke model complexer maakt.

In het derde hoofdstuk van het proefschrift wordt een modelleringsstudie op veldschaal gepresenteerd waarin het verband wordt onderzocht tussen de dagelijkse schommelingen van de grondwaterstand en de opname van grondwater door plantenwortels. Een 3D model werd opgezet om de waargenomen dagelijkse grondwaterfluctuaties in een loofboomperceel en in het aangrenzende grasveld te simuleren. Het model simuleerde de belangrijkste kenmerken van de geobserveerde diurnale grondwaterspiegelschommelingen goed, hoewel een meer geavanceerde vegetatie module nodig zou zijn om de timing van de diurnale schommelingen beter weer te geven. Significante dagpatronen werden gesimuleerd in de tijdreeks van fluxen tussen het boomperceel, het naburige grasperceel en de aangrenzende rivier. Bovendien leidde de opname van water uit het grondwater door plantenwortels tot kleinere (10 tot 30 %) grondwater - oppervlaktewaterfluxen tijdens droge perioden. Dit suggereert dat grondwateropname door planten een belangrijk proces is dat in een stroomgebiedschaalmodel kan worden weergegeven.

In het laatste hoofdstuk van dit proefschrift wordt een steady-state grondwatermodel van het stroomgebied van de Kleine Nete (Noordoost-België) gepresenteerd. Verschillende parametrisaties van grondwatervoeding en grondwater - oppervlaktewaterinteracties en hun effecten op de gesimuleerde grondwaterstanden en -fluxen werden beoordeeld. Met betrekking tot grondwater - oppervlaktewater interacties, werd het gebruik van de nieuwe functie voor grondwater - oppervlaktewater geleidingsparameter vergeleken met het gebruik van een homogene geleidingsparameter die bekomen werd door kalibratie. De grondwatervoeding werd bepaald via een opzoektabel waarin de relaties tussen de diepte van het grondwater, het bodemtype, de vegetatie met al dan niet wateropname door

plantenwortels uit het grondwater en de grondwatervoeding werden samengevat. Deze opzoektabel was gebaseerd op simulaties met een 1D bodemhydrologisch model. Met deze opzoektabel kon het effect van subgrid variabiliteit met betrekking tot vegetatie, bodem en topografie op de grondwatervoeding in de gridcel eenvoudig in rekening gebracht worden. Het relatieve belang van het overwegen van deze factoren op gesimuleerde grondwatervoeding en grondwaterstromingsvelden werd geëvalueerd. De resultaten benadrukken de relevantie van het gebruik van een ruimtelijk variabele grondwater – oppervlaktewater geleidingparameterisatie en het belang van het overwegen van de koppeling tussen de diepte van het grondwater en de grondwatervoeding in laagland met ondiep grondwater.

List of abbreviations

a.s.l	Above Sea Level
DOV	Databank Ondergrond Vlaanderen
DREAM	Differential Evolution Adaptive Metropolis
DTM	Digital Terrain Model
FAO	Food and Agriculture Organization
GR-GD	Groundwater Recharge – Groundwater Depth
GW	Groundwater
HH	Hydraulic Head
HUF	Hydrogeologic Unit Flow package for MODFLOW
IGN/NGI	Belgian National Geographical Institute (“Institut Géographique National“/ “Nationaal Geografisch Instituut“)
IRM/KMI	Royal Meteorological Institute of Belgium (“Institut Royal Météorologique” / “Koninklijk Meteorologisch Instituut”)
KN	Kleine Nete
MAPE	Mean Absolute Percentage Error
MAP	Maximum A Posteriori
MCMC	Markov Chain Monte Carlo
MF	MODFLOW
MM	Metamodel
NAM	Neogene Aquifer Model
NRF	Net Recharge Function package for MODFLOW
NRMSE	Normalized Root mean Square Error

p-p	Peak-to-Peak
R^2	Coefficient of determination
RMSE	Root mean Square Error
RSD	Residual Standard Deviation
S/V	Soil/Vegetation
SCK CEN	Belgian Nuclear Research Center (“Studiecentrum voor Kernenergie” “Centre d'Étude de l'énergie Nucléaire”)
SW	Surface Water
VA	Vertical Anisotropy
VHA	Flemish hydrographic atlas (“Vlaamse Hydrografische Atlas”)
VMM	Flanders Environment Agency (“Vlaamse Milieumaatschappij”)

List of symbols

$C_{\mathrm{GW-SW,3D}}$	3D groundwater – surface water conductance [$L^2.T^{-1}$]
$C_{3D,sb}$	3D groundwater – surface water conductance [$L^2.T^{-1}$], streambed component
$C_{\mathrm{3D,aqui}}$	3D groundwater – surface water conductance [$L^2.T^{-1}$], aquifer component
D	Aquifer thickness [L]
D_{avg}	Vertical discretization of a hydrogeological model cell [L]
ET0	Reference potential evapotranspiration [$L.T^{-1}$]
ET_{GW}	Evapotranspiration from the groundwater [$L.T^{-1}$]
ETp	Potential evapotranspiration [$L.T^{-1}$]
G	Grid cell size G [L]
h_{GW}	Groundwater hydraulic head [L]
h_{SW}	Surface water hydraulic head [L]
k	Vegetation light extinction coefficient [–]
K_{hor}	Saturated hydraulic conductivity of the aquifer, horizontal component [$L.T^{-1}$]
K_{rad}	Saturated hydraulic conductivity of the aquifer, radial component [$L.T^{-1}$]
K_{ver}	Saturated hydraulic conductivity of the aquifer, vertical component [$L.T^{-1}$]
K_{s}	Saturated hydraulic conductivity [$L.T^{-1}$]
K_{sb}	Saturated hydraulic conductivity of the streambed [$L.T^{-1}$]
L	Distance between two surface water bodies [L]
L_{avg}	Horizontal discretization of a hydrogeological model cell [L]

L_{sw}	Length of surface water in a cell [L]
l_{VG} (−)	Tortuosity parameter in the van Genuchten − Mualem model [−]
LAI	Leaf area index [−]
M_{sb}	Streambed thickness [L]
n_{VG}	Shape parameter in the van Genuchten − Mualem model [−]
P0	Pressure head value below which roots start to extract water from the soil in the Feddes model [L]
P2H	Limiting pressure head value below which roots cannot longer extract water at the maximum rate (assuming a potential transpiration rate of *r2H*) in the Feddes model [L]
P2L	Limiting pressure head value below which roots cannot longer extract water at the maximum rate (assuming a potential transpiration rate of *r2L*) in the Feddes model [L]
P3 (m)	Pressure head value below which root water uptake ceases in the Feddes model [L]
POpt (m)	Pressure head value below which roots extract water at the maximum possible rate in the Feddes model [L]
$q_{\mathrm{2D,GW-SW}}$	Groundwater – surface water exchange flux for a stream-aquifer cross section [$L^2.T^{-1}$]
$Q_{\mathrm{GW-SW}}$	Volumetric flow rate between groundwater and surface water [$L^3.T^{-1}$]
Q_i	Volumetric flow rate between groundwater and surface water in a model cell *i* [$L^3.T^{-1}$]
Q_{SW}	Volumetric flow rate to surface water [$L^3.T^{-1}$]
Q_{Ta}	Volumetric flow rate to atmosphere through vegetation [$L^3.T^{-1}$]
Q_{tot}	Volumetric flow rate between groundwater and surface water in all model cells [$L^3.T^{-1}$]
R	Recharge rate [$L.T^{-1}$]
R_W	Average hourly rise of the water table during periods of no evapotranspiration

r2H (m/day)	Potential transpiration rate in the Feddes model [L.T^{-1}]
r2L (m/day)	Potential transpiration rate in the Feddes model [L.T^{-1}]
S_{cell}	Surface area of a grid cell [L^2]
S_y	Specific yield [−]
u	Wet perimeter [L]
W_{sb}	Streambed width [L]
α	Correction factor in the groundwater – surface water conductance metamodel [−]
α_{VG}	Shape parameter in the van Genuchten − Mualem model [L^{-1}]
β	Empirical parameter in the groundwater – surface water metamodel [−]
$\gamma_{\mathrm{2D,aqui}}$	2D Groundwater – surface water resistance, aquifer component [T.L^{-1}]
$\gamma_{\mathrm{3D,aqui}}$	3D Groundwater – surface water resistance, aquifer component [T.L^{-2}]
$\gamma_{\mathrm{3D,metamodel}}$	3D Groundwater – surface water resistance calculated with the metamodel [T.L^{-2}]
$\gamma_{\mathrm{3D,MODFLOW}}$	3D Groundwater – surface water resistance calculated with the classical MODFLOW approach [T.L^{-2}]
$\gamma_{\mathrm{3D,sb}}$	3D Groundwater – surface water resistance, streambed component [T.L^{-2}]
$\gamma_{\mathrm{GW-SW,2D}}$	2D Groundwater – surface water resistance [T.L^{-1}]
$\gamma_{\mathrm{GW-SW,3D}}$	3D Groundwater – surface water resistance [T.L^{-2}]
Δs	Daily decline in groundwater level [L]
ϑr	Residual water content [−]
ϑs	Water content at saturation [−]
ω_{c}	Vegetation interception capacity [L]

Table of contents

“Les herbes de la berge étaient calcinées, presque blanches ; sous le couvert des hêtres la rivière déroulait indéfiniment ses ondulations liquides, d’un vert sombre. Le monde extérieur avait ses propres lois, et ces lois n’étaient pas humaines.”

Michel Houellebecq – Les particules élémentaires

“The grass on the riverbank was scorched, almost white; in the shadow of the beech trees, the river wound on forever in dark green ripples. The world outside had its own rules, and those rules were not human.”

Michel Houellebecq – The Elementary Particles

Chapter I

General introduction

I. General introduction

I.1. Context

Clean fresh water is a priceless resource essential for ecosystems, agriculture and public supply. Threats affecting the quality and quantity of this natural resource are numerous. This thesis contributes to the ongoing efforts made over the last decades to improve our scientific understanding and modeling capability of the terrestrial water cycle.

97 % of the liquid fresh water on earth is found in aquifers (Healy, 2010; Nace, 1967; Shiklomanov and Rodda, 2004) from where it can be readily extracted using water wells. It is estimated that more than 20 % of the global population relies directly on groundwater as a source of potable water (Clarke et al., 1996) and that 38 % of irrigated area (≈ 114 million of ha) are equipped for irrigation with groundwater (Siebert et al., 2010). In Europe, groundwater is the predominant source (about 55 %) for public water supply and represents around 25 % of the water used for agriculture.

The groundwater budget is a balance between water entering (recharge) and leaving (discharge or extraction) the aquifer. These water fluxes are part of the larger terrestrial water cycle and thus integrated within the hydrosphere. Furthermore, water is essential for transporting dissolved elements and solid particles across the geosphere, atmosphere and biosphere. The water fluxes in aquifers and exchange with other environmental compartments are therefore crucial for the fate of elements in the environment and are important processes in other biogeochemical cycles (e.g. carbon, nitrogen, metals) (Aufdenkampe et al., 2011; Austin et al., 2004; Schimel et al., 1991).

Human activity is now global and is the dominant cause of most contemporary environmental change. Hence, the Anthropocene was proposed to name the current geological epoch (Crutzen, 2006; Lewis and Maslin, 2015). Human-induced changes particularly impact the terrestrial water cycle. Additionally to the direct abstraction of groundwater, land use, land cover and climate change are modifying the natural water cycle (Christensen et al., 2004; Crosbie et al., 2013; Mati et al., 2008; Scanlon et al., 2005; Taylor et al., 2013). Therefore, there is an important need for improving our modeling concepts and tools to quantify the

anthropogenic impact on groundwater resources. Another harmful effect of human activities is the pollution of water resources by modifying the nature and quantity of transported elements (Hildebrandt et al., 2008; Schwartz, 2020; Spalding and Exner, 1993). A distinction is commonly made between diffuse pollution (e.g. due to land use and cover changes) and point-source pollution. This thesis is set in the context of such a potential point-source pollution, namely the fate of radionuclides released from nuclear waste surface disposal to the groundwater which is an inevitable pathway in the scenarios evaluated in the framework of long-term safety assessments (Cool et al., 2013; Jacques et al., 2010, 2008; Mallants et al., 2008, 2000).

In permeable media like aquifers, water flow patterns greatly affect solute plume movement and spreading (Bear and Cheng, 2010). Thus, the proper simulation of groundwater flow patterns is a prerequisite for solute transport modeling. Groundwater flow patterns are controlled by topography, hydraulic conductivity distribution, spatio-temporal dynamics of groundwater recharge and groundwater – surface water interactions (Sophocleous, 2002). The present thesis particularly deals with the representation in numerical models of groundwater recharge and groundwater – surface water interactions in lowland temperate areas and more specifically lowland areas of northern Europe. Lowland areas are characterized by flat topography, high groundwater tables, and low surface water flow velocities (Krause et al., 2007; Lam et al., 2012; Schmalz et al., 2009). Thus in these environments, groundwater flow patterns are expected to be significantly influenced by groundwater recharge and interactions with the surface water network. These processes occur at the interface between atmosphere, vegetation, soil and geological material, within the so-called critical zone, which extends from the upper limit of vegetation down to the lower limit of groundwater (Anderson et al., 2007; Brantley et al., 2007; Chorover et al., 2007).

I.2. Critical zone water transfer processes in lowland temperate environments

Although the concept of a critical zone integrating the atmosphere, vegetation, soil, groundwater and surface water dates from the 2000's, water transfer processes within it have been studied for much longer, perhaps sometimes lacking such an integrated perspective. In hydrology, the critical zone used to be sub-divided between (i) the surface (above ground

level), (ii) the sub-surface (below ground level) unsaturated zone (soil) and (iii) the subsurface saturated zone (groundwater) (Figure 1).

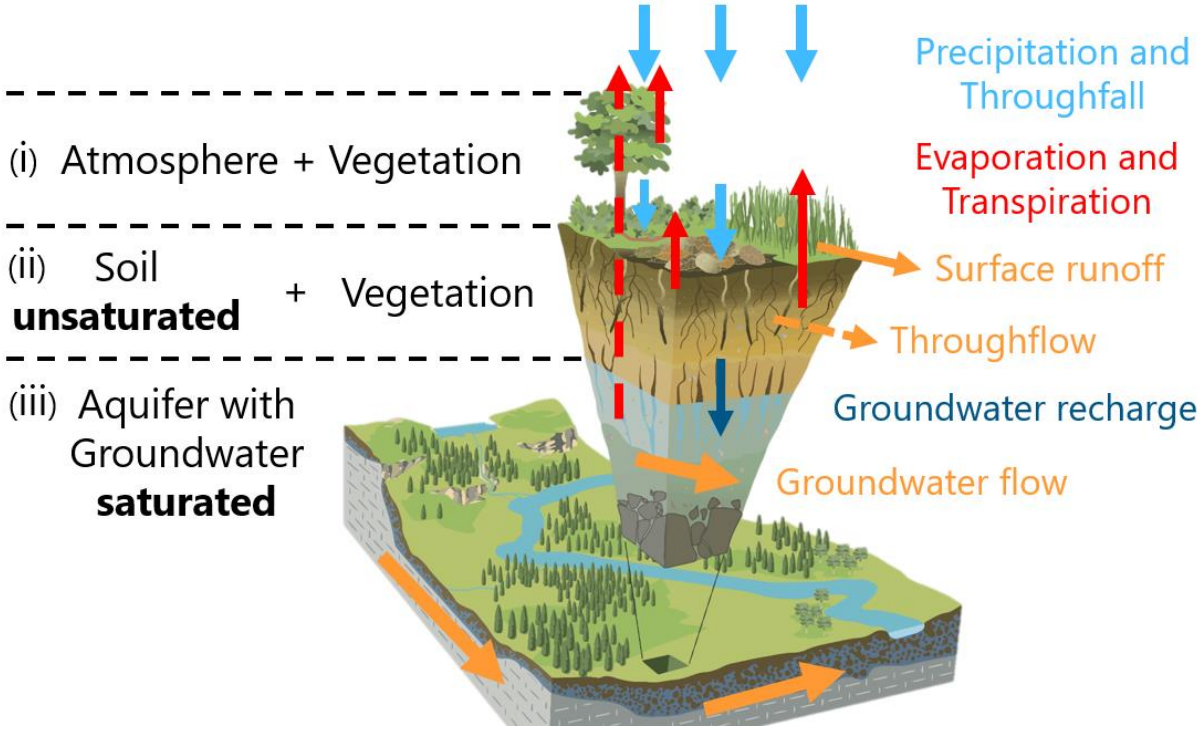

Figure 1: Main water transfer processes and sub-delimitation of the critical zone (Chorover et al., 2007, modified)

At the upper limit, water is entering the critical zone through precipitation and exiting it through evapotranspiration fluxes. Precipitation generation is a complex process occurring higher in the atmosphere and thus falls beyond the borders of the critical zone. It will therefore not be addressed here. Evapotranspiration demand is determined by atmospheric conditions (e.g. radiation, temperature, vapor pressure, wind speed). The partitioning between evaporation and transpiration depends on plant characteristics (e.g. species, leaf area index, height, interception capacity) and antecedent soil moisture conditions. A part of the precipitation is intercepted by the vegetation and may return to the atmosphere through evaporation. The remaining part (throughfall) reaches the soil surface. Throughfall is thus determined by plant characteristics and atmospheric conditions which control evaporation of the intercepted water. Once on the soil surface, water enters the subsurface (sub-zone (ii) in Figure 1) if soil infiltration and/or saturation capacity are not exceeded. When it cannot infiltrate, water remains at the soil surface, and may evaporate/infiltrate later, or flows following the local topography (surface runoff or overland flow). Surface runoff generation is controlled by topsoil and vegetation properties and antecedent moisture conditions. Surface

runoff can flow to a surface water body or infiltrate in soils along the flow path if conditions allow it. In temperate areas, saturation excess is the dominant overland flow mechanism because rainfall rates rarely exceed soil infiltration capacity (Davie and Quinn, 2002). In lowland areas, the shallow groundwater table enhances saturation excess overland flow although relatively flat topography limits surface runoff rates.

Water infiltration into the unsaturated subsurface (sub-zone (ii) in Figure 1) is driven by gravity and capillary forces. Moreover, several processes and heterogeneity complicate water infiltration and redistribution within a soil profile. First, topsoil water may evaporate depending on evaporation demand and topsoil moisture. Drying front caused by evaporation can reach up to few decimeters deep, depending on soil intrinsic properties (Or et al., 2013). Additionally, roots attempt at fulfilling transpiration demand by taking up soil water. However, root water uptake can be limited if soil moisture conditions are too dry or too wet. In excessively dry conditions, the water pressure gets too low for allowing for root water uptake, while in wet conditions, the low oxygen partial pressure limits root water uptake (Aroca et al., 2011). In both cases, the actual transpiration rate will be lower than the potential transpiration. Root water uptake is controlled by the distribution of roots and compensation mechanisms which can lead to a very heterogeneous uptake patterns along soil profiles (Coelho and Or, 1999; Javaux et al., 2013). After uptake, water travels through the roots, stem and leaves where it finally evaporates to the atmosphere. Extracted water can also be transitionally released in dryer soil layers (i.e. hydraulic lift) (Caldwell et al., 1998). Furthermore, soils are layered materials shaped by the interactions between geology, ecology, hydrology, climate and, in the case of anthrosols, human interventions. Different horizons have different hydraulic properties thus distorting infiltration fronts. Additionally, water infiltration in soil can be largely enhanced by flow along macropores created by soil structure, plant roots and soil fauna (Beven and Germann, 2013, 1982). Water that percolates through the soil and reaches the groundwater table is referred to as diffuse groundwater recharge. Between the unsaturated and saturated zone, a capillary fringe develops due to capillary forces pulling up groundwater. In shallow groundwater environments as lowland areas, soil moisture profiles can be largely dependent on groundwater depth (Doble and Crosbie, 2017; Renger et al., 1986; Shah et al., 2007) and thus influence surface runoff, evapotranspiration and groundwater recharge. Furthermore, groundwater can evaporate and/or be extracted by

plant roots either directly or via the capillary fringe (Mould et al., 2010; Vincke and Thiry, 2008). Plants that have roots which can uptake water in the capillary fringe and the saturated zone are called phreatophytes (Naumburg et al., 2005). This adds complexity to diffuse groundwater recharge conceptualization as water can flow both up− and downward. The net result of these interactions is sometimes referred to as net groundwater recharge (Doble et al., 2017; Szilagyi et al., 2013). An additional hydrological process assumed to take place within the unsaturated zone is throughflow, which refers to lateral flow within the unsaturated zone to surface water networks. The mechanisms generating throughflow are still not fully understood, however it is evidently associated with slope and a relatively deep unsaturated zone (Anderson and Burt, 1978; Jackson, 1992; Lv et al., 2013). Therefore, this is not expected to be a significant water transfer process in nearly flat lowland areas with shallow groundwater.

Water flow in the saturated zone (sub-zone (iii) in Figure 1) is driven by gravity and hydrostatic pressure gradients. Groundwater flow patterns have typically larger spatial extents than in the unsaturated zone. Groundwater flow systems have a nested organization with local, intermediate and regional components (Sophocleous, 2002; Todd and Mays, 2005). In lowland temperate areas, groundwater in unconfined aquifers is generally fed by diffuse recharge from soil infiltration and discharges to surface water features. In these environments, groundwater and surface water are connected (no development of unsaturated zone below surface water bodies). Nevertheless, man-made surface water features (e.g. canals) can have higher hydraulic head than the surrounding groundwater, and thus surface water may flow towards groundwater.

I.3. Spatio-temporal variability in the critical zone

The wide range of processes previously described and their complexity result in critical zone water fluxes that are variable at virtually all scales in time (from seconds to eon) and space (from centimeters to continental scale).

Short term variability (< 1 year) mainly comes from atmospheric processes. Rainfall intensity can largely vary at a subhourly time scale while temperature and solar irradiance, which determine potential evapotranspiration, follow a diurnal cycle. Moreover, seasonal cycles also affect atmospheric variables and in turn vegetation development, either naturally or through

agricultural practices. Time variability of atmospheric processes largely impacts water transfer in soil, vegetation and surface water. However, their effect on groundwater flow remains mainly limited to local shallow flow systems (Todd and Mays, 2005). Hence, variability on short time scales is less important in aquifers than in soil, vegetation and surface water. Additionally, land use and cover changes modify the composition of the critical zone. The main triggers to land use and changes at time scales of a year to decades (1–100 years) are human activities; whereby important changes can happen over a few years with crop rotation, agricultural expansion and urbanization (Lambin and Geist, 2008). Climate changes also impact rainfall and evapotranspiration processes at time scale superior to decades (> 10 years). Climate and land use and cover changes directly affect surface and soil hydrology, and their impacts are transferred to groundwater flow through recharge and groundwater – surface water interactions processes. Time delay can reach a few decades for deep unsaturated zone (Scanlon et al., 2005) but should be limited in areas with shallow groundwater. At larger time scales (> 100 years), erosion and pedogenesis modify critical zone properties and thus water transfer. Finally, critical zone is impacted by tectonic changes (e.g. fault formation) over geologic time.

Spatial variability of critical zone water transfer processes at sub-metric scale is due to vegetation architecture and subsurface pore properties distribution. At larger scale, spatial variability of critical zone processes comes from the combinations of climatic, topographical and geological settings which control soil and vegetation developments. Thus, in a natural environment, the different components of the critical zone vary together in organized patterns. However, human activities disrupt these natural patterns, increasing or decreasing spatial heterogeneity, depending on agricultural management practices and urbanization, which affect both soil and land cover. Land cover spatial variability largely depends on local environmental settings and history. Soil spatial variability is usually represented using soil classification in which soils are classified based on their textural and structural properties and profile development. Changes in soil properties at the order level of classification generally take place over relatively large distances, often across a significant climatic and/or topographic gradient. However, even within one horizon of one soil class, soil properties can significantly vary at the field scale (~1–1000 m^2) (Mulla and McBratney, 2002; Vereecken et al., 2014, 2007). Some properties vary by only a few percent (e.g. texture) but others can vary

by few orders of magnitude (e.g. saturated hydraulic conductivity). Groundwater flow patterns are controlled by topography, spatial variability of hydraulic conductivity (e.g. geological layers with distinct hydraulic conductivities), groundwater recharge and groundwater – surface water interactions.

In lowland temperate areas, flat topography suggests that groundwater recharge and interactions with surface water features could significantly influence groundwater flow patterns. On the one hand, groundwater recharge spatial variability depends on precipitation, potential evapotranspiration, land cover, soil properties and groundwater depth spatial distribution (Zomlot et al., 2015). In these environments, weather is usually not a differentiating factor at the regional scale, although localized rainfall events can occur, mainly in the summer. An important characteristic of lowland temperate areas of northern Europe is the heterogenous land cover, resulting from human activities, which show a mixture of meadow, cropland, forest and built-up area, often variable at a sub-kilometric scale (Figure 2). On the other hand, groundwater – surface water interactions spatial variability depends on geometry and density of surface water network bodies as well as geologic characteristics of their beds and surrounding aquifers (Sophocleous, 2002; Todd and Mays, 2005). Lowland temperate areas of northern Europe have a dense surface water network made up of small rivers and agricultural ditch drains. Agricultural ditch drains (Figure 2) were dug for agricultural land claiming and lowering the water table in order to allow agricultural development. The effect of small-scale land cover heterogeneity and dense surface water network on groundwater flow and their representation in catchment scale (~100–1000 km²) hydrogeological models will be investigated in the present thesis.

Figure 2: Typical lowland area landscape in the Kleine Nete catchment (Belgium) with a picture of an agricultural ditch drain

I.4. Modeling of water flow in the critical zone

The representation of the previously described processes and their spatio-temporal variability has been undertaken for decades in mathematical hydro(geo)logical models in various ways.

In catchment scale hydrological models, critical zone water transfer processes have been represented with various levels of details, first implicitly within empirical and conceptual lumped models and later explicitly in spatially distributed physically based models. As this thesis focuses on spatial variability of critical zone water transfer processes, only distributed models will be discussed in this introductory section. The concept of physically based spatially distributed hydrological models have been first proposed as a future project by Freeze and Harlan (1969). In such models, processes are describe explicitly using our knowledge of the distributed physical surface and subsurface phenomena. The flows of water and energy are directly calculated from numerical integration of the coupled governing continuum (partial differential) equations of the sub-systems. These models are usually based on the Darcy-Richards equation for subsurface water flow and Saint-Venant equations for surface water flow (Refsgaard, 1996; Todini, 2007). Early examples of numerical codes based on a physically based distributed modeling concept are SHE/MIKE SHE (Abbott et al., 1986a, 1986b) and IHDM (Beven et al., 1987). More recent implementation of fully coupled models implicitly couple surface and subsurface water flow (Kuffour et al., 2019; Maxwell et al., 2009; Therrien and Sudicky, 2006). In these models, subsurface flow in the unsaturated and saturated zone is represented by solving Richards equation in 3D. However, this detailed description comes with the drawback of important computational costs and data requirements. Moreover, the validity of Richards equation to describe water flow in structured soils at the grid scale (usually > 10 m) has been questioned (Beven, 2001, 1990; Todini, 2007). As a consequence, distributed models based on simplifying assumptions were developed such as, for instance, SWAT (Arnold et al., 2012; Neitsch et al., 2011) and WetSpa(ss) (Batelaan and De Smedt, 2001; Liu and De Smedt, 2004; Wang et al., 1996). Although, the term “physically based” is also often used to classify these models, this term then refers to a larger variety of conceptual descriptions of the physical processes and may in many cases differ significantly from the original idea of partial differential equation based physical models. Simplified representation of physical processes may be appropriate depending on the system aimed to be represented and the purpose of the model. For instance, kinematic wave approximation of water flow in the unsaturated zone can represent water infiltration in deep coarse-textured soil accurately, as it is then essentially driven by gravitational forces. However, in fine-textured soils with shallow groundwater, the kinematic wave approximation may lead to significant errors, as capillary forces play an important role (Twarakavi et al., 2008). Another example is that the simulation

of river discharges in gauged catchments under stationary conditions can be well addressed using simple lumped models, whereas to simulate the effect of land use changes on groundwater flow fields, a more complex and physically based model will be necessary. Therefore, the adequate level of complexity needed to simulate water transfer processes in the critical zone depends partly on the modeling objectives and data availability. As stated by Fatichi et al. (2016): *"Parsimony is convenient but complexity is often necessary".* Nevertheless, the advantages of keeping computational time of a model run at a reasonable level is evident when it comes to parameter estimation and uncertainty analysis, which require a high number of runs (often more than 10 000). Therefore, the application of partial differential equation based physical models can also be limited by the spatial and temporal extent of the modeling study.

Simultaneously, another part of the scientific community developed numerical codes for simulating water flow and transport processes in the vadose zone at sub-catchment scales solving Richards equation. Examples of such codes are HYDRUS (Simunek et al., 2008), SWAP (Kroes et al., 2008; van Dam et al., 2008) and WAVES (Zhang and Dawes, 1998). HYDRUS, arguably the most commonly used, has now evolved in a suite of modeling software able to represent complex processes such as nonequilibrium flow and transport as well as the effect of root water uptake on soil water redistribution in 1, 2 and 3 dimensions (Simunek et al., 2018, 2012, 2005; Simunek and van Genuchten, 2008). An example of a 3D vadose zone model is presented in this thesis (Chapter III). It is used to investigate phreatophytes transpiration and associated fluxes to/from the phreatophyte plot. However, application of such models is limited in the vertical direction to the shallow subsurface and in the horizontal direction to soil column (1D) or field scale (2/3D) studies.

In parallel, the development of hydrogeological models focusing on the saturated zone, has been driven by aquifer water resource problematics. Flow in the saturated zone can be mechanistically described with relatively simple linear differential equations and spatio-temporal dynamics of groundwater flow are often occurring at a coarser scale than for surface hydrology (see section I.3). Therefore, flow processes in the saturated zone are simulated since early studies in a physically-based and spatially distributed way (Staudinger et al., 2019). However, in these models, connections between groundwater, surface water and soil-vegetation-atmosphere continuum are often treated as simple boundary conditions (Dirichlet,

Neuman or Cauchy types). Arguably, the most widely used groundwater models are the finite difference MODFLOW series of codes (Harbaugh, 2005; Langevin et al., 2017; Li et al., 2014; McDonald and Harbaugh, 2003) and the finite element FEFLOW model (Diersch, 2013).

An approach to connect different environmental compartments (groundwater, surface water and soil-vegetation-atmosphere continuum) may lie in coupling of numerical codes that represent a specific compartment. Explicit coupling between these compartments may be efficient as it allows for the representation of water flow with a different spatio-temporal discretization in each sub-system, and water flow processes in the soil-vegetation-atmosphere continuum have higher spatio-temporal variability than in aquifers. This has been done by coupling hydrogeological models (often MODFLOW codes) with distributed catchment hydrological models (Batelaan et al., 2003; Batelaan and De Smedt, 2007; Kim et al., 2008). A more physically based alternative, but still computationally efficient, may lie in coupling 1D variably saturated models with a 3D groundwater model. The UZF package for MODFLOW (Niswonger et al., 2006) follows this approach but only represents gravity-driven water flow. Alternatively, a coupling method between Richards equation-based model HYDRUS-1D (Simunek et al., 2005) and MODFLOW-2000 (Harbaugh et al., 2000) has been developed by Seo et al. (2007), applied by Twarakavi et al. (2008) and latter updated by Beegum et al. (2018). The explicit coupling ensures that MODFLOW receives the recharge flux from each HYDRUS-1D profile and calculates a new groundwater head which is used as pressure head bottom boundary condition in HYDRUS-1D for the next time step. Information exchange occurs at each MODFLOW time step so that water flow in the unsaturated zone can be solved at a smaller time step than in the saturated zone. For computational efficiency, one HYDRUS profile (homogenous vegetation, soil and groundwater depth) can be assigned to several MODFLOW cells and their groundwater depths are averaged. However, the HYDRUS package for MODFLOW cannot be used for a steady state model. Moreover, in low resolution groundwater models sub-grid variability in land cover and groundwater depth can be important in lowland areas and thus several HYDRUS profiles may be needed in each MODFLOW cell. In this case, the NRF package for MODFLOW (Doble et al., 2017) may be a suitable approach. This package integrates the relationship between groundwater recharge and groundwater depth using a look-up table. The latter is built on a number of prior simulations with a variably saturated water model performed for selected combinations of vegetation – soil – groundwater depth.

In the present thesis (Chapter IV), the NRF package for MODFLOW is used to investigate the influence of groundwater depth, phreatophytes and sub-grid variability on groundwater recharge.

Coupling between groundwater and surface water is usually achieved by using a Cauchy boundary condition (head-dependent flux) governed by a proportionality coefficient, called the groundwater – surface water conductance. The most commonly used parameterization of the conductance parameter assumes that the groundwater – surface water conductance is exclusively controlled by streambed properties (Prickett and Lonnquist, 1971). This is correct when the model cells are small enough to represent explicitly the surface water features. However, depending on the spatial scale and the resolution that needs to be considered to simulate the processes in the system of interest, this can be impracticable given available CPU-time and resources. Therefore, in catchment scale hydrogeological models, surface water features are often included implicitly in larger cells, which also integrate a significant aquifer volume. In these settings, a major conceptual problem in the Prickett and Lonnquist (1971) approach is that it neglects the head losses occurring in the aquifer, which can limit groundwater – surface water exchange rates. As a consequence, the conductance parameter is often perceived as a fitting parameter, estimated during model calibration (Bencala, 1984; Mehl and Hill, 2010; Rushton, 2007). However, the calibration of this parameter is often an ill-posed problem given the data availability (Cousquer et al., 2018; Fleckenstein et al., 2010; Hunt et al., 2006). Moreover, when the resistance to flow in the aquifer plays an important role, the calibrated conductance parameters cannot be compared with direct measurements of streambed characteristics (Foglia et al., 2013; Krause et al., 2007). Another related issue, is the grid-size dependency of the groundwater – surface water conductance (Mehl and Hill, 2010) that is not accounted for in the classical parameterization scheme. This leads to the non-transferability of groundwater – surface water conductance values between models with different grid-cell sizes. This problem is expected to be of particular importance when the lateral extent of the grid cells, over which pressure head differences are calculated, is large compared to the dimension of the surface water bodies. Therefore, it is expected to be an important problem at the catchment scale to model the interactions between groundwater and small surface water features (small rivers and ditch drains), which constitute lowland

areas surface water networks. This conceptual gap is addressed in the present thesis (Chapter II and IV).

I.5. Research objectives and general methodology

The thesis investigates the coupling between groundwater and its upper boundaries (atmosphere, vegetation, soil and surface water) in hydrogeological models. As explained in section I.4, a major conceptual issue exists in the current way of coupling groundwater and surface water in regional scale hydrogeological models using a groundwater – surface water conductance parameter. Therefore, the thesis focusses on (i) addressing this issue by integrating the aquifer resistance in the groundwater – surface water resistance/conductance parameterization. Concerning the coupling between groundwater and the soil-vegetation-atmosphere continuum (groundwater recharge), a particular attention is given to the influence of shallow groundwater and its relationship with phreatophytic vegetation. This has been identified as a key aspect in lowland environments (see previous sections). Hence, the thesis focusses on (ii) the investigation of root water uptake by phreatophytes and its relation to fluxes from/to phreatophytes plots and (iii) the representation of groundwater depth and sub-grid variability in groundwater recharge calculations. Finally, this thesis examines (iiii) the relative importance of considering these factors to simulate groundwater flow fields at the catchment scale.

The selected study area is the Kleine Nete catchment (Figure 3), which is located in northeastern Belgium within a lowland area with temperate climate. It is characterized by shallow groundwater, very heterogenous land cover, sandy soils and a dense surface water network including small rivers and ditch drains. A more detailed description of the Kleine Nete catchment can be found in section IV.3.1. A considerable number of piezometers are located within the Kleine Nete catchment. Moreover, a steady-state groundwater model has already been developed for the Nete catchment, which has around twice the area of the Kleine Nete catchment (Gedeon, 2008). This research aims at improving the representation of critical zone water transfer processes in this model. Groundwater modeling in the Kleine Nete catchment is crucial as a surface nuclear waste disposal is planned to be built in Dessel in the near future.

The general approach used in this work is a bottom-up upscaling. First, processes are mechanistically simulated at a smaller scale (point and field scales), considering the small scale

spatio-temporal features of the system. These simulated processes are then averaged or aggregated to a larger scale (grid and catchment scale) and functional relations between larger scale averaged processes and features of the smaller scale structure are derived. In this way, small scale process understanding is effectively used to constrain relations that emerge at larger scales. Hence, the two first chapters of this PhD thesis present field scale modeling studies while the third presents a catchment scale modeling study built on the outcomes of the two first chapters.

The second chapter focuses on the groundwater – surface water conductance parameterization. We derived a new expression to calculate the aquifer component of the GW-SW resistance based on analytical equations and 2D vertical field scale simulations of a stream-aquifer cross section. The expression was then evaluated using simulations with 3D hydrogeological models at different spatial resolutions based on the surface network from an area within the Kleine Nete catchment (Figure 3).

The third chapter is a field scale modeling study which aims at simulating hydraulic head time series measured during the summer 2016 on a phreatophytes tree plot and the adjacent grass plot (Figure 3). The relation between groundwater level diurnal fluctuations, root water uptake and fluxes to/from the tree plot were investigated using numerical simulations performed with a 3D variably saturated model. Important questions were: are the observed diurnal groundwater level fluctuations due to root water uptake in the saturated zone and how do they relate to the spatially heterogeneous land cover and neighboring river and ditch drains?

The fourth and final chapter of this thesis presents the updated version of the Kleine Nete catchment groundwater model. Spatially distributed groundwater recharge was added using HYDRUS-1D simulations and the NRF (Net Recharge Function) package for MODFLOW 2000 (Doble et al., 2017), accounting for groundwater depth, sub-grid variability and root water uptake from the saturated zone by phreatophytes. The relative importance of considering these factors on simulated groundwater recharge and groundwater flow fields was evaluated. Groundwater – surface water interactions were represented using the conductance expression developed in the second chapter. This is compared with two other approaches in which a uniform groundwater – surface water conductance is calibrated against piezometric

data. Finally, the sensitivity of simulated groundwater flow fields to the different groundwater recharge and groundwater – surface water conductance approaches was investigated.

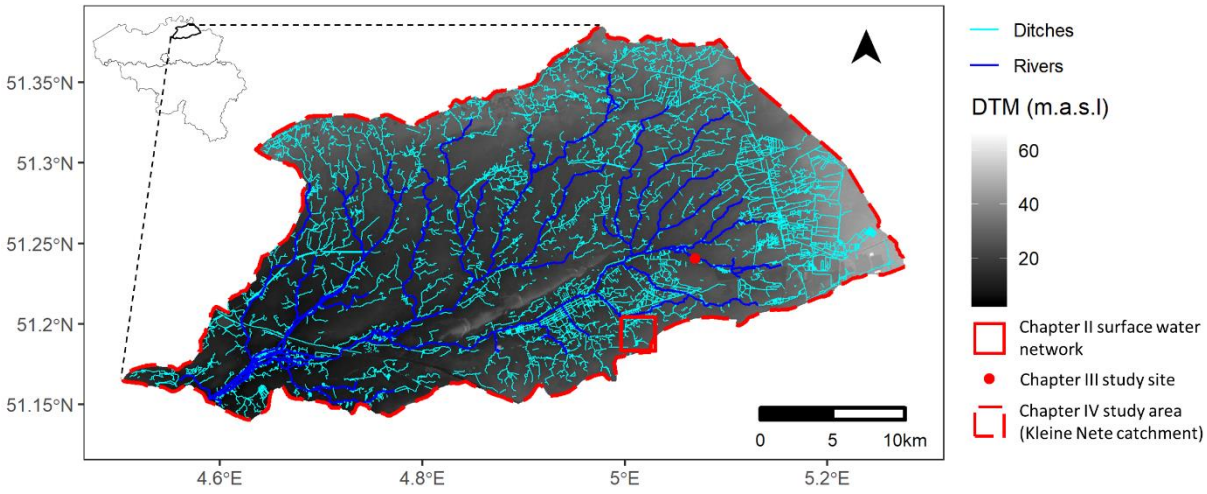

Figure 3: Locations and extents of the areas used in the three different chapters

Chapter II

Scale-dependent parameterization of groundwater − surface water interactions in a regional hydrogeological model

Based on: Di Ciacca, A., Leterme, B., Laloy, E., Jacques, D., Vanderborght, J., 2019. Scale-dependent parameterization of groundwater–surface water interactions in a regional hydrogeological model. J. Hydrol. 576, 494–507. https://doi.org/https://doi.org/10.1016/j.jhydrol.2019.06.072

II. Scale-dependent parameterization of groundwater – surface water interactions in a regional hydrogeological model

II.1. Abstract

In regional hydrogeological models, groundwater – surface water interaction is generally represented with a Cauchy boundary condition, in which a conductance parameter governs the exchange flux rate. In some models, the conductance is controlled by the streambed properties, since it has generally a lower hydraulic conductivity than the aquifer. However, depending on the specific system and the spatial discretization of the hydrogeological model, aquifer conductance can be a limiting factor for groundwater – surface water interactions. The present study introduces a new expression to represent the groundwater – surface water conductance as a function of aquifer properties, surface water network density and model discretization. This expression is based on the Dupuit-Forcheimer theory, the Ernst equation and vertical 2D numerical experiments at the field scale. The main assumptions used to derive our formulation are the presence of a no-flow boundary at the bottom of the hydrogeological model and the homogeneity of the aquifer. The expression is evaluated using simulations with 3D hydrogeological models at different spatial resolutions and compared against previously published parameterization approaches. The results show that the new expression outperforms the other approaches by capturing accurately both the grid-size and the surface water network density dependency of the conductance, which is caused by pressure head losses due to flow within the aquifer grid cell to the surface water, without any additional numerical calculation. Moreover, the proposed expression can be implemented directly in hydrogeological models thereby improving current approaches to represent groundwater − surface water interactions in regional hydrogeological models.

II.2. Introduction

Modeling water exchange between groundwater (GW) and surface water (SW) is of great importance at all scales for a variety of functions some including: river ecology (Boulton et al.,

2010; Stegen et al., 2016), water, mass and energy transfer at the catchment scale (Bailey et al., 2016; Rassam et al., 2008) and even at the continental and global scales as a part of earth system modeling (de Graaf et al., 2017; Maxwell et al., 2015).

In spatially distributed numerical models, the coupling of surface and ground water flows can be simulated in different ways. Recent advances in computational power and coupling methods have led to a new generation of models that solve differential equations of flow in the variably saturated subsurface and equations for SW flow in a fully coupled way (Camporese et al., 2010; Kollet and Maxwell, 2006; Maxwell et al., 2014; Therrien and Sudicky, 2006). However, CPU-time and resources can still be a limiting factor depending on the spatial scale and the resolution that needs to be considered to simulate the processes in the system of interest. For instance, dense surface water networks (i.e. rivers and drains) of drained lowland areas cannot be spatially realistically resolved or represented to a sufficient degree in a regional hydrogeological model without an excessive computational cost. An implicit representation of surface water bodies appears, in this case, to be the only viable solution. In regional hydrogeological models, the GW-SW coupling is usually accomplished with a Cauchy boundary condition (head-dependent flux). In a model cell, the volumetric flow rate between GW and SW ($Q_{\mathrm{GW-SW}}$, [$L^3.T^{-1}$]) is calculated as the product of the conductance ($C_{\mathrm{GW-SW,3D}}$[$L^2.T^{-1}$]) and the difference between the hydraulic heads of groundwater (h_{GW}, [L]) and surface water (h_{SW}, [L]):

$$Q_{\mathrm{GW-SW}} = C_{\mathrm{GW-SW,3D}}(h_{\mathrm{GW}} - h_{\mathrm{SW}})$$

Equation 1

The inverse of the conductance is defined as the resistance ($\gamma_{\mathrm{GW-SW,3D}}$, [$T.L^{-2}$]). Therefore, the resistance represents the whole head losses happening between the GW and the SW. For convenience, in this paper the resistance will be used and thus Equation 1 becomes:

$$Q_{\mathrm{GW-SW}} = \frac{h_{\mathrm{GW}} - h_{\mathrm{SW}}}{\gamma_{\mathrm{GW-SW,3D}}}$$

Equation 2

The volumetric flow between GW and SW can also be expressed per unit length of surface water, considering a vertical cross-section of the stream − aquifer system. In this case the 2D

resistance ($\gamma_{\mathrm{GW-SW,2D}}$) is equal to γ_{3D} multiplied by the length of surface water and has the dimension [T.L^{-1}].

The most commonly used parameterization of the resistance dates from the 1970's (Prickett and Lonnquist, 1971). The approach assumes that the flow mechanism between SW and GW is similar to the leakage through a low permeability layer and therefore depends only on the geometry and hydraulic properties of the streambed. It is used, for instance, in the MODFLOW family of codes, as highlighted by Harbaugh (2005), relies on the assumption that a distinct interface of low permeability (i.e. streambed) between the surface and subsurface exists and that all the head losses occur in the streambed. The resistance of this low permeability layer can then be easily calculated using Darcy law and is referred to as streambed resistance (γ_{sb}). This conceptualization is convenient and might be correct in particular cases because γ_{sb} can indeed be an important parameter governing the GW – SW interactions. However, it suffers the major conceptual problem of not considering the head losses occurring in the aquifer (i.e. aquifer resistance, γ_{aqui}). This shortcoming was well known by the authors of the original MODFLOW code and discussed in McDonald and Harbaugh (1988). Assuming that the resistances of the streambed and of the aquifer act in series, the GW − SW resistance is related to these resistances as follows:

$$\gamma_{GW-SW} = \gamma_{\mathrm{sb}} + \gamma_{\mathrm{aqui}}$$

Equation 3

The importance of aquifer resistance relatively to the streambed resistance depends on the geometry and the hydraulic properties of the streambed and the aquifer. Some field studies have shown that a clear interface between the surface and subsurface is not always present (Bayani and Zlotnik, 2003; Ghysels et al., 2018; Kollet and Zlotnik, 2007, 2003). Including the aquifer resistance is essential in such conditions. Moreover, even if the hydraulic conductivity is lower in the streambed than in the aquifer, the aquifer resistance can still be important because the distance over which the flow takes place is usually much larger than the streambed dimensions. This problem is expected to be of particular importance when a low spatial resolution is used in the numerical model and the lateral extent of the grid cells over which pressure head differences are calculated is large compared to the dimension of the surface water bodies. A solution would be to keep the hydrogeological model cell size small enough for the aquifer resistance to be negligible. Haitjema et al. (2001) proposed a criterion,

depending on the aquifer transmissivity and the streambed resistance, which should not be exceeded by the cell size. However, this is not always possible in practice and does not solve the conceptual problem. Furthermore, Ghysels et al. (2019) recently introduced a new approach for modelling GW-SW interactions in MODFLOW, which includes riverbed heterogeneity and river bank seepage. In this approach, the river is modelled as a separate constant head cell and thus a detailed model discretization around the river is required.

Another issue lies in the fact that the GW − SW interactions can occur not only through the streambed but also through the river banks (Anibas et al., 2018) especially in managed ditches, rivers or drains, which are deepened and in which the bed sediments are often removed. In this case, the resistance of the streambed would not be the main limiting factor for the water exchange between the groundwater and surface water. As a consequence, the resistance parameter, γ, is often perceived as a lumped fitting parameter that needs to be estimated during model calibration (Bencala, 1984; Mehl and Hill, 2010; Rushton, 2007). However, the calibration of γ is often an ill-posed problem given the data availability (Cousquer et al., 2018; Fleckenstein et al., 2010; Hunt et al., 2006). Moreover, when the resistance to flow in the aquifer plays an important role, the calibrated resistance parameters cannot be compared with direct measurements of streambed characteristics (Foglia et al., 2013; Krause et al., 2007). Another related issue is the grid-size dependency of γ (Mehl and Hill, 2010). This leads to the non-transferability of γ values between models with different grid-cell sizes. A detailed investigation of GW − SW resistance has been done in some studies using 2D mechanistic models of a stream − aquifer cross section. Rushton (2007) highlights the importance of aquifer hydraulic conductivity on the GW − SW resistance and provides guidance for estimating the aquifer resistance value. Furthermore, Cousquer et al. (2017) show that grid-cell size and aquifer hydraulic conductivity have a predominant role over streambed geometry and hydraulic properties. They suggest that 2D vertical models should be used for the prior estimation of the resistance as a step forward in the calibration and uncertainty analysis of surface − subsurface models. However, this implies a significant amount of additional 2D model runs in order to consider the specific characteristics of the GW − SW interfaces in a regional scale model.

Furthermore, analytical equations have been proposed to calculate the aquifer resistance for aquifer-river interactions (Anderson, 2005, 2003a, 2003b; Morel-Seytoux, 2009; Morel-

Seytoux et al., 2014). Progress towards the integration of an analytical solution within hydrogeological models have been achieved recently by Morel-Seytoux et al. (2017) and Morel-Seytoux et al. (2018). However, their results are limited to 2D field-scale models including a single surface water body only.

Another field dealing with GW − SW interactions is drainage design. In drainage design studies, the most widely used analytical solutions for the calculation of aquifer resistance are the Hooghoudt (1940) and Ernst (1962) equations. The theory behind these equations is detailed by Ritzema (1994). However, these equations were derived to help in the design of man-made drainage networks and not to be included in hydrogeological models. Consequently, their use to specify γ_{GW-SW} in hydrogeological models is impracticable because, among others, they require the GW hydraulic head between two SW bodies as input and estimate the aquifer resistance for the whole aquifer system.

Furthermore, De Lange (1999) presented an analytical solution for the interaction between any number of surface water bodies and a regional aquifer. This equation was evaluated and compared to other approaches in a set of numerical experiments by Pauw et al. (2015). Their results showed that the equation of De Lange (1999) performed better than the other approaches. However, this equation was derived under the assumption that two distinct aquifers exist (the regional and the phreatic aquifer), separated by an aquitard. Consequently, when the hydrogeological settings deviate from this conceptualization, this equation is impracticable to use.

Finally, two alternatives to the classical MODFLOW approach were proposed by Mehl and Hill (2010), which aimed at including the resistance due to the vertical flow between the bottom of the streambed and the cell center. However, the results of their numerical experiments highlight that the resistance formulations considered, including the commonly used, fail to account for the grid-size dependency in the horizontal and vertical directions. Nonetheless, these two alternatives approaches remain today the only ones which have been implemented directly in a MODFLOW model to account for the aquifer resistance in the GW-SW resistance expression.

It should be noted that all the approaches discussed in this introduction as well as the new approach proposed in this article are only meant to represent a connected GW – SW system (i.e. without an unsaturated zone below the SW body).

In this work, we propose a new model for the calculation of aquifer component of the GW-SW resistance that is required to simulate GW − SW interactions using a Cauchy boundary condition. A novel term is proposed for the horizontal resistance and the Ernst (1962) equation is used for the radial resistance, but with a correction derived from detailed numerical experiments of flow through a stream − aquifer cross sections at the field scale. Because of this empirical correction, we refer to our model as a metamodel. A metamodel can be broadly defined as a model of a model (Barton, 1994; Fraser et al., 2013; Jin et al., 2001). In our case, numerical simulation outputs are used to expand an analytical model, which thus become a metamodel.

The remainder of this paper is organized as follows. Section II.3 presents the theoretical underpinnings of the proposed metamodel. Next, section II.4 details both the detailed 2D numerical experiments that are used to define part of our metamodel and the upscaling experiment involving a 3D hydrogeological model that is used to demonstrate our proposed approach against the usual MODFLOW approach and the two alternatives proposed by Mehl and Hill (2010). This experiment is similar to that used by Mehl and Hill (2010) but further includes ditch drains in addition to the river network. In section II.5, our evaluation results are analyzed. Finally, section II.6 discusses the advantages and limitations of our approach and outline possible future developments before section II.7 concludes with a summary of the most important findings.

II.3. Aquifer resistance metamodel

II.3.1. Aquifer resistance in two dimensions (2D)

To derive the metamodel for aquifer resistance, we are considering parallel surface water bodies with a hydraulic head, h_{SW} [L], which are separated by a distance, L [L], and are located at a height, D [L], above the impermeable, horizontal bottom of the aquifer. A uniform recharge R [L.T^{-1}] is assumed, and thus RL equates to $q_{\mathrm{2D,GW-SW}}$ [L^2.T^{-1}], the groundwater discharge to the surface water. We resort to two additional variables to represent the

discretization of a hydrogeological model in the horizontal and vertical directions: L_{avg} [L] and D_{avg} [L], respectively. They correspond to the distance over which the groundwater pressure head field is averaged in the horizontal and vertical directions, respectively. The datum is the aquifer bottom. A schematic view of this conceptualization is shown in Figure 4.

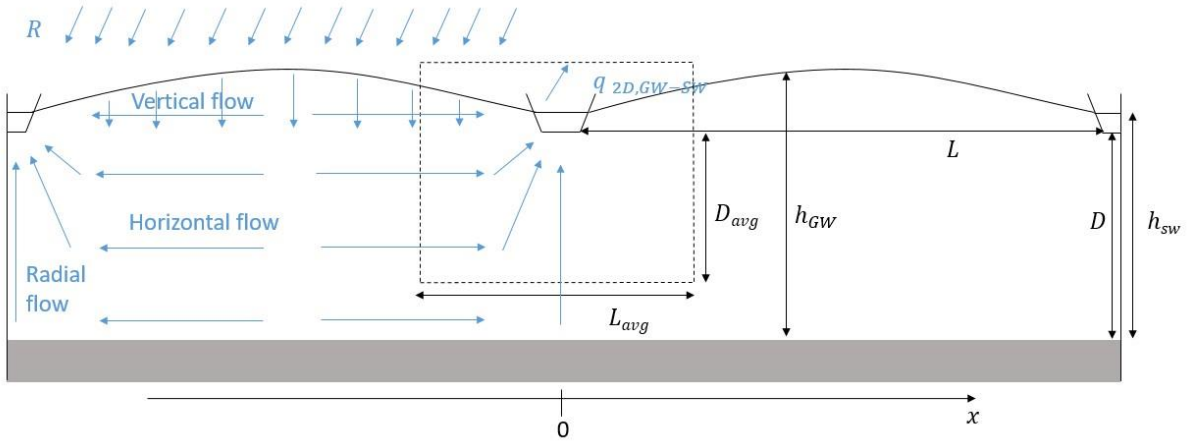

Figure 4: Schematic view of the model conceptualization where L [L] is the distance between two surface water bodies, D [L] is the thickness of the aquifer, h_{GW} [L] is the groundwater hydraulic head, h_{SW} [L] is the surface water hydraulic head, L_{avg} [L] is the horizontal discretization of a hydrogeological model, D_{avg} [L] is the vertical discretization of a hydrogeological model, x [L] is the horizontal coordinate, R [L.T⁻1] is recharge flux and $q_{2D,GW-SW}$ [L².T⁻1] is the GW – SW flux

Similar to the approach of Ernst (1962) as published by van Beers (1976) and Ritzema (1994), the flow domain is divided in a vertical, a horizontal and a radial component (Figure 4). A resistance is associated to each of these components and referred to as the vertical ($\gamma_{\mathrm{aqui,ver}}$), horizontal ($\gamma_{\mathrm{aqui,hor}}$) and radial ($\gamma_{\mathrm{aqui,rad}}$) resistances. Assuming that these resistances act in series, the aquifer resistance (γ_{aqui}) is given by:

$$\gamma_{\mathrm{aqui}} = \gamma_{\mathrm{aqui,ver}} + \gamma_{\mathrm{aqui,hor}} + \gamma_{\mathrm{aqui,rad}}$$

Equation 4

The vertical resistance, which is due to the infiltration of water from the soil surface, is generally small compared to the horizontal and radial resistances (Ritzema, 1994). This is because the vertical resistance only applies above the SW bottom level. Therefore, the vertical flow domain is generally smaller than the horizontal and radial flow domain located below the SW bottom level (i.e. $h_{GW} \approx h_{sw} \approx D$). Therefore, in the derivation of the metamodel, the vertical resistance is neglected, and Equation 4 becomes:

$$\gamma_{\text{aqui}} = \gamma_{\text{aqui,hor}} + \gamma_{\text{aqui,rad}}$$

Equation 5

For the derivation of the horizontal resistance, it is also assumed that $h_{GW} \approx h_{sw} \approx D$. This makes the resistance parameter independent of both the groundwater and surface water hydraulic heads and therefore facilitates its integration in hydrogeological models.

Two limitations following the above assumptions are that (i) in the case of a thin aquifer and/or highly incised channels, the simplification $h_{GW} \approx h_{sw} \approx D$ cannot be assumed; and (ii) in the case of an aquifer with a significant vertical anisotropy, the vertical resistance can be relatively important.

Hereafter, the derivation of the horizontal aquifer resistance is first presented, followed by the derivation of the radial resistance.

II.3.1.1. Horizontal aquifer resistance

The horizontal aquifer resistance is derived by considering only the horizontal flow processes. Thus, the Dupuit-Forcheimer theory applies that describes the hydraulic head at a given x ($h(x)$, [L]) as:

$$h_{GW}{}^2(x) = -\frac{R}{K_{\text{hor}}}x^2 + \frac{RL}{K_{\text{hor}}}x + h_{\text{SW}}{}^2$$

Equation 6

where K_{hor} [L.T^{-1}] is the horizontal hydraulic conductivity, R [L.T^{-1}] is the recharge flux, L [L] is the spacing between 2 surface water bodies, h_{SW} [L] is the surface water hydraulic head and x [L] is the horizontal coordinate.

From Equation 6 we can derive the mean hydraulic head ($h_{\text{GW,mean}}(x)$) over a given domain from 0 to x:

$$h^2{}_{\text{GW,mean}}(x) = -\frac{R}{3K_{\text{hor}}}x^2 + \frac{RL}{2K_{\text{hor}}}x + h_{\text{SW}}{}^2$$

Equation 7

Rearranging this equation and considering that $q_{\text{2D,GW-SW}} = RL$, we obtain the following relationship between the GW – SW exchange flux ($q_{\text{2D,GW-SW}}$) and the hydraulic heads, aquifer and geometric properties:

$$q_{2D,GW-SW} = \frac{h_{GW,mean}(x) + h_{sw}}{\frac{x}{2K_{hor}} - \frac{x^2}{3K_{hor}L}} (h_{GW,mean}(x) - h_{SW})$$

Equation 8

where x can be replaced by $\frac{L_{avg}}{2}$ which leads to:

$$q_{2D,GW-SW} = \frac{h_{GW,mean} + h_{sw}}{\frac{L_{avg}}{4K_{hor}} - \frac{{L_{avg}}^2}{12K_{hor}L}} (h_{GW,mean} - h_{SW})$$

Equation 9

where L_{avg} [L] is the horizontal averaging distance of the aquifer hydraulic head.

By analogy with Equation 1, the 2D horizontal aquifer resistance ($\gamma_{2D,aqui,hor}$ [T.L^{-1}]) can be expressed as:

$$\gamma_{2D,aqui,hor} = \frac{\frac{L_{avg}}{4K_{hor}} - \frac{{L_{avg}}^2}{12K_{hor}L}}{h_{GW,mean} + h_{SW}}$$

Equation 10

Considering that $h_{GW,mean} \approx h_{sw} \approx D$ (the aquifer thickness, [L]), the horizontal aquifer resistance can be approximated as:

$$\gamma_{2D,aqui,hor} = \frac{\frac{L_{avg}}{4K_{hor}} - \frac{{L_{avg}}^2}{12K_{hor}L}}{2D} = \frac{3LL_{avg} - {L_{avg}}^2}{24LK_{hor}D}$$

Equation 11

This equation relates the horizontal aquifer resistance ($\gamma_{2D,aqui,hor}$, [T.L^{-1}]) to the horizontal aquifer hydraulic conductivity (K_{hor}, [L.T^{-1}]), the aquifer thickness (D, [L]) and the horizontal discretization of the hydrogeological regional model (L_{avg}, [L]).

II.3.1.2. Radial aquifer resistance

The radial aquifer resistance is expressed in the same way as by Ernst (1962):

$$\gamma_{2D,aqui,rad} = \frac{\ln\left(\frac{D}{u}\right)}{\pi K_{rad}}$$

Equation 12

where u [L] is the wetted perimeter of the surface water body and K_{rad} [L.T^{-1}] the radial hydraulic conductivity calculated as $\sqrt{K_{hor}K_{ver}}$ (Kroes et al., 2008). Note that the geometry factor equals to 1 because of the aquifer homogeneity.

However, a correction to the radial aquifer resistance is needed to account for the cases where the vertical discretization of the hydrogeological model (D_{avg}) is smaller than the aquifer thickness (D). Therefore, a correction factor α [−] is included, which should be equal to 1 when $D_{avg} = D$ and when $L_{avg} = L$. It is applied as a weighting factor of the radial aquifer resistance and is written as:

$$\alpha = 1 - \beta\left(1 - \frac{L_{avg}}{L}\right)\left(1 - \frac{D_{avg}}{D}\right)$$

Equation 13

in which D_{avg} [L] is the vertical averaging distance of the aquifer hydraulic head. The β parameter is determined from the numerical experiments. It is fitted to the outputs of the mechanistic 2D numerical experiments (i.e. fitted resistances, see section II.4.1). The α parameter is the reason why we refer to our model as a metamodel. Note that if $D_{avg} = D$ or $L_{avg} = L$, then α = 1 and thus the model is purely analytical. When $L_{avg} > L$, we consider that $L_{avg} = L$ (only for the calculation of α) and thus α = 1. D_{avg} cannot exceed D by definition.

II.3.1.3. Aquifer resistance

The total aquifer resistance is therefore given by:

$$\gamma_{2D,aqui} = \gamma_{aqui,hor} + \alpha.\gamma_{aqui,rad}$$

Equation 14

$$\gamma_{2D,aqui} = \frac{3LL_{avg} - {L_{avg}}^2}{24LK_{hor}D} + \left[1 - \beta\left(1 - \frac{L_{avg}}{L}\right)\left(1 - \frac{D_{avg}}{D}\right)\right]\frac{\ln\left(\frac{D}{u}\right)}{\pi\sqrt{K_{hor}K_{ver}}}$$

Equation 15

The principle relationships outlined in equations 13-14 link the aquifer resistance to the aquifer hydraulic conductivities (K_{hor}, K_{ver}), the aquifer thickness (D), the wetted perimeter of the SW bodies (u), the distance between two SW bodies (L) and the horizontal discretization of the hydrogeological model in the horizontal (L_{avg}) and vertical (D_{avg}) direction. They apply to isotropic and anisotropic aquifers. In the application presented hereafter however, only isotropic aquifers are considered.

II.3.2. Aquifer resistance in three dimensions (3D)

In a model cell, the 3D aquifer resistance ($\gamma_{\mathrm{3D,aqui}}$, [T.L^{-2}]) is straightforward to calculate from the 2D aquifer resistance ($\gamma_{\mathrm{2D,aqui}}$, [T.L^{-1}]). As the volumetric flow is an integration of the 2D fluxes over the length of surface water features within a cell (L_{sw} [L]), $\gamma_{\mathrm{3D,aqui}}$ is equal to $\gamma_{\mathrm{2D,aqui}}$ divided by L_{sw}:

$$\gamma_{\mathrm{3D,aqui}} = \frac{\gamma_{\mathrm{2D,aqui}}}{L_{\mathrm{sw}}} = \frac{M}{K_{sb} W_{sb} L_{\mathrm{sw}}} + \frac{3 L L_{\mathrm{avg}} - {L_{\mathrm{avg}}}^2}{24 L K_{hor} D L_{\mathrm{sw}}} + \left[1 - \beta \left(1 - \frac{L_{\mathrm{avg}}}{L}\right)\left(1 - \frac{D_{\mathrm{avg}}}{D}\right)\right] \frac{\ln\left(\frac{D}{u}\right)}{\pi \sqrt{K_{\mathrm{hor}} K_{\mathrm{ver}}} L_{\mathrm{sw}}}$$

Equation 16

However, in 3D, the distance between surface water bodies (L) is not a straightforward variable to specify because the surface water network can be far from the ideal case of parallel bodies assumed in the derivation of the metamodel. Therefore, the next section presents a method to calculate a representative L all over a 3D modeling domain.

II.3.2.1. Representative distance between surface water bodies in 3D

To calculate $\gamma_{\mathrm{aqui,3D}}$ a representative distance between surface water bodies (L) has to be determined in each model grid cell of size G ([L]), containing one or more surface water bodies. L is calculated as:

$$L = \frac{S_{\mathrm{cell}}}{L_{\mathrm{sw}}} = \frac{G^2}{L_{sw}}$$

Equation 17

where S_{cell} is the surface area of the grid cell [L²] and L_{sw} is the length of the surface water features in the cell [L]. However, in each grid cell, if L_{sw} is smaller than the grid cell diagonal ($D = G\sqrt{2}$, [L]), we consider that only one surface water feature is present in the cell and thus L cannot be determined with this grid resolution. In this case we look for a larger G in which more surface water features are included and $L_{\mathrm{sw}} > D$. Therefore, the calculation of L should start with a fine-resolution grid (i.e. small G), then G should be increased iteratively until S_{cell} gets close to the whole domain area and/or a value of L has been assigned to all fine-resolution cells.

In this work, the modeling domain is a 2400 m by 2400 m square in the horizontal directions. Thus, grids with increasing horizontal resolutions are generated: 5, 10, 20,50, 100, 200, 300, 400, 600, 800, 1200 and 2400 m. Starting at the finest resolution (5 m), the values of L calculated using Equation 17 are attributed to the corresponding cells where L_{sw} is larger than D. For grid cells where L_{sw} is smaller than D, L is calculated using the next larger G value. This is done iteratively until the grid resolution reaches 2400 m. Thus, S_{cell} is equal to the whole modeling domain and a value of L has been assigned to all 5 m resolution cells.

II.4. Numerical experiments

Section II.4 investigates the conditions of an unconfined aquifer, with rather high hydraulic conductivities, drained by a dense complex network of small rivers and ditch drains using the numerical experiments presented below. The variables are representative of the well-documented Nete catchment around Mol, Belgium (Batelaan and De Smedt, 2007; Dams et al., 2012; Gedeon, 2008; Leterme et al., 2013).

II.4.1. 2D Field scale numerical experiments

II.4.1.1. Modeling domains and boundary conditions

The modeling domain consists of 2D vertical cross sections with half a surface water body at the left boundary and a drainage divide at the right boundary. The length of the modeling domain ($\frac{L}{2}$) is 100 m, representing half of the distance between two parallel surface water bodies. The surface slope, represented by the top boundary, is 1 %. The depth of the SW body (H_{d}) is 1 m. The bottom width of the SW body (W_d) is 1 m, and the top width is 2 m. Through

symmetry, only half of the SW body needs to be represented. An example of the modeling domain is shown in Figure 5.

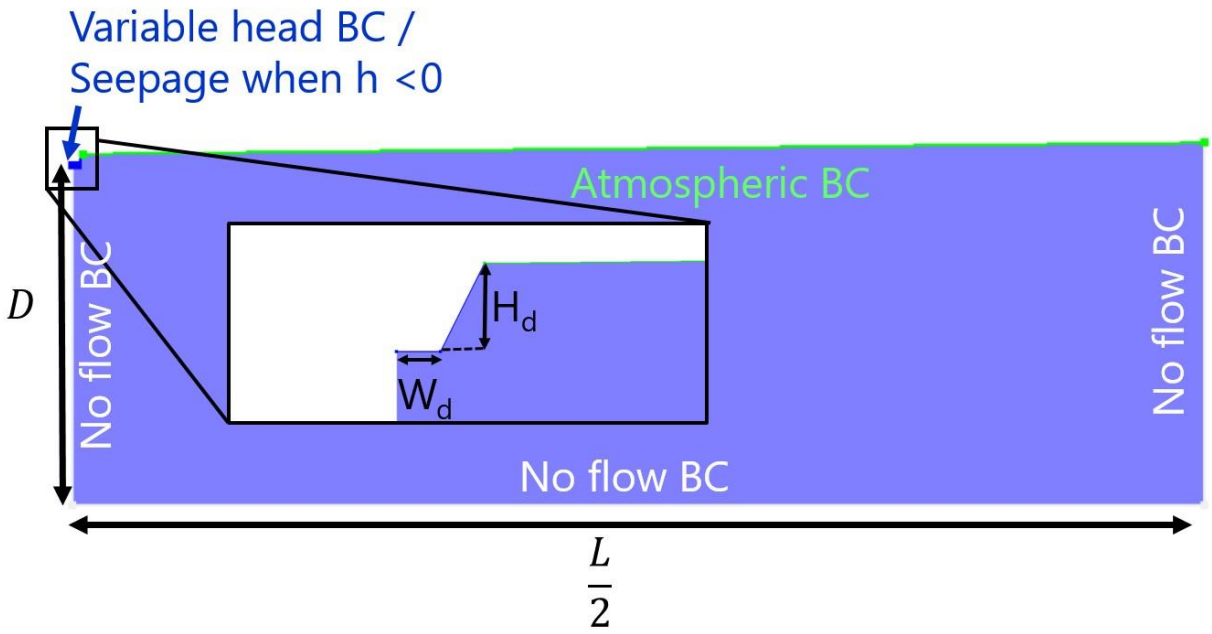

Figure 5: 2D field scale modeling domain where L/2 is the length of the modeling domain, D is the thickness of the aquifer, Wd and Hd are respectively the width and the height of the half surface water body

A three-year model was simulated using the HYDRUS 2D/3D software (Simunek et al., 2012), which solves Richards equation in variably saturated media. The mass balance error tolerance was 1 % as it is a standard use with this software. The soil hydraulic properties were specified using the model of van Genuchten (1980)) and textural classes were represented by the conclusions of Carsel and Parrish (1988).

The top boundary condition was set to atmospheric conditions using meteorological data recorded from September 1st, 2012 until the September 1st, 2015 at SCK•CEN (Belgian nuclear research center, Mol, Belgium). The side and bottom boundary conditions were set to no flow conditions to represent the drainage divide on the right, the middle of the drain on the left and the bottom of the aquifer at the bottom. In the surface water body, the boundary condition was set to a specific boundary condition, which is a variable head but switches to a seepage face when the pressure head at the boundary drops below zero. The variable head was specified using a piezometric time series from a drained area close to Mol (Belgium).

The soil textural class, aquifer hydraulic conductivity (K_s) and thickness of the aquifer (D) were varied between different scenarios and are summarized in Table 1. Combination of these variables led to 9 models.

Table 1: Investigated variables in the 2D field scale numerical experiments

Variable	Values
Soil textural class	**Sand, loamy-sand, sandy-loam**
Hydraulic conductivity Ks (m/d)	**7.5, 3.5, 1**
Thickness of aquifer D (m)	**10, 30, 50**

II.4.1.2. Averaging of groundwater hydraulic head

At each time step where water was present in the surface water body, the hydraulic head simulated in HYDRUS was averaged over different domains by varying the vertical (D_{avg}) and horizontal (L_{avg}) extents (Figure 6). The different values used for L_{avg} and D_{avg} are summarized in Table 2. Therefore, each model output time series is processed considering each value of L_{avg} and D_{avg}, resulting in 900 different domains (9 models x 5 D_{avg} x 20 L_{avg}).

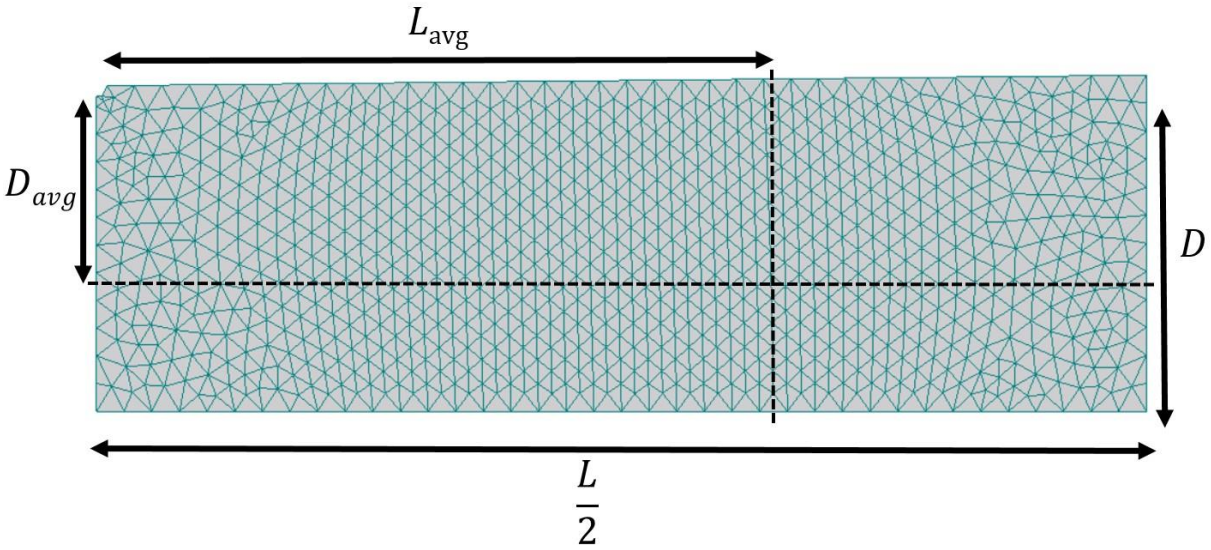

Figure 6: Schematic view and examples of the averaging length (L_{avg}) and thickness (D_{avg})

Table 2: L_{avg} and D_{avg} values

Variable	Values
L_{avg} (m)	5, 10, 15, 20, …, 100
D_{avg} (m)	0.1.D, 0.2.D, 0.4.D, 0.6.D, D

L_{avg} and D_{avg} allow evaluation of cases where the boundaries of a grid cell do not coincide with the no flow bottom or lateral boundaries, which respectively represents the bottom of the aquifer and the water divide between two surface water bodies. L_{avg} thus denotes the horizontal grid boundary and D_{avg} signifies the vertical grid boundary.

II.4.1.3. Aquifer resistance estimation

In the numerical experiments, for each time step, the surface water hydraulic head is known as it is one of the boundary conditions. The averaged groundwater hydraulic head was calculated by averaging the pressure field for the different averaging distances as described in the previous section, while the flux towards the surface water body is known as model output. Therefore, the only unknown in Equation 1 is the conductance. A conductance value representative of all-time steps is estimated, for each numerical experiment, using a linear regression of the simulated fluxes against the pressure head differences. The resistances are then calculated as the inverse of the conductances. The resistances derived in this way are referred to as fitted resistances. The accuracy of these regressions is assessed by the coefficient of determination (R^2) and residual standard deviation (RSD). These statistics measure how the GW − SW water flow interaction can be approximated using a constant conductance approach in these transient numerical experiments.

The estimated resistances are only representative of the aquifer because no resistance of the streambed was considered. The simulations led to the creation of a dataset consisting of one value of resistance (and conductance) for each combination of averaging scales (i.e. L_{avg} and D_{avg}), soil hydraulic parameters, and aquifer thicknesses. The obtained resistances were compared with resistances calculated from the properties of the aquifer, the drainage network and the spatial discretization of the hydrogeological model using the proposed metamodel (derived in section II.3). This comparison considered two criteria, the root mean

square error (RMSE) and the mean absolute percentage error (MAPE) between the two resistances.

II.4.2. Upscaling of a 3D hydrogeological model

A synthetic upscaling experiment was designed to evaluate the accuracy of the aquifer resistance provided by the proposed metamodel within a steady-state 3D hydrogeological model. The analysis consisted of simulating GW − SW interactions over the same domain but with various horizontal and vertical discretizations. The model with the finest horizontal and vertical discretizations is considered as a reference because it is the model in which the least aquifer volume is integrated into the GW-SW resistance. The GW − SW fluxes simulated by the metamodel-based approach and the classical MODFLOW approach are evaluated against the reference model GW − SW fluxes outputs by calculating both the total and spatialized errors. Ultimately, the performance of the two approaches are compared.

II.4.2.1. Modeling domain

The MODFLOW modeling domain is a rectangular block of 2400 x 2400 x 40 m (Figure 7). The domain includes both rivers and ditch drains. The river and ditch drain networks are representative of the Kleine Nete catchment (Belgium) and are taken from, respectively, the Flemish hydrographic atlas (“Vlaamse Hydrografische Atlas”, VMM 2017) and the IGN/NGI dataset (IGN/NGI 2017). The topography was set to a linear slope between 25 m at the southern boundary and 20 m at the northern boundary. The elevation of the water level in the rivers was defined as the ground elevation minus 1.5 m and the water elevation in the ditch drains as the ground elevation minus 1 m. The wetted perimeter of the surface water bodies was set to their width.

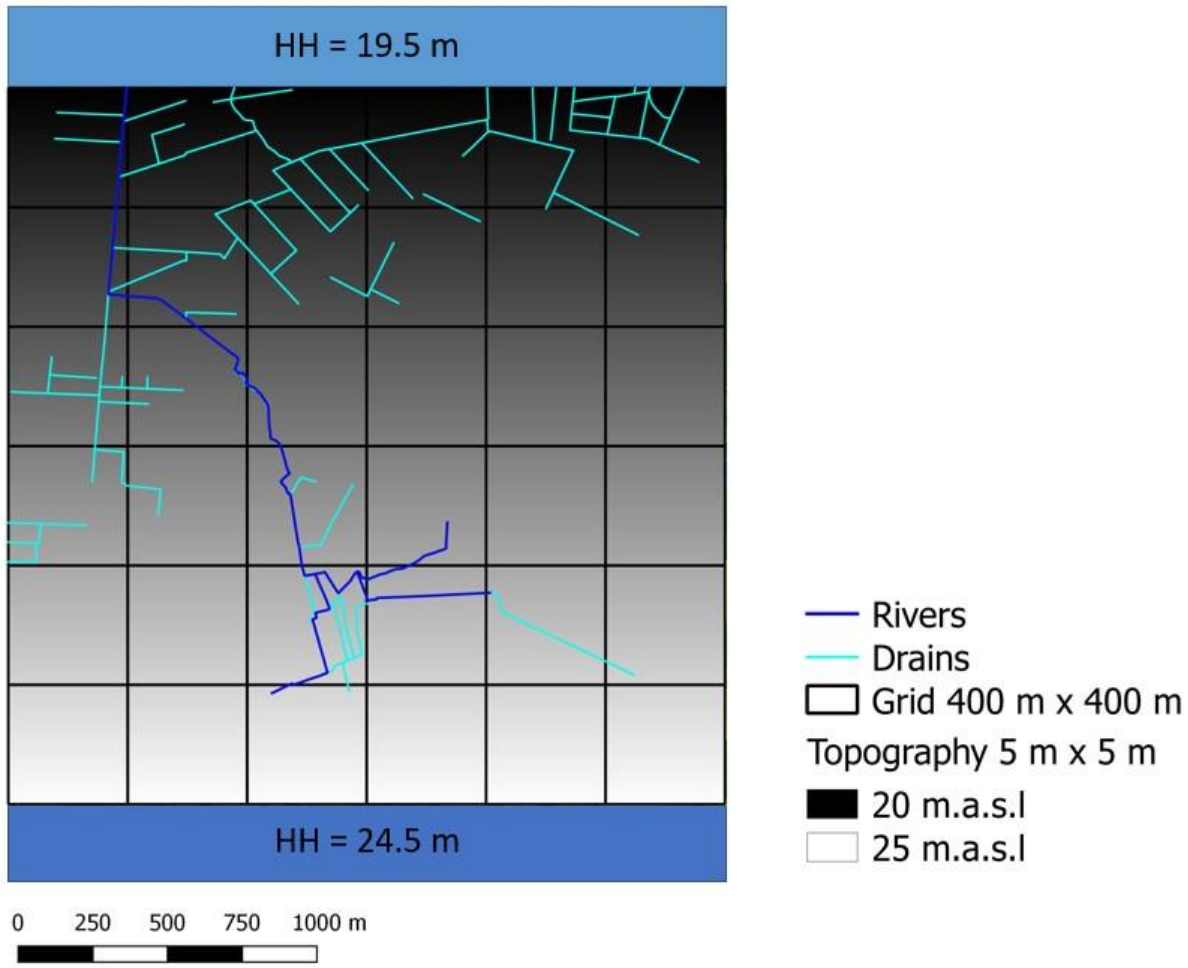

Figure 7: Horizontal domain of the 3D hydrogeological upscaling study. HH *stands for the hydraulic head boundary conditions defined at the northern and southern boundaries*

The boundary conditions were set to "no flow" at the bottom and at the eastern and western boundaries, and to constant head at the northern and southern boundaries. Vertically, a homogenous layer with a hydraulic conductivity of 1 m/d was considered. The streambed properties for rivers and ditches were set to a thickness of 0.1 m, a hydraulic conductivity of 0.5 m/d and a width of 1 m and 0.5 m, respectively.

II.4.2.2. Reference and upscaled models

The model with the finest discretization (i.e. 5 m × 5 m × 5 m) was used as a reference to evaluate the upscaled models (with larger discretization in horizontal and vertical directions). This was done for four different ways of calculating the GW – SW resistance, γ: the classical MODFLOW approach ($\gamma_{3D,\mathrm{MODFLOW}}$) which considers only the streambed resistance (Equation 18), our proposed metamodel ($\gamma_{3D,\mathrm{metamodel}}$) that accounts for the aquifer resistance as well

(Equation 19) and the two approaches proposed by Mehl and Hill (2010) (Equation 20 and 21), which are referred to as Mehl_01 and Mehl_02.

$$\gamma_{\mathrm{3D,MODFLOW}} = \gamma_{\mathrm{3D,sb}} = \frac{M_{\mathrm{sb}}}{K_{\mathrm{sb}} W_{\mathrm{sb}} L_{\mathrm{sw}}}$$

Equation 18

$$\begin{aligned}\gamma_{\mathrm{3D,metamodel}} &= \gamma_{\mathrm{3D,sb}} + \gamma_{\mathrm{3D,aqui,meta}} \\ &= \frac{M_{\mathrm{sb}}}{K_{sb} W_{sb} L_{\mathrm{sw}}} + \frac{3LL_{\mathrm{avg}} - {L_{\mathrm{avg}}}^2}{24LK_{hor}DL_{\mathrm{sw}}} \\ &+ \left[1 - 0.5\left(1 - \frac{L_{\mathrm{avg}}}{L}\right)\left(1 - \frac{D_{\mathrm{avg}}}{D}\right)\right] \frac{\ln\left(\frac{D}{u}\right)}{\pi\sqrt{K_{\mathrm{hor}} K_{\mathrm{ver}}} L_{\mathrm{sw}}}\end{aligned}$$

Equation 19

$$\gamma_{\mathrm{3D,Mehl\_01}} = \gamma_{\mathrm{3D,sb}} + \gamma_{\mathrm{3D,aqui,Mehl\_01}} = \frac{M_{\mathrm{sb}}}{K_{sb} W_{sb} L_{\mathrm{sw}}} + \frac{\frac{D_{\mathrm{avg}}}{2} - M_{\mathrm{sb}}}{K_{ver} L_{avg} L_{\mathrm{sw}}}$$

Equation 20

$$\gamma_{\mathrm{3D,Mehl\_02}} = \gamma_{\mathrm{3D,sb}} + \gamma_{\mathrm{3D,aqui,Mehl\_02}} = \frac{M_{\mathrm{sb}}}{K_{sb} W_{sb} L_{\mathrm{sw}}} + \frac{\frac{D_{\mathrm{avg}}}{2} - M_{\mathrm{sb}}}{K_{ver} W_{sb} L_{\mathrm{sw}}}$$

Equation 21

where $\gamma_{\mathrm{3D,aqui}}$ are the aquifer resistance calculated by the different models [$L^{-2}.T$], $\gamma_{\mathrm{3D,sb}}$ is the streambed resistance [$L^{-2}.T$], M_{sb} is the streambed thickness [L], K_{sb} is the streambed hydraulic conductivity [$L.T^{-1}$], W_{sb} is the streambed width [L], L_{sw} is the length of surface water in a cell [L], L is the spacing between two surface water bodies [L], K_{hor} is the horizontal hydraulic conductivity [$L.T^{-1}$], K_{ver} is the vertical hydraulic conductivity [$L.T^{-1}$], u is the wetted perimeter of the surface water body [L], D is the aquifer thickness [L], L_{avg} is the horizontal discretization of the groundwater model [L] and D_{avg} is the vertical discretization of the groundwater model [L].

However, the aquifer resistance in the reference model needs to be considered in order to have a unique reference model for both resistance expressions and avoid any bias in the

comparison. Still, this is not expected to have a major impact on the results. This is done using the metamodel and Equation 18becomes:

$$\gamma_{\mathrm{3D,MODFLOW}} = \frac{M_{\mathrm{sb}}}{K_{\mathrm{sb}}.W_{\mathrm{sb}}.L_{\mathrm{sw}}} + \gamma_{\mathrm{3D,aqui,ref}}$$

Equation 22

where $\gamma_{\mathrm{aqui,3D,ref}}$ is the aquifer resistance calculated by the metamodel in a 5 m × 5 m × 5 m grid (reference model) [L^{-2}.T].

This is done only for the model using the usual MODFLOW expression because the models Mehl_01 and Mehl_02 already account for the aquifer resistance. Consequently, the reference models of Mehl_01 and Mehl_02 have different values of GW – SW resistance.

Regarding the discretization of the upscaled models, grid with block side lengths of 5, 10, 50, 100, 200 and 400 m in the horizontal plane and thicknesses of 5, 10, 20 and 40 m were considered. All combinations of these 6 horizontal and 4 vertical discretizations were investigated, leading to 24 configurations.

II.4.2.3. Evaluation of the upscaled models

First, the sum of the GW – SW fluxes in all model cells were compared. Then, the total absolute error and the absolute value of the relative error were calculated as:

$$total\ error\ = Q_{\mathrm{tot\_ref}} - Q_{\mathrm{tot}}$$

Equation 23

$$relative\ total\ error = |\frac{Q_{\mathrm{tot_{ref}}} - Q_{\mathrm{tot}}}{Q_{\mathrm{tot_{ref}}}}|$$

Equation 24

with:

- $Q_{\mathrm{tot\_ref}}$ = sum of groundwater fluxes to rivers or ditch drains in all reference model cells
- Q_{tot} = sum of groundwater fluxes to rivers or ditch drains in all upscaled model cells

In a second step, the spatial distribution of the GW − SW fluxes were evaluated. The fluxes computed by the reference model were aggregated in the upscaled model cells and the errors per model cell were calculated as:

$$error_i = Q_{\mathrm{ref},i} - Q_i$$

Equation 25

with:

- $Q_{\mathrm{ref},i}$ = aggregated flux of the reference model in cell *i* of the upscaled model
- Q_i = flux in cell *i* in the upscaled model

In a third step, the GW − SW fluxes errors per cell are summarized by calculating the RMSE as:

$$RMSE = \sqrt{\frac{\sum_{i=1}^{n}(error_i)^2}{n}}$$

Equation 26

with:

- *n* = number of cells with rivers or ditch drains in the upscaled model

The magnitude of the GW − SW fluxes in a grid cell generally increases with the horizontal area of the grid cell, resulting in an increase of the error. The RMSE was normalized using the spatial variation of the aggregated fluxes of the reference model (Equation 27) in order to compare the performance of the models with different horizontal discretizations. The normalization was done in this way because the GW – SW fluxes can be both positive and negative, therefore the normalization with the mean value could be problematic.

$$NRMSE = \frac{RMSE}{\sqrt{\frac{\sum_{i=1}^{n}(Q_{\mathrm{ref},i})^2}{n} - \frac{Q_{\mathrm{tot\_ref}}^2}{n^2}}}$$

Equation 27

II.5. Results

II.5.1. 2D field scale numerical experiments

This section presents the results of the 2D field scale numerical experiments. First, two examples of the regressions used to calculate the GW − SW resistances from the 2D numerical experiments (fitted resistances) as well as the accuracy of all of them are shown. Secondly,

the results of the comparison between the fitted resistances and the metamodel resistances are highlighted.

II.5.1.1. Estimation of the GW − SW conductances

Two examples of the regression used to calculate the GW − SW conductance from the numerical experiments are presented in Figure 8. An overview of the coefficients of determination (R^2) and residual standard deviations (RSD) of all the regressions is displayed in Figure 9.

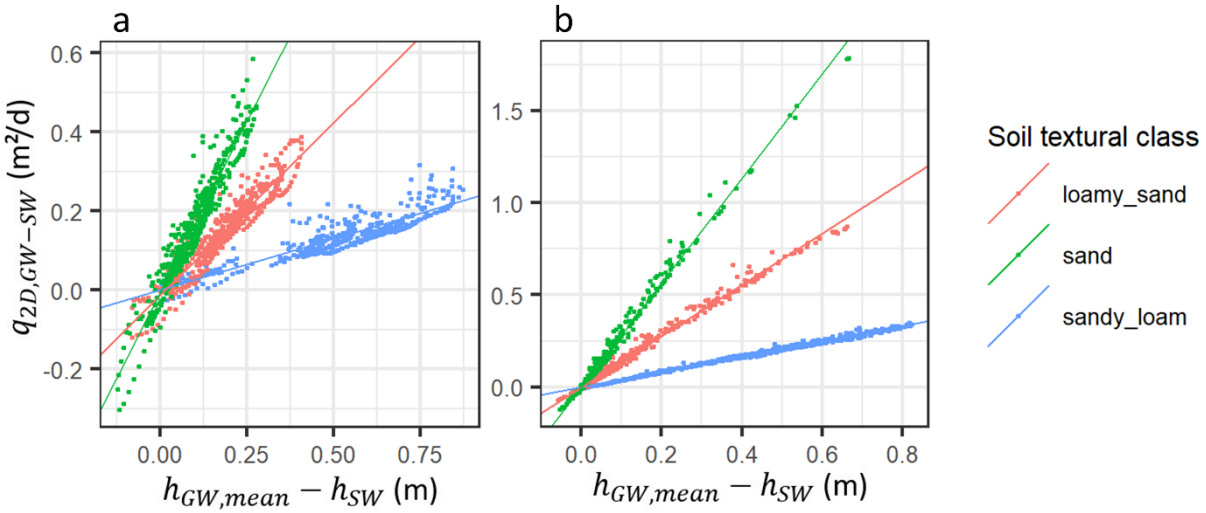

Figure 8: Examples GW − SW flux ($q_{2D,GW-SW}$) as a function of the hydraulic gradient ($h_{GW,mean} - h_{SW}$) and the linear regressions associated, for models with (a) an aquifer thickness (D) = 10 m, a vertical averaging length (D_{avg}) = 10 m and a horizontal averaging length (L_{avg}) = 100 m (a) and (b) D = 50 m , D_{avg} = 50 m and L_{avg} = 100 m (b)

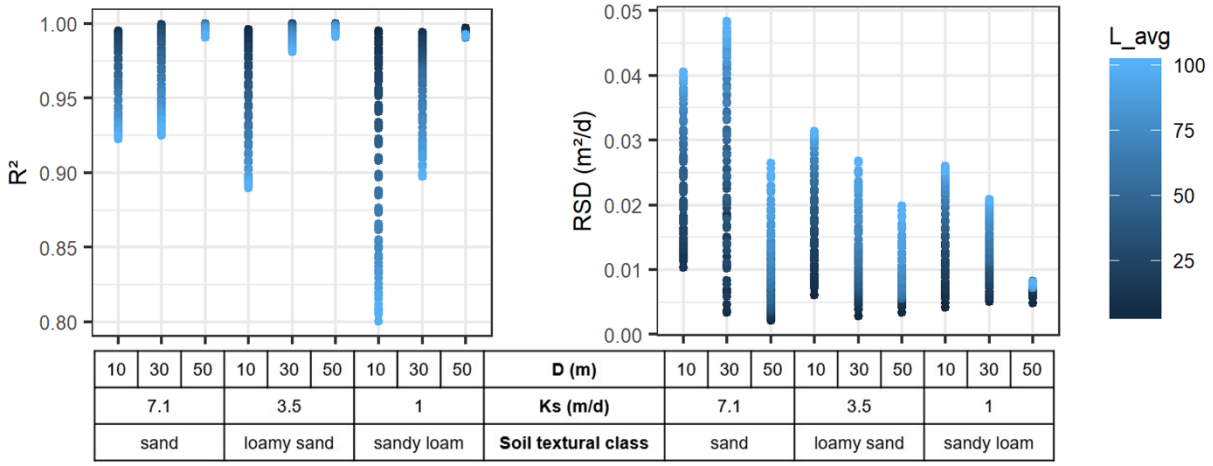

Figure 9: Coefficient of determination (R^2) and residual standard deviation (RSD) of the linear regressions used to calculate the conductance, for different combinations of aquifer thicknesses (D) and hydraulic conductivity (Ks)

The results show that the resistance approach with a time constant parameter can appropriately represent GW − SW water flow exchanges in the numerical experiments. It can be noticed however, that the errors increase as D and L_{avg} decrease.

II.5.1.2. Comparison of the fitted and the metamodel resistances

The comparison between the resistance calculated from the 2D numerical experiments and the metamodel with and without the correction coefficient α is presented in Figure 10. The ratio between D_{avg} and D is set as color scale. When not using the coefficient α, a significant deviation of the metamodel is observed for cases with D_{avg} smaller than D. The RMSE and MAPE are respectively 0.20 d/m and 31.2 %. This deviation is corrected quite well by introducing α with a manually fitted β value of 0.5 (see section II.3.1.2 for the equations associated). The fit is better and the RMSE and MAPE improve to 0.13 d/m and 16.8 %.

The metamodel presents a slight overall overestimation of the resistance, which could be due to an overestimation of the length over which the hydraulic resistance is calculated. Note that the use of the α coefficient is not aimed to correct this overestimation.

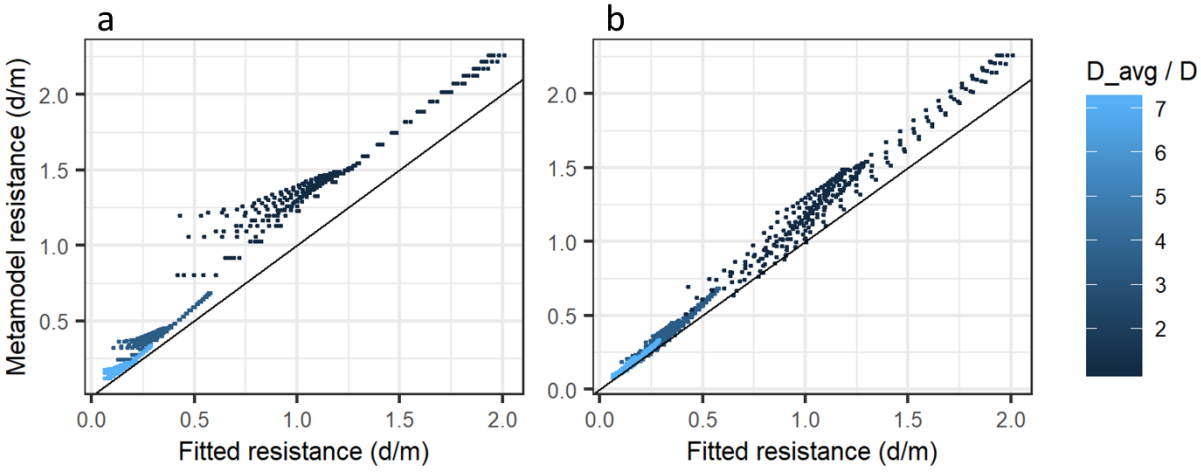

Figure 10: Comparison of the resistance calculated from the 2D numerical experiments (fitted resistances) and by the metamodel, without (a) and with (b) the correction coefficient α

II.5.2. 3D hydrogeological model upscaling study

This section presents the results of the 3D hydrogeological model upscaling study. First, examples of the calculation of L (the representative distance between surface water bodies) are given. Secondly, the comparison of the total GW – SW net fluxes is presented and finally the results of the evaluation of the upscaled models against the reference model are

discussed. Note that in the results presented in this section, negative fluxes are from GW towards SW.

The results of the two approaches proposed by Mehl and Hill (2010) (Mehl_01 and Mehl_02) are not presented in detail here because they show the same shortcomings as in the original study and are not commonly used approaches in hydrogeological models. These results are in line with the original study conclusions and are presented in the supplementary material (Appendix A). Briefly summarized, the Mehl_01 approach leads to a decrease of the GW – SW resistance when the horizontal discretization increases. However, the numerical experiments show that the GW – SW resistance and the horizontal discretization are positively correlated. Moreover, in the vertical direction, this approach overestimates the increase in GW – SW resistance due to the increase in vertical discretization. Concerning the Mehl_02 approach, the GW – SW resistance does not increase with the horizontal resistance and the overestimation of the GW – SW resistance when the vertical discretization increases is even more pronounced than for Mehl_01.

II.5.2.1. Representative distance between surface water bodies ($\boldsymbol{L}$) in 3D

Figure 11 shows the map of the calculated representative distance between the rivers and ditch drains, for horizontal discretizations of 50 and 400 m as examples. The representative distance calculated for the two resolutions are similar because they are both an aggregation at different scales of the same 5 x 5 m grid data. L values for rivers vary over a large range; from 55 to approximately 3000 m. The smaller values are mainly located in the confluence areas. The distance between surface water bodies, represented by L, varies from 45 to 815 m.

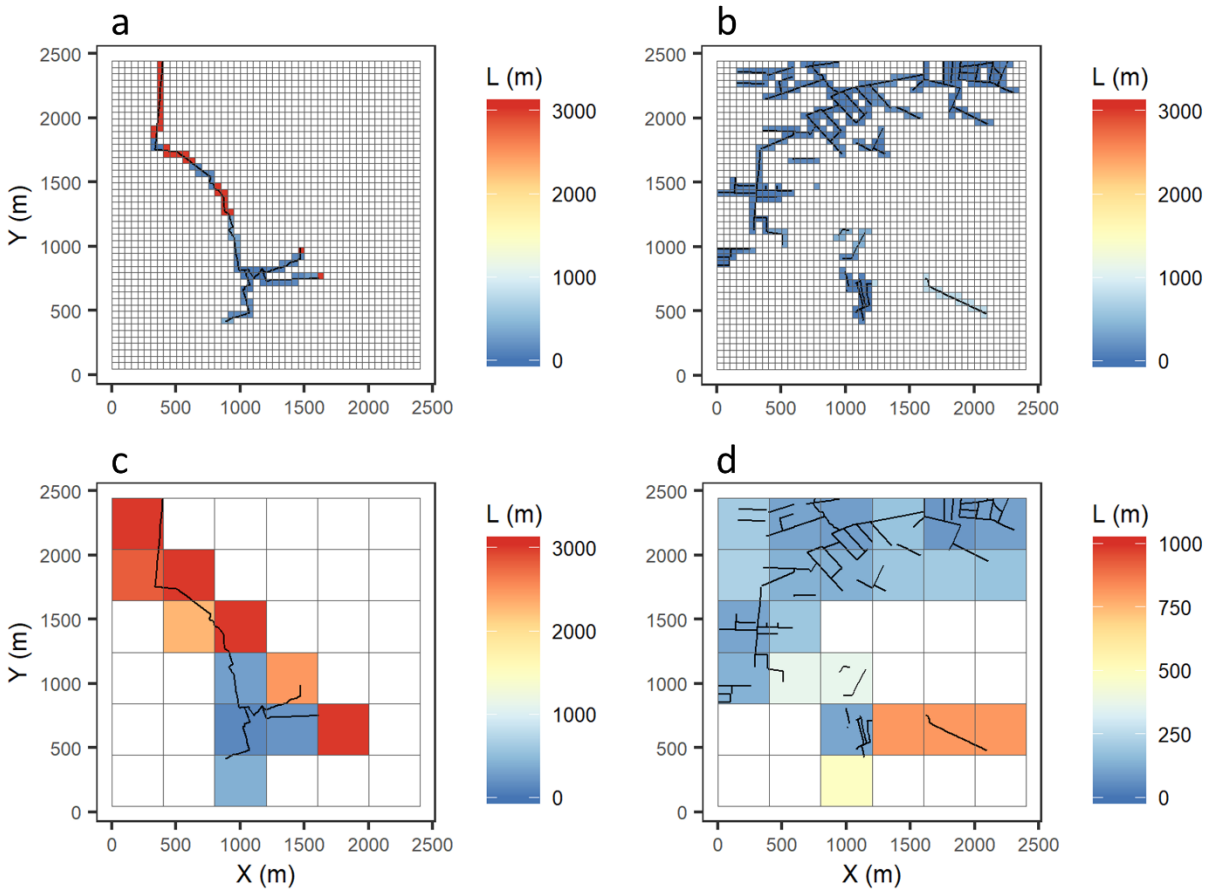

Figure 11: Map of the calculated representative distance between surface water bodies (L) for a horizontal discretization of 50 m (a: rivers, b: ditch drains) and 400 m (c: rivers, d: ditch drains). Note the different color scales for the rivers (a and c) and drains (b and d)

II.5.2.2. Comparison of the total GW – SW net fluxes

The total net rivers – groundwater and ditch drains − groundwater fluxes in all the upscaled models as well as the associated mean 2D resistances considering the MODFLOW expression are shown in Figure 12. Figure 13 shows the results when considering the metamodel resistance expression.

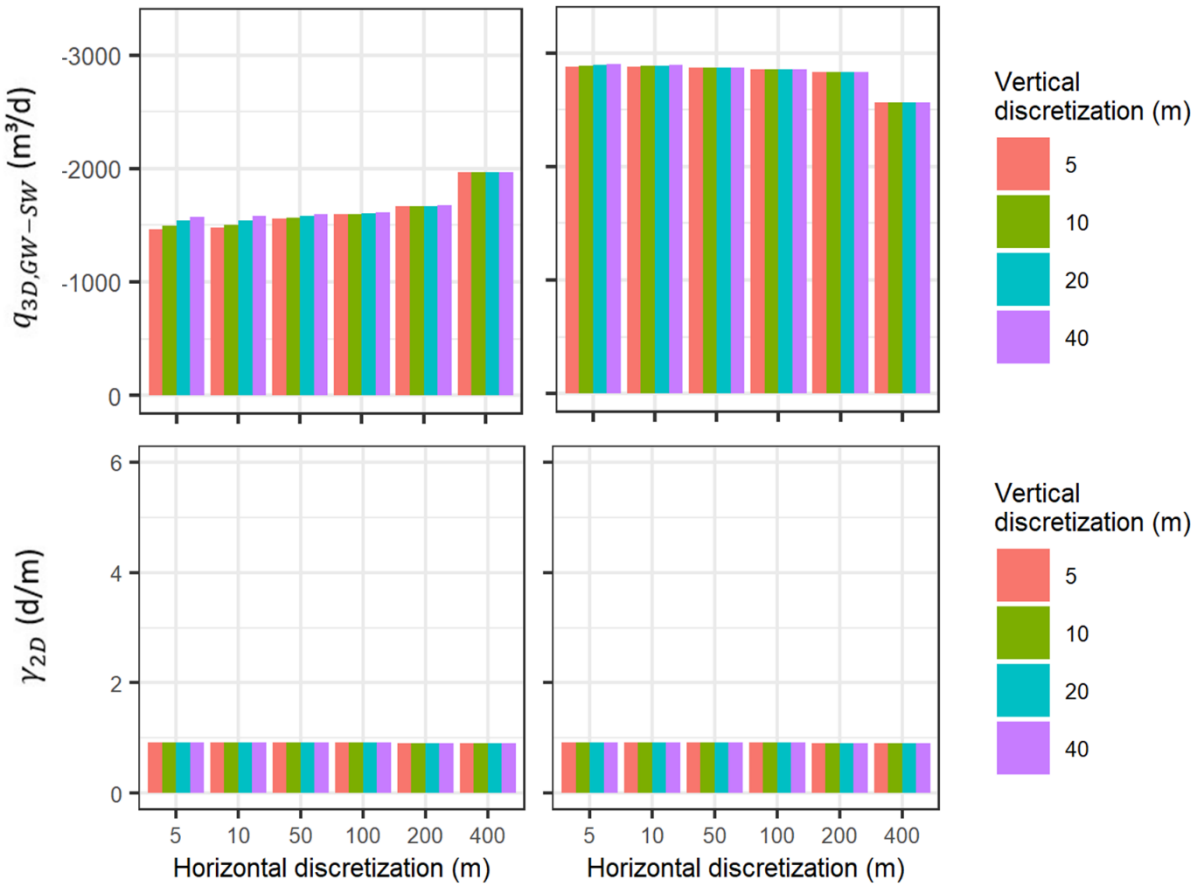

Figure 12: Total net rivers – groundwater and ditch drains − groundwater fluxes ($q_{3D,GW-SW}$) in all the upscaled models considering the MODFLOW resistance and the associated mean 2D resistances (γ_{2D})

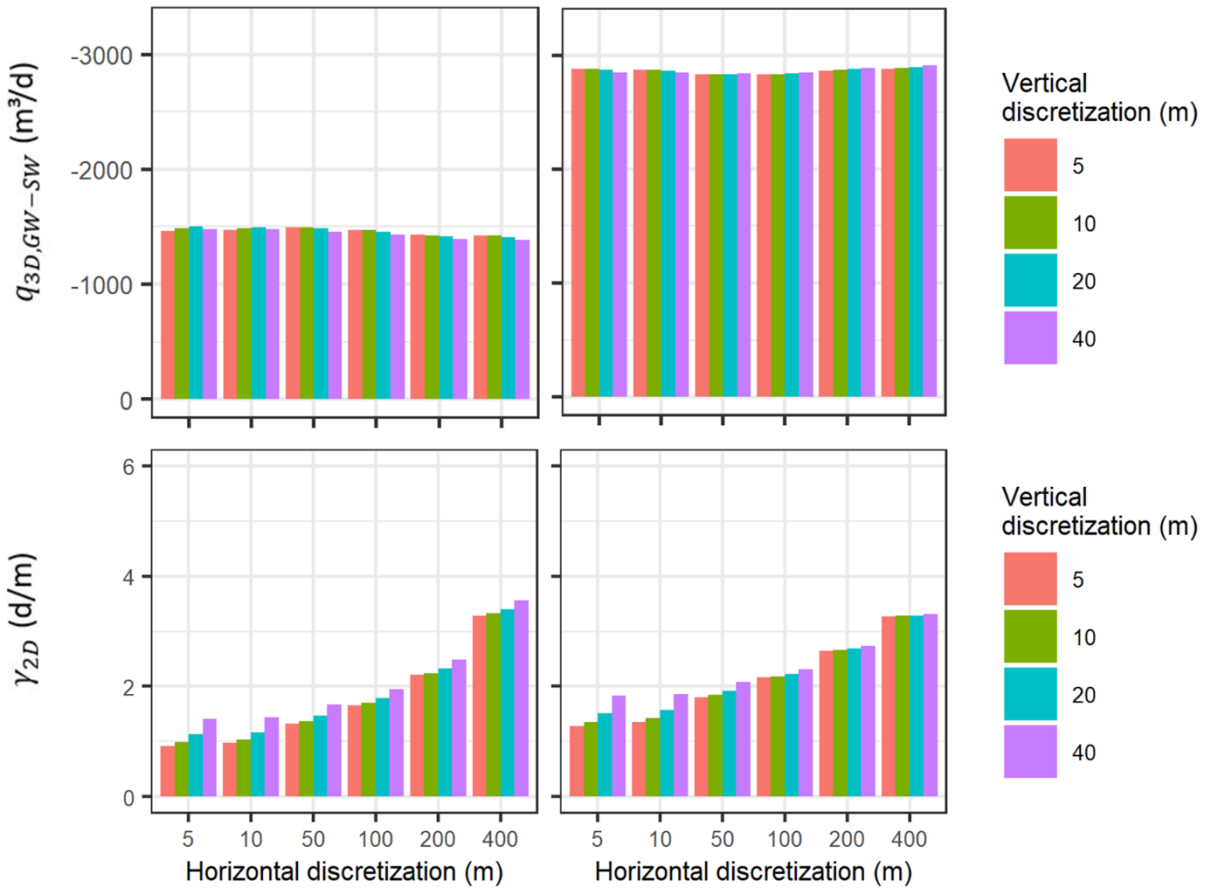

Figure 13: Total net rivers – groundwater and ditch drains − groundwater fluxes ($q_{3D,GW-SW}$) in all the upscaled models considering the metamodel resistance and the associated mean 2D resistances (γ_{2D})

The results reveal that with the MODFLOW expression, the total groundwater − rivers fluxes increase with the horizontal discretization. This leads to an important overestimation at the coarsest resolution of 400 m. To a lesser extent, an overestimation of the fluxes is also observed when the vertical discretization increases. This overestimation is more important for the smallest horizontal discretization and seems to be negligible when the horizontal discretization is superior to 100 m. The observed overestimation of groundwater − river fluxes by the MODFLOW parameterization as the horizontal and vertical discretization increase is because the MODFLOW resistance does not consider the aquifer resistance. Indeed, the 2D resistances remain constant as the discretization gets coarser.

Concerning the groundwater – ditch drains fluxes, the vertical discretization seems not to have any noticeable impact. However, when the horizontal discretization increases the fluxes are underestimated. This is because when fluxes to rivers are overestimated, hydraulic heads drop, and smaller fluxes to the ditch drains is computed. This behavior caused groundwater to drop below the ditch drains, in a part of the domain, so fluxes were no longer computed in

these cells. The inactivity of ditch drains in part of the domain increases with the horizontal discretization size in the MODFLOW resistance models as is illustrated in Figure 14 (a) for a vertical discretization of 5 m (the patterns are similar for the others vertical discretizations). This behavior is also observed, although less importantly, when the vertical discretization increases as shown in Figure 14 (b) for a horizontal discretization of 5 m.

Conversely, the fluxes to ditch drains and rivers simulated by the proposed metamodel remain rather constant as the horizontal discretization increases. This indicates that the metamodel properly upscales the resistances. Concerning the vertical discretization, some improvement can be seen for the rivers in models with horizontal discretizations smaller than 50 m. However, for the horizontal discretizations larger than 100 m, the metamodel slightly underestimates the fluxes. A small bias can also be seen when looking at the effect of the vertical discretization on the groundwater – ditch drains fluxes. This is most probably due to the α correction parameter in the metamodel expression, as it is the only term that accounts for the vertical discretization size. However, these small inconsistencies cover a very low error range of a few percent.

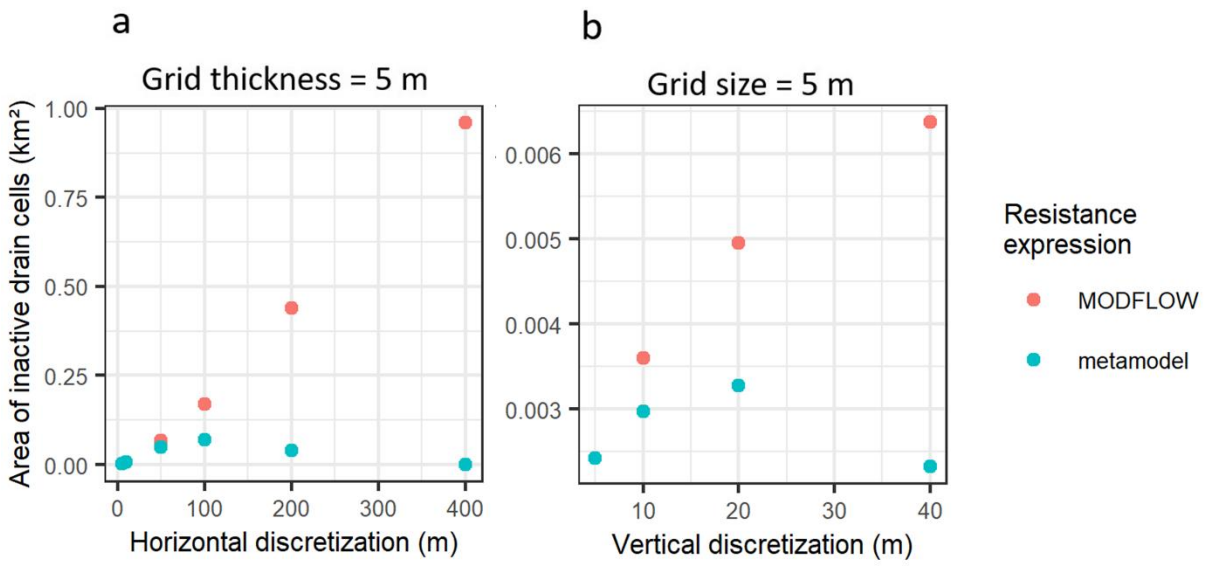

Figure 14: Area of inactive drain cell plotted against the horizontal discretization size (a) and the vertical discretization size (b)

II.5.2.3. Evaluation of the upscaled models

The section discusses some selected results from the complete comparison between upscaled models and the reference model. For the horizontal upscaling, only the results of the models

with a vertical discretization of 5 m are presented. For the vertical upscaling, only the results of the models with a horizontal discretization of 5 m are presented. The remaining results are presented as tables in the supplementary material (Appendix A).

II.5.2.3.1. Evaluation of total GW – SW fluxes

The absolute and relative total errors of the upscaled models, compared to the reference model, for the horizontal upscaling are presented in Figure 15. The same results for the vertical upscaling are presented in Figure 16.

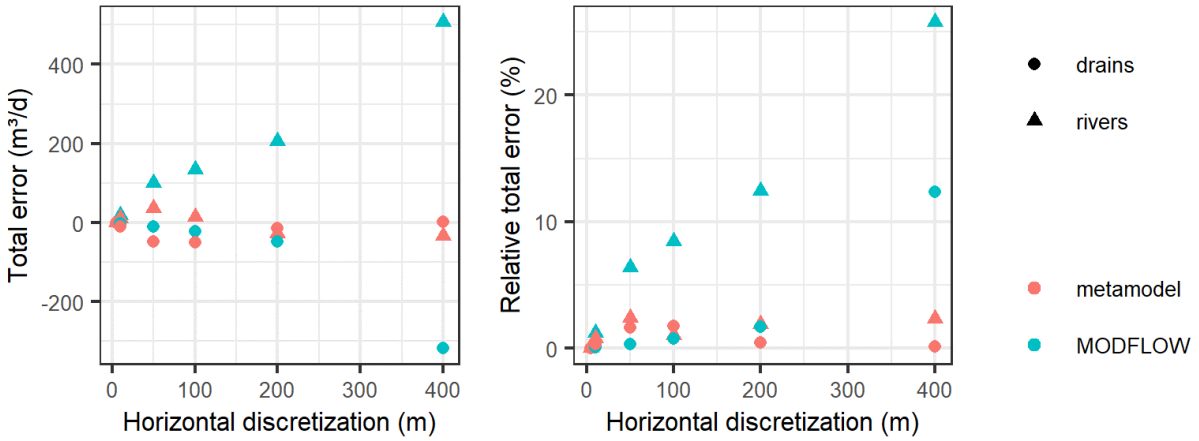

Figure 15: Absolute and relative errors of GW – SW total fluxes for the horizontal upscaling study for the models of 5 m vertical discretization

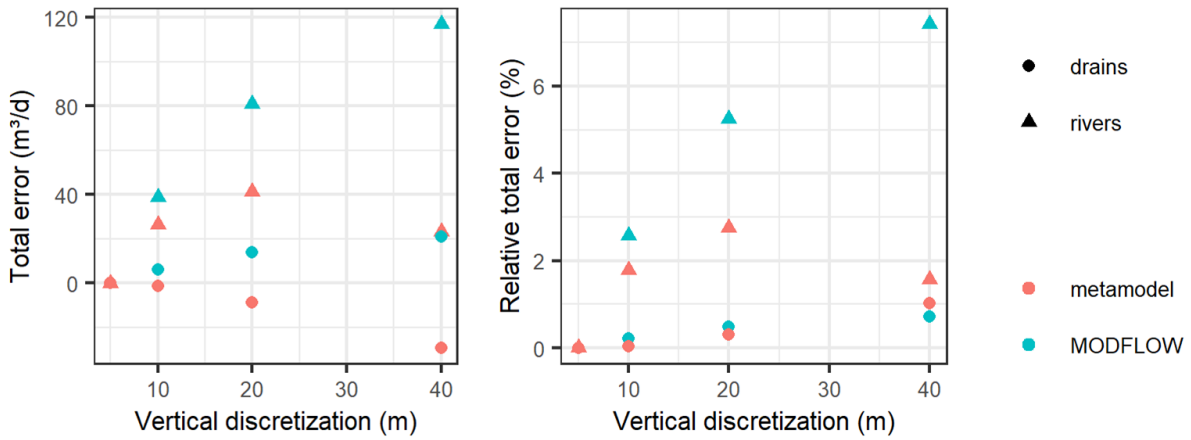

Figure 16: Absolute and relative errors of GW – SW total fluxes for the vertical upscaling study for the models of 5 m horizontal discretization

Concerning the horizontal upscaling, the total errors associated with the MODFLOW resistance expression reach more than 500 m³/d or 25 % of the total flux for the rivers and more than 300 m³/d or 10 % of the reference flux for the ditch drains. In contrast, total errors

for the models using the proposed metamodel remain lower than 50 m^3/d or 5% of the reference flux for both rivers and ditch drains. With respect to this criterion and as far as the ditch drains are concerned, the models based on the MODFLOW resistance expression perform better than the ones relying on our metamodel for horizontal discretizations from 5 to 100 m (Figure 15). However, this should be regarded with caution as two different sources of error are compensating each other here. The underestimated resistance leads on the one hand to an overestimation of the fluxes to the rivers, and on the other hand, this resistance underestimation causes a drop in groundwater head together with a subsequent underestimation of the fluxes to the ditch drains.

Regarding the vertical upscaling, the absolute and relative total errors observed are much smaller than for the upscaling in the horizontal direction, probably because the upscaling is done over a smaller scale range. The models using the MODFLOW expression show a total error of the groundwater – rivers fluxes of approximately 7 %, for a vertical discretization of 40 m. The relative total errors of the groundwater – ditch drains fluxes remain below 2%. In contrast, using the metamodel resistance expression, relative total errors remain below 3 % for the rivers and below 2 % for the ditch drains.

II.5.2.3.2. Evaluation of GW − SW fluxes per cell

To illustrate GW − SW fluxes model outputs, maps of the GW − SW fluxes for the models with a horizontal discretization of 400 m and a vertical discretization of 5 m are presented in Figure 17. On the Figure 18, the map of GW − SW fluxes errors between the reference model and the two upscaled models as well as the associated histograms are presented.

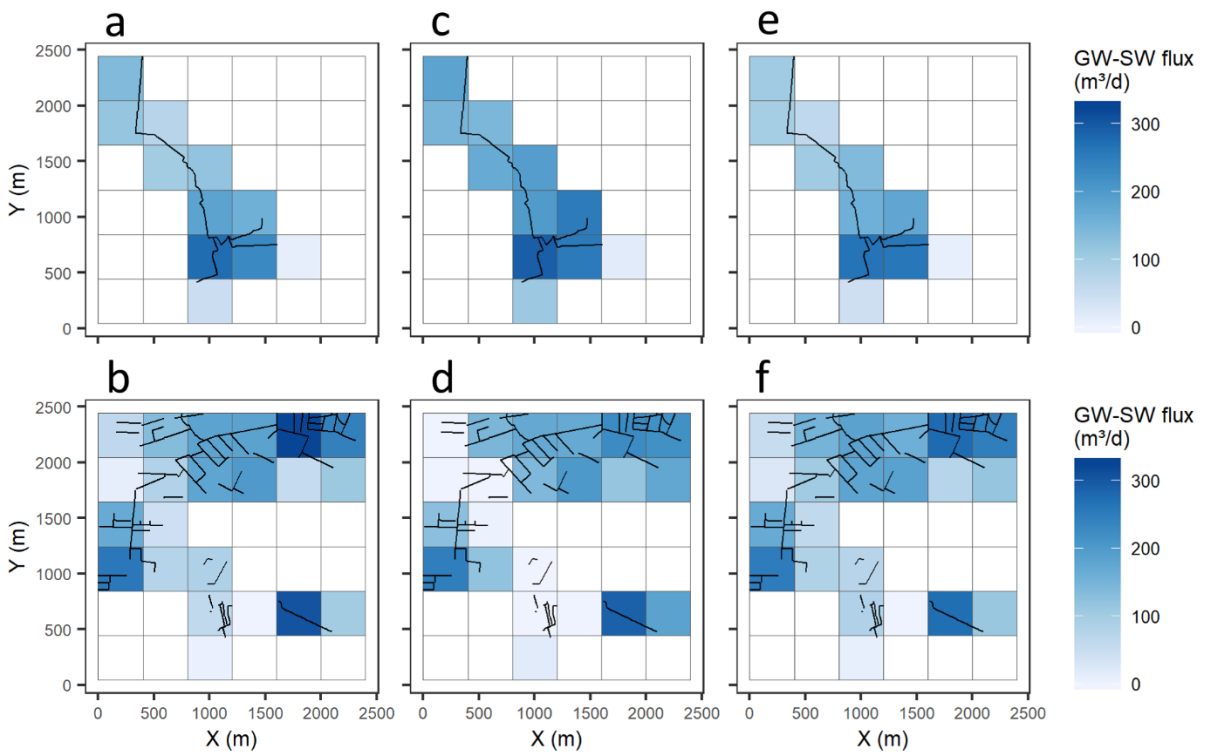

Figure 17: Map of the GW − SW fluxes for the model with a horizontal discretization of 400 m and a vertical discretization of 5 m. a and b are the outputs of the reference model for the rivers and ditch drains respectively, c and d the outputs of the model using the usual MODFLOW resistance, e and f the outputs of the model using the metamodel resistance

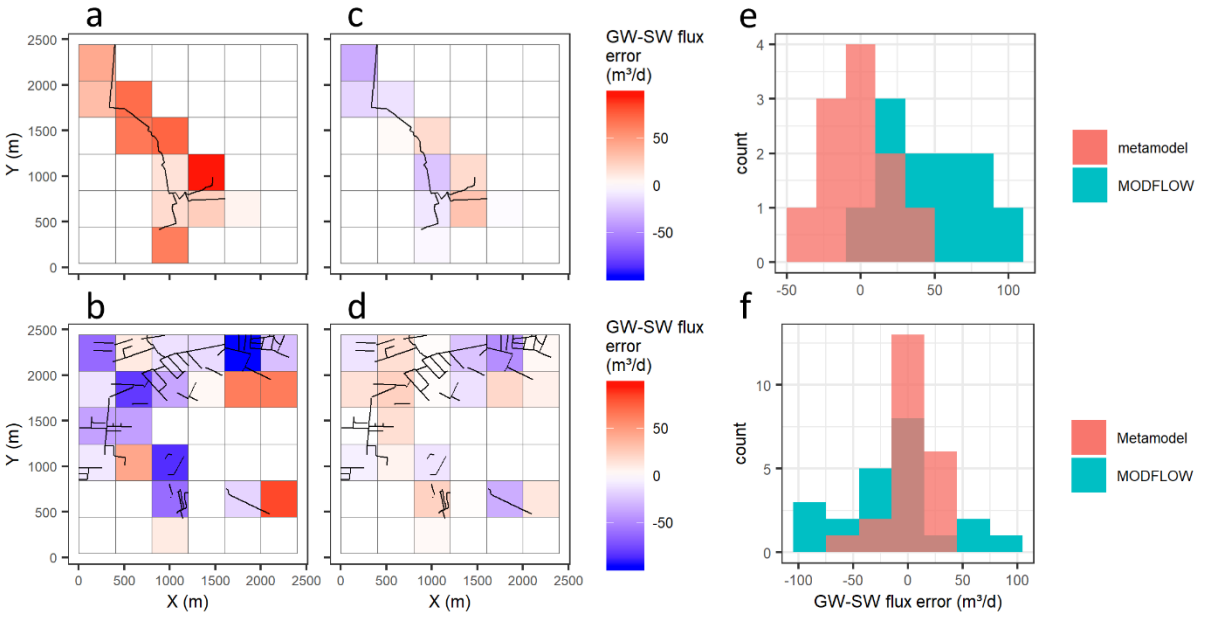

Figure 18: Map of errors between the GW − SW fluxes computed by the reference model and the upscaled models with a horizontal discretization of 400 m and a vertical discretization of 5 m as well as the histograms associated. a and b are the map of errors observed using the MODFLOW expression for the rivers and drains respectively, c and d the map of errors observed using the metamodel expression, e and f are the histograms associated for the rivers and drains respectively

Concerning the rivers, the distribution of the errors observed when using the MODFLOW expression is spread between approximately 0 and 100 m^3/d. In contrast, when using the metamodel, the distribution of errors is spread approximately between −50 and 50 m^3/d and is centered on 0. This shows that the use of the metamodel removes the bias observed when the aquifer resistance is neglected.

Concerning the drains, the distribution of errors when using the MODFLOW expression is approximately between −100 and 100 m^3/d. In contrast, when using the metamodel, the distribution of errors approximately between −50 and 50 m^3/d.

The RMSE of the GW − SW fluxes per cell of the upscaled models compared to the reference model are shown in Figure 19 and Figure 20**Error! Reference source not found.** for the horizontal and vertical upscaling, respectively.

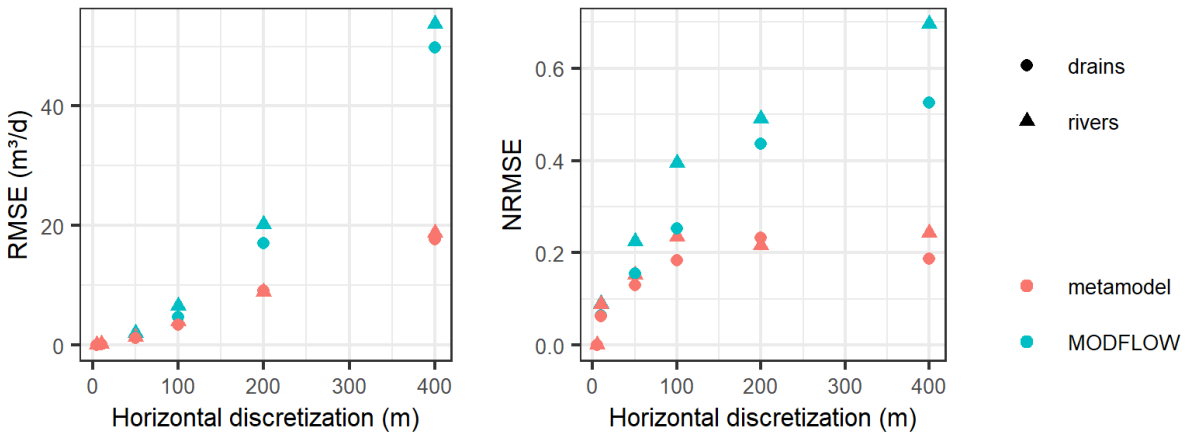

Figure 19: RMSE and NRMSE of GW − SW fluxes per cell for the horizontal upscaling for the models of 5 m vertical discretization

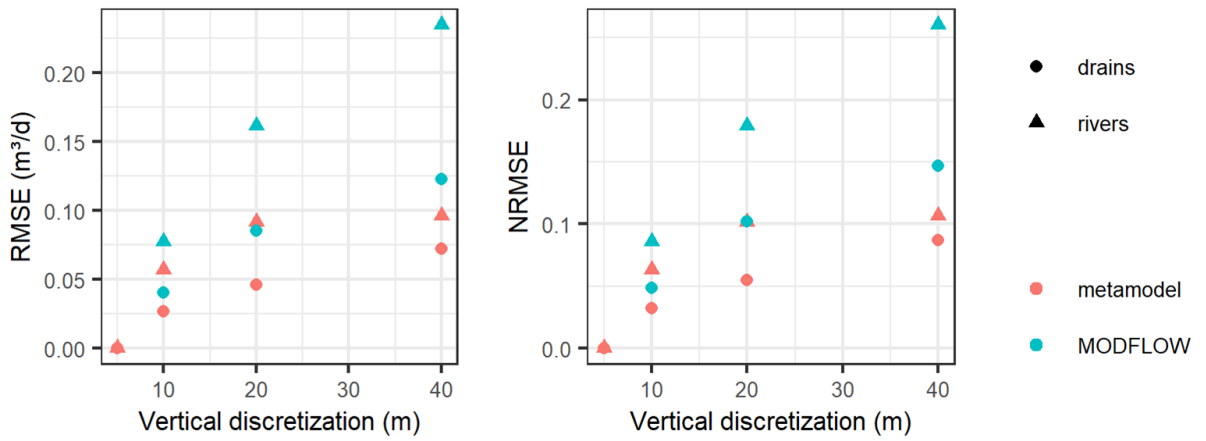

Figure 20: RMSE and NRMSE of GW – SW fluxes per cell for the vertical upscaling for the models of 5 m horizontal discretization

Regarding the upscaling in horizontal direction, the RMSE increases to approximately 50 m³/d for the MODFLOW expression, which represents around 0.5 of the standard deviation of the reference model for the ditch drains and around 0.7 for the rivers. In the case of the metamodel expression, the RMSE remains below20 m³/d or 0.25 of the standard deviation of the reference model fluxes for both the rivers and the ditch drains. These values remain relatively high for both approaches. However, the improvement of the metamodel approach can be clearly seen. It is likely that a part of the RMSE increase is not linked to the scale dependency of the resistance but to other upscaling issues (e.g. averaging of hydraulic head, boundary conditions effect).

For the upscaling in the vertical direction, this criterion shows also a much lower error range for the metamodel. The models with the MODFLOW approach show a RMSE increasing to around 0.12 m³/d for the ditch drains and around 0.25 m³/d for the rivers. These values represent 0.15 for the ditch drains and 0.25 for the rivers of the standard deviation of the reference models fluxes per cell. Concerning the models using the metamodel resistance expression, the values are always lower, with RMSE lower than 0.1 m³/d for both rivers and ditch drains, which is around 0.1 of the standard deviation of the reference models fluxes per cell.

II.6. Discussion

This work presents a new metamodel to estimate aquifer component of the GW-SW resistance in Cauchy boundary conditions used to simulate groundwater − surface water

interactions in regional hydrogeological models. This is achieved by deriving a new analytical equation and empirically correcting the equation of Ernst (1962) to obtain an expression which can be used in hydrogeological models.

Our metamodel is tested against 2D and 3D numerical experiments and shows good estimation of the groundwater − surface water fluxes as it manages to capture the scale dependency of the resistance that is caused by the flow processes occurring in the aquifer. Moreover, the proposed metamodel can be directly implemented in hydrogeological models, for any number of surface water bodies within a groundwater model cell, without requiring any additional numerical calculation.

It is important to note that the metamodel expression is derived under the assumption of a homogeneous aquifer. For a layered aquifer with horizontal layers, the derivation of representative horizontal and vertical hydraulic conductivities should be straightforward and could be used in the metamodel equation. For more general cases, the estimation of representative hydraulic conductivities would be trickier. However, it could be achieved, for instance, by upscaling the hydraulic conductivities field and/or using inverse modeling.

A second assumption in our analysis is the presence of a no flow boundary at the bottom of the hydrogeological model. It should be noted though that the approach can be used for vertical discretizations that are less than the thickness of the aquifer so that vertical flow across the bottom of a grid cell in contact with surface water is in fact accounted for. For other kinds of boundary conditions at the bottom of the hydrogeological model, some additional testing would be required.

A third assumption made in the derivation of the metamodel is that the GW and SW hydraulic heads can be approximated by the aquifer thickness. This seems to be a reasonable simplification for the majority of hydrogeological models because the aquifer thickness is usually much larger than the hydraulic head above the surface water bottom. It simplifies greatly the use of the metamodel in hydrogeological models. The resistance could be derived without this simplification but would then depend on the hydraulic head in the groundwater and the surface water, which would result in a nonlinear model and thus add complexity to the numerical modeling exercise. However, in the case where this assumption is unrealistic (e.g. highly incised channels), a possible alternative would be to choose a level above the

surface water bottom for the calculation of the horizontal head losses. Note that, for the calculation of the radial aquifer resistance the surface water bottom level should be chosen anyway. Another geometrical assumption is that neighboring surface water features have the same streambed and water level. While this seems to be a reasonable assumption in virtually flat lowland areas, it may be an oversimplification in areas with higher topographic gradient.

The metamodel still needs to be evaluated for loosing rivers (i.e. flux from surface water toward groundwater) because the examples presented in this paper mainly consider gaining surface water features.

A next step would be to use the proposed metamodel in a real-world case study, either to parameterize directly hydrogeological models or to be incorporated in a calibration framework. Because it improves the conceptualization of the GW – SW resistance approach by decoupling the aquifer resistance from the streambed resistance, our approach should allow for transferring calibrated values in models of different horizontal and vertical discretizations. Moreover, it could also help for the investigation of streambed resistances and hyporheic processes.

II.7. Conclusion

A new expression for groundwater – surface water interactions in regional hydrogeological models is proposed. The main new aspect is that it includes the aquifer component of the GW-SW conductance in Cauchy boundary conditions as usually implemented in such models. The expression takes into account site-specific factors such as the hydraulic conductivity, the aquifer thickness and the distance between two surface water bodies but also model factors as the grid-cell size in both vertical and horizontal directions. One of the main advantages is that streambed and aquifer resistances are transferable between different model discretizations. The expression is derived from the Dupuit-Forcheimer theory, the Ernst drain design equation and an empirical correction parameter derived from detailed 2D (cross sectional) numerical experiments at the field-scale. Our expression appears to capture in a satisfactory way the relationship observed in the 2D numerical experiments between the aquifer component of the GW-SW conductance and the aquifer characteristics. It is also tested in a 3D hydrogeological model upscaling study (both in horizontal and vertical directions) and compared with the MODFLOW expression, which shows grid-size dependency problems, and

the alternatives proposed by Mehl and Hill (2010). The proposed expression outperforms the other approaches and is found to capture a substantial part of the conductance grid-size dependency without adding any complexity to the numerical modeling exercise. We therefore argue that it is an improvement over the existing approaches for representing groundwater – surface water interactions in regional hydrogeological models.

Chapter III

Unraveling the link between diurnal groundwater fluctuations and root water uptake using HYDRUS-3D simulations

III. Unraveling the link between diurnal groundwater fluctuations and root water uptake using HYDRUS-3D simulations

III.1. Abstract

This study presents an attempt to model groundwater consumption by plants as observed in a lowland temperate area. Piezometric data were recorded at high frequency in a deciduous tree plot as well as the adjacent grass plot. Diurnal groundwater fluctuations were observed in both piezometer time series. To evaluate whether these fluctuations are related to tree root water uptake from the groundwater, we carried out a simulation study. Our modeling framework included the FAO (Food and Agriculture Organization) 56 Penman-Monteith evapotranspiration equation, a canopy water balance model and a 3D variably saturated subsurface flow model. The model simulated the main features of the observed diurnal groundwater level fluctuations properly, though a more advanced vegetation compartment would be needed to represent the timing of the diurnal fluctuations. We also evaluated the White method (White, 1932) for estimating transpiration from diurnal groundwater level fluctuations using specific yield estimates proposed by Loheide et al. (2005). When applied to the simulated piezometric levels, it shows good agreement with simulated transpiration from groundwater. Thus, this method was applied to the measured piezometric levels and compared to the simulated transpiration from groundwater. Finally, an analysis of the simulated fluxes at the boundaries of the tree plot shows significant diurnal patterns caused by tree transpiration. Moreover, excluding root water uptake from groundwater in our simulation scenario led to larger (10 to 30 %) groundwater – surface water fluxes during dry periods. It is therefore concluded that adequately representing groundwater consumption by plants is essential for modeling subsurface flow in such environments.

III.2. Introduction

Transpiration is globally the dominating terrestrial evapotranspiration flux (Jasechko et al., 2013). Some ecosystems rely on groundwater to satisfy whole or a part of their transpiration

demand. These ecosystems are recognized as groundwater-dependent and include lowland areas, riparian zones and wetlands (Kløve et al., 2011; Orellana et al., 2012).

Potential transpiration demand is determined by atmospheric conditions (e.g. radiation, temperature, vapor pressure, wind speed) and plant characteristics (e.g. species, leaf area index, height, interception capacity). This demand is then transferred as hydraulic gradients to the roots that take up water. Water uptake can be limited by the soil water status if conditions are too dry or too wet. In excessively dry conditions, the water pressure gets too low to allow for root water uptake while in wet conditions, the low oxygen partial pressure limits root water uptake (Aroca et al., 2011). In both cases, the actual transpiration will be lower than the potential transpiration. For most plants, root water uptake is only possible in the unsaturated zone. However, some plants, the phreatophytes, are able to access water in the saturated part of the soil.

One of the first extensive studies of phreatophytes was done by Meinzer (1927) and later updated by Robinson (1958). They identified phreatophyte species and their main characteristics in relation to groundwater depth of their habitat. Since then, numerous studies on phreatophytes were conducted including a review of monitoring and modeling techniques used to study water – phreatophytes interactions (Orellana et al., 2012). Most of the studies focused on arid and semiarid environments where groundwater is often the only viable source of water for plants (Bauer et al., 2004; Miller et al., 2010), but some also considered more humid environments where transpiration from groundwater can largely impact the hydrological cycle (Mould et al., 2010; Vincke and Thiry, 2008).

One of the consequences of groundwater extraction by phreatophytes is diurnal fluctuations of the groundwater level. Groundwater level drops during the day when transpiration occurs and recovers during the night after transpiration stopped. White (1932) used these fluctuations and the aquifer specific yield value to estimate daily groundwater evapotranspiration (ET_{GW}). Groundwater evapotranspiration refers to the water losses from groundwater due to both transpiration, i.e., direct water uptake through roots from groundwater or the capillary fringe, and direct evaporation, i.e., evaporation of water at the water table which is then transported through the unsaturated zone to the land surface in the vapor phase (Orellana et al., 2012). The so-called White method, is still used today (Fan et al., 2016; Gribovszki et al., 2008; Salama et al., 1994). A detailed description of the method is given

in section III.3.3.1. Using numerical experiments, Loheide et al. (2005) showed that the White method overestimates ET_{GW} up to a factor 20 for fine textured soil, when calculating the specific yield as the difference between the saturated and residual water contents. Therefore, they proposed to use corrected values of the specific yield, referred to as readily available specific yield, defined on the basis of their numerical model simulations. These corrected values have the advantage of taking into account the drainage time considered in the application of the White method (< 12 hours). The White method used together with the specific yield estimates proposed by Loheide et al. (2005) has been widely applied (Lautz, 2008; Marchionni et al., 2019). However, its evaluation has been considerably limited by the difficulty to estimate ET_{GW} from field measurements. Fahle and Dietrich (2014) evaluated the performance of the White method for a temperate grassland using a weighable lysimeter. Zhang et al. (2016) performed a similar evaluation in a desert riparian forest where groundwater is the only source of evapotranspiration, which could therefore be measured with an eddy covariance system. Their studies concluded that the estimated ET_{GW} (White) does not show important discrepancies with measured ET_{GW} (eddy covariance, lysimeter) at the seasonal scale. However, at the daily scale, the estimations can differ significantly from the measurements, sometimes showing deviations larger than 1 mm/d, for observed value ranging from 0 to 6 mm/d. In humid shallow groundwater environments, evapotranspiration fluxes are composed of soil evaporation and plant transpiration from the unsaturated and the saturated zones. Therefore, ET_{GW} cannot be measured in natural conditions. Nevertheless, the link between diurnal groundwater fluctuations and root water uptake from the groundwater can be investigated through detailed numerical modeling. It can also provide representative values of ET_{GW} for a given system and set of meteorological conditions.

Water uptake from the groundwater (or saturated zone) by phreatophytes has been modelled in various ways. In conceptual and groundwater models, the tight coupling between root water uptake and water flow in the unsaturated and saturated zone is not represented. Therefore, water uptake from the groundwater is modeled with simple empirical approaches which assume a given relationship (e.g. linear, piecewise linear, bell-shaped) between groundwater depth and transpiration from groundwater (Baird et al., 2005; Pumo et al., 2010). In variably saturated flow models that consider both the groundwater and the unsaturated zone, the impact of root water uptake on water redistribution is described in a more physical

way. The potential transpiration is distributed along the root depth and the actual transpiration calculated using a pressure head reduction function. The most common root water uptake pressure head reduction function is the Feddes function (Feddes et al. 1978), in which two parameters determine at what pressures anoxic stress is occurring. Additionally, Simunek and Hopmans (2009) added a compensation factor to compensate for water stress in some parts of the root zone. Although variably saturated flow models and the Feddes function have been extensively used with and without root water uptake compensation (Galleguillos et al., 2017; Markewitz et al., 2010; Shah et al., 2007), applications to root water uptake by phreatophytes remain scarce. Loheide et al. (2005) used a 2D variably saturated model of groundwater consumption by phreatophytes to evaluate the White method considering different hydraulic properties and flow geometries (see section III.3.3.1). However, the simulations were numerical experiments of hypothetic systems and were not compared with actual field data. More recently, Gou et al. (2018) incorporated several new functions representing groundwater dependent vegetation into the coupled subsurface-land surface model ParFlow.CLM (Maxwell and Miller, 2005). This model was used to conduct three-dimensional, standscale simulations of a Mediterranean oak savanna in California, which showed good agreement with evapotranspiration and soil moisture field data at daily time scale as well as latent heat measurements at diurnal time scale. However, no comparison was shown between the simulated and observed diurnal groundwater level fluctuations.

A challenge with the observations of diurnal water level fluctuations, especially for small fluctuations (a few millimeters), is the reliability of the water and atmospheric pressure measurements used to calculate the water level. Although they are supposed to be corrected for temperature variations, pressure measurements often show temperature-induced biases (McLaughlin and Cohen, 2011). It is therefore important to verify that such corrected diurnal fluctuations are actually due to root water uptake and not influenced by temperature fluctuations. For the present study, this issue is addressed in the supplementary material (Appendix B).

Diurnal fluctuations due to phreatophyte transpiration were also observed in river stage and discharge monitoring studies (Bond et al., 2002; Deutscher et al., 2016; Yashi et al., 1990). Gribovszki et al. (2010) published a review on diurnal fluctuations in shallow groundwater level and streamflow rate including diurnal fluctuations induced by evapotranspiration.

Diurnal fluctuations in groundwater – surface water exchange fluxes are suggested to be the result of water consumption by phreatophytes. Moreover, Nachabe et al. (2005) showed that diurnal patterns in subsurface water flow can also occur between adjacent ecosystems. However, these flux patterns are difficult, if not impossible, to observe in detail. Therefore, numerical modeling of transpiration by phreatophytes and associated fluxes appears to be of great interest to get insights into diurnal fluctuations of subsurface water fluxes and their importance relative to other hydrological fluxes.

The present study evaluates if diurnal fluctuations in groundwater level caused by phreatophytes transpiration can be represented using a three-dimensional variably saturated subsurface flow model. Piezometric measurements are compared with simulation outputs to assess the appropriateness of the conceptual model for explaining diurnal fluctuations. A second objective is to evaluate the impact of tree groundwater uptake on subsurface fluxes to and from phreatophytes areas and their diurnal dynamics. Finally, a third objective is to evaluate the performance of the White method when used with the specific yield estimation guidelines proposed by Loheide et al. (2005) to estimate ET_{GW} for the considered case study and compare the White method ET_{GW} estimates to our simulated ET_{GW}.

III.3. Materials and methods

III.3.1. Experimental set-up

The study area is located in north-eastern Belgium within the Campine area and the Kleine Nete catchment. The experimental set-up consisted of three groundwater level monitoring sites equipped with Solinst levelogger Edge M5 pressure sensors (sites A, B and C) and one weather station where atmospheric pressure is recorded (Figure 21). The pressure sensors also measure temperature, which is internally used to correct the pressure measurements. The atmospheric pressure data were used to correct the groundwater level records. At site C, with a groundwater deeper than > 1.5 m and a vegetation with shallow rooting depth (10 cm), no groundwater uptake and fluctuations were expected whereas fluctuations were expected at sites A and B with trees and a shallow groundwater table (< 1.5 m). Additionally, two laboratory tests were performed. Only site A was modeled in a detailed three-dimensional set-up. The White method was applied to site A and B datasets. The other three datasets (sites C and laboratory tests) were only used to assess the sensor reliability for measuring small

diurnal groundwater level fluctuations and to test the hypothesis that diurnal groundwater fluctuations can be related to root water uptake from the groundwater. Hence, they are presented and discussed in the supplementary material (Appendix B).

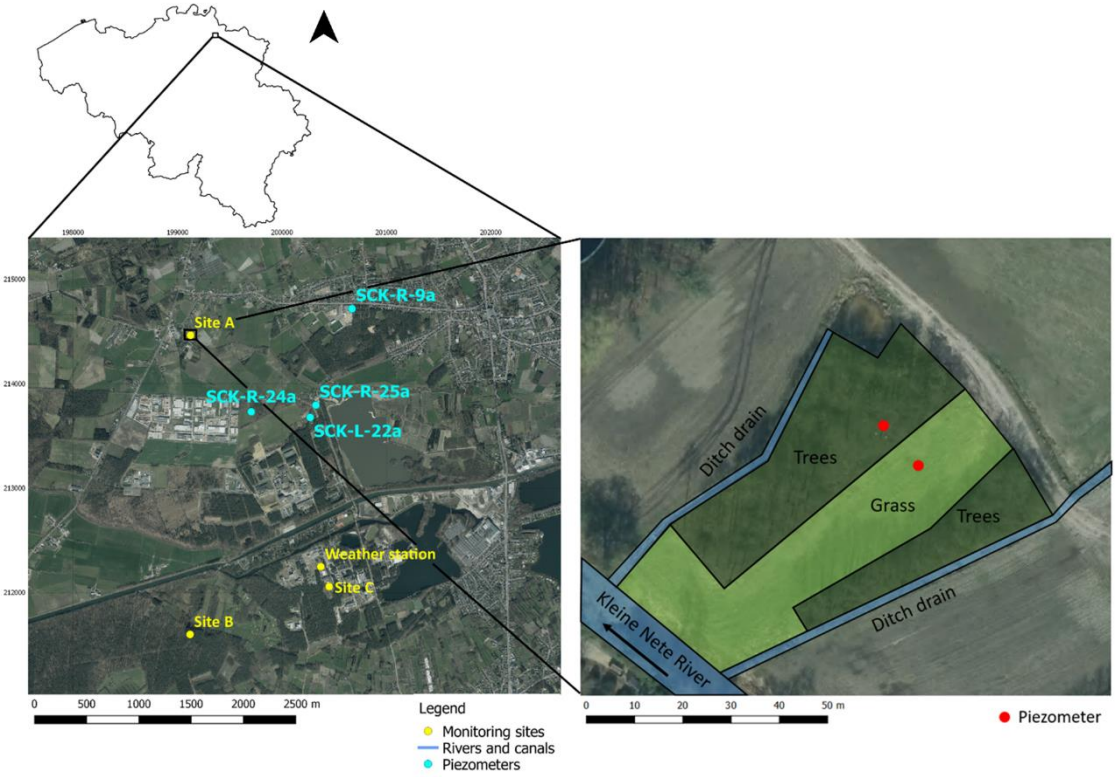

Figure 21: Map of the monitoring sites, the weather station and the four piezometers used to derive the numerical flow model upstream boundary condition (left) and detailed map of site A (right)

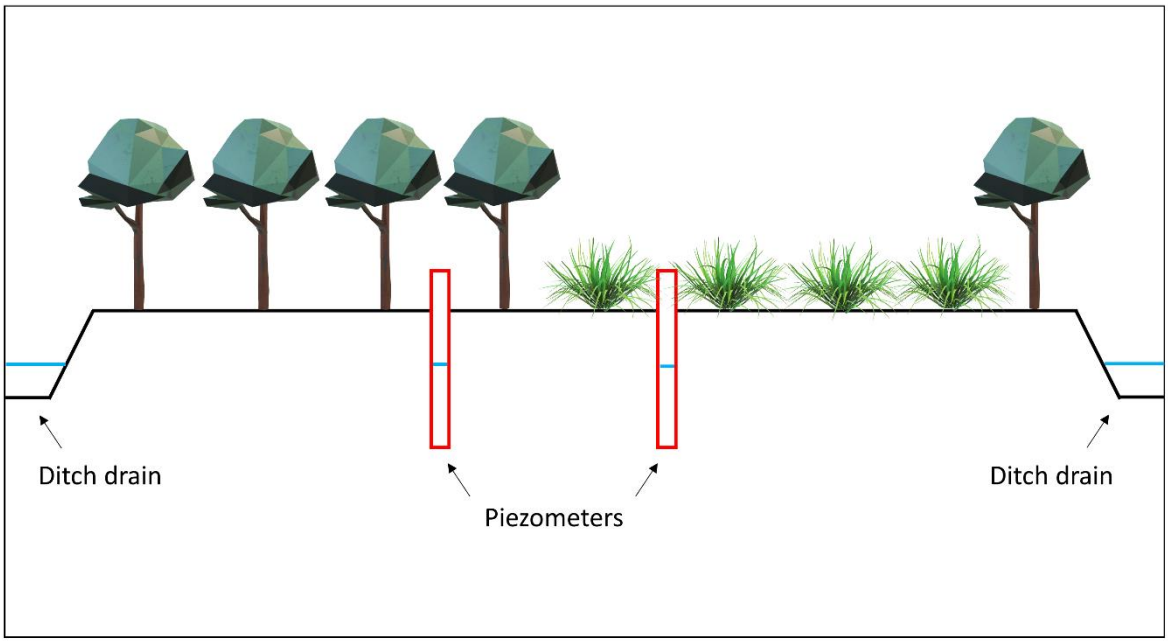

Figure 22: Schematic cross-sectional view of the monitoring design

The study focuses on the summer of 2016, from the 12th of June until the 24th of August.

The rainfall data used in the modeling and interpretation of the piezometric time series were measured every 15 min by the VMM (Flanders Environment Agency) in Herentals, approximately 20 km away from the study sites.

III.3.1.1. Site A

Site A is the core of this study. It consists of a plot of approximately 80 m by 50 m delimited by the Kleine Nete river and two agricultural ditch drains (Figure 21, right). The fourth border is open to lateral groundwater inflow. The plot is covered by two distinct vegetation covers: mixed deciduous trees dominated by black and grey alder (*Alnus glutinosa and Alnus incana*) and grassland. On the 7th of June 2016 a standpipe was installed in each of the vegetation cover areas, up to a depth of approximately 1.5 m. These standpipes were equipped with pressure sensors measuring groundwater level and temperature every 10 minutes. A filter was placed at their bottom where they are open to groundwater conditions.

The soil profile is similar under the tree and the grass vegetation, i.e. an approximately 50 cm thick sandy A horizon with a high organic matter content over a loamy subsoil. Because of the presence of the river and the ditch drains together with a rather flat topography, a high

groundwater table was expected. Moreover, tree roots were spotted below a depth of 1 m. This suggested a possible connection between tree roots and groundwater.

III.3.1.2. Site B

Site B is located in the Scots pine stand investigated by Vincke and Thiry (2008) and Schneider et al. (2013). In the study of Vincke and Thiry (2008), diurnal groundwater level fluctuations due to root water uptake were observed and the White method was used to estimate ET_{GW}. Site B was instrumented with a pressure sensor of the same type as used on site A and is used to evaluate if the expected groundwater diurnal fluctuations are measurable with these sensors. Additionally, the White method was applied to piezometric measurements at site B.

III.3.1.3. Data processing

All pressure data from the field sites and the laboratory tests were corrected by subtracting the atmospheric pressure measured at the weather station to obtain the water level.

III.3.1.3.1. Removal of fluctuations at scales larger than a day

In a second step, the water level data were processed to remove trends at time scales longer than a day by subtracting moving averages of the levels with a window width of one day. The resulting detrended values are the diurnal fluctuations of water level.

The diurnal fluctuations are shown and discussed in detail below for two periods, from the 17th until the 21st of July 2016 (referred as P1 period) and from the 15th until the 19th of August 2016 (referred as P2 period). These two periods were selected because they are the two longest periods without any precipitation event during the summer of 2016, but both having a distinct temperature regime. During P1, maximum daily temperatures reached 35 °C, while during P2 temperatures remained below 30 °C. P2 is representative of usual warm summer days in Belgium, but P1 appears to be a more extreme case, representative of the warmest days of the year.

III.3.2. Modeling of site A

The modeling framework of site A includes three steps. First, the reference potential evapotranspiration (*ET0*) was calculated using the FAO 56 Penman − Monteith equation (Allen et al. (1998); section III.3.2.1). Then, *ET0* and precipitation were distributed between

interception, potential evaporation of the intercepted water, throughfall, potential soil evaporation and potential transpiration for each vegetation cover (section III.3.2.2). Finally, the three-dimensional numerical model of site A was run using atmospheric boundary conditions calculated in the previous stages (section III.3.2.3).

The model simulation timeframe was split between two periods: (i) a warm-up period used to obtain realistic initial conditions for (ii) the focus period, for which model outputs were compared to field measurements. The warm-up period was set to one year, from the 1st of June 2015 until the 1st of June 2016, and used boundary conditions at a time resolution of one day. The focus period represents the summer 2016 from the 2nd of June until the 25th of August using boundary conditions with a time step of one hour.

III.3.2.1. Calculation of the reference evapotranspiration (*ET0*)

ET0 was calculated using the Ref-ET software (Allen, 2009). The input data for the focus period were the air temperature, solar radiation, and dew point temperature measurements, all recorded at the VMM weather station located in Herentals. Additionally, wind speed measurements from the weather station of Melsele, approximately 50 km away from the study sites, were used. For the warm-up period, relative humidity measurements were used rather than dew point temperatures because of inconsistencies in the measurements. Moreover, solar radiation measurements for June and July 2015 were taken from the weather station of Melsele. The 15-min time step measurements were aggregated to hourly (focus period) and daily (warm-up period) data.

III.3.2.2. Water balance canopy model

A water balance canopy model was used to separate *ET0* in potential transpiration and potential evaporation and to calculate the throughfall for each vegetation covers. The governing equations of the water balance canopy model have been described in Leterme et al. (2012) and are briefly explained hereafter.

The model requires precipitation, *ET0* and following vegetation parameters: the crop factor (*Kc*, [−]), the leaf area index (*LAI*, [−]), the interception capacity (ω_c, [L]) and the light extinction coefficient (*k*, [−]). The value of *k* was set to 0.5. The values of *Kc*, *LAI*, ω_c and *k* were derived from literature (Breuer et al., 2003; Granier et al., 1999; Jacques et al., 2011; Lawrence and

Slingo, 2004; Meyus et al., 2004) and adapted to daily time steps. The *Kc* for the tree plot was corrected to take into account the clothesline effect induced by the shape of the tree plot (Allen et al. 1998). The values of the vegetation parameters are shown in Figure 23.

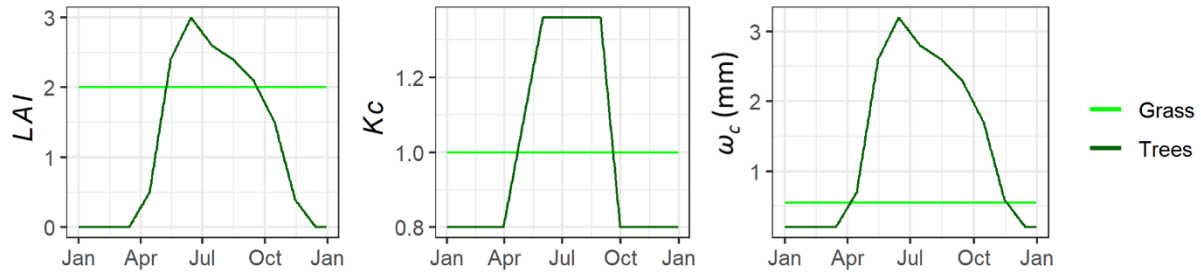

Figure 23: Annual variation of leaf area index (LAI), crop factor (Kc) and interception capacity (ωc) for the grass and tree covers (Breuer et al. 2003, Granier et al. 1999, Jacques et al. 2011, Lawrence and Slingo 2004, Meyus et al. 2004).

III.3.2.3. 3D variably saturated flow model

The 3D variably saturated flow model was setup using HYDRUS 2D/3D (Simunek et al., 2012). A modified version of the code was used, allowing for the representation of two vegetation covers. The geometry of the model is presented in Figure 24, showing the main features of site A. Two soil horizons were considered (topsoil until 50 cm depth and subsoil), as observed during the soil survey. The unsaturated soil hydraulic properties were described using the van Genuchten − Mualem model (Mualem, 1976; van Genuchten, 1980). The soil hydraulic parameters of these two horizons were obtained through pedotransfer functions using the Rosetta module (Schaap et al., 2001) based on soil texture information in the Belgian soil map (1/20000) and profile database (Van Orshoven et al., 1988). The saturated hydraulic conductivity estimate of the subsoil layer was adjusted to better describe the groundwater hydraulic head observations. The initial value of the subsoil saturated hydraulic conductivity was 0.01 m/h and the final value of all soil hydraulic parameters are presented in Table 3.

Table 3: Soil hydraulic parameters of the van Genuchten model estimated using the Rosetta code (Schaap et al., 2001)

	ϑr (−)	ϑs (−)	α_{VG} (m^{-1})	n_{VG} (−)	Ks (m/h)	l_{VG} (−)
Topsoil	0.041	0.39	4.2	2.1	0.073	0.5
Subsoil	0.078	0.43	3.6	1.6	0.083	0.5

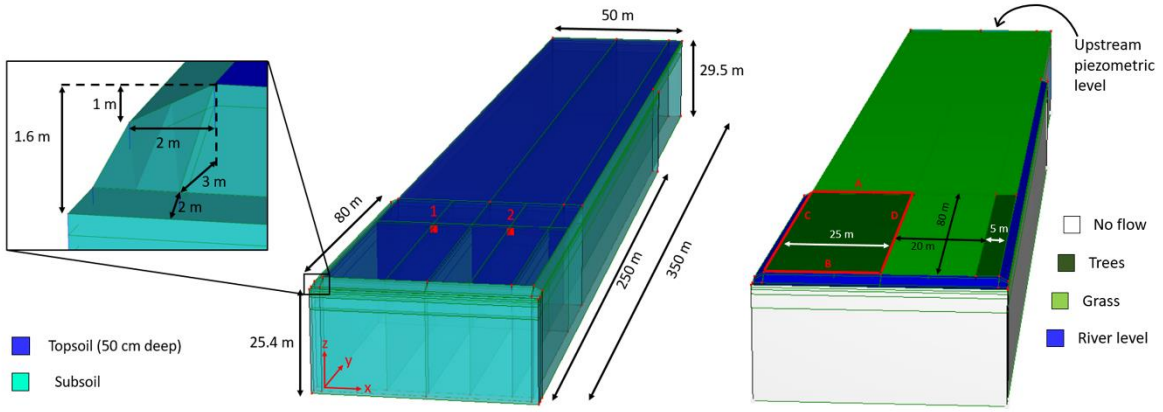

Figure 24: Geometry of the numerical flow model and observation nodes (left). Boundary conditions and vertical planes (A, B, C, D) through which lateral fluxes are investigated (right). The Kleine Nete river is at the front and the two drains are at the left (80 m-long ditch) and right (250 m-long ditch) sides.

Although the length of the field plot is around 80 m, the model was extended to a length of 350 m in order to reduce the influence of the northeast boundary conditions on the simulation results in the area of interest. The x, y and z directions refer to the river, the ditches and the vertical direction respectively. The origin of the 3D coordinate system was located at the bottom of the modeling domain (z = 0), the downstream ditch bank (x = 0) and the river bank (y = 0; see Figure 24). The elevation of the top surface was constant in the x direction but increased along the y direction, being 27 m at y equal to 0 m and 29.5 m at y equal to 350 m. This resulted in a slope of approximately 0.7 %, pending towards the river stretch. The elevation of the bottom surface was set to a constant value of 0. The river bottom had a uniform elevation of 25.4 m above the datum. The ditch drain bottoms were set to 26 m at x equal to −2 and 52 m and follow the same slope than the ground elevation along the y direction.

The boundary conditions of the model are illustrated in Figure 24. The ditch drains and the river used the same time series as variable head boundary condition. These time series were measured at a VMM monitoring station 200 m downstream and are shown, for both the warm-up and focus periods, in Figure 25, the reference level is the river bed. These values were specified all over the corresponding surface boundaries. The code is only applying pressure heads which are adjusted according to the z-coordinates of the surface elements. The upper boundary conditions were set to represent the two different vegetation covers using the outputs of the canopy water balance model described above. The root depths were set to 0.5 m for the grass and 2 m for the trees, while both root profiles were considered

constant with depth and time. The root uptake reduction function was specified according to the Feddes function (Feddes et al., 1978). Parameters used for each vegetation cover were taken from the HYDRUS database (Table 4, Simunek et al. (2012)). P0 and POpt for the trees were set to positive values to allow for groundwater uptake. Boundary conditions for the lateral sides and bottom surface were set to no flow.

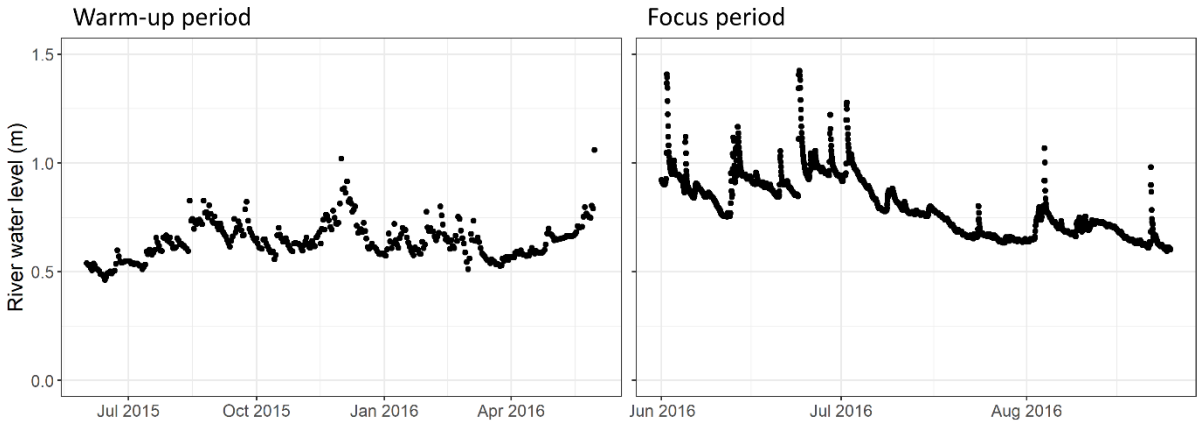

Figure 25: Time series of the river and drains variable head boundary condition for the warm-up (left) and focus period (right). The reference level is the river bed.

Table 4: Root water uptake pressure head reduction function parameters according to the Feddes model

	Trees	**Grass**
P0 (m)	3	−0.1
POpt (m)	2	−0.25
P2H (m)	−5	−3
P2L (m)	−8	−10
P3 (m)	−80	−80
r2H (m/d)	0.005	0.005
r2L (m/d)	0.001	0.001

The upstream piezometric level boundary condition was derived from monthly measurements of a regional piezometer network. Four piezometers located in the vicinity of site A were selected (Figure 21) and the distance from each piezometer to the river was measured. For every month, a polynomial function was used to describe the relationship between the

groundwater head above the river water level and the distance to the river. An example of this fit is presented in Figure 26 for June 2016. Finally, a spline interpolation in time was performed to obtain the time series of variable head boundary conditions at 350 m away from the river. The time series for the warm-up and focus periods are presented in Figure 27.

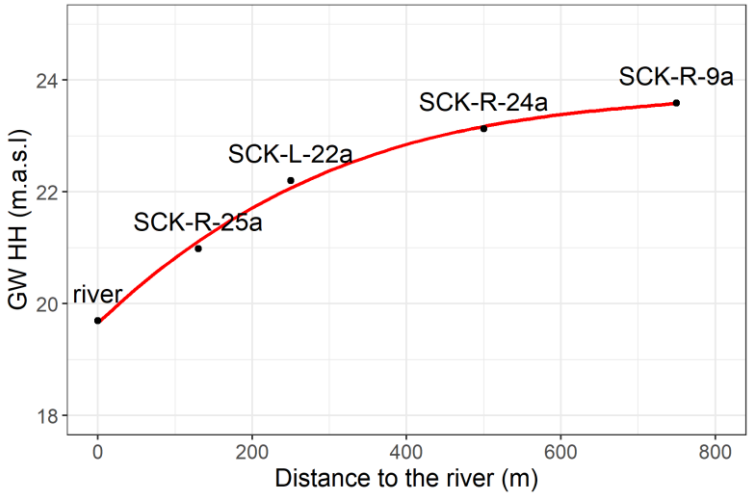

Figure 26: Example of a polynomial function describing for June 2016 the groundwater hydraulic head (GW HH) above the river water level as a function of the distance to it

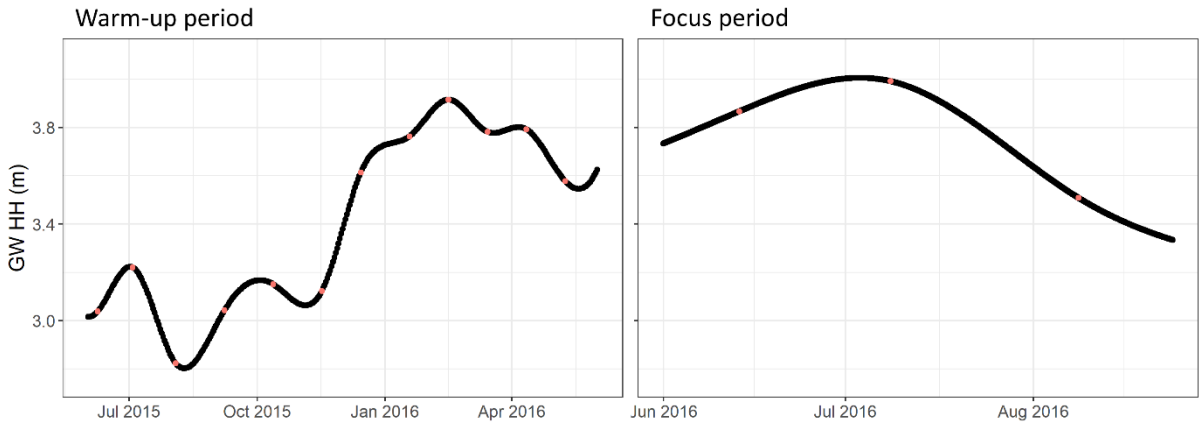

Figure 27: Upstream northeast boundary condition time series of the numerical flow model for the warm-up (left) and focus (right) periods. GW HH refers to the groundwater hydraulic head considering the river bed as datum.

III.3.2.4. Model output processing

III.3.2.4.1. Comparison with field data

Two observation nodes were used to compare the model outputs with the field measurements (Figure 24). Observation node number 1 (x = 15 m, y = 55 m, z = 25.792 m, depth = 1.6 m) was compared with the piezometer under the trees and observation node number 2 (x = 35 m, y = 55 m, z = 25.792 m, depth = 1.6 m) with the piezometer within the

grassland. The simulated groundwater levels were treated using the same procedure as the field data to extract the diurnal fluctuations (section III.3.1.3.1).

III.3.2.4.2. Fluxes through the lateral borders of the tree plot

The lateral fluxes through four planes (A, B, C, D; Figure 24) were calculated from the 12th until the 31st of July at an hourly time step. For each plane, the simulated Darcy velocity field was interpolated using a Voronoï diagram. Volumetric flows were computed as the product of each node velocity value by the associated polygon surface. These volumetric flows were then summed up to calculate the total volumetric flow through each plane. Finally, the obtained values were normalized by the whole plane area (unsaturated and saturated zone), in order to obtain the mean flux, for comparing between the different planes.

III.3.2.5. Alternative simulations with no root water uptake from the saturated zone

Three additional simulations were performed to verify that the simulated diurnal groundwater level fluctuations are due to root water uptake within the saturated zone. These simulations are referred to as Alt 01, Alt 02 and Alt 03. In the three alternative simulations, root water uptake was limited to the unsaturated zone by setting the Feddes parameters of the trees *P0* and *POpt* to negative values (*P0* = −0.1 m and *POpt* = −0.25 m). In the first alternative simulation (Alt 01), the root profile depth was set to 2 m as in the standard simulation presented in the previous sections while in the second (Alt 02) it was set to 1 m, which is above the water table during the considered period. The third alternative simulation (Alt 03) used a root water uptake compensation factor (Simunek and Hopmans 2009) set to 0.01 in order to simulate full compensation of water and oxygen stress. The root profile depth was set to 2 m. Therefore, the key difference between these simulations is that Alt 01 simulates a case in which anoxic stress occurs due to the large fraction of roots below the water table while Alt 02 and Alt 03 simulate cases where anoxic stress is limited by the root depth and root water uptake compensation respectively. The alternative simulation outputs were processed in the same way as for the standard simulation.

The alternative simulations were compared to the observations and the reference simulation regarding the amplitude of diurnal groundwater level fluctuations during P1 and P2 period. Moreover, the simulated volumetric flows from the tree plot to the river and ditch (Q_{SW}) were compared between the different simulations for the period from the 12th until the 31st of July.

III.3.3. Application and evaluation of the White method

III.3.3.1. Original method and further modifications

The White equation for estimating groundwater evapotranspiration is written as Loheide et al. (2005):

$$ET_{GW} = S_y\left(\frac{\Delta s}{t} + R\right)$$

Equation 28

where ET_{GW} is the rate of groundwater evapotranspiration averaged over a 24-hour period [$L.T^{-1}$], S_y is the specific yield (dimensionless), Δs is the daily change in groundwater level [L], R is the average net inflow (recovery) rate during periods of no evapotranspiration [$L.T^{-1}$] and t is the time period of one day expressed in the appropriate time units [T]. Figure 28 illustrates the determination of R and Δs using diurnal groundwater level fluctuation measurements. It is important to note that groundwater levels in Figure 28 are not detrended.

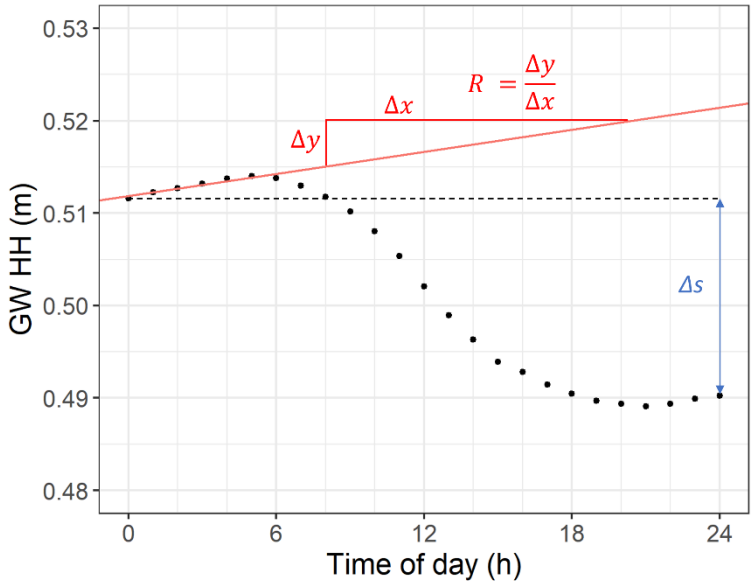

Figure 28: Example of a diurnal groundwater level (GW HH) fluctuations on which the White method is applied. GW HH data were measured on site B the 19th of July 2016. R is the average hourly rise of the water table during periods of no evapotranspiration [L/T] and Δs is the daily change in groundwater level [L].

White (1932) hypothesized that the source of the recovery is groundwater inflow from depth, while Davis and De Wiest (1966) imply that the recovery is caused by groundwater lateral inflow from outside the phreatophytes covered area. Loheide et al. (2005) showed that the White method could work for both flow systems.

As summarized by Loheide et al. (2005), the White method relies on four assumptions: (1) The diurnal water table fluctuations are caused solely by plant water use. (2) Groundwater uptake by the plants is negligible during periods of no evapotranspiration. (3) A constant rate of groundwater flow into the near-well region occurs over the entire day. (4) A representative value of the specific yield can be determined. Different time spans have been used for the period of no evapotranspiration, during which *R* is calculated. Originally, White (1932) set it to between midnight and 4 am, while Loheide (2008) used a slightly longer period from midnight to 6 am. Even longer periods were used, e.g. from 6 pm to 6 am (Rushton, 1996) or from 10 pm to 7 am (Miller et al., 2010). Fahle and Dietrich (2014) and Zhang et al. (2016) evaluated the effect of these different time spans on the output of the White method. They showed that in general, using longer time span is beneficial and averaging *R* calculation over two nights (the nights before and after the day of interest) improves the quality of ET_{GW} estimates. However, depending on the vegetation and meteorological settings, the length of the daily period with no evapotranspiration can differ. Therefore, the optimal time span to calculate *R* is likely to be site specific. Moreover, a more critical issue is the definition of the specific yield (S_y in Eq. 1). As mentioned in the introduction, Loheide et al. (2005) published specific yield values for different soil textures and specific use in the White method. These values, referred to as readily available specific yield, are used in the present study.

III.3.3.2. Evaluation on model outputs

The White method was evaluated on site A simulation outputs for the P1 and P2 periods. Specific yield was first set to 0.1 according to the estimation guidelines given by Loheide et al. (2005). It was then slightly adjusted on the simulation outputs to a very similar value of 0.115 in order to improve the fit on the simulated ET_{GW}. The recovery rate (R_W) was calculated over two nights from 10 pm to 6 am alike in the study by Miller et al. (2010) but stopping one hour earlier in the morning because evapotranspiration begins.

The simulated transpiration from the groundwater was calculated by multiplying the actual transpiration by the fraction of roots in the saturated zone. This approach could be used since no water stress was simulated during the considered time periods. The values thus obtained were considered as the reference for evaluating the White method.

III.3.3.3. Application to piezometric measurements

The White method was applied to the piezometric measurements of sites A and B for the P1 and P2 periods. For site A, the specific yield was 0.115 as in the evaluation on model outputs presented above, while it was set to 0.17 for site B according to the soil texture in site B and based on the guidelines of Loheide et al. (2005) and the study of Vincke and Thiry (2008). As the piezometric measurements show some delay in the increase of groundwater level observed during the night, *R* had to be calculated over a shorter time span than for the simulation outputs. It was thus calculated between 2 am and 6 am for site A and between midnight and 6 am for site B.

ET_{GW} values estimated using the White method were compared with the potential evapotranspiration (*ETp*). For site A, covered by deciduous trees, *ETp* was calculated within the modeling framework presented in section III.3.2, the corresponding *Kc* value for the P1 and P2 periods is 1.36. For site B, covered by pine trees, a *Kc* value of 1.16 was used (Meiresonne et al., 2003).

III.4. Results

III.4.1. Site A

III.4.1.1. Groundwater hydraulic head time series

Figure 29 shows the rainfall data, the simulated infiltration (corrected for interception by vegetation) and the simulated and observed hydraulic heads for the summer of 2016. The

datum is set to the riverbed level, which is 1.8 m below the ground surface at the piezometer location.

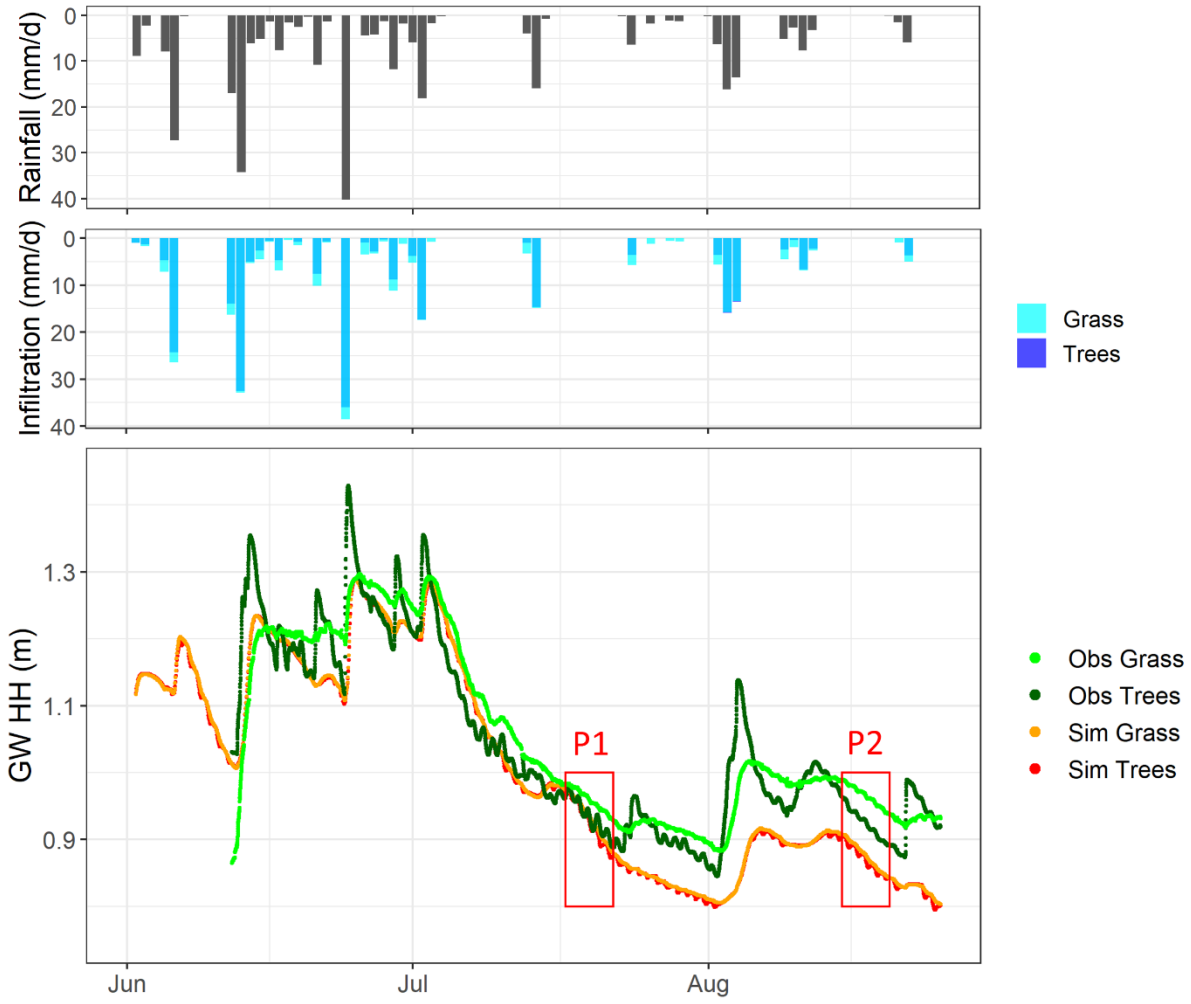

Figure 29: Rainfall measured at the Herentals weather station (first row), simulated infiltration (second row) and simulated (sim) and measured (obs) piezometric (GW HH) time series (third row) for the summer 2016 at site A

The simulated piezometric levels are close to the measurements until the end of P1 period, even though no model calibration was performed except a slight adaptation of the subsoil saturated hydraulic conductivity. However after P1 period, they remain 5 to 10 cm lower. Although the two piezometers are separated by only 10 m and located at a similar distance to the river and ditches, they show different behaviors. The piezometer in the tree plot reacts stronger and faster to rainfall events than the piezometer in the grass plot. Moreover, during dry periods, the decrease is faster in the tree plot than in the grass plot. On the other hand, the simulated piezometric time series show almost no difference between the grass and the tree plot. Another difference between the two measured piezometric time series is that

diurnal groundwater fluctuations can be spotted clearly under the trees while at this scale they are barely visible under the grass. The same can be noticed in the simulation outputs.

III.4.1.1.1. Zoom on P1 and P2

Figure 30 presents the simulated and measured groundwater levels, extracted diurnal fluctuations, simulated potential and actual transpiration and measured groundwater temperature diurnal fluctuations for the P1 and P2 periods.

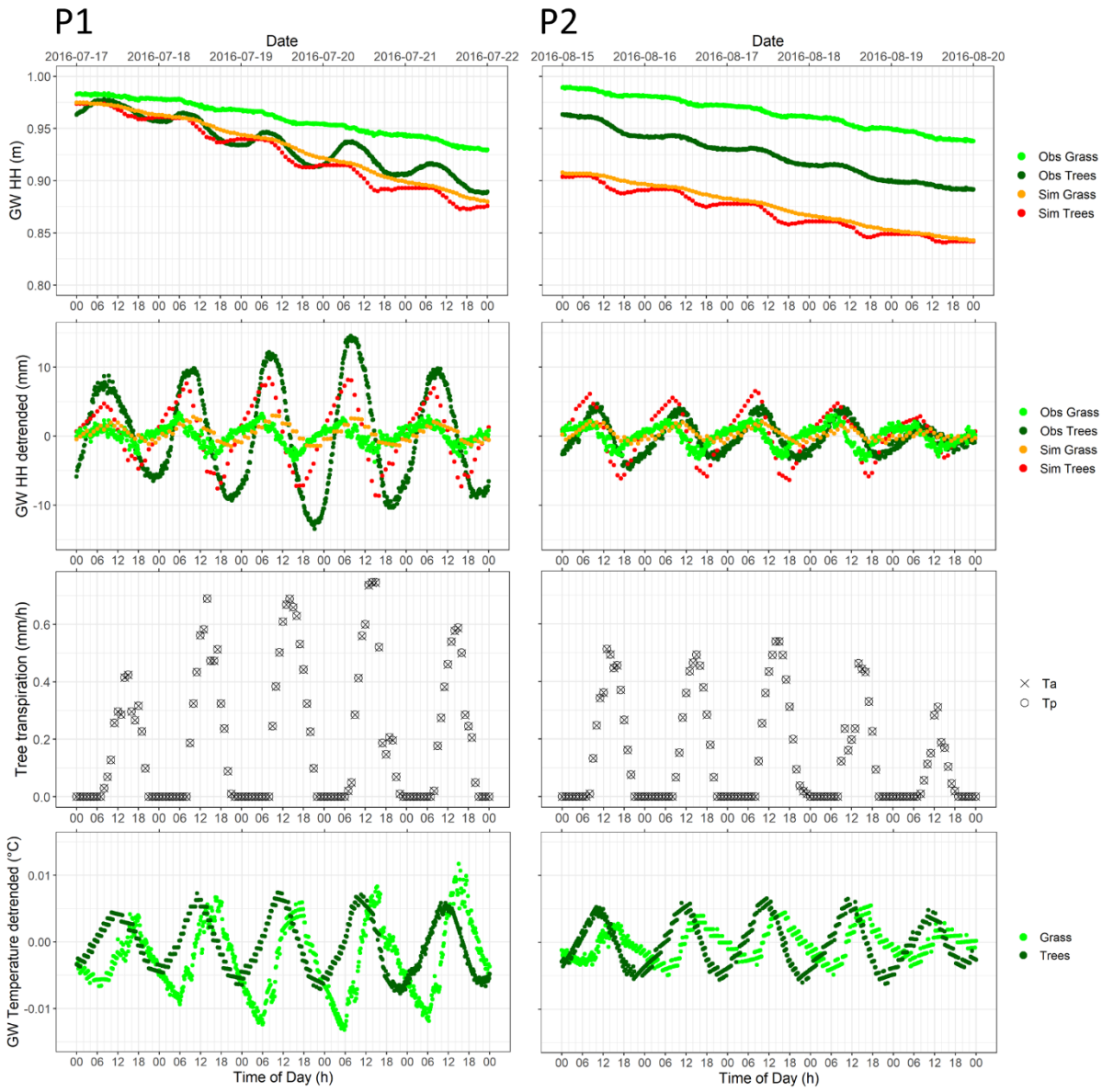

Figure 30: Groundwater level (GW HH) simulated and measured (first row), detrended fluctuations (second row), potential (Tp) and actual (Ta) transpiration (third row) and groundwater temperature detrended fluctuations (fourth row) for the P1 (left) and P2 (right) periods at site A

Under the trees, peak-to-peak (p-p) amplitudes of the measured diurnal groundwater level fluctuations are in the range of 15 to 25 mm for the P1 period. For the same period, the simulated diurnal groundwater level fluctuations are in the range of 10 to 15 mm which underestimate the observations by 30 to 40 %. During P2, observed p-p amplitudes are smaller than during P1; in the range of 5 to 10 mm. The simulated groundwater level also shows smaller p-p amplitudes than during P1, although slightly higher than the observations. Under the grass, the measured and simulated diurnal groundwater level fluctuations have a p-p amplitude of approximately 5 mm for the two selected periods.

The simulated potential and actual trees transpiration fluxes are almost identical, showing the absence of water stress for this vegetation cover. The simulated tree transpiration is in the range of 3 to 6 mm/d for the P1 period. The maximum daily values are from 0.4 to 0.7 mm/h. For the P2 period, tree transpiration is lower, varying between 1.5 and 4.5 mm/d. The maximum daily values are between 0.3 and 0.5 mm/h.

Regarding the timing of the fluctuations, measured groundwater levels reach a maximum at around 8 am under the trees and 6 am under the grass for both periods. The minimum is reached at around 10 pm under the trees and 4 pm under the grass. However, the simulated groundwater levels show a different timing. The simulated diurnal fluctuations occur simultaneously for the grass and tree vegetation. The simulated groundwater levels show a daily maximum around 8 am, when the potential transpiration starts. This is similar to the pattern observed under the trees, but slightly later than is the maximum observed under the grass (6 am). The minimum of the simulated daily diurnal fluctuations is reached around 4 pm in the tree plot and around 6-8 pm in the grass plot. For the trees, this corresponds roughly to the maximum of the actual (and potential) transpiration but happens earlier than in the observations. For the grass, the simulated minimum occurs later than in the observations.

Concerning groundwater temperature fluctuations, p-p amplitudes are around 0.02 °C under the trees and 0.015 °C under the grass during P1 and around 0.01 °C under the trees and the grass during P2. Note that these values are below the temperature sensor accuracy, which is 0.05°C, but higher than the sensor resolution, which is 0.003 °C. The timing of the diurnal temperature fluctuations under the grass is in line with the atmospheric temperature fluctuations, increasing from 6 am to 4 pm and then decreasing. Under the trees, however, a

time shift can be observed, the timing corresponds roughly to the groundwater level diurnal fluctuations.

III.4.1.2. Fluxes through the lateral borders of the tree plot

This section presents the groundwater fluxes through the four planes bordering the tree plot for the period from the 12th until the 31st of July 2016. Fluxes are considered positive when entering the plot and negative when leaving it.

III.4.1.2.1. Volumetric flow through every plane

Figure 31 shows all the simulated volumetric flows to/from the tree plot including lateral fluxes, evapotranspiration and infiltration.

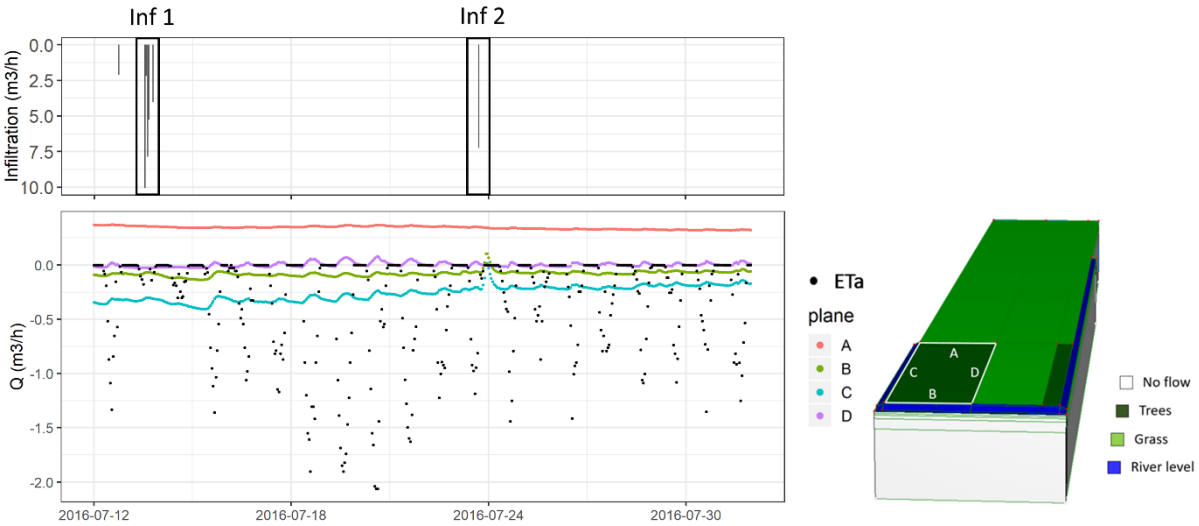

Figure 31: Simulated volumetric flows (Q) to/from the Site A tree plot. Positive flows are entering the plot, negative flows are leaving. Infiltration episodes 1 (Inf 1) and 2 (Inf 2) summed up to approximately 16 and 3.5 mm of infiltration over one day, respectively.

Regarding the lateral volumetric flows, groundwater is entering the plot mainly through plane A (upstream). However, it can be noted that several times groundwater is also incoming through plane D (i.e. from the grass plot) – though in small volumes. Groundwater is leaving the tree plot through plane B (to the river) and C (to the ditch drain). The volumetric flows towards the ditch are more than twice those towards the river. Note that the ditch reach is also much longer (80 m) than the river reach (25 m) and that this is accounted for in the mean lateral fluxes presented hereafter. Volumetric flows through all planes show diurnal fluctuations. However, infiltration episodes disrupt the diurnal fluctuations. Following the first

infiltration episode (Inf 1), almost no diurnal fluctuation occurs over the next two days and the fluxes absolute values towards the river (plane B) and the drain (D) increase almost steadily. Following the second infiltration episode (Inf 2), no diurnal fluctuations of fluxes occur over the next day. The absolute values of the fluxes towards the river and the drain decrease. The simulation shows also a flux from the river to the tree plot during a short time period after the second infiltration episode because of a fast rise in the river level following the rainfall event. Such an increase in river level was not observed after the first infiltration episode (river level data not shown).

The following sub-section discusses the mean flux time series through each plane for the P1 period. This normalization allows for a better comparison of the fluxes between planes with different dimensions and their diurnal dynamics.

III.4.1.2.2. Mean lateral fluxes for the P1 periods

Figure 32 presents the mean lateral fluxes to/from the tree plot for the P1 period. These fluxes correspond to the volumetric flow normalized by the cross-sectional area.

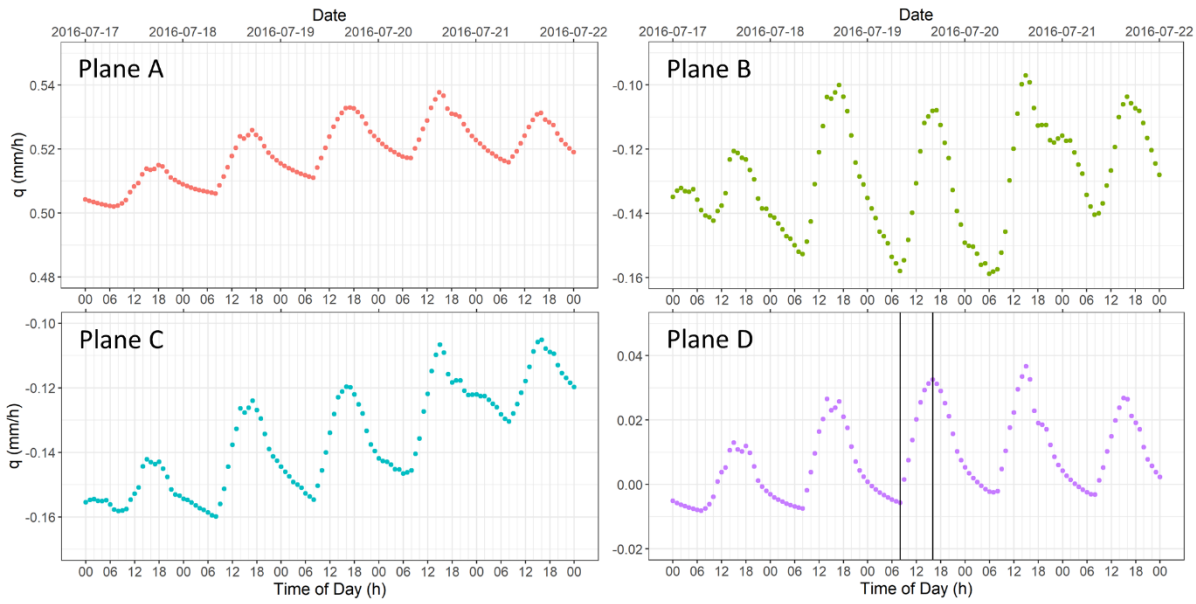

Figure 32: Mean lateral fluxes (q) to/from the Site A tree plot for the P1 period. Positive fluxes are entering the plot, negative fluxes are leaving. The vertical lines represent the two times for which fluxes distributions through plane D are shown in Figure 33.

The mean flux absolute values are the highest through plane A (> 0.5 mm/h). Mean flux absolute values through plane B and C are in a similar range (between 0.1 and 0.16 mm/h). Regarding mean fluxes through plane D, their absolute values are much lower than for the

other planes, they remain close to 0 during the night and increase to a maximum of around 0.04 mm/h during the day. To investigate further the fluxes dynamics through this plane, the cross-sectional fluxes distributions at 6 am and 4 pm for the 19th of July are shown in Figure 33.

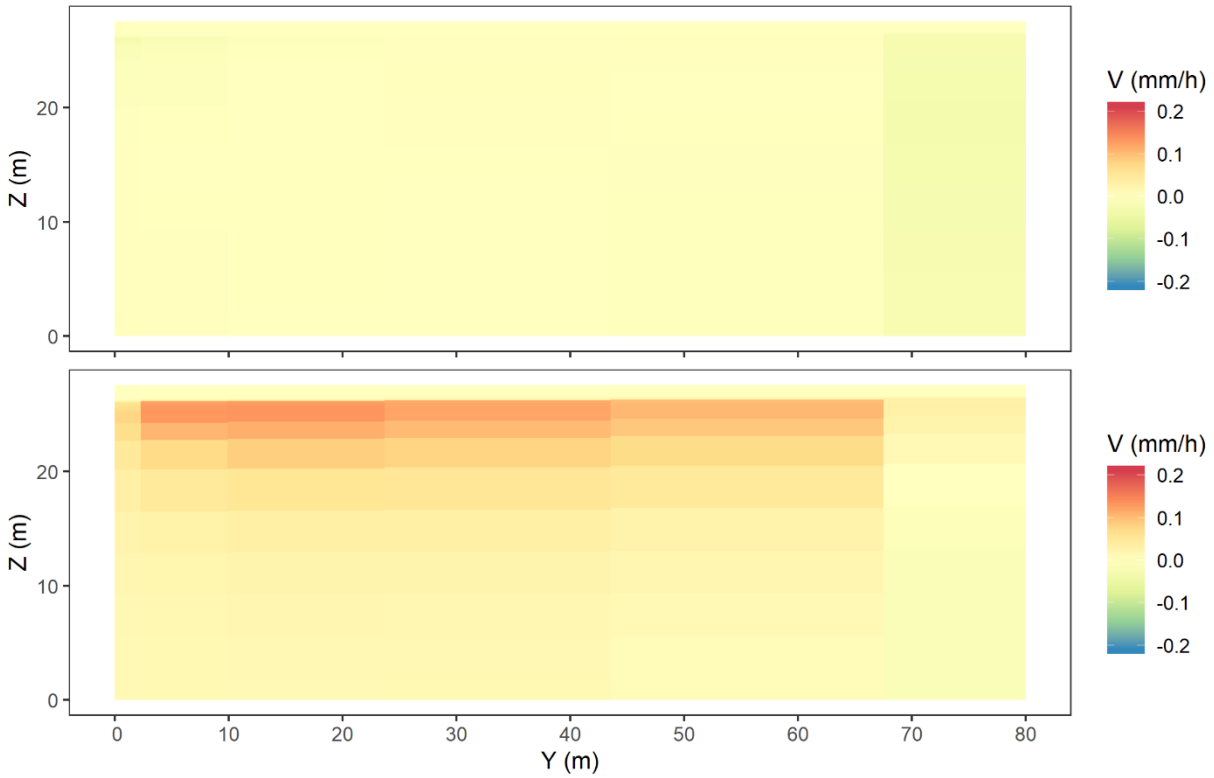

Figure 33: Simulated fluxes cross-sectional distributions through plane D for the 19th of July 2016 at 6 am (top row) and 4 pm (bottom row)

A general diurnal pattern can be seen in these simulation outputs, the fluxes entering the tree plot (planes A and D) reach a maximum around 4 pm, when the daily transpiration is the highest. They reach a minimum around 8 am, when the daily transpiration starts. The difference between the maximum and minimum is around 0.02 mm/d and 0.035 mm/d, for planes A and D respectively. It can be clearly seen on Figure 33 that during the day trees transpiration activates fluxes from the grass to the tree plot mainly in the shallow groundwater. These lateral fluxes only occur in the saturated zone.

The fluxes leaving the tree plot (planes B and C) show an opposite pattern. They reach a maximum around 8 am and a minimum around 4 pm. The difference between the maximum and minimum is around 0.05 mm/d and 0.03 mm/d, for planes B and C respectively.

These results demonstrate that tree root water uptake from the groundwater induce significant diurnal fluctuations of the fluxes to and from the phreatophytes area.

III.4.1.3. Alternative simulations with no root water uptake from the saturated zone

Observed and simulated groundwater levels and diurnal fluctuations under both vegetation covers for the cases without root water uptake from the saturated zone are presented in Figure 34, together with the simulated potential and actual transpiration.

In the first alternative simulation (Alt 01), only very limited groundwater level diurnal fluctuations under both tree and grass plot are present. Although the second (Alt 02) and third (Alt 03) alternative conceptualizations simulate a bit more diurnal fluctuations than Alt 01, they still strongly underestimate the observed p-p amplitudes under the trees – by a factor 3 and 2 for the P1 and P2 periods respectively. They remain two times smaller than the p-p amplitudes of the reference case (considering tree root water uptake from the saturated zone). Similar results are obtained under the grass. The groundwater level fluctuations simulated by the alternative simulations are probably due to capillary movements caused by root water uptake in the unsaturated zone. These results demonstrate that the relatively large diurnal fluctuations of the reference simulation under the tree plot are due to root water uptake within the saturated zone and that fluctuations under the grass plot partly result from the diurnal water table fluctuations of the tree plot.

The smaller groundwater level diurnal fluctuations in Alt 01 and Alt 02 can be explained by a reduction of the actual transpiration due to root water uptake stress. In Alt 01 (root depth = 2m as in the reference simulation), important anoxic stress is caused by the large fraction of the roots located below the groundwater table. In Alt 02 (root depth = 1 m), the root depth is limited to remain above the groundwater table. However, this leads to a larger amount of water extracted from the unsaturated zone which causes water stress in the topsoil. For the same reason, water stress is also simulated under the grass (root depth = 0.5 m) for all the reference and alternative simulations. On the other hand, in Alt 03 (root depth = 2 m), the actual transpiration reaches its maximum potential value as in the reference simulation because of root water uptake compensation balancing water stress under the water table and in the dry topsoil. The smaller groundwater level diurnal fluctuations compared to the reference simulation are therefore not due to actual transpiration reduction but rather to a

different allocation of root water uptake. As a consequence, the unsaturated soil moisture is globally lower than in the reference simulation but the groundwater table higher. This induces larger volumetric flows to the river and ditch simulated in the alternative simulations (Table 5). During the period from 12th until the 31st of July, the differences between the cumulative volumetric flow to surface water are 38 m^3 (= Alt 01 – Ref), 17 m^3 (= Alt 02 – Ref) and 47 m^3 (= Alt 03 – Ref) (Table 5). This corresponds to relative differences of 23, 10 and 29 %, respectively.

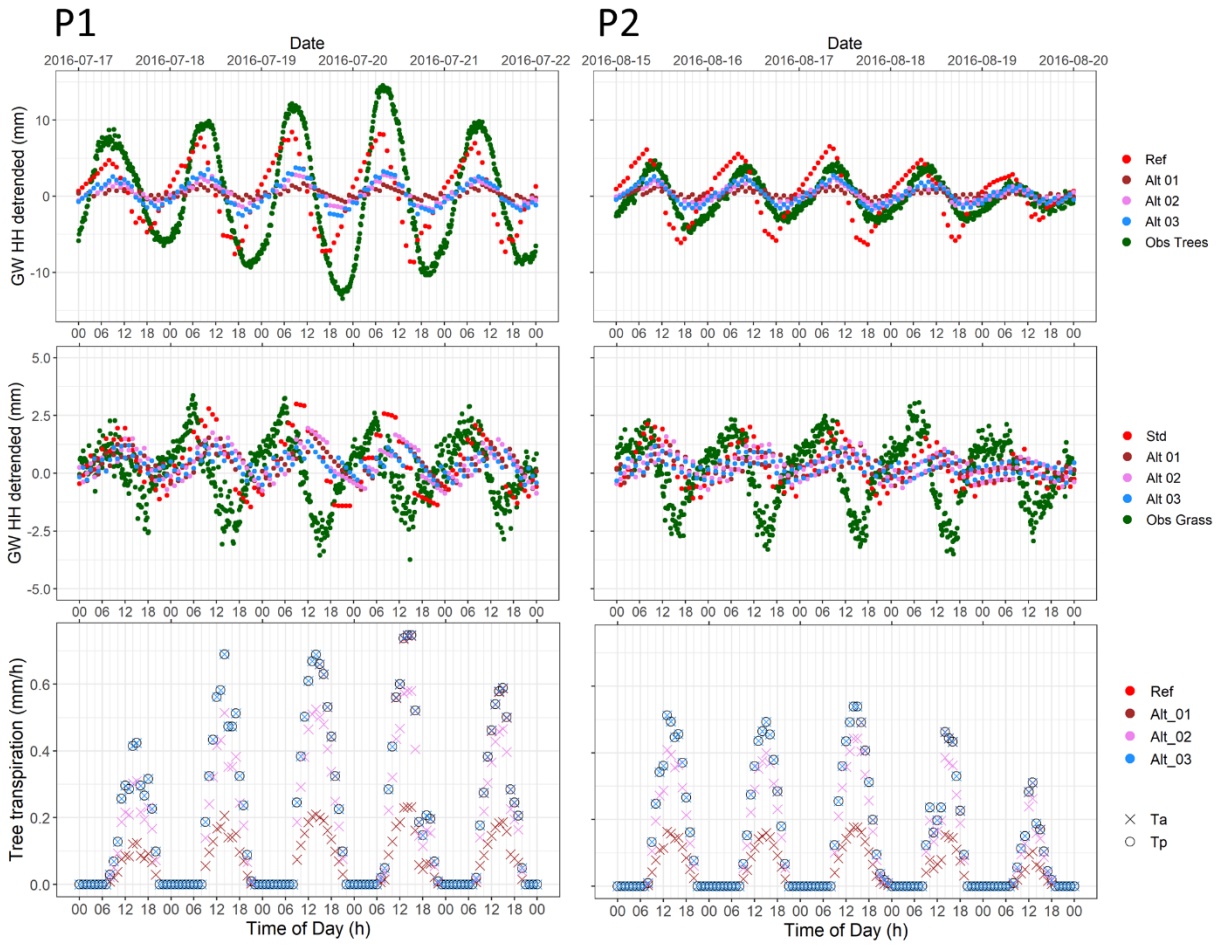

Figure 34: Groundwater level (GW HH) diurnal fluctuations simulated and measured in the tree plot (top row), in the grass plot (middle row) and potential (Tp) and actual (Ta) transpiration (bottom row) for the P1 and P2 periods at site A considering the 3 alternative conceptualizations (Alt 01, Alt 02 and Alt 03) in which tree root water uptake can not occur in the saturated zone. The results of the reference simulation (Ref, presented in the previous sections) are shown for comparison purposes.

*Table 5: Cumulative volumetric flow from the tree plot subsurface to surface water (Sum Q_{SW}) and to atmosphere through vegetation (*Sum Q_{Ta}*) simulated by the reference (Ref) and alternatives (Alt 01, Alt 02, Alt 03) simulations for the period from 12th until the 31st of July*

Simulation	Sum Q_{Ta} (m^3)	Sum Q_{SW} (m^3)	Difference to Ref (m^3)	Relative difference to Ref (%)
Ref	390	161	0	0
Alt 01	123	199	38	23
Alt 02	307	178	17	10
Alt 03	391	209	47	29

III.4.1.4. Evaluation and application of the White method

Figure 35 presents the calculated daily evapotranspiration from groundwater (ET_{GW}) using the White method on the simulated and observed groundwater levels, for the two selected periods P1 and P2. It also shows the ET_{GW} derived from the flow model output, together with the tree potential evapotranspiration (*ETp*).

Firstly, it can be seen that ET_{GW} values calculated by the White method applied to the simulated groundwater level are very similar to those calculated by the flow model. The two datasets actually overlap for the P1 period. Assuming that the numerical model accounts for all relevant processes, this suggests that the White method applied to the observed piezometric head would give reliable estimates of ET_{GW} for this site. Thus, they can be compared to the daily transpiration values simulated by our flow model.

ET_{GW} values estimated by applying the White method to the observed groundwater levels (ET_{GW} White obs in Figure 35) are approximately twice the estimates from the flow model (ET_{GW} White sim) during P1 period, equivalent to a difference of around 2 mm/d. This means that the White method estimates that a larger proportion (between 60 and 75 %) of the total evapotranspiration comes from groundwater than what is simulated in the flow model (between 30 and 35 %). For the P2 period, ET_{GW} values estimated by the flow model and the White method applied to the observations are closer as the simulated diurnal groundwater level fluctuations amplitudes are similar to the observed ones.

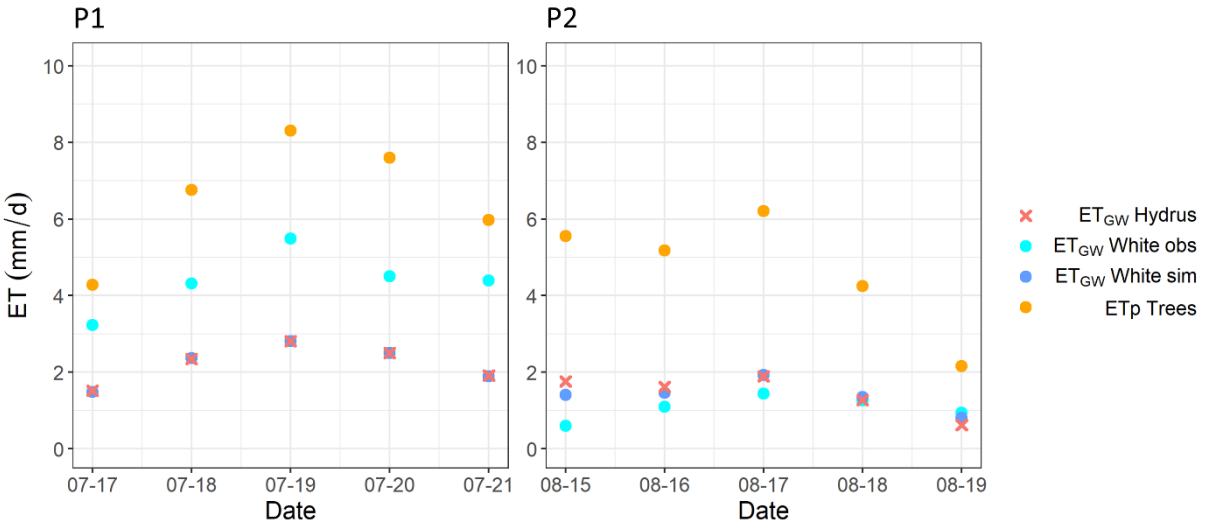

Figure 35: Daily evapotranspiration fluxes from groundwater (ET_{GW}*) on site A for the P1 and P2 periods. Fluxes are (i) calculated using the White method applied to simulated (White sim) and observed (White obs) water levels, or (ii) extracted from the flow model (Hydrus). Daily potential tree evapotranspiration is plotted as well (*ETp *trees).*

III.4.2. Site B

III.4.2.1. Groundwater hydraulic head time series

Figure 36 shows the rainfall data and piezometric measurements for the summer of 2016. The datum is set to the sensor level at 1.64 m below the soil surface. Groundwater level diurnal fluctuations are observed during the dry periods.

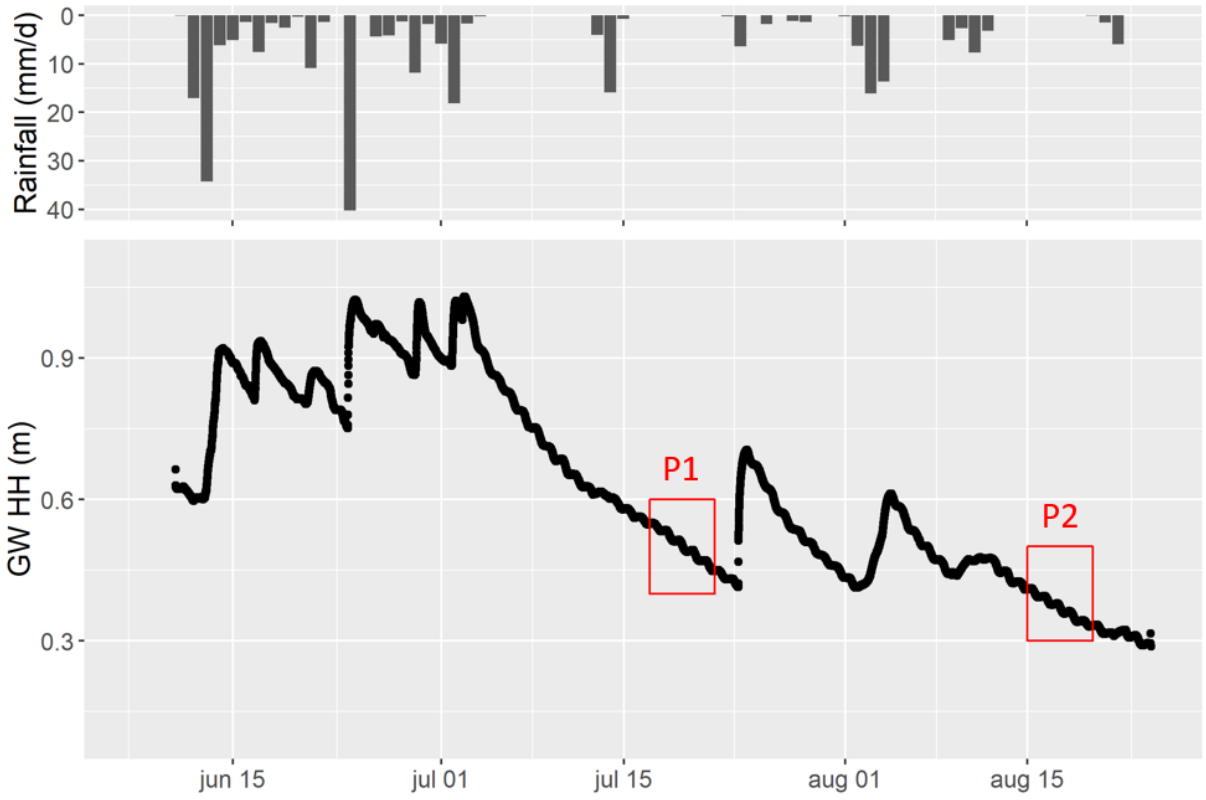

Figure 36: Groundwater level (GW HH) time series for the summer 2016 measured on site B and rainfall measured at the Herentals weather station

III.4.2.1.1. Zoom on P1 and P2

Figure 37 shows the measured groundwater levels and detrended diurnal fluctuations for the P1 and P2 periods.

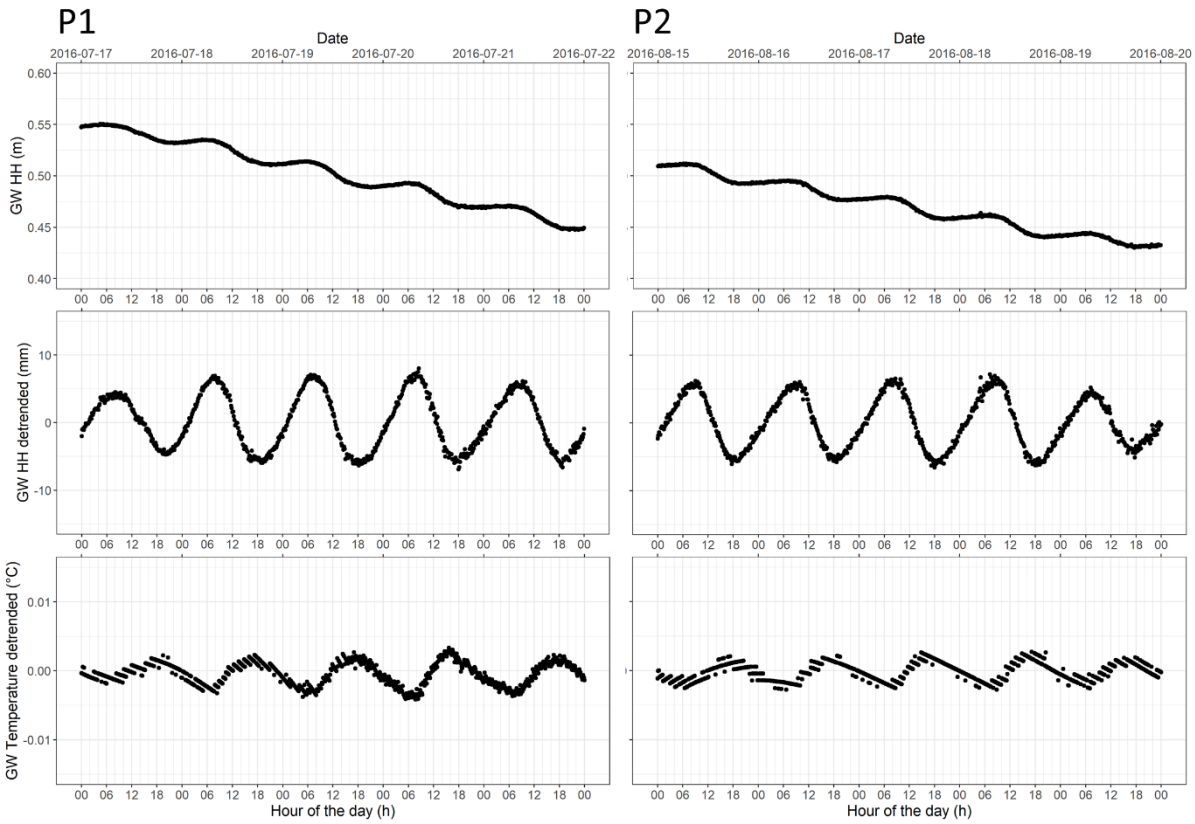

Figure 37: Groundwater level (GW HH) measured (first row) and extracted diurnal fluctuations of the groundwater level (second row) and temperature (third row) for the P1 (left) and P2 (right) periods at site B

The p-p amplitude and timing of groundwater level and temperature fluctuations are similar for both periods. The p-p amplitude of the groundwater level diurnal fluctuations is around 10 mm. Regarding their timing, the groundwater levels reach a maximum around 8 am and a minimum around 6 pm. The p-p amplitude of the groundwater temperature diurnal fluctuations is around 0.005 °C, which is one order of magnitude below the sensor accuracy (0.05 °C) but still slightly higher than the resolution (0.003 °C).

In comparison to site A, the drop in groundwater level over the same time periods is larger at site B and the p-p amplitudes of the groundwater level diurnal fluctuations are higher, especially during P2.

III.4.2.2. Application of the White method to piezometric measurements

The daily ET_{GW} values for the P1 and P2 periods, estimated using the White method on the piezometric measurements of site B, are shown in Figure 38 together with the potential transpiration for trees.

The daily ET_{GW} values estimated using the White method are very close to the potential evapotranspiration daily value. According to this method, the proportion of evapotranspiration coming from groundwater is always above 70 %. Although ET_{GW} values larger than potential evapotranspiration are impossible and probably due to uncertainties in the calculation methods, these results suggest that for some days potential evapotranspiration is satisfied completely, or almost completely, by transpiration from the groundwater. This is in line with the results published by Vincke and Thiry (2008), who showed that groundwater contributed to 98.5% of the water uptake during a drought period in June 2005, at the same location.

In comparison with site A this would indicate a stronger coupling between transpiration processes and groundwater on site B for the periods considered.

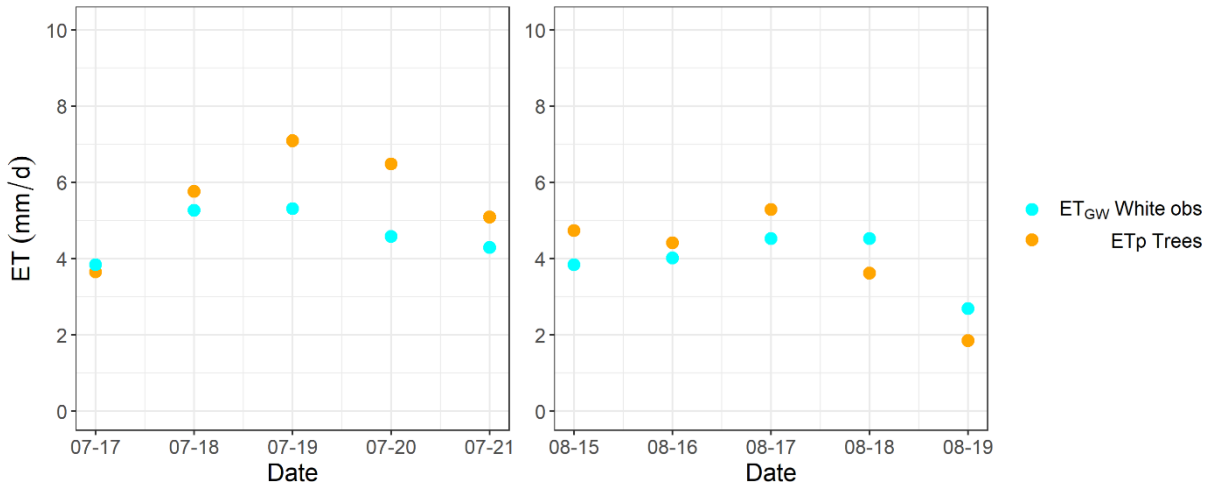

Figure 38: Daily evapotranspiration from groundwater (ET_{GW}) calculated by the White method applied to the observed (obs) groundwater level and daily potential trees evapotranspiration (ET_p) for the P1 and P2 periods on site B

III.5. Discussion

III.5.1. Sensor reliability to measure groundwater level diurnal fluctuations

A detailed discussion on the sensors reliability to measure groundwater level diurnal fluctuations is presented in the supplementary material (Appendix B). The main conclusion is that even though the water pressure sensors show a bias linked to the temperature correction, this bias is significant only for temperature fluctuations larger than 0.5 °C. Therefore, our measurements, which show maximal temperature fluctuations around 0.01 °C

are not significantly affected by this temperature-induced bias. However, there remain an important concern when atmospheric pressure is measured using this kind of sensors or water temperature diurnal fluctuations are close to 0.5 °C.

III.5.2. Comparison of simulated against observed piezometric level on site A

III.5.2.1. Absolute values

The piezometer in the tree plot appears to react much more to rainfall events than the piezometer in the grass plot. This could be due to preferential infiltration in the tree plot. Preferential infiltration can be due to natural processes (e.g. stemflow and infiltration along the root system, Cape et al. (1991); Lange et al. (2009); Spencer and van Meerveld (2016)) or due to infiltration along the piezometer. Preferential infiltration is not observed for the piezometer located in the grass plot but is observed at site B, covered by trees but with a deeper groundwater table. This suggests that preferential infiltration occurs as a result of natural processes such as tree roots enhancing fast infiltration. Another possible process that could explain these results is the spatial variation of specific yield. At locations with a lower specific yield, groundwater level fluctuations would be more important. Preferential infiltration and spatial variation of specific yield are not represented in our model which, therefore, simulates similar infiltration patterns under the trees and the grass after a rainfall event. To take the process of preferential infiltration into account one possibility is for example to consider different soil hydraulic properties for the soils in the tree plot and the grass plot or to represent the hydraulic properties with a dual porosity model (Durner, 1994; Durner et al., 1999). Trying to improve the fit of simulated vs. observed water content in the soil profiles under the trees and under the grass was beyond the scope of this study but could be addressed by implementing the approaches described above.

The simulated piezometric heads are also significantly smaller than the observations after the P1 period. This seems to be due to the infiltration event happening immediately after the end of P1. This rainfall event is probably underestimated in our model boundary conditions, which are derived from meteorological measurements recorded 20 km away from the study site. However, rainfall intensity can be highly variable locally, especially in summer.

III.5.2.2. Diurnal fluctuations

III.5.2.2.1. Amplitudes

In the tree plot, the model simulates correctly the diurnal groundwater level fluctuation amplitudes for the P2 period but underestimates them for the P1 period by 30 to 40 %. This is shown with the White method to correspond to an underestimation by a factor 2 of the transpiration from groundwater for the P1 period. These two periods differ in the prevailing meteorological conditions. While P2 is a usual summer period in Belgium with maximum daily temperature remaining below 30 °C, P1 is a more extreme period with maximum daily temperature reaching 35 °C. The amplitude underestimation during the unusually warm P1 period could be due to an underestimation of potential transpiration. Another explanation could be that, as the upper unsaturated soil becomes drier, root water uptake compensation occurs and root water uptake in the deeper saturated soil increases. Root water uptake compensation is independent of water stress and may occur even under relatively wet conditions, as soon as soil water head distribution is not uniform, due to hydraulic gradient at the soil–root interfaces of a plant (Javaux et al., 2013). This is not represented in our model in which root water compensation is assumed to be due to water stress in part of the root profile. Finally, groundwater level diurnal fluctuations will also depend on how much water is actually taken from the groundwater, which is defined by the fraction of the root zone below the groundwater table in our model. In the current study, root density was assumed to be constant with depth, however, a variable description of root density as a function of depth could improve the representation of the observed groundwater level diurnal fluctuation amplitudes. Under the grass, the model correctly simulates the diurnal groundwater fluctuations driven by root water uptake from the adjacent tree plot.

III.5.2.2.2. Timing

In the tree plot, there is a time shift between the simulated and observed diurnal groundwater level fluctuations which can be seen especially at the end of the daily transpiration period. This could be explained by a capacity effect of the trees. These processes have been extensively described in plant physiology studies (Čermák et al., 2007; Phillips et al., 2003; Richards and Caldwell, 1987) but are often not implemented in hydrological models. Two different types of capacity effects, which are not represented in the model, can explain this time shift. The first is the capacity within the trees. In the morning, trees first loose the water

stored in their tissues and only later the roots start taking up (ground)water. In the evening, the water uptake lasts longer than the transpiration because the trees need to restore their inner water storage. The second effect is hydraulic lift. When the hydraulic head is higher in the aquifer than in the upper soil layers, water moves during the night upwards through the plant root system from the aquifer to the drier soil layers. This water is first taken up in the next morning. With hydraulic lift, the water is stored in the unsaturated soil rather than in the trees. Our model applies directly the transpiration (calculated for the canopy level) to the root level, thus neglecting plant hydraulic and capacity effects.

Therefore, a more advanced representation of the vegetation compartments would probably improve the simulation of root water uptake from groundwater. There are alternative root water uptake models to the Feddes model, in which root water uptake is proportional to the hydraulic conductivity so that more water is taken from more saturated regions (Bresler, 1987; Nimah and Hanks, 1973a, 1973b). More recently, Gou et al. (2018) modified the root uptake functionality of Parflow.CLM, integrating several functions to represent plant hydraulic properties and redistribution. Moreover, a version of HYDRUS-1D representing root hydrology was recently used by Cai et al. (2018) and Cai et al. (2018b) to simulate water uptake by winter wheat in different soils and under different water stress conditions. A similar improvement would be beneficial to HYDRUS 2D/3D.

III.5.3. Relative importance of phreatophytes transpiration on groundwater fluxes

The analysis of the simulated fluxes shows that tree transpiration impacts significantly the fluxes to and from the tree plot. For our particular case study, trees transpiration leads to diurnal variations in groundwater fluxes towards the ditch and river of more than 20 %. Moreover, during the period from the 12th until the 31st of July the simulation considering root water uptake from groundwater simulates a water flow to the river and ditch that is significantly lower (from 10 to 29 %) than simulated by the alternative conceptualizations (Alt 01, 02 and 03) which consider root water uptake only from the unsaturated zone. This highlights the importance of simulating this process in larger scale models. The relative importance of this flow pattern over other hydrologic fluxes depends on the time scale considered as root water uptake is mainly occurring during summer. A relevant example would be that not considering root water uptake from the saturated zone in a riparian zone

could lead to a significant overestimation, in the case of a gaining river, or underestimation, in the case of a losing river, of the groundwater – surface water exchange rate. An additional proof of the existence of such flow pattern is that slight diurnal water level fluctuations are also present in the measured river water level 200 m downstream the tree plot (data not shown).

III.5.4. Impact of the model structure and parametrization

It should be noted that the model parameterization could have an important impact on the simulation results. For instance, the root depth distribution defines the fraction of water that is taken up from the groundwater while the *Kc* factors determine the total potential transpiration rates. Uncertainties on *Kc* values for the two vegetation covers remain high and could not be evaluated in this study due to lack of appropriate measurements. Moreover, tree root depth was observed on the field but only until the water table depth (≈ 1 m) and no information on greater depth or root density were gathered. Furthermore, the soil hydraulic parameters define the specific yields, which in turn define the impact of root groundwater on diurnal variations in groundwater level. Due to spatial variability and layering, specific yield may vary significantly with location but also with the groundwater level. Specific yield spatial variability is out of our reach given the measurements we currently have. Next to the model parameterization, there is also some uncertainty left about the model structure itself. Some processes like preferential flow, root water uptake compensation and hydraulic lift are not yet represented in the model but could have an impact on the relation between groundwater level fluctuations, transpiration from groundwater and subsurface fluxes. Investigating these sources of uncertainties was beyond the scope of this study, even if the alternative simulations consider a few additional scenarii regarding root water uptake conceptualization.

III.5.5. Evaluation of the White method

The results of our evaluation of the White method show a good agreement between the ET_{GW} estimates obtained by using the White method and the ET_{GW} calculated by the flow model (Figure 35). This may be surprising as the assumption that a constant rate of groundwater flow into the near-well region occurs over the entire day is clearly violated (Figure 31 and 32). An explanation could be that having a constant rate of groundwater flow is not crucial and that using an average net inflow rate (*R*) is sufficient. *R* was calculated by fitting a linear model to

the piezometric data (Figure 28). Another explanation could be that the specific yield estimates derived from variably saturated flow model simulations by Loheide et al. (2005) compensate for this deviation from the White method assumptions. Anyway, these results suggest that the White method when used together with the Loheide et al. (2005) specific yield estimates is a robust method to estimate groundwater evapotranspiration.

III.6. Conclusion

Diurnal groundwater level fluctuations as a result of uptake by phreatophytes were measured in a mixed deciduous tree and grass plot drained by two ditch drains and a river in the Kleine Nete catchment. They were simulated using the FAO 56 Penman − Monteith equation, a canopy water balance model and a variably saturated flow model considering root water uptake from the saturated zone. The simulation represents well the main features of the measured piezometric time series, including the groundwater level diurnal fluctuations, without any advanced calibration, only adaptation of the subsoil saturated hydraulic conductivity. However, the amplitude of the diurnal groundwater level fluctuations is underestimated for some periods. Additionally, the timing of the diurnal fluctuations is not represented correctly in the simulation, most probably because tree capacity was not represented in our model. The simulation was also used to evaluate the White method (White, 1932) together with the specific yield estimation guidelines of Loheide et al. (2005). This evaluation shows that the White method represents properly the simulated transpiration from groundwater. These fluctuations are also significant for the simulated groundwater discharge to surface water bodies and cause lateral fluxes between neighboring plots covered by a different vegetation. This highlights the potential importance of representing groundwater consumption by phreatophytes in catchment and larger scale models.

Chapter IV

Upscaling groundwater recharge and groundwater – surface water interactions in a catchment scale model

IV. Upscaling groundwater recharge and groundwater – surface water interactions in a catchment scale model

IV.1. Abstract

Water flow in the critical zone at the catchment scale is currently represented using various modeling approaches in a compromise between process representation and computational efficiency. This study investigates a modeling framework to describe groundwater flow in a lowland catchment with a temperate humid climate, the Kleine Nete catchment in Belgium, in which groundwater depth is strongly coupled to recharge from the unsaturated zone and exchange with a dense surface water network. The study focuses on the conductance parameter used to simulate groundwater – surface water interactions in hydrogeological models and on the integration of groundwater recharge calculations, performed using 1D variably saturated models into a 3D groundwater model. We tested a recently developed groundwater – surface water conductance expression which aims at correcting the omission of aquifer resistance in the standard approach. We also investigated the influence of considering variable groundwater depth, sub-grid variability and tree root water uptake from the saturated zone in our groundwater recharge calculations. Results show that using the new groundwater – surface water conductance expression reduces uncertainties on groundwater – surface water conductance values. Furthermore, the spatial variability induced by the new expression influences significantly simulated groundwater flow fields. Moreover, we highlight the importance of considering groundwater depth for simulating groundwater recharge in lowland areas with shallow groundwater. Lastly, we show that accounting for sub-grid variability of groundwater depth, soil and land cover can also be important for modeling the spatial variability of groundwater recharge.

IV.2. Introduction

Groundwater systems are connected to the land surface through interactions with soil, vegetation and surface water. It is through these interactions that changes in atmospheric

conditions are transferred towards the water table and influence flow and transport in aquifers (Maxwell and Kollet, 2008; Scibek et al., 2007; Smerdon, 2017). Accurately representing the processes at the boundaries between aquifers and land surface and their spatio-temporal variability in hydrogeological models is therefore of paramount importance to model groundwater flow under current and future climatic conditions.

In lowland temperate environments, groundwater is generally recharged by rainwater infiltrating through vegetation and soil (diffuse recharge) and discharges into the surface water network. This water distribution occurs in a variably saturated environment sometimes referred to as the critical zone (Anderson et al., 2007; Brantley et al., 2007; Chorover et al., 2007). Diffuse groundwater recharge is the net water flux to the water table resulting from different processes: rainfall, vegetation interception, surface run-off, soil evaporation and root water uptake. Therefore, meteorological conditions together with soil and vegetation properties and status control diffuse groundwater recharge. In shallow groundwater areas, an additional feedback emerges as groundwater depth turns out to have a considerable influence on evapotranspiration, surface runoff and hence groundwater recharge (Doble and Crosbie, 2017; Renger et al., 1986; Shah et al., 2007). Furthermore, root water uptake from groundwater by phreatophytes can even lead to a net negative recharge (Batelaan et al., 2003; Miller et al., 2010; Mould et al., 2010; Vincke and Thiry, 2008). Groundwater discharge into the surface water network is controlled by local pressure gradients, the surface network geometry and subsurface hydraulic properties (Sophocleous, 2002). Groundwater diffuse recharge and discharge to surface water network are highly variable in space, due to surface and subsurface characteristics, and in time, mainly due to weather and climatic variability.

Many methods with various complexity levels are currently available to represent interactions between groundwater, atmosphere, vegetation, soil and surface water. On the one hand, specified flux and head-dependent flux boundary conditions, originally implemented in groundwater models, may neglect important hydrological controls, non-linearity of coupling relationships with groundwater depth and/or spatio-temporal variability. Examples of such methods can be found for instance in the original MODFLOW packages to simulate recharge (specified flux) and evapotranspiration (groundwater depth-dependent flux) (Banta, 2000; Harbaugh, 2005). On the other hand, recent fully integrated models solving Richard's equation in 3D (Kuffour et al., 2019; Therrien and Sudicky, 2006; Thoms et al., 2006) allow detailed

representation of water flow in the critical zone. However, they may incur a prohibitive computational cost, especially when a large number of runs is required for model calibration and uncertainty analysis. The compromise between detailed process representation and computational cost depends a lot on the scale and resolution of the study as well as available computer resources. This study investigates alternative approaches for representing diffuse groundwater recharge and interactions with surface water in a lowland catchment scale steady-state hydrogeological model (Kleine Nete catchment, Belgium), which aim at improving model realism at reasonably low computational cost, thus allowing for comprehensive calibration and uncertainty analysis. This study focuses on two aspects of the coupling between groundwater and land surface hydrology, (1) The groundwater – surface water (GW-SW) conductance used to simulate GW-SW interactions in hydrogeological models and (2) the calculation of diffuse groundwater recharge using 1D variably saturated models and their integration into a 3D groundwater model.

GW-SW interactions are usually described in groundwater models as a Cauchy boundary condition (head-dependent flux) governed by a proportionality coefficient called the GW-SW conductance. The most commonly used parameterization of the conductance parameter assumes that the GW-SW conductance is exclusively controlled by streambed properties (Prickett and Lonnquist, 1971). A major conceptual problem in this approach is that it neglects the head losses occurring in the aquifer, which can limit GW-SW exchange rate especially in low-resolution models. This shortcoming was well known to the authors of the original MODFLOW code and is discussed in McDonald & Harbaugh (1988). As a consequence, the conductance parameter is often perceived as a fitting parameter estimated during model calibration (Bencala, 1984; Mehl and Hill, 2010; Rushton, 2007). Parameterization difficulties have motivated the development of more comprehensive but also more computationally intensive coupling methods (Kollet and Maxwell, 2006). Recently, Di Ciacca et al. (2019) proposed a computationally efficient representation of the conductance parameter aiming at implicitly representing flow processes within the aquifer. This formulation was derived from analytical equations and 2D vertical field scale simulations of stream-aquifer cross sections and is referred to herein as aquifer conductance metamodel. It links the conductance to aquifer hydraulic properties, the geometry and discretization of the groundwater model, and the density of the surface water network. The expression was shown to perform well using

simulations with 3D hydrogeological models at different spatial resolutions (Di Ciacca et al. (2019)). However, it has so far only been applied to numerical experiments considering a homogenous aquifer. The present study applies the Di Ciacca et al. (2019) conductance metamodel to a real world calibration/evaluation exercise in which uncertain model parameters are calibrated using a probabilistic inversion method. With regard to the conductance parametrization and model calibration, two approaches were tested first : (i) spatially distributed GW-SW conductances were calculated using the Di Ciacca et al. (2019) conductance metamodel (no calibration of this parameter); (ii) a uniform value of conductance was calibrated. Calibration using approach (ii) failed to find the parameter sets fitting the best our observations, which led us to test a third calibration approach: (iii) a uniform value of conductance was calibrated but with prior information calculated using the GW-SW conductance metamodel. Parameter uncertainties, fit on piezometric and river discharge data as well as simulated GW-SW and groundwater fluxes are compared for the three different approaches.

Concerning diffuse groundwater recharge, a relevant compromise between process representation and computational requirements may lie in using 1D variably saturated models coupled with a 3D groundwater model. The UZF package for MODFLOW (Niswonger et al., 2006) follows this approach but only represents gravity-driven water flow, which can be an oversimplification in shallow groundwater environments where upward capillary flow can be important (Twarakavi et al., 2008). Moreover, in low resolution groundwater models sub-grid variability in land cover and groundwater depth can be important. In this case, the NRF (Net Recharge Function) package for MODFLOW (Doble et al 2017) may be a suitable approach. This package integrates the relationship between groundwater recharge and groundwater depth using a look-up table. The latter is built on a number of prior simulations with a variably saturated water model performed for all combinations of vegetation – soil – groundwater depth present in the model. Until now the NRF package has been applied to a steady-state groundwater model representing the South East region of South Australia (29 000 km²). In the present study, groundwater recharge calculations consider spatially variable groundwater depth, tree root water uptake from the saturated zone (phreatophytes) and sub-grid variability of groundwater depth, soil texture and land cover. The relative importance of considering these factors on simulated groundwater recharge and groundwater flow fields is

evaluated. Finally, we compare the influence of the considered groundwater recharge and GW-SW conductance parameterizations on simulated groundwater fluxes.

IV.3. Methodology

IV.3.1. Study area

The study area covers the Kleine Nete catchment (≈ 800 km^2) in north-eastern Belgium (Figure 3). This catchment is characterized by shallow groundwater, sandy soils and a very heterogeneous land cover. The following sub-sections describe the hydrogeology, surface water network, soil and land cover of the study area.

IV.3.1.1. Hydrogeology

In the present study, we adopt the hydrogeological model of the Kleine Nete catchment by Gedeon (2008). This model considers an aquifer system that consists of seven main hydrostratigraphic units: Kempen clay-sand complex, Pliocene sand, Kasterlee clay, Diest sand, Berchem sand, Voort sand, and that is delimited at the bottom by the Boom Clay aquitard. These units are inclined towards the East and some of them wedge out within the catchment leading to a variable aquifer thickness from 400 m at the eastern (upstream) border to less than 50 m at the western (downstream) border (Figure 39) (Gedeon and Wemaere, 2003; Meyus, 1998).

The Kasterlee Clay formation was divided into 3 different zones (Figure 40): (1) the main zone covering the major part of the Kleine Nete catchment, (2) a more permeable zone located close to the Kasterlee Clay outcrop area where hydraulic conductivities are 5 times higher than in zone (1), (3) a third zone behind the Rauw fault where hydraulic properties are different and not correlated to those in zones (1) and (2).

Table 6 summarizes the minimum and maximum hydraulic conductivity values of the different hydrostratigraphic units derived from pumping tests (Vandersteen et al., 2014). The Kempen clay-sand complex and the Kasterlee clay have anisotropic hydraulic conductivities. Berchem and Voort sand are considered as one undifferentiated unit in this dataset.

*Table 6: Hydraulic conductivity (*Ks*) measurements range of the different hydrostratigraphic units derived from pumping tests* (Vandersteen et al., 2014)

Hydrostratigraphic unit	***Ks* minimum ($m.d^{-1}$)**	***Ks* maximum ($m.d^{-1}$)**
Kempen clay-sand complex, horizontal	2	2×10^{1}
Kempen clay-sand complex, vertical	2×10^{-5}	3×10^{-2}
Pliocene sand	1×10^{-1}	4×10^{1}
Kasterlee clay, horizontal	1×10^{-1}	8×10^{-1}
Kasterlee clay, vertical	2×10^{-4}	7
Diest sand	1	6×10^{1}
Berchem/Voort sand	5×10^{-2}	2×10^{1}

A considerable number of piezometers is located within the Kleine Nete catchment. Piezometric data were obtained from SCK CEN (Belgian Nuclear Research Center) and the Flemish underground dataset (DOV, "Databank Ondergrond Vlaanderen"). Piezometers with available time series longer than one year were selected. Time series of the resulting selection of 888 piezometers were averaged to obtain for each piezometer a single value of groundwater head comparable to the simulated steady-state hydraulic heads (see section IV.3.3.3). The location of these piezometers and their filter depth are presented in Figure 39.

Moreover, several pumping wells are located within the Kleine Nete catchment, 74 of them were implemented in the hydrogeological model by Gedeon (2008). The most important pumping wells, in term of pumping rate, are shown on Figure 39 and their time averaged pumping rate are presented in Table 7.

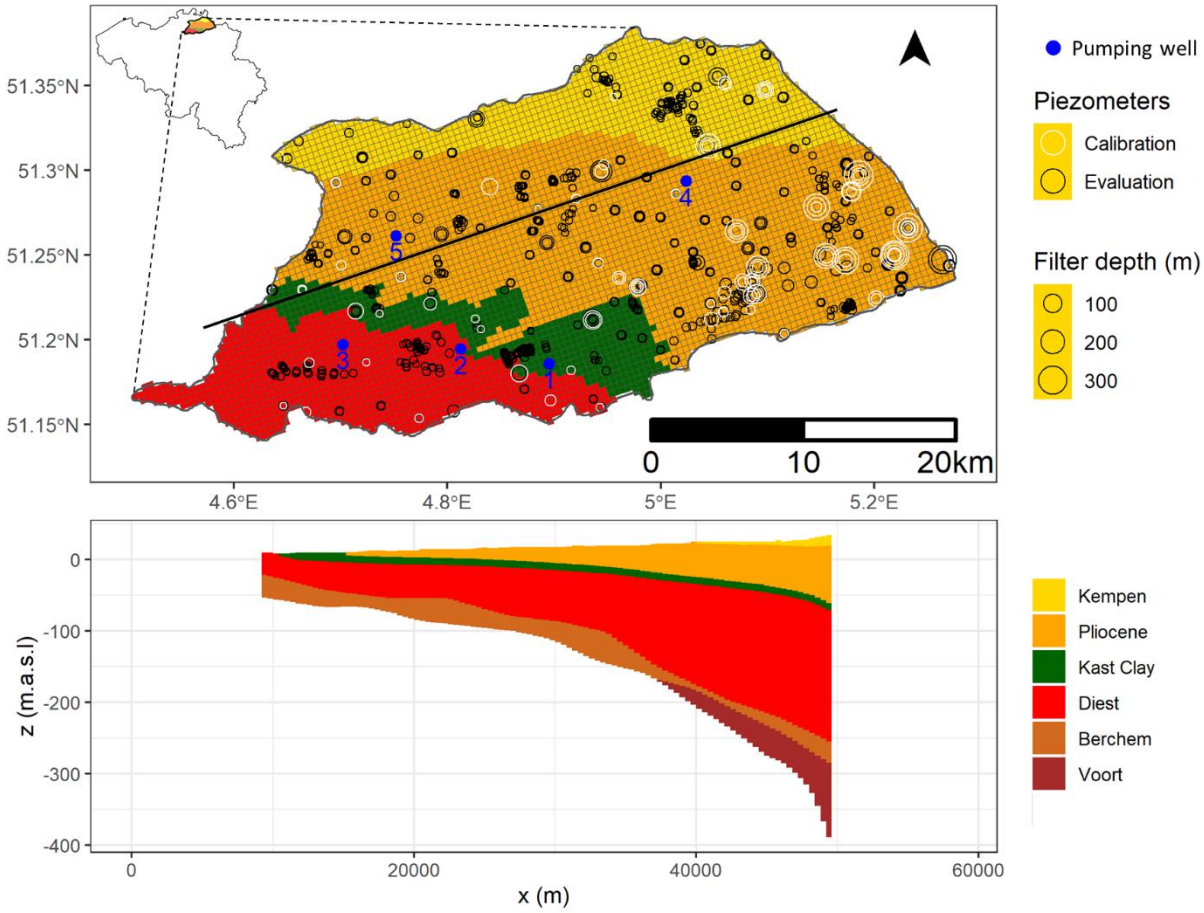

Figure 39: Hydrogeological units (map and SW-NE cross-section), piezometers and most important pumping wells in the Kleine Nete catchment

Table 7: Pumping rate of the most important pumping wells located within the Kleine Nete catchment

ID	Pumping rate ($m^3.d^{-1}$)
1	6891
2	9034
3	13837
4	9849
5	9287

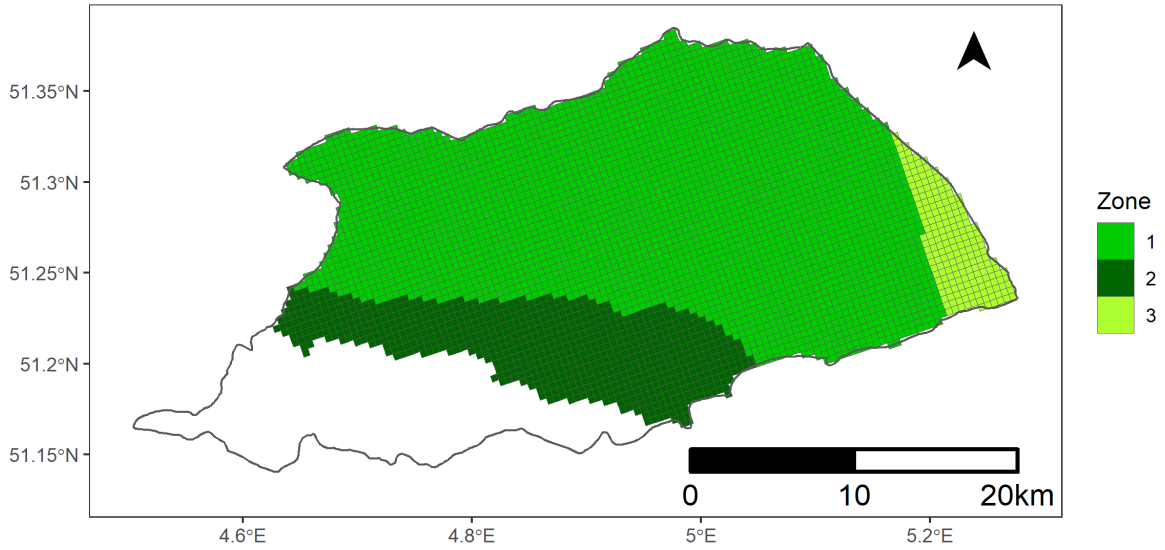

Figure 40: Map of the Kasterlee Clay zones with different hydraulic properties

IV.3.1.2. Surface water network

The surface water network in the Kleine Nete catchment is characterized by a dense and complex network of canals, rivers of variable order and agricultural ditch drains (Figure 41). Furthermore, a few lakes are located within the catchment, the most important being in the south-eastern part of the catchment as a result of white (Pliocene) sand mining. The surface water network used in this study was derived from the Flemish hydrographic atlas (VHA, "Vlaamse Hydrografische Atlas" distributed by VMM, 2019) and the IGN/NGI dataset (distributed by IGN/NGI, 2017).

Several gauging stations measuring water level and flow are located within the catchment. Four of them were selected based on the length of the available time series (Table 8). Their locations are presented on Figure 41 together with their associated sub-catchment, delimited based on the surface water network and digital terrain model (DTM) (distributed by "Informatie Vlaanderen", 2015).

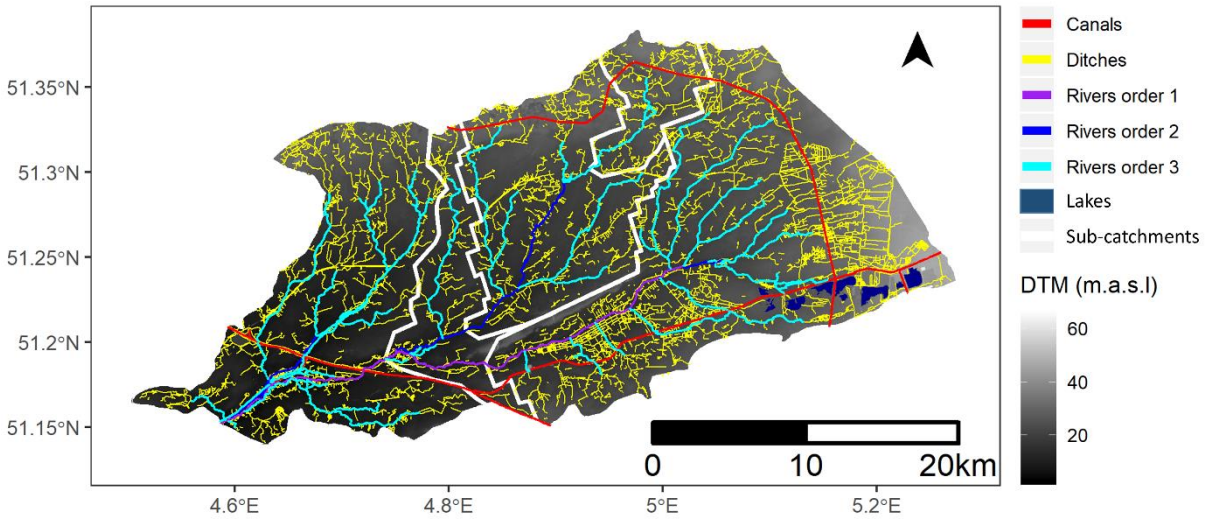

Figure 41: Surface water network, river gauging stations and associated sub-catchments (AA01, AA02, KN01 and KN02) and Digital Terrain Model of the Kleine Nete catchment. "AA" stands for the Aa river and "KN" for the Kleine Nete river.

Table 8: River gauging station time series length

Gauging station	Time series length
Aa 01 (Turnhout)	1986-2011
Aa 02 (Vorselaar)	1976-2011
KN 01 (Herentals)	1988-2019
KN 02 (Grobbendonk)	1984-2019

IV.3.1.3. Soil and land cover

The Kleine Nete catchment is mainly covered by sandy soils (≈ 60%) with locally some dunes, formed by recent aeolian sand deposition. However, finer textured soils can also be found, mainly in alluvial plains and in the western part of the catchment (Figure 42a). The main soil profile developments are podzol, plaggic anthrosol and fluvisol.

Land cover in the Kleine Nete catchment is very heterogeneous, showing a significant percentage of meadow (37 %), forest (31 %), cropland (21 %) and built-up area (15 %) (Figure 42b). Land cover is highly variable at a sub-kilometric scale, displaying often in a patchwork of meadow, cropland, woodland and built-up area.

The soil information was derived from the Belgian soil map (1/20000, distributed by "Databank Ondergrond Vlaanderen (DOV)") while information about the land cover was obtained from the Flemish land cover map (25 m resolution, 2001, distributed by "Informatie Vlaanderen").

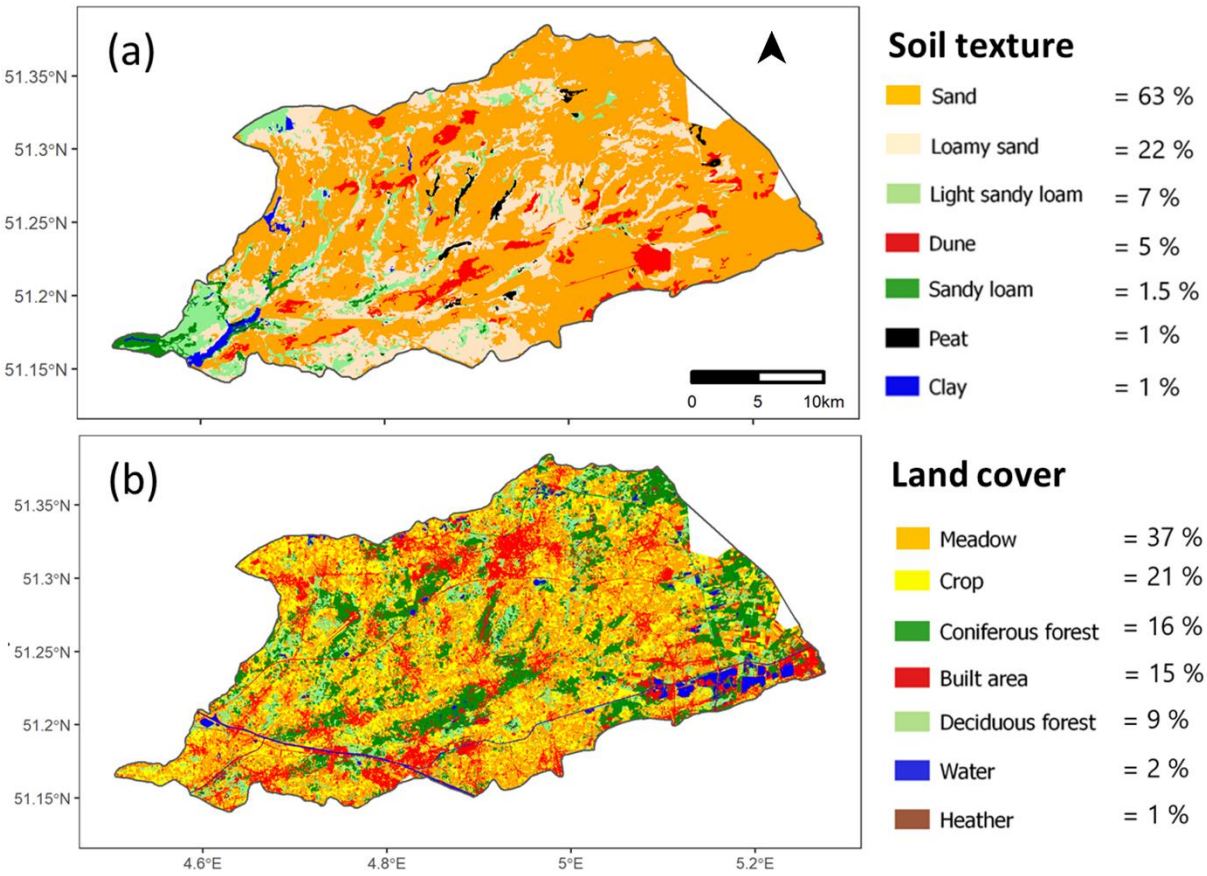

Figure 42: Soil texture and land cover maps of the Kleine Nete catchment

IV.3.2. Groundwater recharge vs groundwater depth calculation

Groundwater recharge calculations prior their integration in the NRF package were performed using HYDRUS 1D (Simunek et al., 2005). The following sub-sections describe how the soil hydraulic parameters, root water uptake parameters and boundary conditions (atmospheric and groundwater depth) were derived. The simulations represent 28 years of meteorological records from 1990 to 2017. The first 6 years were repeated one time as a spin-up period.

Intersections of the soil texture and land cover spatial datasets were computed excluding built-up and water covered areas for which no groundwater recharge calculations were made. This resulted in 35 soil / vegetation (S/V) combinations. A 1D vadose zone model, representing

a 5 m deep soil profile, was set-up for each combination. Maize is the dominant crop in the Nete catchment and was taken as the representative cover for cropland (Leterme and Mallants, 2012). Groundwater recharge under built-up area was considered to be 70 % of grassland, because of the land cover map resolution and the nature of residential and industrial built-up surfaces in the study area (Dams et al., 2013). Not mapped area at the eastern border of the catchment are considered as a combination of sandy soil and meadow.

IV.3.2.1. Soil hydraulic parameters

The van Genuchten − Mualem model (Mualem, 1976; van Genuchten, 1980) was used in HYDRUS-1D for solving the Richards equation of water flow in variably saturated media. The soil hydraulic parameters were obtained through pedotransfer functions using the Rosetta module (Schaap et al., 2001). These pedotransfer functions require the percentage of sand, silt and clay for each textural class considered in our study area. The Aardewerk database (Van Orshoven et al., 1988) was used to obtain representative soil profiles within the Kleine Nete catchment. If, for a textural class, less than 20 profiles were available within the catchment, profiles up to a distance of 30 km around the Kleine Nete catchment were used. No soil layering was considered in this study thus sand, loam and clay percentage were averaged over the depth of each profile and then for each class. Table 9 summarizes the average fraction of sand, silt and clay, the corresponding standard deviation and number of soil profiles considered for each textural class. Table 10 shows the soil hydraulic parameters of the van Genuchten − Mualem model for each textural class.

For peat soils, only two profiles were available in the area therefore parameter values were taken from the study by Gnatowski et al. (2010) who determined van Genuchten − Mualem model parameters for 87 peat soil samples.

Table 9: Average and standard deviation of sand, silt and clay percentage and number of soil profile considered for each textural class

Textural class	Mean sand fraction (%)	Mean silt fraction (%)	Mean clay fraction (%)	Standard deviation sand fraction (%)	Standard deviation silt fraction (%)	Standard deviation clay fraction (%)	Number of soil profiles
Dune	95	3.	2	3	2	1	17
Sand	92	6	2	4	3	2	111
Loamy sand	80	14	6	8	5	4	22
Sandy loam	52	35	13	13	14	5	23
Light sandy loam	65	25	9	12	9	6	31
Clay	69	9	22	11	5	8	10

Table 10: Soil hydraulic parameters of the van Genuchten – Mualem model for each textural class. Parameter values for peat soils were taken from the study by Gnatowski et al. (2010)

Texture class	ϑr (–)	ϑs (–)	α_{VG} (m^{-1})	n_{VG} (–)	Ks ($m.d^{-1}$)	l_{VG} (–)
Dune	0.051	0.38	3.5	3.4	7.5	0.5
Sand	0.048	0.38	3.6	2.9	4.8	0.5
Loamy sand	0.040	0.39	4.1	1.7	0.96	0.5
Sandy loam	0.049	0.39	1.6	1.4	0.21	0.5
Light sandy loam	0.041	0.39	3.1	1.4	0.42	0.5
Clay	0.062	0.38	2.8	1.3	0.19	0.5
Peat	0.18	0.91	2.3	1.3	0.073	0.5

IV.3.2.2. Root water uptake

In our model, root density profiles control the distribution of potential transpiration over the soil profile depth and root water uptake reduction functions determine the actual rate of water uptake depending on local pressure head.

Normalized root density profiles for the different vegetation types considered here were inferred from the literature (Aerts et al., 1992; Gale and Grigal, 1987; Jacques et al., 2011; Roberts, 1976; Vincke and Thiry, 2008) and are presented in Figure 43.

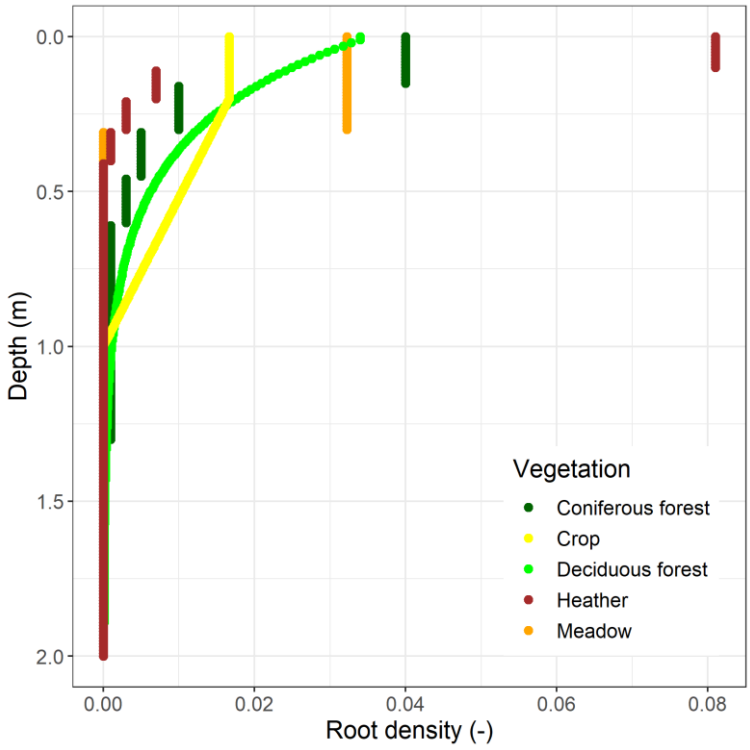

Figure 43: Normalized root density profile for the different vegetation covers

Concerning root water uptake, two different parameterizations were considered: (i) all plants can only extract water from the unsaturated zone and (ii) trees (phreatophytes) can extract water from the saturated zone. The root uptake reduction function was specified according to the model of Feddes et al. (1978). Parameters used for each vegetation cover were taken from the HYDRUS database (Simunek et al., 2012) and presented in Table 11. When trees were considered to be phreatophytes, *P0* and *POpt* were set to positive values to allow for groundwater uptake.

Table 11: Root water uptake pressure head reduction function parameters of the Feddes model for each vegetation cover

Vegetation	*P0* (m)	*POpt* (m)	*P2H* (m)	*P2L* (m)	*P3* (m/h)	*r2H* ($m.d^{-1}$)	*r2L* ($m.d^{-1}$)
Meadow	−0.1	−0.25	−2	−8	−80	0.005	0.001
Corn	−0.1	−0.30	−3.25	−8	−80	0.005	0.001
Heather	−0.1	−0.30	−3	10	−80	0.005	0.001
Coniferous trees	−0.1	−0.25	−5	−8	−80	0.005	0.001
Deciduous trees	−0.1	−0.25	−5	−8	−80	0.005	0.001
Coniferous trees (phreatophytes)	3	2	−5	−8	−80	0.005	0.001
Deciduous trees (phreatophytes)	3	2	−5	−8	−80	0.005	0.001

IV.3.2.3. Boundary conditions

An atmospheric boundary condition was used at the top of the soil profile and a constant pressure head, representing groundwater depth, was defined at the bottom of soil profile (5 m below the soil surface). Simulations were run for different groundwater depths that ranged between 0 and 5 m depth with an increment of 0.1 m between 0 and 2 m depth and 0.5 m between 2 and 5 m.

For the atmospheric boundary conditions, the approach used in Leterme et al. (2012) was followed. Daily reference potential evapotranspiration (*ET0*) was calculated using the FAO 56 Penman-Monteith equation (Allen et al., 1998) within the Ref-ET software (Allen, 2009). The input data were daily minimum and maximum air temperature and relative humidity, average wind speed and sunshine hours recorded at the IRM/KMI (Institut Royal Météorologiques/Koninklijk Meteorologisch Instituut) weather station in Kleine-Brogel, approximately 15 km away from the eastern catchment boundary. Because of missing data, the number of sunshine hours were replaced from the year 2005 onwards by solar radiation measured at the IRM/KMI weather station in Diepenbeek, located approximately 40 km south-east of the catchment. Then, for each vegetation type, a water balance canopy model

described in Leterme et al. (2012) was used to split *ET0* into potential transpiration and potential evaporation and to calculate throughfall, which are the required inputs for the variably saturated water flow model.

The canopy model uses as input data, precipitation, *ET0* and several vegetation parameters: the crop factor (*Kc*, [−]), leaf area index (*LAI*, [−]), interception capacity (*ωc*, [L]) and light extinction coefficient (*k*, [−]). The value of *k* was set to 0.5. The values of *Kc*, *LAI* and *ωc* were derived from the literature (Breuer et al., 2003; Granier et al., 1999; Hall, 1985; Heijmans et al., 2008; Jacques et al., 2011; Lawrence and Slingo, 2004; Leuschner, 2001; Meiresonne et al., 2003; Meyus et al., 2004; Verstraeten et al., 2005; Vincke and Thiry, 2008) and changed over the entire year with daily time steps. Table 12 summarizes the average annual Kc factors for the different vegetation types considered.

*Table 12: Mean annual crop factor (*Kc*) values*

Vegetation	Mean annual Kc (−)
Meadow	1
Corn	0.57
Deciduous trees	0.84
Coniferous trees	1.14
Heather	0.67

The combination of 27 groundwater depths, 7 vegetation types and 7 soil types resulted in a total of 945 simulations that each spanned a period of 28 years (plus 6 years of spin-up).

IV.3.2.4. Groundwater recharge output processing

Groundwater recharge was taken as the flux at the bottom of the soil profile. For each S/V combination, time series of daily groundwater recharge were averaged over the entire simulation period to derive a recharge rate for the steady-state groundwater flow simulations

We hence obtained for each S/V combination a groundwater recharge – groundwater depth (GR-GD) look-up table. For each forest vegetation type, two look-up tables were obtained: one assuming tree root water uptake from the groundwater and one considering only uptake from

the unsaturated zone. The same procedure was used to relate run-off to groundwater table depth.

IV.3.3. Groundwater modeling

The groundwater model used in this study is based on the Neogene Aquifer Model (NAM) (Gedeon, 2008), implemented in MODFLOW-2000 (Harbaugh et al., 2000), but limited to the Northern part representing the Kleine Nete catchment. Hydrostratigraphy and model discretizations remain unchanged compared to Gedeon (2008), while groundwater recharge, surface water boundary conditions and calibrated parameter values were updated.

The hydrogeological model represents the hydrostratigraphic units (Figure 39) using a regular 400 by 400 m grid (horizontal discretization) and 16 numerical layers (Table 13).

Table 13: Top elevation of the 16 numerical layers used in the hydrogeological model

Layer number	Top elevation
1	Ground surface elevation, GSE (m.a.s.l)
2	0.5*GSE
3	0.1*GSE
4	Uniform −5 m.a.s.l
5	Uniform −10 m.a.s.l
6	Uniform −15 m.a.s.l
7	Uniform −20 m.a.s.l
8	Uniform −27 m.a.s.l
9	Uniform −35 m.a.s.l
10	Uniform −45 m.a.s.l
11	Uniform −58 m.a.s.l
12	Uniform −75 m.a.s.l
13	Uniform −100 m.a.s.l
14	Uniform −145 m.a.s.l
15	Uniform −220 m.a.s.l
16	Uniform –300 m.a.s.l

We used the Hydrogeologic Unit Flow (HUF) package (Anderman and Hill, 2000) to represent hydrostratigraphic units independently from the numerical model layers. HUF calculates effective hydraulic properties of a grid cell based on the hydraulic properties of the hydrostratigraphic units in the grid cell.

IV.3.3.1. Groundwater recharge

Five different groundwater recharge approaches were implemented (Figure 44), all based on the groundwater recharge simulations presented in section IV.3.2. Four of them use the NRF package for MODFLOW (Doble et al., 2017) and one uses the original recharge (RCH) package

(Harbaugh, 2005). The NRF package for MODFLOW is a modification of the Segmented Evapotranspiration (ETS) package for MODFLOW 2000 (Banta, 2000) allowing the use of GR-GD lookup tables to select the groundwater recharge values to be applied in each cell. Net recharge for each cell is calculated by linearly interpolating net recharge for the nearest groundwater depth above and below the groundwater depth value generated by MODFLOW. Net recharge is added to MODFLOW's mass balance equation, and both groundwater elevation and net recharge are solved iteratively. More detailed explanation can be found in Doble et al. (2017).

Our Reference approach uses a representation of sub-grid variability described hereafter and considers tree root water uptake in the groundwater (phreatophytes). The first alternative scenario calculates recharge and surface runoff considering a uniform groundwater depth of 2 m in the recharge calculations (≈ average value on the catchment) and is referred to as GWD2m. The second scenario considers no tree water uptake in the saturated zone (see section IV.3.2.2) and is referred to as RTUnsat. The third and fourth scenarios (NoSubGridE and NoSubGridESV) explore the impact of the representation of sub-grid variability for the GR-GD relations that consider water uptake from groundwater by trees.

The grid cell resolution in the groundwater model was 400 m. Therefore, sub-grid variability in soil, land cover and elevation can be important, especially since the relation between GR and GD is strongly non-linear. Each groundwater cell was subdivided in subunits defined by the intersections of the soil texture and land cover spatial datasets. The GR-GD look-up table of each S/V subunit within a cell was corrected to take into account the differences between the average elevations of the different subunits. GR-GD relationships for the different S/V subunits within a cell were also averaged using their respective area as weight. This approach was used for the Reference, RTUnsat and GWD2m scenario. The NoSubGridE scenario did not consider differences in elevation within a grid cell but did still represent S/V variability. The NoSubGridESV scenario did not consider any sub-grid variability neither elevation nor S/V, and thus the S/V combination covering the largest area within a grid-cell was selected to look up the recharge values in the GR-GD tables. Alternative upscaling scenarios were only implemented for groundwater recharge simulations that consider tree root water uptake in the saturated zone.

The same approaches were considered for surface runoff calculated in each groundwater model cell. However, surface runoff was not routed to the groundwater model but was directly used for the comparison with river discharge measurements (see section IV.3.3.3.2).

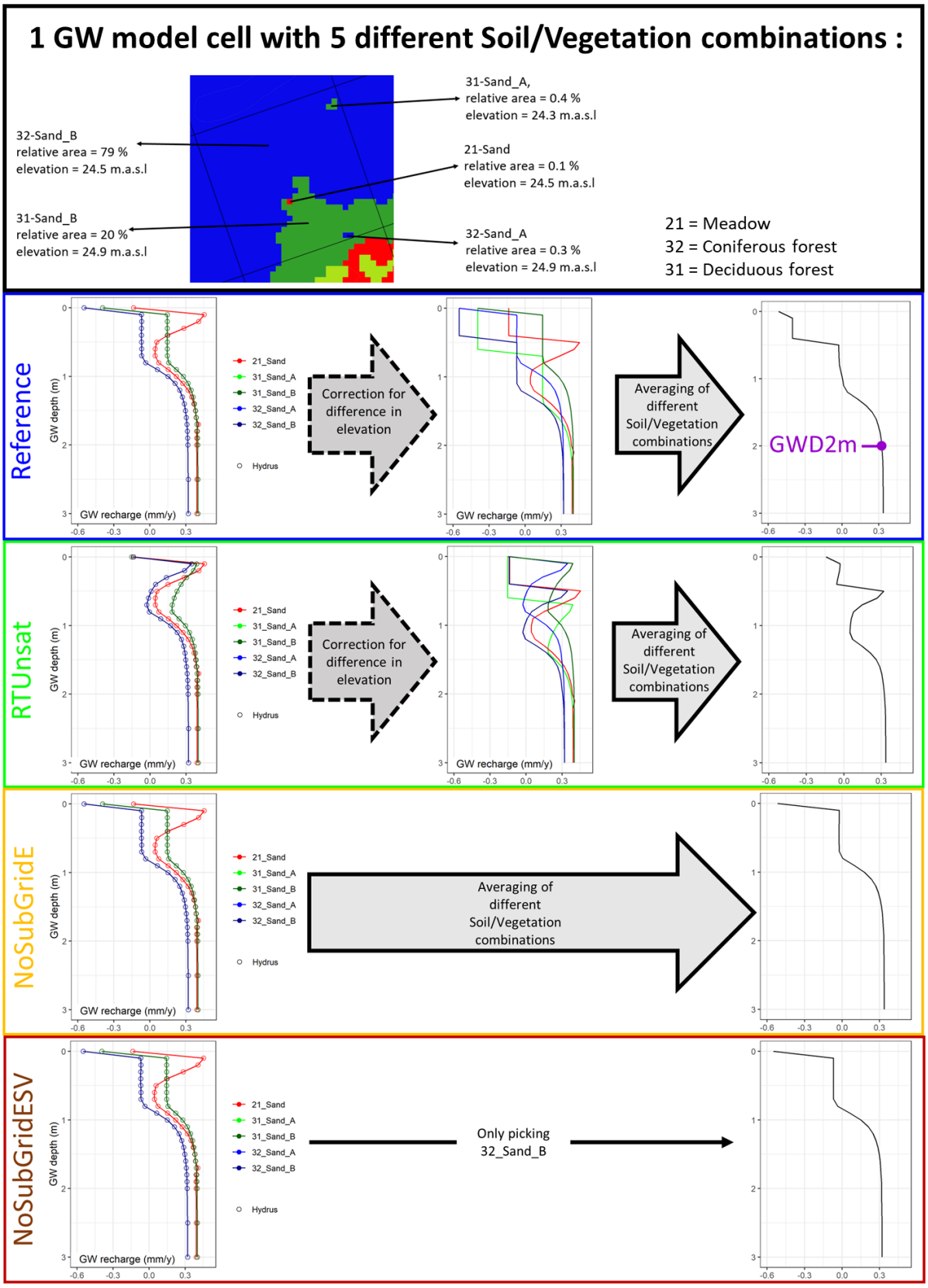

Figure 44: Implementation of the different groundwater recharge approaches illustrated for one random groundwater model cell. Circles indicate the HYDRUS simulations outputs and lines the linear interpolation.

IV.3.3.2. Groundwater – surface water interactions

The surface water network presented in Figure 41 was used to parameterize the groundwater model. Rivers of different orders, canals and lakes were represented with the MODFLOW River package which allows water exchange in two directions, to and from surface water. Ditches were represented with the MODFLOW Drain package which only allows water flow from groundwater to surface water.

In the MODFLOW River and Drain packages GW-SW flow exchanges are calculated by multiplying the hydraulic head difference between groundwater and surface water with a conductance value. Parameterization of conductances and surface water levels are presented in the next sub-sections for the rivers and ditches. Lakes and canals have not been modified from the previous model version and are beyond the scope of the present study. Lakes were assigned a quite high conductance value (5 d^{-1}) to ensure a good connection with groundwater and canals a low conductance value to simulate their isolation from the surrounding aquifer (from 10^{-7} to 10^{-2} d^{-1} depending on the canal).

Two different approaches to calculate river and ditch conductance were tested in this study. The first is the standard approach used in MODFLOW (MF) in which the GW-SW conductance is viewed as the streambed conductance. The groundwater model using this approach is later referred to as MFCond. Following this approach, the conductance ($C_{3D,sb}$ [$L^3.T^{-1}$]) is calculated as:

$$C_{3D,sb} = \frac{K_{\mathrm{sb}} W_{\mathrm{sb}} L_{\mathrm{sw}}}{M_{\mathrm{sb}}}$$

Equation 29

where M_{sb} [L] is the streambed thickness, K_{sb} [$L.T^{-1}$] is the streambed hydraulic conductivity, W_{sb} [L] is the streambed width, L_{sw} [L] is the length of surface water in a cell.

The streambed width was considered to be equal to the wetted perimeter and was set to 15 ,10 and 5 m for the first, second and third order rivers respectively based on the 1 m resolution DTM. Ditches streambed width was set to 2 m. The streambed thickness and hydraulic conductivity are unknown. Their ratio was estimated using inverse modeling (see section IV.3.3.3) and is referred hereafter as 1D GW-SW conductance (GW-SW conductance per unit area, [T^{-1}]).

The second approach uses a metamodel that takes into account aquifer conductance (Di Ciacca et al., 2019) to calculate the GW-SW conductance (MMCond). Although the metamodel approach can be used in combination with the standard approach to represent both the streambed and aquifer conductance, only the aquifer conductance was considered in this study in order to test the hypothesis that the GW-SW resistance is mainly due to the aquifer in our case study. The conductance ($C_{3D,aqui}$ [$L^3.T^{-1}$]) is calculated as:

$$C_{\mathrm{3D,aqui}} = \frac{1}{\frac{3LL_{\mathrm{avg}} - {L_{\mathrm{avg}}}^2}{24LK_{hor}DL_{\mathrm{sw}}} + \left[1 - 0.5\left(1 - \frac{L_{\mathrm{avg}}}{L}\right)\left(1 - \frac{D_{\mathrm{avg}}}{D}\right)\right]\frac{\ln\left(\frac{D}{u}\right)}{\pi\sqrt{K_{\mathrm{hor}}K_{\mathrm{ver}}}L_{\mathrm{sw}}}}$$

Equation 30

where L [L] is the representative spacing between two surface water bodies, K_{hor} [$L.T^{-1}$] is the aquifer representative horizontal hydraulic conductivity, K_{ver} [$L.T^{-1}$] is the representative aquifer vertical hydraulic conductivity, u [L] is the wetted perimeter of the surface water body, D [L] is the aquifer thickness, L_{avg} [L] is the horizontal discretization of the groundwater model and D_{avg} [L] is the vertical discretization of the groundwater model. All parameters in Equation 2 can be calculated directly from available input data.

The aquifer thickness (D) was taken as the thickness between the surface water level and the top of the Boom Clay aquitard. The maximum thickness considered was limited to $\frac{1}{4}L$ (Ernst, 1962; Ritzema, 1994). Wet perimeters (u) were set to 15, 10 and 5 m for the first, second and third order rivers respectively, based on the 1 m resolution DTM. For the ditches u was set to 2 m.

The representative hydraulic conductivities (K_{hor} and K_{ver}) were obtained by averaging the hydraulic conductivities weighted by the layer thicknesses below the surface water level (limited to a total aquifer thickness of $\frac{1}{4}L$) in each grid cell. The horizontal representative hydraulic conductivities were calculated using arithmetic means and the vertical ones using harmonic means. Note that the application of the metamodel to an heterogenous aquifer was not addressed by Di Ciacca et al. (2019). Therefore, this way of calculating representative K_{hor} and K_{ver} has not been previously evaluated and constitutes a new implementation.

The representative spacing between two surface water bodies was calculated using the iterative procedure described in Di Ciacca et al. (2019). In this case, iterations were made for grid resolution of 400, 800, 1200, 1600, 2400, 3200, 3600, 4800, 7200, 9600 and 14400 m.

River water level was set using the 1 m resolution DTM. First, the minimum elevation value was computed in each model grid cell. Second, the computed values were manually corrected in cells where the minimum elevation value was not located within the river channel. The riverbed was set to 1 m below the river water level. Ditches water level was set to 0.5 m below the cell topographic level, corresponding to what is generally observed in the study area.

IV.3.3.3. Comparison against piezometric and river discharge data

Simulation outputs were compared with measurements in two different manners. First, a Bayesian calibration was performed using a selection of 100 piezometers distributed across the study area (Figure 39). The calibration was undertaken for the hydraulic conductivities of the different hydrogeological layers and the vertical anisotropy of the Kasterlee clay layer. Second, simulation outputs were evaluated on the remaining 788 piezometers (Figure 39) and river discharge measurements from 4 gauging stations (Figure 41).

IV.3.3.3.1. Probabilistic calibration using piezometric measurements

The calibration or inverse problem can be represented as:

$$\mathbf{d} = F(\theta) + e$$

Equation 31

where $\mathbf{d} = (d_1, \dots, d_N) \in \mathbb{R}^N$, $N \geq 1$ is the measurement data vector (in our case groundwater hydraulic heads), $F(\theta)$ is the groundwater model with parameters θ and the noise term e lumps all sources of errors.

Following Bayesian theory, parameters in θ are considered as random variables. Their posterior pdf, $p(\theta \mid \mathbf{d})$, is given by:

$$p(\theta \mid \mathbf{d}) = \frac{p(\theta)p(\mathbf{d} \mid \theta)}{p(\mathbf{d})} \propto p(\theta)L(\theta \mid \mathbf{d})$$

Equation 32

where $L(\theta \mid \mathbf{d}) \equiv p(\mathbf{d} \mid \theta)$ is the likelihood function of θ. $p(\mathbf{d})$ is a normalization factor which is not required when the parameter dimensionality is fixed.

Groundwater model calibration is a non-linear inverse problem. Therefore, $p(\theta \mid \mathbf{d})$ cannot be calculated analytically and we used Markov Chain Monte Carlo (MCMC) simulations to explore the parameter space and approximate numerically $p(\theta \mid \mathbf{d})$. More specifically, the $DREAM_{ZS}$ algorithm was used (Laloy and Vrugt, 2012; Vrugt, 2016).

Parameters included in the calibration are presented in Table 14 together with their assumed uniform prior range or distribution. Bounds of the range for hydraulic conductivities and vertical anisotropy were defined based on existing information on the associated subsurface layers (Table 6, Gedeon, 2008; Vandersteen et al., 2014) with some added flexibility to explore potentially unexpected values. As assumed by Gedeon (2008), vertical anisotropy of the Kempen clay-sand complex was set to a fixed value of 10. Concerning the Kasterlee clay unit, horizontal hydraulic conductivity and vertical anisotropy were calibrated independently for the zone (1) and (3) (Figure 40). Horizontal and vertical hydraulic conductivities of the zone 2 were assumed to be 5 times higher than in zone (1).

Table 14: Parameters included in the calibration and explored ranges of values. Ks *refers to saturated hydraulic conductivity and* VA *to vertical anisotropy.* Z1 *and* Z3 *refers to the zone 1 and 3 of the Kasterlee Clay (Figure 40).*

Parameter	Lower bound	Upper bound
Ks Kempen clay-sand complex ($m.d^{-1}$)	0.1	100
Ks Pliocene sand ($m.d^{-1}$)	0.1	100
Ks Kasterlee clay Z1 ($m.d^{-1}$)	0.01	100
Ks Kasterlee clay Z3 ($m.d^{-1}$)	0.01	100
VA Kasterlee clay Z1	1	10000
VA Kasterlee clay Z3	1	10000
Ks Diest sand ($m.d^{-1}$)	0.1	100
Ks Berchem sand ($m.d^{-1}$)	0.1	100
Ks Voort sand ($m.d^{-1}$)	0.1	100
1D River conductance (d^{-1})	0.01	10000

Calibration was first undertaken for the two different GW-SW conductance models (MFCond and MMCond) and the Reference groundwater recharge approach (see section IV.3.3.1). For MMCond, no calibration was made for the river conductance as it is calculated from the calibrated hydraulic conductivities and other model characteristics (Equation 30). GW-SW conductance for the ditches were not included in the calibration and set to 1 d^{-1} according to the average value given by the GW-SW conductance metamodel. Calibration using the MFCond approach failed to find the parameter sets fitting the best our observations, which led us to test a third calibration approach (MFCondPMM). It uses the same conceptualization as MFCond, but prior information about the GW-SW conductance obtained from the metamodel was given to the inversion algorithm. To obtain this prior information, first the metamodel was applied to 1000 realizations randomly sampled in the posterior distributions of the parameter values of the MFCond model and an average value was computed for each realization. This gave a distribution of spatially averaged GW-SW conductance values. This distribution was then extended by using a Gaussian distribution centered on the same mode

(0.3 d^{-1}) and with a standard deviation of 20 d^{-1}(Figure 45). For the three models, the calibration was achieved with 60 000 model runs.

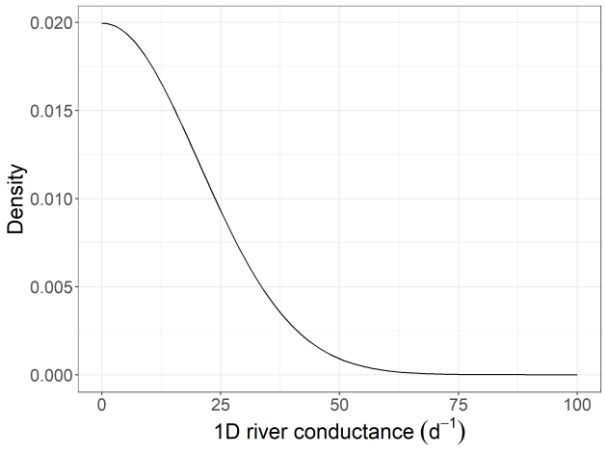

Figure 45: Prior distribution of the 1D river conductance used for the calibration of MFCondPMM model

The different groundwater recharge approaches were investigated using the MMCond approach for calculating GW-SW conductances and a set of parameters taken from its posterior distribution.

IV.3.3.3.2. Evaluation on river discharge

Simulated flow to surface water by all the models (5 groundwater recharge and 3 GW-SW conductance approaches) were evaluated against time-averaged values of river discharges (Figure 41, Table 8). First, GW-SW fluxes simulated in all cells of a sub-catchment were summed up to obtain a flow value that can be compared with the time-averaged river discharge of the corresponding station. Second, surface runoff fluxes simulated with the HYDRUS models (for deriving the GR-GD look-up tables), in each sub-catchment, were added to the corresponding aggregated GW-SW flow. However, no HYDRUS simulations were made for impermeable areas, which are assumed to be 30 % of built-up areas. Therefore, we considered a value of 0.35 ± 0.05 $m.y^{-1}$ of surface runoff on impermeable areas based on the results of the modeling study by Batelaan & De Smedt (2007), who calculated surface runoff , evapotranspiration and groundwater recharge on the Nete catchment for different land covers and soil types. Surface runoff on impermeable areas was added to the aggregated simulated GW-SW and runoff flow ahead of the comparison with river discharge for each sub-catchment to obtain the total flow to surface water.

IV.4. Results

IV.4.1. Groundwater recharge vs groundwater depth calculation

Time-averaged groundwater recharge, evaporation, transpiration and surface runoff as a function of groundwater depth simulated for sandy soils with coniferous trees are presented in Figure 46 (a). Figure 46 (b) shows the simulated GR-GD functions for different vegetation types covering sandy soils. In this section, only these results are discussed, however simulated GR-GD functions for the other soil textures are provided as supplementary material (Appendix C, Figure A).

The characteristics of groundwater recharge as a function of ground water depth in case of root water uptake from the saturated zone is considered are explained first. When the groundwater level reaches the soil surface (groundwater depth = 0 m), groundwater recharge is negative since the precipitation that does not evaporate runs off and the transpiration and evaporation losses need to be compensated by upward flow. Groundwater recharge increases sharply with increasing groundwater depth until a groundwater depth of 0.1 m due to surface runoff decrease (no infiltration excess runoff). Groundwater recharge then remains constant with groundwater table depth until 0.7 m of groundwater depth and slightly negative because the potential transpiration of trees is for the considered climate larger than the precipitation. Below this point, evaporation and transpiration start to decrease with increasing groundwater table depth due to water stresses occurring during dry periods and consequently, groundwater recharge is increasing with groundwater table depth. Finally, a maximal groundwater recharge is reached for groundwater table depths below approximately 2 m. When no root water uptake occurs in the saturated zone, groundwater recharge increases, and transpiration decreases with increasing groundwater table depth when groundwater table is above 1.0. to 0.5 m depth as a result of anaerobic stress in a fraction of the root zone. Differences between vegetation types are mainly due to different *Kc* values (Table 12), and to different root density profiles (Figure 43). The *Kc* determines the potential transpiration. The root density profile controls the shape of the GW-GD relationships. Differences between fine and coarse soil textural classes are as important as between the different vegetations, with finer texture leading to lower recharge values and smoother GW-GD relationships. However,

fine textured soils cover only a small part of the catchment (Figure 42) and differences between the two most common soil textures (sand and sandy-loam) are relatively small.

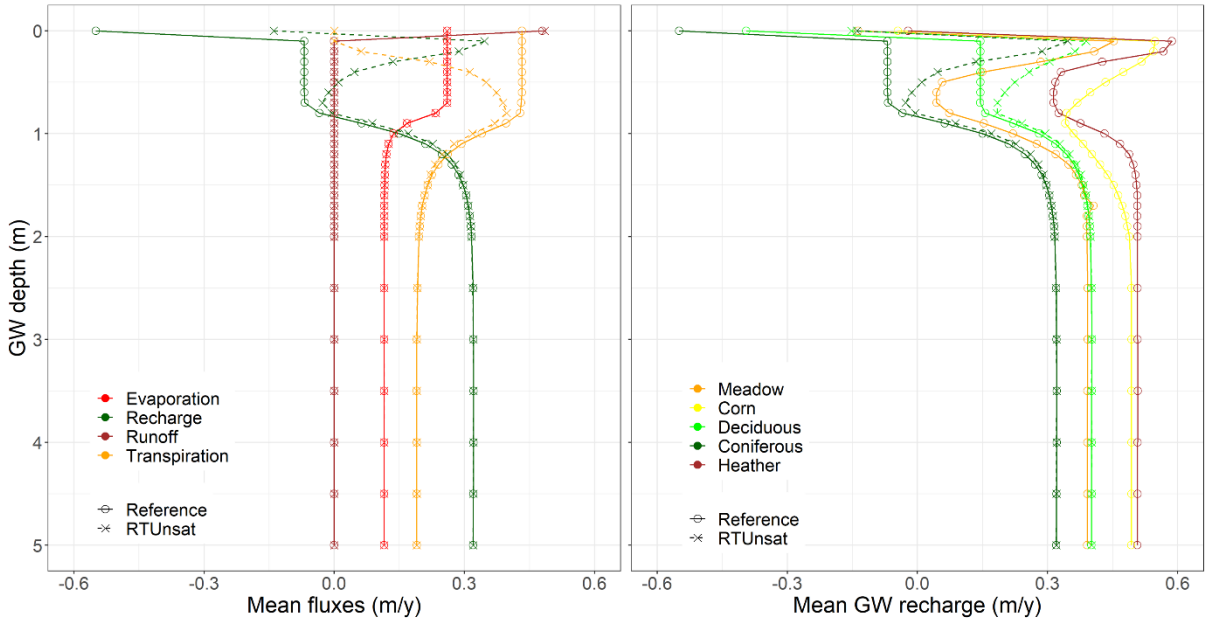

Figure 46: (a) Time-averaged groundwater recharge, evaporation, transpiration and surface runoff as a function of groundwater depth (GW depth) simulated for sandy soils with coniferous trees. (b) Groundwater recharge as a function of groundwater depth simulated for sandy soils with different vegetation covers. Fluxes are presented for simulations considering tree water uptake from the saturated zone (Reference) and excluding it (RTUnsat). Circles indicate the HYDRUS simulations outputs and lines the linear interpolation.

IV.4.2. Groundwater models

Results of the groundwater modeling are discussed in two distinct sections. The first section presents the results of the probabilistic calibration of the different GW-SW conductance approaches, describes the derived parameter posterior distributions and discussed model evaluation against piezometric and river gauging data. The second section presents a comparison of simulation outputs obtained with the different GW-SW conductance and groundwater recharge approaches.

IV.4.2.1. Calibration and evaluation

For the three calibrated models (MMCond, MFCond and MFCondPMM), parameter posterior distributions were derived using the 30 000 last runs. Posterior distributions of the hydraulic conductivities and vertical anisotropies are presented in Figure 47. Figure 48 displays the posterior distributions of the river conductance. Although no calibration of the river conductance parameter was done when using the metamodel (MMCond), a posterior

parameter distribution and maximum a posteriori (MAP) parameter set were calculated by applying the metamodel to the posterior hydraulic conductivities (using a sample of 1000 posterior realizations), averaging the spatially distributed river conductances for each realization and normalizing by the wetted perimeter to obtain the 1D GW-SW conductance.

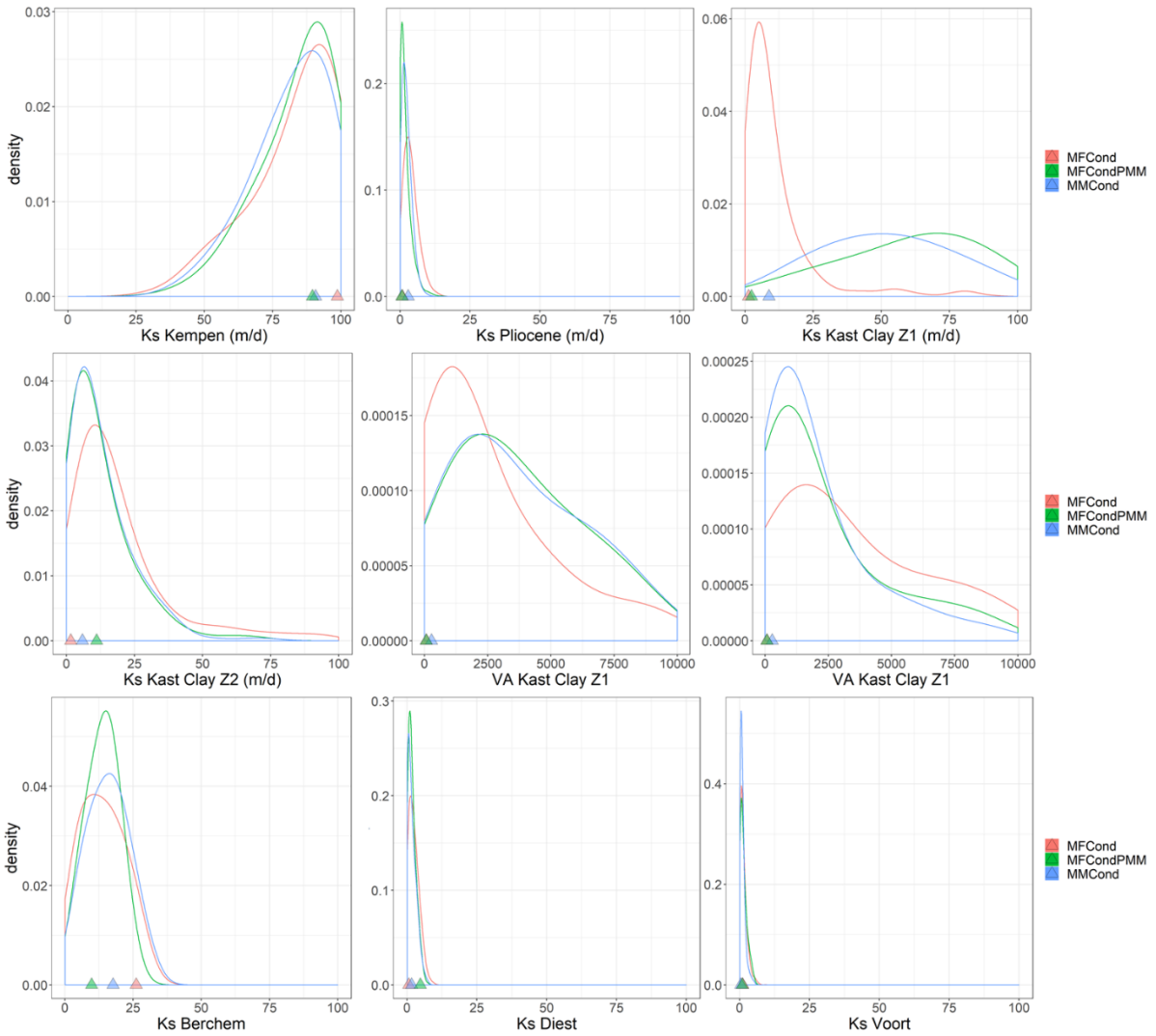

*Figure 47: Posterior distributions of the calibrated hydraulic conductivities (*Ks*) and vertical anisotropies (*VA*) of the different hydrogeological units (Figure 39 and Figure 40) obtained with the different GW-SW conductance approaches. Triangles indicate Maximum A Posteriori (MAP) values. MFCond simulations use a calibrated homogenous 1D river conductance value obtained without prior information, MFCondPMM simulations use a calibrated homogenous 1D river conductance value obtained with prior information from the metamodel and MMCond simulations consider spatial variability of the river conductance due to aquifer properties calculated with the metamodel.*

Hydraulic conductivities of the Pliocene, Diest and Voort sand are well resolved by the measurement data. Their posterior distribution spread between 0.1 and 10 $m.d^{-1}$. Posterior values of Berchem sand hydraulic conductivity are higher, from 1 to 30 $m.d^{-1}$. Regarding the Kempen clay-sand complex, the posterior distribution spreads from 25 to 100 $m.d^{-1}$. This

suggests that this parameter is not well determined, and its posterior distribution is limited by the upper bound of the investigation range (100 $m.d^{-1}$). For all the aforementioned parameters, no notable differences between the different GW-SW conductance approaches are observed.

Regarding Kasterlee Clay horizontal hydraulic conductivities, posterior distributions for the zone 1 show important differences between the considered approaches. Posterior values for MFCond spread from 0.1 to 25 $m.d^{-1}$ (MAP = 1.3 $m.d^{-1}$), while for MMCond and MFCondPMM the posterior distributions of this parameter range from 1 to 100 $m.d^{-1}$ (MAP around 70 $m.d^{-1}$). For the zone 2, which covers a much smaller area than zone 1 (Figure 40), no significant differences are observed with posterior distributions between 0.1 and 50 $m.d^{-1}$ and MAP values around 1 $m.d^{-1}$. Regarding the Kasterlee Clay vertical anisotropy, all posterior distributions display a similar spreading over the whole exploration range even though values around 1000 have a higher density.

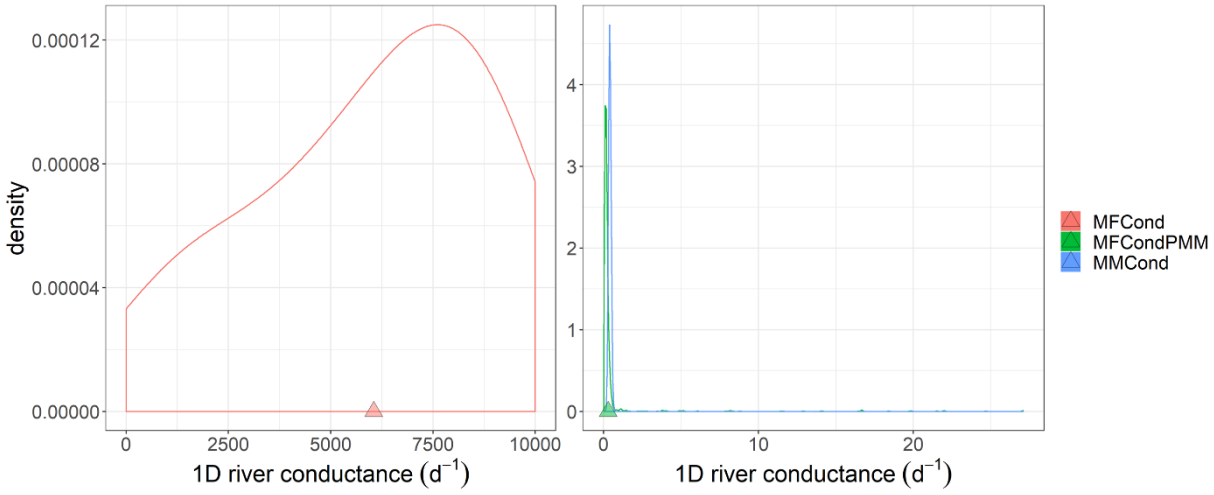

Figure 48: Posterior distribution of the calibrated river conductances obtained with the three approaches, displayed on two different Figures with different axis limits for clarity. Triangles indicate Maximum A Posteriori (MAP) values. MFCond simulations use a calibrated homogenous 1D river conductance value obtained without prior information, MFCondPMM simulations use a calibrated homogenous 1D river conductance value obtained with prior information from the metamodel and MMCond simulations consider spatial variability of the river conductance due to aquifer properties calculated with the metamodel.

Posterior distributions of the 1D river conductance show major differences between the calibration without prior information (MFCond) and the two other approaches (MFCondPMM and MMCond). In MFCond, the calibration algorithm fails at resolving the river conductance, as shown by a marginal posterior distribution spreading over the whole exploration range (Figure 9, left). However, when prior information from the metamodel or when the

metamodel is used directly, a quite narrow posterior distribution ranging from 0.03 to 0.75 d^{-1} is determined (Figure 48, right). Looking at the corresponding data misfits (Figure 10) and likelihoods (not shown), it is observed that the posterior conductance distribution of the MFCond case (Figure 48, left) induces slightly too large data misfits and much too large likelihoods (not shown) compared to the posterior conductance distributions of the MMCond and MFCondPMM cases (Figure 48, right). The larger posterior conductance distribution of the MFCond case (Figure 48, left) is therefore incorrect. The difference between the prior and posterior conductance distribution for the MFCondPMM case shows that this is not forced by the prior distribution which is much wider and has much smaller densities (Figure 45). The mode of the posterior distributions for MMCond and MFCondPMM is slightly lower for MFCondPMM (0.13 d^{-1}) than for MMCond (0.38 d^{-1}) but the two distributions overlap substantially.

To investigate model performances on the piezometric evaluation dataset and simulated GW-SW fluxes, 1000 realizations were randomly sampled in the posterior distributions. The results presented hereafter are derived from this sample.

Figure 49 presents the root mean square error (RMSE) calculated on the evaluation piezometric dataset (788 piezometers) as a function of the RMSE calculated on the calibration dataset (100 piezometers) for the three calibration approaches. On the calibration dataset, RMSE values vary between 0.86 and 1.11 m for MFCond while they range from 0.83 to 1.03 m for MMCond and between 0.78 and 1.01 m for MFCondPMM. These results show that a slightly better calibration fit was obtained by integrating the metamodel directly and even a better one when the metamodel was used to obtain prior information.

RMSE on the evaluation dataset are not well correlated with the RMSE on the calibration dataset and show less disparities between the different approaches. MFCond shows the most dispersion with RMSE values between 0.89 and 1.20 m. MMCond shows slightly less dispersion, with RMSE ranging from 0.92 to 1.13 m. MFCondPMM leads to RMSEs between 0.91 and 1.17 m. These disparities do not seem significant, highlighting the low sensitivity of these measurements to GW-SW conductance values. Moreover, a scatter plot of simulated vs observed piezometric heads does not show significant disparities between the different GW-SW conductance approaches (supplementary material in Appendix C, Figure B).

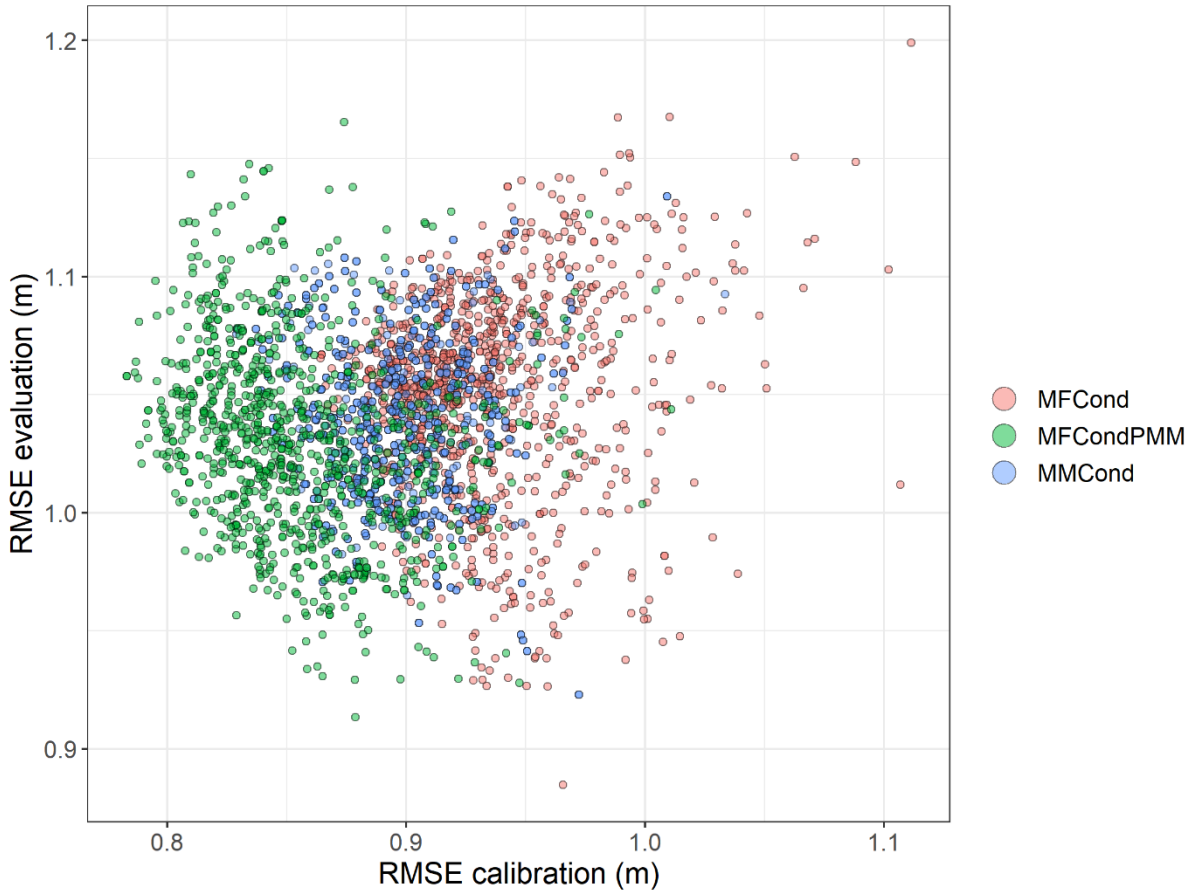

Figure 49: Root mean square error (RMSE) on the calibration piezometric dataset as a function of RMSE on the evaluation dataset. MFCond simulations use a calibrated homogenous 1D river conductance value obtained without prior information, MFCondPMM simulations use a calibrated homogenous 1D river conductance value obtained with prior information from the metamodel and MMCond simulations consider spatial variability of the river conductance due to aquifer properties calculated with the metamodel.

Figure 50 presents the comparison between simulated flow to surface water and time-averaged values of river discharge measurements for the different GW-SW conductance and groundwater recharge parameterization approaches. The comparison with the different GW-SW conductance approaches (Figure 50, a) was performed for the 1000 realizations randomly sampled in the posterior distributions. MMCond and MFCondPMM simulate very similar flow to surface water in the four sub-catchments (Figure 41). Observations fall within the uncertainty range due to parameter values for Aa 02 and KN 01, however for Aa 01 and KN 02 sub-catchments, the models slightly overestimate the water flow to surface water. MFCond simulates slightly higher groundwater fluxes to surface water than MMCond and MFCondPMM and slightly overestimates flow to surface water in KN 01 sub-catchment. Most of the differences between the different GW-SW conductance approaches and between simulated and measured value are in the range of the uncertainties we consider on urban-

runoff (Figure 50, b). Only the overestimation of river discharge at Aa 01 gauging station by the three models exceed this uncertainty range.

Concerning the groundwater recharge approaches (Figure 50, c), they all overestimate flow to surface water in Aa 01 sub-catchment and these errors are larger than the uncertainties we estimated on parameter values (Figure 50, a) and we assume on urban-runoff (Figure 50, b). For the three other gauging stations (Aa 02, KN 01 and KN 02), the three models that consider variable groundwater depth in the groundwater recharge simulations (Reference, RTUnsat, NoSubGridE and NoSubGridESV) simulate flow to surface water within the uncertainty range estimated on parameter values and assumed on urban-runoff. Nevertheless, RTUnsat predicts higher flow to surface water than Reference, RTUnsat, NoSubGridE because it simulates less transpiration and hence more recharge (see section IV.4.2.2.2) and surface runoff (not shown). The two approaches that does not consider groundwater depth sub-grid variability (NoSubGridE and NoSubGridESV) predict slightly more recharge but less surface runoff than the Reference model, thus a compensation occurs and simulated flow to surface water are similar. However, these differences can lead to different groundwater and GW-SW fluxes simulations (see section IV.4.2.2). Finally, the model that considers a homogenous groundwater depth of 2 m in the groundwater recharge calculations (GWD2m) simulates values exceeding the upper bound of the uncertainty range for KN 01 and especially KN 02 sub-catchments. This indicates that this model overestimates groundwater recharge in these sub-catchments.

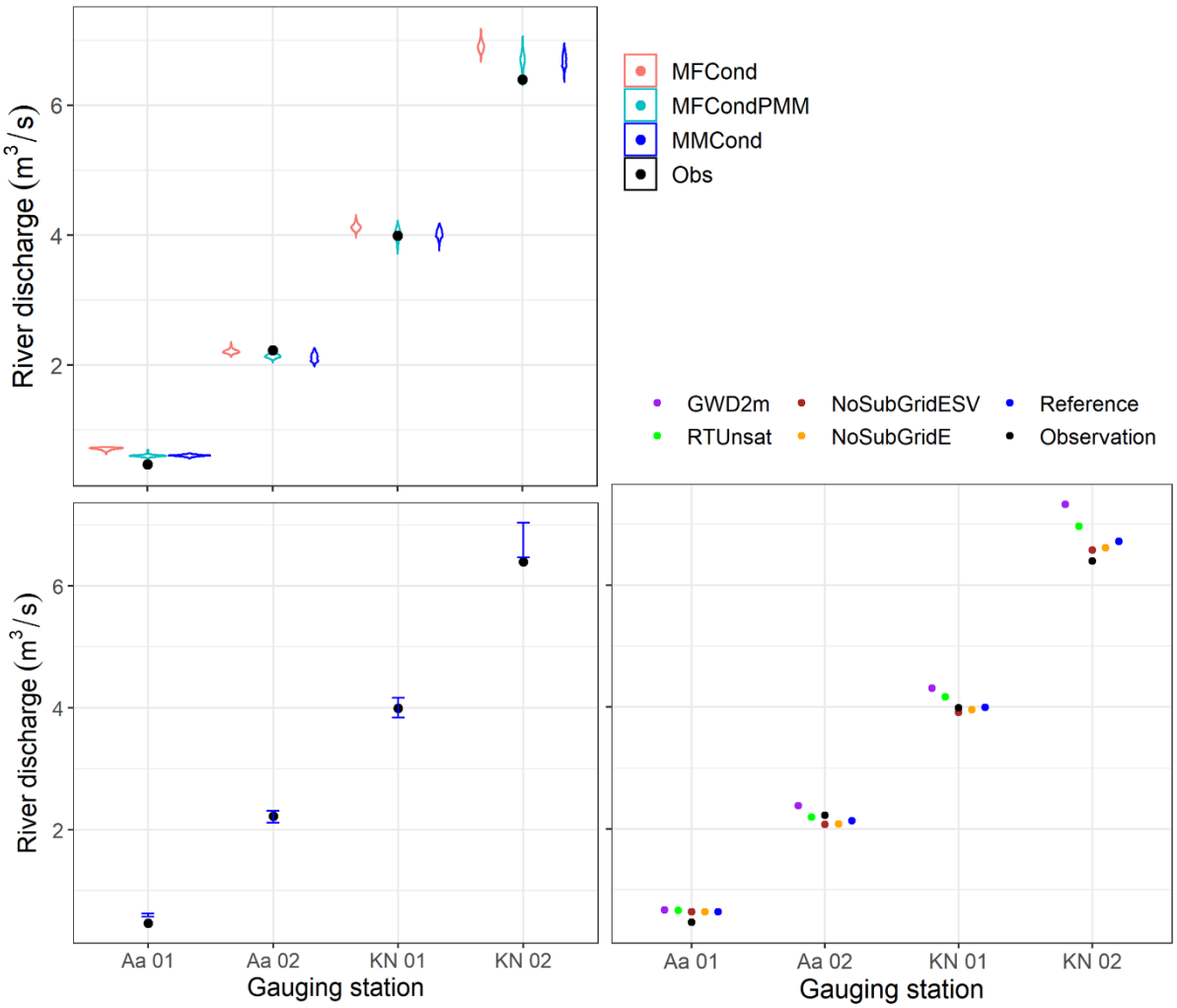

Figure 50: Comparison between simulated flow to surface water and time-averaged values of river discharge measurements for the different sub-catchments (Figure 41). Plot (a) shows the three different GW-SW approaches that have been calibrated, the violin plots display the density obtained by sampling the posterior distributions. Plot (b) illustrates the estimated uncertainties as a result of runoff on built-up areas (0.3 to 0.4 m.y^{-1}). Plot (c) presents the differences due to the different groundwater recharge approaches. MFCond simulations use a calibrated homogenous 1D river conductance value obtained without prior information, MFCondPMM simulations use a calibrated homogenous 1D river conductance value obtained with prior information from the metamodel and MMCond simulations consider spatial variability of the river conductance due to aquifer properties calculated with the metamodel and its MAP set of parameters is used in (b) and (c). In (c), the Reference simulation considers spatially variable groundwater depth, tree root water uptake from the saturated zone and sub-grid variability in the groundwater recharge calculations. GWD2m considers a homogenous groundwater depth of 2m in the groundwater recharge calculations, RTUnsat does not consider tree root water uptake from the saturated zone. NoSubGridESV does not consider sub-grid variability of groundwater depth, soil and land cover and NoSubGridE considers only sub-grid variability of soil and land cover but not of groundwater depth.

IV.4.2.2. Model intercomparison

This section discusses the sensitivity of simulated fluxes spatial distribution to the different groundwater recharge and GW-SW conductance approaches using one set of aquifer hydraulic parameters. First, simulated GW-SW fluxes are compared for the three different GW-SW conductance approaches. Second, simulated groundwater recharge outputs are compared for

the five different groundwater recharge approaches. Finally, simulated groundwater vertically averaged cell-by-cell fluxes are compared for the three GW-SW conductance approaches and three selected groundwater recharge approaches (Reference, GWD2m and NoSubGridESV).

To isolate the effect of GW-SW conductance and groundwater recharge, all simulations use the same aquifer hydraulic parameters (Table 15). MFCondPMM uses a river conductance value equivalent to the average value calculated by the metamodel in MMCond. MFCond uses a value of 20 d^{-1} as in Gedeon (2008), which seems reasonable if only streambed conductance is considered. For instance, it could correspond to a streambed with a thickness of 0.1 m and a hydraulic conductivity of 2 $m.d^{-1}$. All parameter values and associated data misfits are within the range of the derived posterior distributions presented in Figure 47 and 48.

Figure 51 shows the groundwater hydraulic heads and depths simulated with the reference approach, which uses MFCond description of the GW-SW conductance and considers variable groundwater depth, tree root water uptake from the saturated zone and sub grid variability of groundwater depth, soil and land cover in the groundwater recharge simulations. Groundwater is flowing towards the West. Moreover, the drawdown due to some important pumping wells (Figure 39 and Table 7) can be clearly seen. Simulated groundwater depth is shallow in most of the catchment, 65 % of the 400x400 m model cells have a groundwater depth lower than 2 m and 30 % lower than 1 m. Groundwater depth is lower in the eastern (upstream) part of the catchment. Relatively high dune areas in the central part of the catchment show deep groundwater table (> 5m).

Table 15: Aquifer hydraulic parameter values used for the model intercomparison of the different recharge and GW-SW conductance approaches. Ks *refers to saturated hydraulic conductivity and* VA *to vertical anisotropy.* Z1 *and* Z3 *refers to the zone 1 and 3 of the Kasterlee Clay (Figure 40).*

Parameter	MMCond	MFCond	MFCondPMM
Ks Kempen ($m.d^{-1}$)	91	91	91
Ks Pliocene ($m.d^{-1}$)	2.9	2.9	2.9
Ks Kasterlee Clay Z1 ($m.d^{-1}$)	8.8	8.8	8.8
Ks Kasterlee Clay Z3 ($m.d^{-1}$)	5.8	5.8	5.8
VA Kasterlee Clay Z1	278	278	278
VA Kasterlee Clay Z3	824	824	824
Ks Diest ($m.d^{-1}$)	1.7	1.7	1.7
Ks Berchem ($m.d^{-1}$)	17.6	17.6	17.6
Ks Voort ($m.d^{-1}$)	0.47	0.47	0.47
1D River conductance (d^{-1})	Spatialized	20	0.47
RMSE (m)	0.85	0.94	0.85

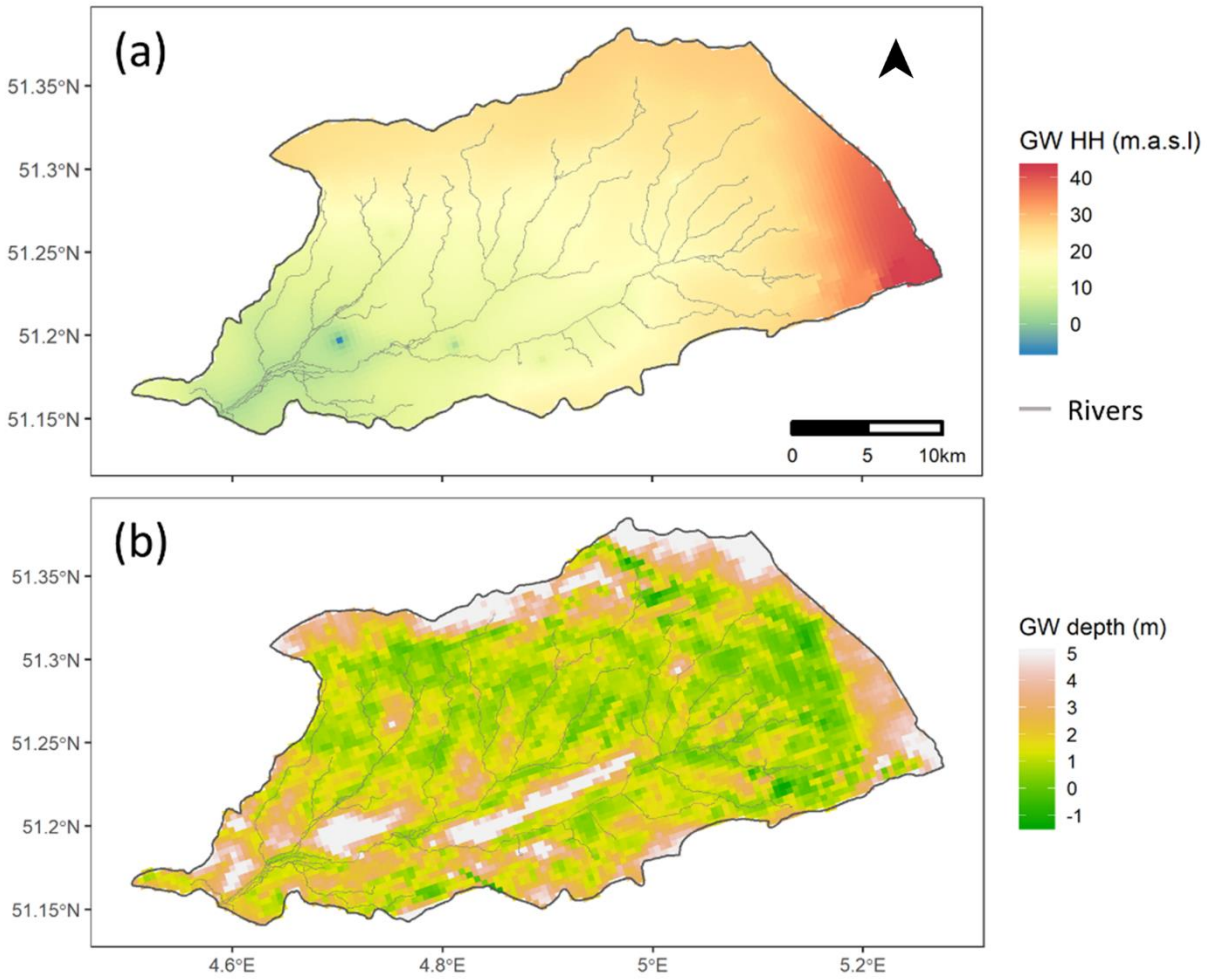

Figure 51: Map of groundwater hydraulic head (GW HH) and groundwater depth (GW depth) simulated with the reference approach

IV.4.2.2.1. Groundwater – surface water exchange fluxes

The spatially distributed GW-SW conductances obtained with the reference approach (MMCond) and the difference to MFCond and MFCondPMM are shown in Figure 52 for the rivers and in Figure 53 for the drains. The main factor affecting the metamodel GW-SW conductance in our case study is the hydraulic conductivity of the subsurface. River and drain conductance calculated with the metamodel are higher in the north-eastern part of the catchment, where it is influenced by the hydraulic conductivity of the Kempen clay-sand complex, and in south-eastern part of the catchment, where it is mainly influenced by the hydraulic conductivity of the Berchem sand. The influence of the low vertical hydraulic conductivity of the Kasterlee Clay can be seen in the middle of the catchment. Furthermore, the influence of surface water network density generates local heterogeneity. For the other approaches (MFCond and MFCondPMM) the 1D GW-SW conductance parameter (see Table

15 for river and equal to 1 d^{-1} for drains) is multiplied by the streambed width, which depends on the surface water body classification (Figure 41, 15 ,10 and 5 m for the first, second and third order rivers respectively), to obtain the 2D GW-SW conductance. Regarding river conductance in MMCond, the calibrated value of 20 d^{-1} lead to much higher 2D conductance values all over the catchment than in the reference case (MMCond). On the other hand, the 1D river conductances used in MMCond and drain conductances used in both MFCond and MFCondPMM have similar average value than the reference case. In these cases, 2D GW-SW conductance differences reflect the metamodel spatialization. 2D GW-SW conductances calculated with the metamodel (MMCond) are higher in the north-eastern and south-eastern part of the catchment and smaller in the central part.

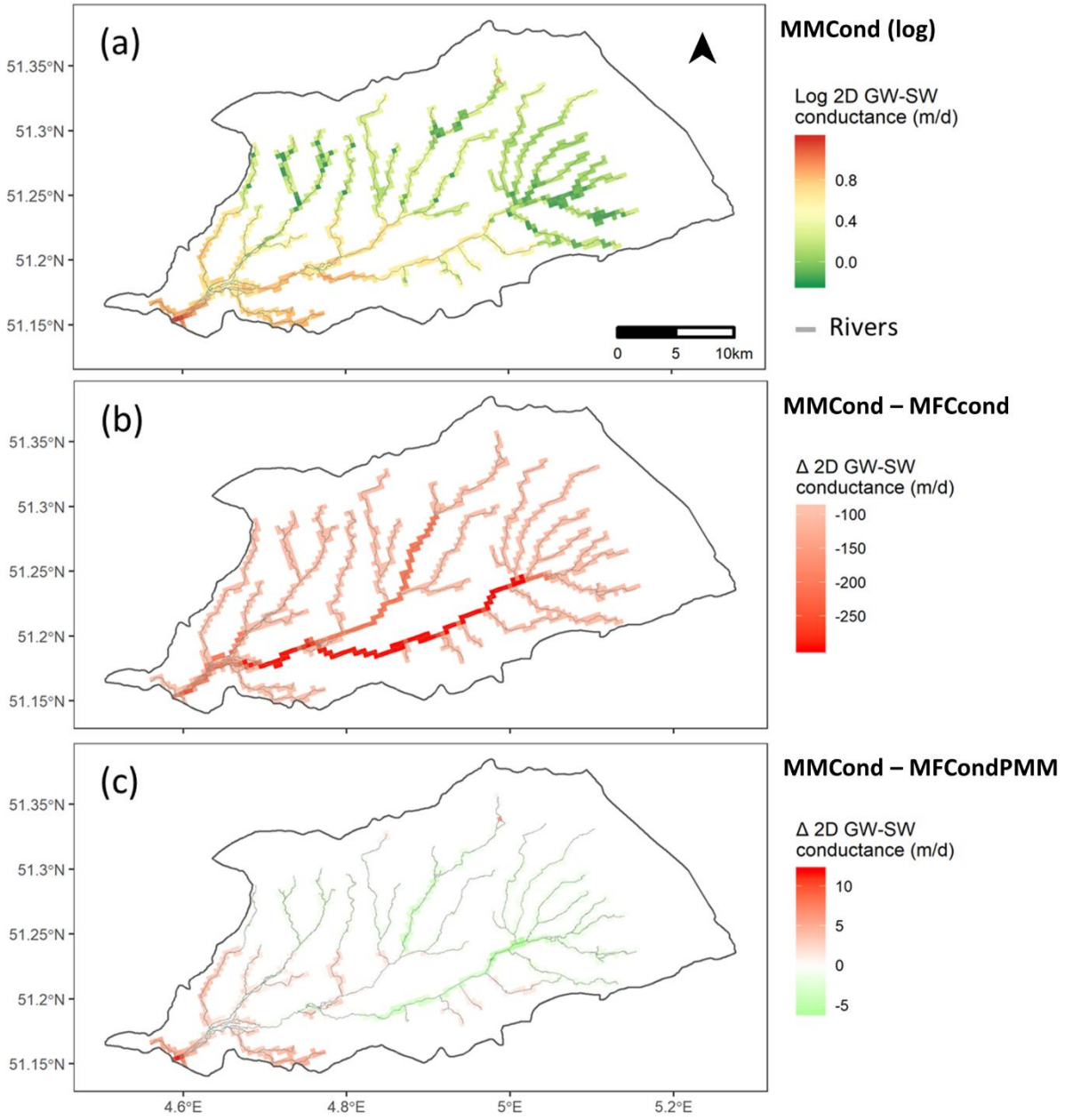

Figure 52: Maps of (a) 2D groundwater – surface water (GW-SW) conductances of the rivers calculated with the metamodel and used in the reference simulation (MMCond), differences to (b) the 2D GW-SW conductances calibrated and considered in the MFCond simulation (MMCond − MFCond) and (c) the 2D GW-SW conductances calibrated with prior information from the metamodel and considered in the MMCondPMM simulation (MMCond − MFCondPMM)

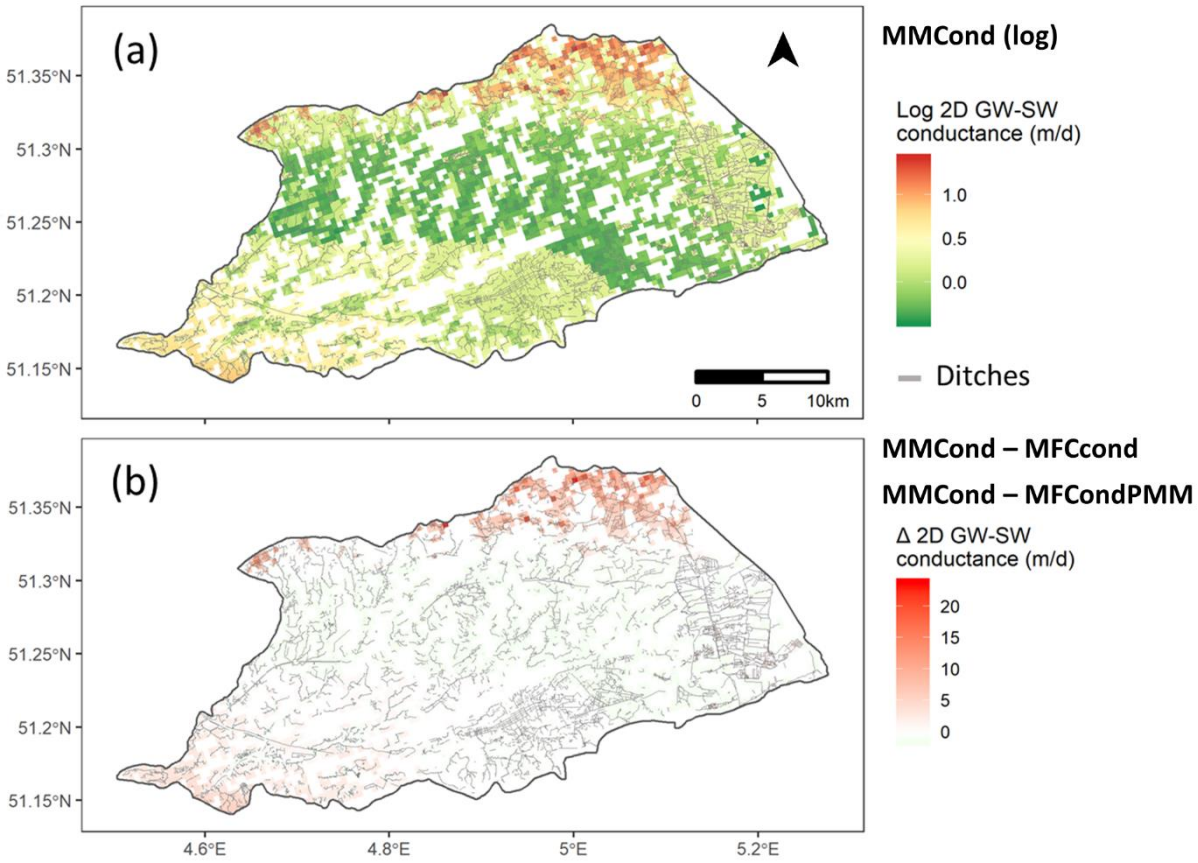

Figure 53: Maps of (a) 2D groundwater – surface water (GW-SW) conductances of the drains calculated with the metamodel and used in the reference simulation (MMCond) and differences to (b) the 2D GW-SW conductances calibrated and considered in the MFCond and MFCondPMM simulation (MMCond – MFCond and MMCond – MFCondPMM)

These differences of GW-SW conductance are reflected in GW-SW fluxes spatial distribution. This is highlighted in Figure 54, which shows the map of simulated GW-SW fluxes (rivers plus drains) in the reference approach (MMCond) and maps of differences between the simulations. GW-SW volumetric flows were normalized by the grid cell area (16000 m²) and negative fluxes indicate fluxes from groundwater to surface water. GW-SW fluxes simulated by the reference model (MMCond) vary from −9.4 $m.y^{-1}$ to 2.6 $m.y^{-1}$ with an average value of 0.68 $m.y^{-1}$. Differences with fluxes simulated with MFCond (MMCond − MFCond) vary from −7.4 to 9.1 $m.y^{-1}$ with an average value of 0.088 $m.y^{-1}$. Differences from MFCondPMM to MMCond (MMCond – MFCondPMM) are less important, varying between −3.6 and 1.3 $m.y^{-1}$, with an average value of −0.0018 $m.y^{-1}$. Note that mean values are strongly influenced by cells with drains where very little flow occurs.

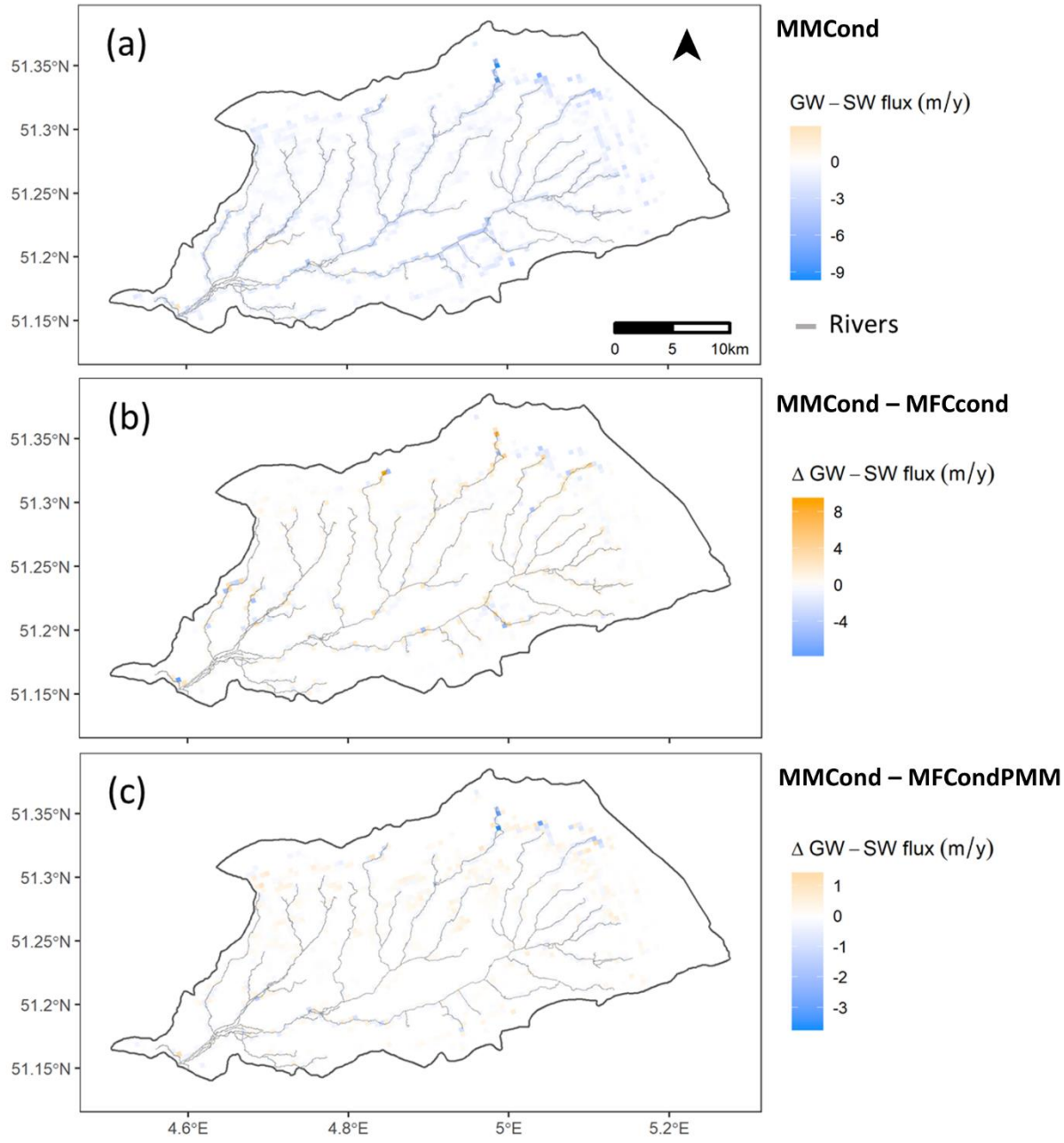

Figure 54: Maps of (a) simulated groundwater – surface water (GW-SW) fluxes (rivers plus drains) by the MMCond (spatialized river conductance from the metamodel) model, differences to (b) the GW-SW fluxes simulated by the MFCond (calibrated river conductance) model (MMCond – MFCond) and (c) the GW-SW fluxes simulated by the MFCondPMM (calibrated river conductance with a priori information from the metamodel) model (MMCond – MFCondPMM). GW-SW fluxes refer to GW-SW volumetric flows normalized by the grid cell area and negative fluxes indicate fluxes from groundwater to surface water

IV.4.2.2.2. Groundwater recharge

Probability density functions (PDF) and mean values of the simulated spatially distributed groundwater recharge are presented in Figure 55 for the different approaches. They spread over a large range from −0.55 to 0.55 m.y^{-1}, with modal values around 0.3 m.y^{-1}.

Considerable differences are observed between GWD2m (groundwater recharge calculated with a groundwater depth of 2 m) and the other simulations, which consider variable groundwater depth in the groundwater recharge calculations. Setting the groundwater depth to 2 m leads to overall larger groundwater recharge and a narrower range of values (mean = 0.33 $m.y^{-1}$, min = −0.13 $m.y^{-1}$, max = 0.48 $m.y^{-1}$). The Reference approach that considers variable groundwater depth, tree root water uptake from the saturated zone and sub-grid variability, generates a larger groundwater recharge distribution with mean values around 0.27 m y^{-1}, minimum values around −0.39 $m.y^{-1}$ and maximum values around 0.47 $m.y^{-1}$. Tree root water uptake from the saturated zone mainly affects the lower end of the groundwater recharge range. Not considering this process (RTUnsat) limits minimum values to around −0.18 $m.y^{-1}$ whereas it does not impact strongly the average value (0.28 $m.y^{-1}$). Although the Reference model, NoSubGridE and NoSubGridESV have similar mean values (0.27 $m.y^{-1}$), the shape of their generated probability distribution functions differs significantly, especially for NoSubGridESV with no sub-grid variability in elevation and vegetation. This leads to a multimodal distribution. NoSubGridE generates distribution more similar to the Reference model with differences mainly in the lower range of recharge values. Not considering sub-grid variability leads to the simulation of more extreme minimum and maximum values (min = −0.41 and −0.55, max = 0.50 and 0.59 $m.y^{-1}$ for NoSubGridE and NoSubGridESV respectively).

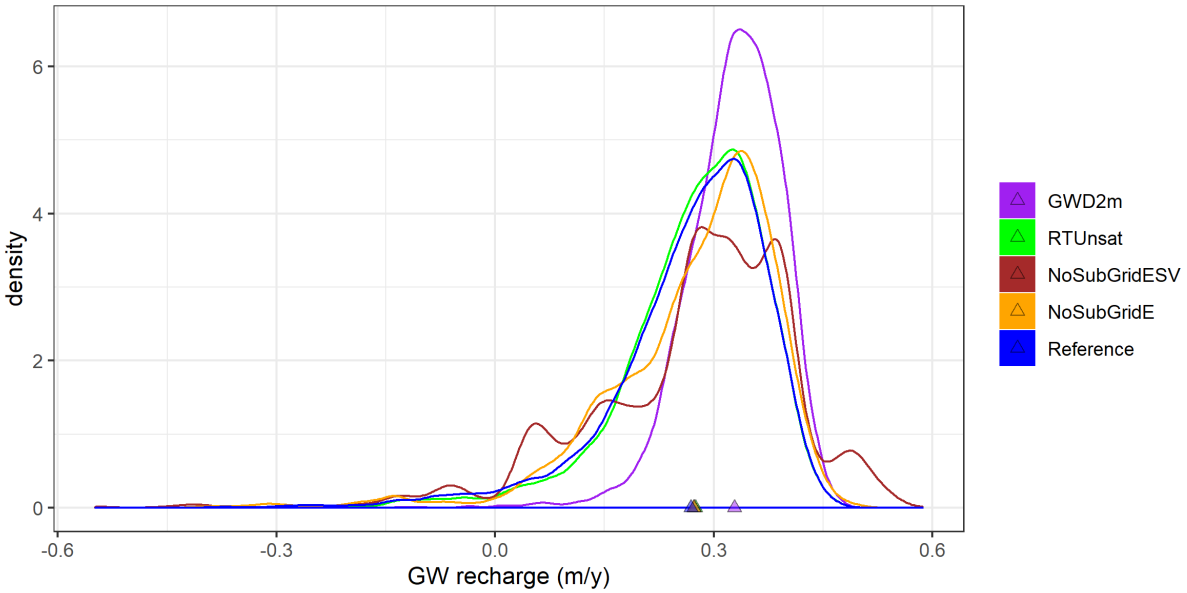

Figure 55: Probability density functions of the spatially distributed steady-state groundwater recharge calculated from the HYDRUS simulations obtained with different approaches. Triangles indicate mean recharge values. The Reference simulation considers spatially variable groundwater depth, tree root water uptake from the saturated zone and sub-grid variability in the groundwater recharge calculations. GWD2m considers a homogenous groundwater depth of 2m in the groundwater recharge calculations, RTUnsat does not consider tree root water uptake from the saturated zone. NoSubGridESV does not consider sub-grid variability of groundwater depth, soil and land cover and NoSubGridE considers only sub-grid variability of soil and land cover but not of groundwater depth

The spatial distribution of groundwater recharge as a function of the modeling approach is investigated in Figure 56, mapping groundwater recharge in the Reference approach and showing the differences compared to the other approaches.

In the Reference approach, groundwater depth (Figure 51) is the main factor controlling the spatial variability of simulated groundwater recharge. Recharge is lower where groundwater is shallow as in the eastern part of the catchment, where it even becomes negative locally. Furthermore, the influence of land cover and soil can be discerned when comparing the groundwater recharge map with the land cover and soil texture maps presented in Figure 42. The influence of land cover can be mainly seen with lower recharge in urban areas and in forest enhancing negative recharge in shallow groundwater areas as a result of root water uptake from the groundwater. The influence of soil texture can be discerned in the western part of the catchment where soil texture is finer than in the rest of the study area covered mainly by sandy soils and thus is an area with lower groundwater recharge.

Differences between the groundwater recharge simulated with the Reference approach and with the other approaches reveal some important factors. The most significant is the effect of groundwater depth highlighted with the difference to GWD2m. The difference map shows that calculating groundwater recharge only with groundwater depth of 2 m (approximately the average groundwater depth simulated on the catchment) generates larger (up to around 0.67 $m.y^{-1}$) simulated groundwater recharge in areas with shallow groundwater (depth < 2m) and smaller recharge (up to 0.4 $m.y^{-1}$), in areas with deeper groundwater (depth > 2 m). The simulation that does not consider tree water uptake in the saturated zone (RTUnsat) shows much less difference compared to the Reference approach than the GWD2m simulation. However, locally, in areas with trees and shallow groundwater, it simulates groundwater recharge up to 0.26 $m.y^{-1}$ higher than in the Reference case. Finally, the two simulations considering no elevation (NoSubGridE) and elevation and land cover (NoSubGridESV) sub-grid variability show important (> 0.5 $m.y^{-1}$) differences relative to the Reference case, in which sub-grid variability is accounted for. These differences are spread all over the catchment. Differences to the Reference case are roughly two times more important for NoSubGridESV than for NoSubGridE. This shows that sub grid variability in elevation and in S/V combinations are equally important in our groundwater recharge simulations.

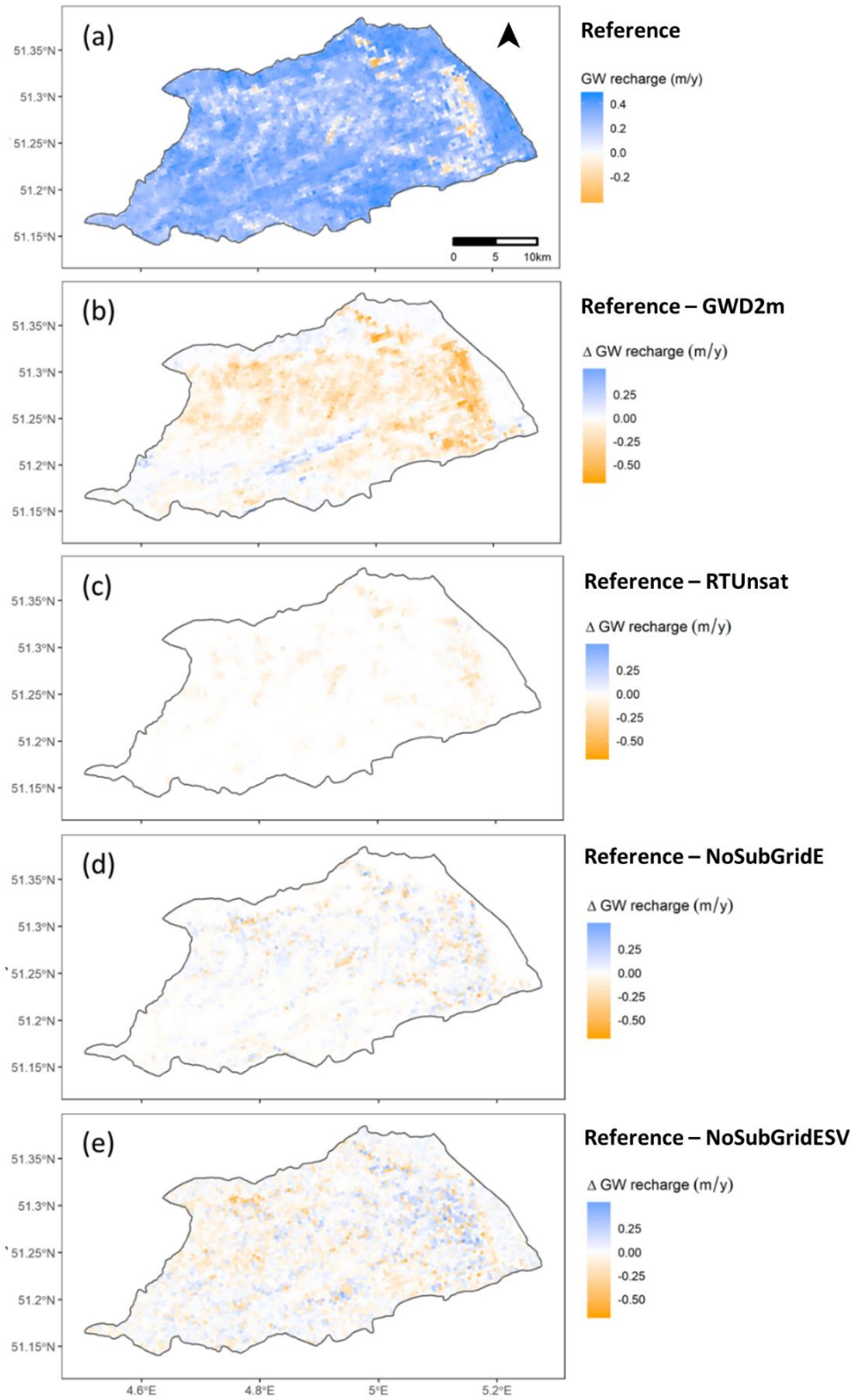

Figure 56: Maps of (a) simulated groundwater (GW) recharge by the Reference simulation, differences to (b) the simulation considering homogenous groundwater depth of 2 m in the groundwater recharge simulations (Reference − GWD2m), (c) the simulation not considering tree root water uptake from the saturated zone (Reference – RTUnsat), the simulations not considering sub-grid variability of groundwater depth (d, Reference − NoSubGridE) and of soil, vegetation and groundwater depth (e, Reference – NoSubGridESV)

IV.4.2.2.3. Groundwater fluxes

Figure 57 presents the vertically averaged cell-by-cell groundwater fluxes simulated by the Reference model, which uses the metamodel to calculate GW-SW conductance (MFCond) and consider variable groundwater depth, tree root water uptake from the saturated zone and sub-grid variability of groundwater depth, soil and vegetation to calculate groundwater recharge. The impact of different groundwater recharge and GW-SW conductance parametrization approaches on the simulated vertically averaged cell-by-cell groundwater flux magnitudes is shown respectively in Figure 58 and Figure 59. Concerning groundwater recharge, only the simulation that does not account for groundwater depth variability (GWD2m) and the simulation that does not consider sub-grid variability of soil, land cover and groundwater depth (NoSubGridESV) are compared to the Reference simulation. Groundwater recharge and GW-SW fluxes have been excluded as they are presented in previous figures.

The Reference simulation shows groundwater fluxes up to 33 $m.y^{-1}$ with a mean value around 3 $m.y^{-1}$. The influence of the aquifer thickness can be seen with higher flux magnitudes towards the west (Figure 39). Moreover, high groundwater fluxes induced by pumping wells appear clearly.

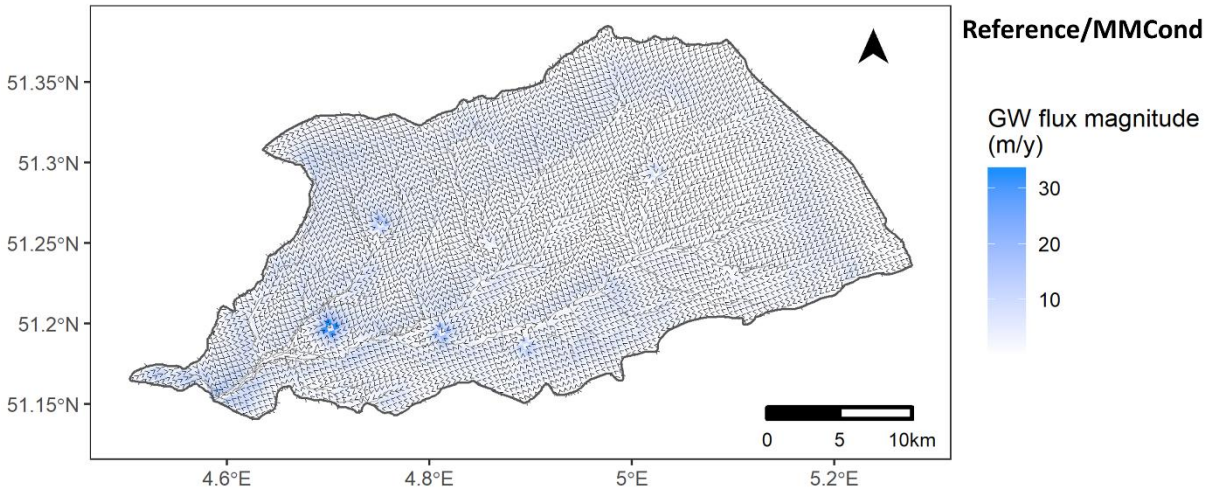

Figure 57: Map of vertically averaged cell-by-cell groundwater fluxes magnitude (color scale) and direction (black arrows) simulated by the Reference model, which uses the metamodel to calculate GW-SW conductance (MMCond) and consider variable groundwater depth, tree root water uptake from the saturated zone and sub-grid variability of groundwater depth, soil and land cover in groundwater recharge calculations

The groundwater recharge simulation that does not consider variable groundwater depth (GWD2m) induces groundwater flux magnitudes up to around 1 $m.y^{-1}$ higher and 1.5 $m.y^{-1}$ lower than in the Reference case. Approximately 50 % of model cells show groundwater flux

magnitude with more than 0.1 $m.y^{-1}$ difference to the Reference simulation and around 3.2 % show difference of more than 0.5 $m.y^{-1}$. The groundwater recharge simulation that does not consider sub-grid variability (NoSubGridESV) induces smaller differences, up to 1.9 $m.y^{-1}$ higher and 0.4 $m.y^{-1}$ lower. Approximately 20 % of model cells show groundwater flux magnitude with more than 0.1 $m.y^{-1}$ difference from the Reference simulation and only 0.2 % show difference of more than 0.5 $m.y^{-1}$.

The differences in flux magnitudes induced by the different GW-SW conductance approaches are higher. The simulation with higher river conductance values all over the catchment than the reference case (MFCond) simulates groundwater flux magnitudes up to around 13 $m.y^{-1}$ higher and 2.6 $m.y^{-1}$ lower than the reference case. The frequency distribution of the groundwater flux magnitude differences between MFCond and the reference simulation indicates that 63 % of the model cells show difference of more than 0.1 $m.y^{-1}$ and 15 % more than 0.5 $m.y^{-1}$. On the other hand, the simulation with similar average value of river and drain conductance than the reference case but not considering the spatial distribution due to aquifer conductance (MFCondPMM), simulates groundwater flux magnitudes up to around 1.3 $m.y^{-1}$ higher and 2.1 $m.y^{-1}$ lower than the reference case. The frequency distribution of the groundwater flux magnitude differences between MMCondPMM and the reference simulation indicates that 40 % of the model cells show difference of more than 0.1 $m.y^{-1}$ and 2.3 % more than 0.5 $m.y^{-1}$.

Therefore, among the different approaches we have considered, MFCond, which used much higher river conductance than the Reference simulation, appears to lead to the most different vertically averaged groundwater flux spatial distribution. GWD2m (fixed groundwater depth in groundwater recharge calculations) and MFCondPMM (no spatial variability of GW-SW conductance due to aquifer and surface network properties) show similar differences, which can be locally important. Finally, not considering sub-grid variability (NoSubgridESV) appears to have little effect on vertically averaged cell-by-cell groundwater fluxes.

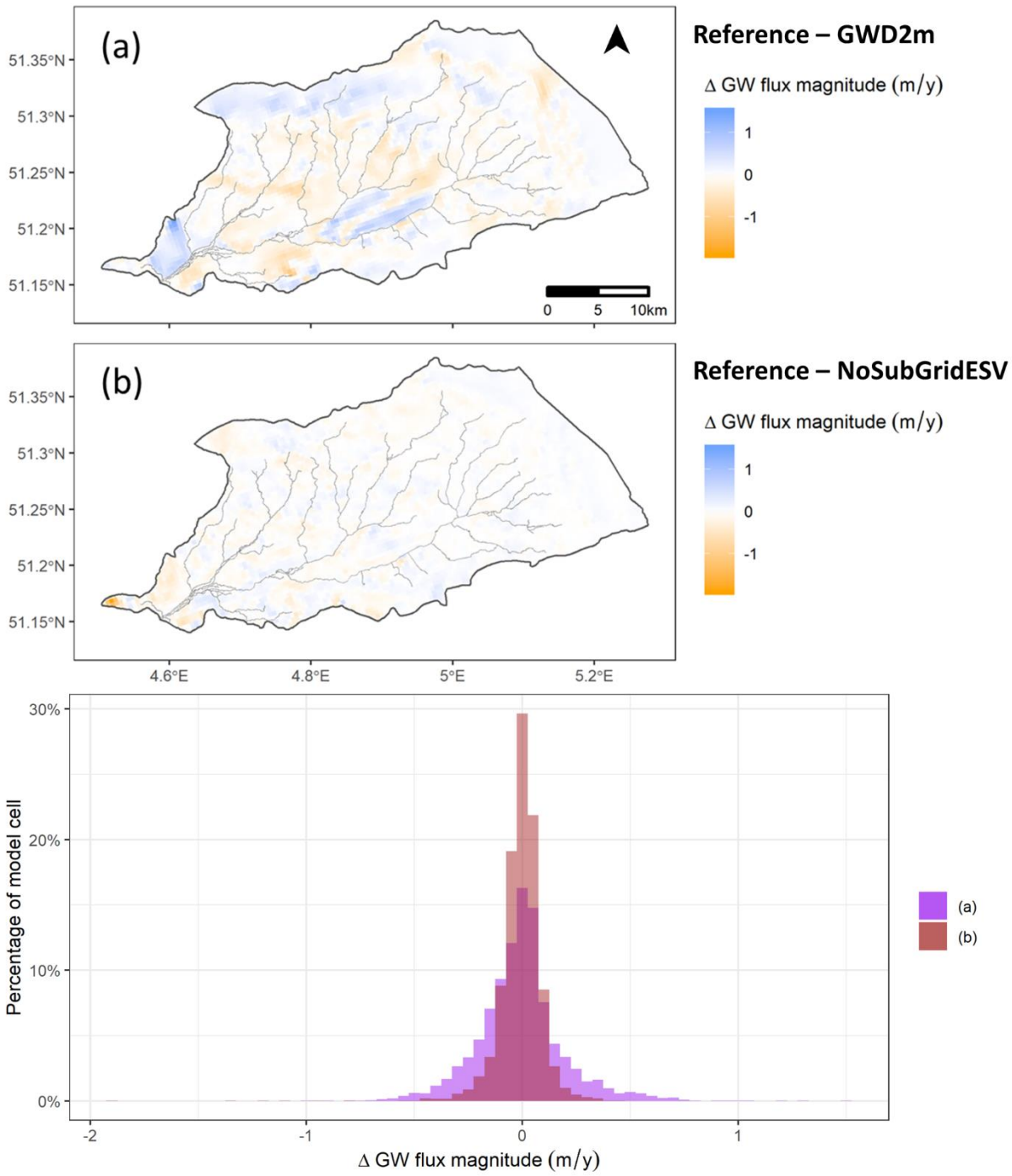

Figure 58: Maps of simulated groundwater (GW) flux magnitudes differences from the reference simulation considering variable groundwater depth and sub-grid variability (Figure 57) to (a) the simulation considering homogenous groundwater depth of 2 m in groundwater recharge simulation (Reference – GWD2m) and (c) the simulation not considering sub-grid variability (Reference – NoSubGridESV). (c) shows the histogram of the differences

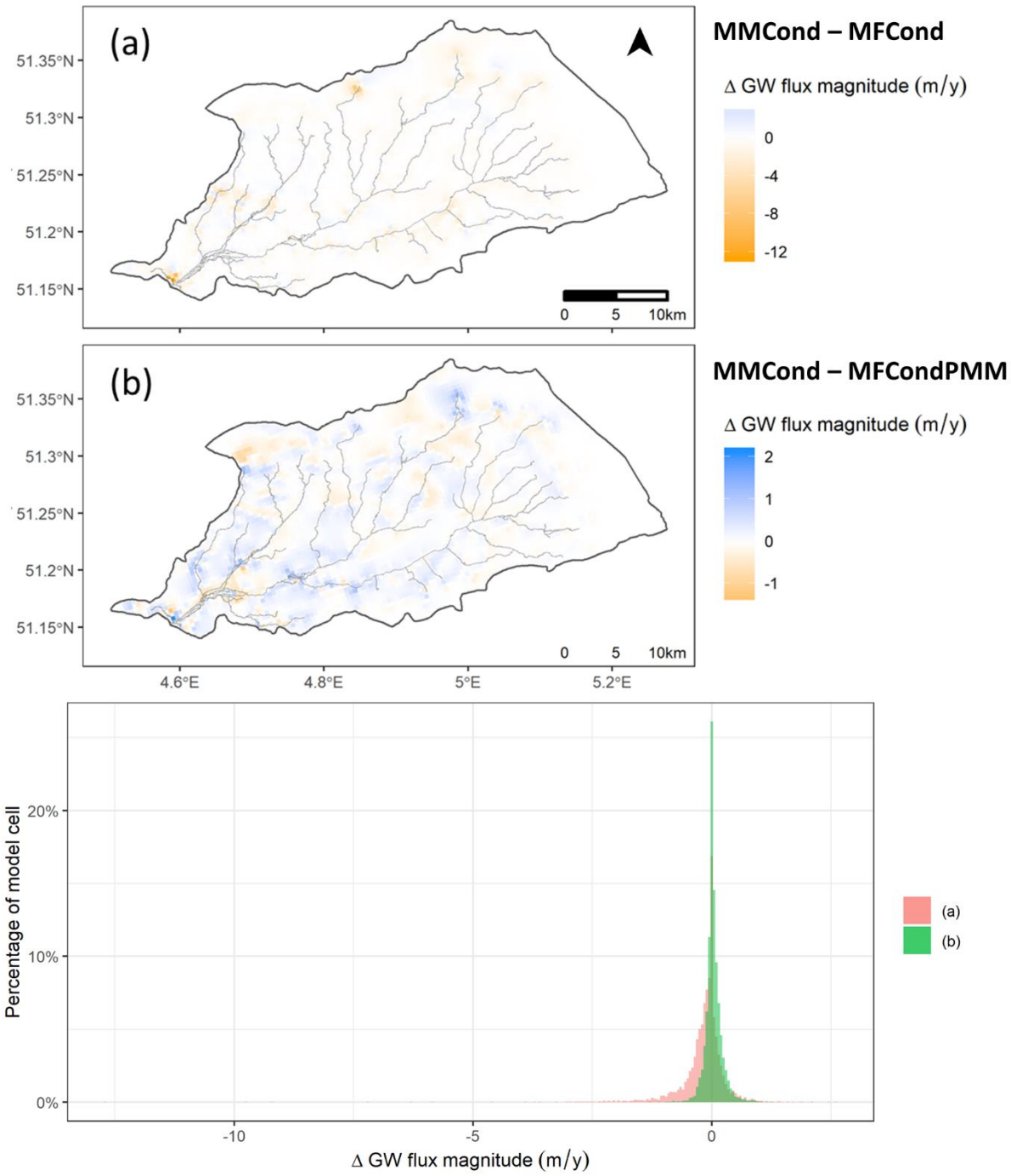

Figure 59: Maps of simulated groundwater (GW) flux magnitudes differences from the reference (spatialized river conductance from the metamodel) simulation (MMCond, Figure 57) to (a) the MFCond (calibrated conductance) simulation (MMCond – MFCond) and (b) the MFCondMM (calibrated conductance with a priori information from the metamodel) simulation (MMCond – MFCondPMM).(c) shows the histogram of the differences.

IV.5.Discussion

The calibration of aquifer hydraulic properties presented some difficulties. Posterior distributions of the Kempen clay-sand complex show unexpectedly high values, exceeding the measurements upper bound (Table 6), and this was found for all the GW-SW approaches

considered. Since the hydraulic heads in the piezometers of the evaluation dataset in the region where the Kempen clay-sand complex is present are underestimated by the calibrated models (supplementary material in Appendix C, Figure C), the high values probably overestimate the reality and the calibration dataset did not contain sufficient information about this hydrogeological layer. This probably explain the overestimation of flow to surface water in the Aa 01 sub-catchments as well. Regarding Kasterlee clay, problems arise for MMCond and MFCondPMM which show wide posterior distributions, exceeding the upper bound of measurements (Table 6). This seems to be due to model convergence issues when low river conductance values are used.

Concerning GW-SW conductance, we show that following the standard approach in which the conductance is viewed to depend on streambed properties only, calibration of this parameter can be problematic as the sensitivity of piezometric measurements to GW-SW conductance is low. In our case study, the posterior river conductance distribution for MFCond is excessively large (as shown by too low likelihoods) and formally incorrect. The associated results are thus also incorrect. However, this is what we got from running a state-of-the-art MCMC sampler on MFCond. Therefore, one is very likely to get wrong uncertainty estimates for the considered case study. The metamodel proposed by A. Di Ciacca et al. (2019), which limits the GW-SW conductance depending on the aquifer conductance, allowed a better identification of this parameter. Two different applications of the metamodel were investigated. First, we used it to directly calculate conductances from aquifer conductivities and other model characteristics (MMCond) and second to define an a-priori distribution used to calibrate the river conductance (MFCondPMM). These two ways of using the metamodel led to similar average GW-SW conductance and other hydraulic parameter values. MFCondPMM led to a slightly lower average GW-SW conductance and a better performance on the calibration piezometric dataset. Nonetheless, performances on the evaluation dataset are similar and river conductance posterior distributions obtained with the two approaches are overlapping. Furthermore, MMCond produces spatially variable GW-SW conductances whereas in MFCondPMM, a constant conductance for the entire catchment is calibrated. The spatial distribution of GW-SW conductance could not be evaluated using the available observation dataset but its influence on simulated GW-SW and groundwater fluxes was demonstrated.

The slightly different average river conductance posterior distributions obtained with MFCond and MFCondPMM could be due to the influence of streambed conductance not taken into account in MMCond or to the implementation of the metamodel (e.g. calculation of aquifer thickness and representative hydraulic conductivities, representative distance between surface water bodies). An alternative to the approaches presented in this study would be to use the metamodel to estimate aquifer conductance while still calibrating an additional streambed conductance. This would lead to a spatially variable GW-SW conductance. The overall conductance would then correspond with the harmonic average of both conductances. When both conductances differ a lot, then the overall conductance will depend mainly on one of the two − the smallest one − and thus, this approach will not be very different from the approaches presented in this study. However, when both conductances have similar values this approach could be relevant. Furthermore, more testing would be needed on the calculation of representative hydraulic conductivities in the case of heterogenous aquifers. In our study, piezometric and river discharge measurements are not sensitive to GW-SW conductance and this is likely to happen in other studies. Therefore, evaluation of GW-SW conductance parameterization would require spatialized estimates of GW-SW and/or groundwater fluxes as it was shown to be sensitive simulation outputs to this parameter. Although measurement methods for estimating GW-SW fluxes have considerably improved over the last decades (Fleckenstein et al., 2010; González-Pinzón et al., 2015; Kalbus et al., 2006; Le Lay et al., 2019; Mamer and Lowry, 2013), the scale discrepancy between observations/estimations and regional model outputs remains a challenge. If we would be able to measure GW-SW fluxes in a spatially distributed way and to compare them with model outputs, we could estimate from these measurements the GW-SW conductance, which in turn depends on the hydraulic aquifer properties. This could help to reduce the uncertainty of the estimated hydraulic aquifer properties. One additional issue is the spatial variability of aquifer properties. In the present study we assumed a uniform hydraulic conductivity for each hydrostratographic unit (except Kasterlee clay which is separated in 3 different zones). However, the spatial variability of the hydraulic conductivity also affects the spatial variability of GW-SW conductances and fluxes. Alternatively, GW-SW conductance parameterization for heterogenous aquifers could be investigated using numerical experiments. This may lead to better implementation of the metamodel in future studies.

Regarding groundwater recharge, the approaches tested rely on 1D variably saturated water flow modeling. Groundwater recharge simulations were not coupled to the groundwater model but implemented using a look-up table (NRF package for MODFLOW). This has the advantage to be simple and computationally efficient while including presumably important processes. Furthermore, the spatio-temporal discretization of the 1D variably saturated models and of the groundwater model are independent. In this study, for instance, groundwater recharge was calculated at a daily time step (with even smaller time steps used for numerical solutions) whereas the groundwater model is in a steady-state mode. Moreover, the number of 1D variably saturated models is not set by the spatial discretization of the groundwater model but by the combinations of soil, vegetation and groundwater depth considered. This allows the representation of sub-grid variability with a relatively low number of variably saturated 1D models. However, the main drawback of this approach is that there is no coupling of fluxes or groundwater depths between groundwater recharge simulations and the groundwater model. Groundwater recharge simulations are done using constant head bottom boundary conditions and therefore do not consider dynamic water table level (e.g. seasonal variation). Further research would be needed to evaluate the uncertainties induced by this simplification. However, in the case of a steady-state groundwater model this seems to be an adequate approach as groundwater level temporal dynamics are not simulated.

Although our groundwater recharge modeling approach aimed at describing properly the spatial variability of groundwater recharge, still some variability was ignored. Soil layering and therefore spatial variability in soil development was not represented. Parameterization of different soil profile developments would require more variably saturated 1D models. The sensitivity of groundwater recharge to soil layering for a particular case could be assessed beforehand to justify this increase in modeling complexity. Preliminary calculations suggest that soil layering is not a major factor to calculate steady-state groundwater recharge in sandy soils typical of the Kleine Nete catchment (not shown). Another issue lies in the root water uptake parameterization. We used one root profile for each vegetation cover, however in reality, these may vary in space (e.g. because of adaptation to groundwater depth) and time (e.g. growing season) (Ghazavi et al., 2008; Thomas et al., 2012). A better approach could be to define root profiles as a function of groundwater depth. Another simplification is that only one crop type (corn) was considered. Furthermore, our groundwater recharge simulations

were run using 28 years of meteorological records (from 1990 to 2017), however the land use/cover changes were neglected. This could be implemented in our modeling framework but would require land cover maps representative of different time periods. Alternatively, land use changes can be predicted using stochastic land use change models (Dams et al., 2008).

Nevertheless, our Reference recharge approach performs quite well when compared with river discharge measurements in most of the catchment area, with errors within the range of parameter and urban-runoff uncertainties. We could show that not considering spatial variability of groundwater depth in the groundwater recharge calculations would lead to an overestimation of flow to surface water network. However, evaluation of groundwater recharge spatial distribution is beyond the reach of available measurements and thus the relevance of our implementation of sub-grid variability and phreatophytes root water uptake remains questionable. Nevertheless, the results obtained with our Reference groundwater recharge approach show good agreement, in term of summary statistics, with the simulation performed by Batelaan & De Smedt (2007) on an area including the Kleine Nete catchment, but approximately five times larger. They simulated a mean groundwater recharge of 0.25 $m.y^{-1}$ for their whole study area and of 0.28 $m.y^{-1}$ for the Nete catchment (approximately two times larger than the Kleine Nete catchment), their minimum and maximum values for the whole study area were, respectively, −0.38 and 0.46 $m.y^{-1}$. We simulated a groundwater recharge spatial distribution on the Kleine Nete catchment with a mean value of 0.27 $m.y^{-1}$, a minimum value of −0.38 $m.y^{-1}$ and a maximum value of 0.47 $m.y^{-1}$. As Batelaan & De Smedt (2007) stated about their WetSpass model: “The development of the model and the parameter estimation is not the result of an a priori ‘upward’ physical approach, but rather a ‘downward’ process, starting from a simple water balance approach, which subsequently evolved by introducing relevant concepts and input data step by step”. In our case, we followed an a priori ‘upward’ physical approach. Our groundwater recharge calculations were performed without parameter calibration and uncertainty analysis. However, some work to include parameters of the GR-GD curves in an uncertainty analysis framework are currently undertaken within the framework of another study (R. Doble, personal communication, 2019).

IV.6. Conclusion

Different approaches were investigated for simulating groundwater recharge and groundwater – surface water (GW-SW) interactions in a steady-state catchment scale groundwater model representing the Kleine Nete catchment (Belgium). Regarding GW-SW interactions the study focused on the parameterization of the GW-SW conductance parameter. Regarding groundwater recharge, the NRF package (Doble et al., 2017) was used to integrate HYDRUS-1D simulation outputs to a MODFLOW model.

The metamodel proposed by Di Ciacca et al. (2019), to consider the spatial variability of GW-SW conductance due to aquifer conductance, is found to slightly improve the simulation of groundwater heads and strongly decreases uncertainties on river conductance values. Additionally, we highlighted the low sensitivity of piezometric head and river discharge to GW-SW conductance in our case study. However, GW-SW conductance average value and spatial distribution are found to influence significantly the spatial variability of GW-SW fluxes. Moreover, the representation of spatially variable groundwater depth in groundwater recharge simulations appears to be of paramount importance in shallow groundwater areas. Furthermore, the consideration of sub-grid variability seems to be important to represent the small-scale spatial variability of groundwater recharge. Among the different approaches we have considered, constraining the river conductance with the aquifer conductance to avoid unrealistically high values by using the metamodel appears to be the one that influences the most simulated groundwater flow fields. Considering variable groundwater depths in groundwater recharge calculations and the spatial variability of GW-SW conductance due to aquifer and surface water network properties have an impact on simulated groundwater flow fields as well, but to a lesser extent.

Chapter V

Summary, conclusions and outlook

V. Summary, conclusions and outlook

V.1. Summary

The overall goal of this thesis was to improve the representation of critical zone water transfers and their spatial distribution in groundwater models of temperate lowland areas. In particular, we focused on diffuse groundwater recharge and groundwater – surface water interactions. In shallow groundwater systems, there is a critical interaction between the groundwater table depth and groundwater recharge because of upward capillary flow from the groundwater to the soil surface. Moreover, the relation between groundwater depth and upward flow is strongly non-linear. This non-linearity has the consequence that small lateral variations in groundwater table depth (due to local topographic changes) have an impact on local groundwater recharge. Furthermore, in lowland areas, the horizontal distance is small between rivers and ditches, which are in direct contact with the groundwater table and where groundwater is discharging. These effects make that groundwater – surface water interactions vary over a small distance such that high spatial resolution is needed in numerical models to represent explicitly these interactions. In addition, very heterogenous land cover variability induces small scale spatial variability of transpiration demand and root density profiles. This results in a tight and non-linear connection between groundwater depth, groundwater recharge and groundwater surface – water interactions, which remains challenging to represent in catchment scale hydrogeological models, given its complexity and small-scale spatial variability. This thesis aimed at contributing to the development of models capable of representing these processes and their spatial variability efficiently. We proposed a new approach to capture more precisely aggregated effects of interactions between groundwater and small surface water elements as well as small-scale variability of groundwater recharge. The general approach we used in this work is a bottom-up upscaling. Processes are first mechanistically simulated at a smaller scale (point and field scales), considering the small scale spatio-temporal features of the system. These simulated processes are then averaged or aggregated to a larger scale (catchment scale) and functional relations between larger scale averaged processes and features of the smaller scale structure are derived. In this way, small

scale process understanding is effectively used to constrain relations that emerge at larger scales. We used the Kleine Nete catchment (Belgium) as a case study.

Regarding groundwater-surface water interactions, the thesis concentrated on the conductance parameter used to simulate water exchange as a Cauchy boundary condition in groundwater models. This approach has been largely criticized because it is built on the assumption that a streambed exists and concentrates all head losses, which is questionable in many cases. To replace the conductance approach, new approaches were developed in the framework of fully coupled hydrological models (Kollet and Maxwell, 2006; Therrien and Sudicky, 2006). Although a conductance approach may not be as accurate as a full coupling, it is still a relevant approach for simpler models. Furthermore, the underlying assumption of the conductance approach (proportionality between hydraulic difference and flux) seems to be reasonable in our considered cases (Chapter II, section 4.1.1). As shown by other studies (Mehl and Hill, 2010; Pauw et al., 2015) and confirmed in ours (Chapter II section 4.2), the current parameterization of the conductance parameter suffers from a conceptual problem because it neglects aquifer conductance, leading to a scale dependency not taken into account. Therefore, we derived a new expression (Chapter II, section 2) to calculate the aquifer component of the GW-SW conductance as a function of aquifer properties, surface water network density and model discretization. This expression, referred to as metamodel, is based on the Dupuit-Forcheimer theory, the Ernst equation and vertical 2D numerical experiments at the field scale. The main assumptions used to derive our formulation are the presence of a no-flow boundary at the bottom of the hydrogeological model and the homogeneity of the aquifer. This expression was shown to represent well the scale dependency of the conductance parameter in synthetic 3D hydrogeological simulations with different spatial resolutions of a homogenous aquifer (Chapter II, section 4.2). In contrast with the original parameterization, our new expression introduces a spatially variable groundwater – surface water conductance due to the variability of surface water network density, aquifer properties and model discretization. It was then applied in the Kleine Nete catchment groundwater model, considering a layered aquifer, and compared to homogenous catchment scale calibrated conductance values (Chapter IV). Because of the low sensitivity of piezometric heads to GW-SW conductances, the Bayesian calibration of the groundwater – surface water conductance on piezometric data without a priori information from the metamodel led in our

case to an incorrectly wide posterior distribution. This is likely to be the case in other applications as well when only piezometric data are used for the calibration. In a Bayesian framework, this translates to wrong uncertainty estimates of this parameter. In a local calibration framework this could be even worse as the final value would be strongly dependent on the initial value. However, when prior information on GW-SW conductance values from the metamodel were used, a much narrower posterior distribution could be obtained which corresponded quite well with the metamodel spatially averaged value. Nevertheless, the sensitivity of piezometric data to groundwater – surface water conductance appears to be low and thus the spatial variability of conductance introduced by our new expression could not be firmly evaluated using the available dataset. Therefore, the validity of our implementation of the metamodel for a layered aquifer is still unproven. However, we demonstrated that groundwater – surface water conductance global value and spatial distribution has a considerable influence on groundwater fluxes inside the aquifer and to the surface water network. It is important to note that the proposed metamodel does not add much complexity to the modeling of GW-SW interactions and uses parameters already needed elsewhere in the model.

Concerning groundwater diffuse recharge, the thesis particularly focusses on the effect of small-scale vegetation spatial variability and shallow groundwater. First, we have set up a field scale modeling study to investigate the relation between groundwater diurnal fluctuations and tree root water uptake using a 3D variably saturated model (Chapter III). This allowed to explore the influence of different root water uptake parameterizations on simulated groundwater level diurnal fluctuations as well as on fluxes between the tree plot, neighboring grass plot and surface water bodies. Although uncertainties in the model parameterization remain high, it appears that allowing tree water uptake in the saturated zone improved the representation of diurnal groundwater level fluctuations, and significantly decreased simulated fluxes towards the ditches and river. Thus, tree root water uptake from the saturated zone was considered in the 1D variably saturated models used to calculate groundwater recharge for the Kleine Nete catchment steady-state groundwater model (Chapter IV). Moreover, different approaches to integrate the groundwater recharge simulation outputs to the groundwater model were investigated. One approach only considered groundwater recharge simulated using a groundwater depth (specified head

boundary condition) of 2 m (catchment scale average groundwater depth). The three others considered groundwater recharge simulated using all selected groundwater depths (from 0 to 5 m) but handled sub-grid variability in different ways. The reference approach considered sub-grid variability of groundwater depth, soil and land cover. The first alternative approach did not consider sub-grid variability of groundwater depth (but considered soil and land cover sub-grid variability). The second alternative approach did not consider any sub-grid variability (neither groundwater depth nor soil and land cover). The most important differences were obtained between the groundwater model simulation that considered only groundwater recharge simulated using a groundwater depth of 2 m and the other approaches, which considered variable groundwater depth to calculate groundwater recharge. Shallow groundwater (< 2m) decreases significantly simulated groundwater recharge, leading to a lower average value and different spatial patterns when variable groundwater depth was considered. These differences in simulated groundwater recharge translated to important differences in simulated vertically averaged groundwater flow fields. Moreover, only considering groundwater recharge simulated using a groundwater depth of 2 m led to an overestimation of flow to surface water in most of the catchment. On the other hand, considering sub-grid variability of vegetation, soil and groundwater depth did not modify the average simulated groundwater recharge value but changed significantly the simulated grid-scale groundwater recharge, although with no clear spatial pattern. This means that in some cases, the local sub-grid variability decreased the simulated grid-scale groundwater recharge and in other cases it increased it. Hence, the influence of considering sub-grid variability on simulated vertically averaged groundwater flow fields appeared to be minor. However, its influence on shallow groundwater fluxes and thus on solute transport in the shallow aquifer may still be important. Finally, the influence of tree water uptake from the saturated zone on simulated groundwater recharge was minor at the scale of the Kleine Nete catchment, although local differences can be significant.

V.2. Conclusions

This thesis proposes and demonstrates the appropriateness and relevance for lowland environments of a new expression (metamodel) to relate GW-SW conductance to the aquifer hydraulic conductivity and thickness as well as the spatial discretization of the groundwater

model and the surface water network density. Furthermore, we propose a method to represent sub-grid variability of groundwater depth, soil and vegetation in groundwater recharge calculations using the NRF package for MODFLOW (Doble et al., 2017). This work also shows that in lowland temperate environments root water uptake from the saturated zone by phreatophytes can activate groundwater fluxes to the phreatophytes plot from neighboring non-phreatophytes plots. Moreover, root water uptake from the saturated zone by phreatophytes can decrease fluxes to surface water bodies where they are the dominant land cover, especially during dry periods. On the other hand, sub-grid variability of groundwater depth and land cover seems to be an important feature to consider for simulating groundwater recharge spatial variability in lowland temperate environments, because of the highly non-linear relation between groundwater recharge and groundwater depth and the very heterogenous land cover. Nevertheless, its influence on simulated vertically averaged groundwater flow fields remains limited. Of higher importance is the consideration of groundwater depth to simulate groundwater recharge in shallow groundwater environments. This appears to be essential to simulate groundwater recharge spatial distribution and important to simulate groundwater flow fields and flow to surface water correctly. Finally, using our new expression to calculate spatially variable groundwater – surface water conductance has a major impact on simulated groundwater – surface water fluxes and hence groundwater flow fields, exceeding the effects of the different groundwater recharge conceptualizations we considered.

V.3. Outlook

The proposed metamodel improves the simulation of GW-SW interactions in hydrogeological models of lowland environments without adding significant complexity to the numerical model. Therefore, the use of the metamodel in further studies on lowland areas should be encouraged. Regarding groundwater recharge, coupling the vadose zone to groundwater depth appears to be essential for a more realistic simulation of groundwater recharge, and thus groundwater fluxes, in shallow groundwater environments. This adds complexity to the modeling of groundwater recharge (increase in data and computational resource requirements), but a particular effort should be made on this aspect for further modeling studies. Although in our study vertically averaged groundwater fluxes were only marginally

influenced by sub-grid variability of groundwater recharge processes, this was an important feature in the simulation of groundwater recharge spatial variability. Therefore, sub-grid variability of groundwater recharge processes in low-resolution hydrogeological models of lowland areas should be considered if one is interested in grid-scale groundwater recharge variability. Furthermore, it may still be important to consider sub-grid variability of groundwater recharge processes in the Kleine Nete catchment to simulate shallow groundwater fluxes and thus solute transport in the shallow aquifer. Additional simulations would be needed to test this sensitivity, preferably carried on with a solute transport model.

The developed upscaling methodologies differ for groundwater recharge and groundwater – surface water conceptualizations. For the groundwater – surface water interactions on the one hand, upscaling was performed by summarizing the 2D stream-aquifer flow field in a unique parameter (i.e. the conductance/resistance). The approach mainly relies on analytical equations although complemented with information from 2D-field scale numerical experiments for cases where groundwater model vertical discretization is smaller than the aquifer thickness. Groundwater – surface water conductance is explicitly defined as a function of groundwater model discretization sizes. On the other hand, upscaling of groundwater recharge has been done under the main assumption of 1D flow in the unsaturated zone and relies solely on numerical simulations. The 1D assumption allows for straightforward aggregation of different soil and vegetation profiles over an area. Despite these methodological differences, we developed a method to represent flow processes occurring at sub-grid scale for both groundwater recharge and groundwater – surface water interactions. Thus, the resolution of the groundwater model does not limit the representation of the spatial variability of water transfer processes occurring at its upper boundary. This could be relevant for models with lower resolution than presented in this thesis (e.g. regional/continental scale model with resolution ≥ 1km).

A limitation of our work lies in the lack of data that can evaluate the different conceptualization of groundwater recharge and groundwater surface – water interactions considered. As shown in Chapter IV, piezometric and river gauging measurements are not sufficient to thoroughly evaluate our different catchment scale simulations and confirm/infirm some of our assumptions. A particularly valuable insight would be given by measurements of water fluxes in soils and aquifers as well as at their interface with surface water. These data

are usually obtained through indirect measurements of state variables (e.g. temperature, hydraulic head, solute concentration) which are related to flux values using analytical/empirical/numerical calculations. An example of such measurement techniques is the White method (White, 1932) used in Chapter III, in which piezometric time series are used to derive evapotranspiration from groundwater. Other relevant examples include heat and other tracers (Brouyère et al., 2008; Fleckenstein et al., 2010; González-Pinzón et al., 2015; Kalbus et al., 2006), which can be used in aquifers and at the interface with surface water. A more direct estimation of groundwater – surface water exchange fluxes can be obtained using seepage meter (Rosenberry, 2008; Rosenberry et al., 2020). However, comparing fluxes data and model outputs is often challenging because of scale discrepancy between the measurement scale and the scale of the model output variables (fluxes averaged over grids). Those measurements mainly observe spatial variability that emerges from streambed conductance heterogeneity, whereas we would need grid-scale (≈ 10-100 m) average estimates of the groundwater-surface water exchange. A promising measurement technique to bridge this scale discrepancy could be distributed temperature sensor (DTS) fiber-optic cables (Le Lay et al., 2019; Mamer and Lowry, 2013). Investigation of such measurement techniques could be beneficial to further modeling studies. This has already been done using heat as an environmental tracer on the Aa river located within the Kleine Nete catchment (Anibas et al., 2018). In this study, spatio-temporal patterns of groundwater – surface water interaction could be identified over an approximately 1 km-long river reach. On a larger scale, an ongoing PhD project at SCK CEN investigates the added value of groundwater temperature and some other tracer data to calibrate a groundwater model of the Nete catchment. The latter is essentially an updated version of the original model from which the groundwater model presented in Chapter IV has been derived. This could be an interesting opportunity to evaluate further some aspects of the work presented in this thesis. One important remaining question is on the validity of our implementation of the GW-SW conductance metamodel for heterogenous (e.g. layered) aquifers. Evaluation of this implementation could also be undertaken in a synthetic case in the same way as presented in Chapter II, but considering a heterogenous aquifer. This would have the advantage to be easy to implement with straightforward fluxes evaluation.

It is important to note that in the present thesis the influence of groundwater recharge and groundwater – surface water conductance on groundwater fluxes has been studied with steady-state models. However, groundwater recharge and groundwater – surface water interactions are essentially transient processes. We are therefore missing some important temporal dynamics due to the time variable atmospheric conditions and surface water levels. Furthermore, the effect of the approaches considered on groundwater fluxes could be different in a transient model. For instance, the effect of root water uptake parameterization is more important during summer, whereas this effect is mitigated in a steady-state model. Similarly, the local temporal dynamics of simulated groundwater discharge to the surface network are probably significantly influenced by groundwater – surface water conductance value and its spatial variability. Further evaluation with transient models is needed to assess the relative importance of these effects. On the other hand, the integration of HYDRUS simulation outputs through the NRF package (Doble et al., 2017), as done in Chapter IV, seems to be more suitable for steady-state than for transient simulations, as the HYDRUS simulations are performed with a constant head boundary condition. For a transient groundwater model, using the HYDRUS package for MODLFOW (Beegum et al., 2018; Twarakavi et al., 2008) would probably be a better option. A convenient alternative could be to iterate between steady-state and transient simulations in order to obtain groundwater depth values that can then be used to select groundwater recharge values in each cell. Furthermore, the conversion of the catchment scale model to a transient model would probably require the addition of a more comprehensive surface water module with runoff routing and temporally variable surface water levels to compare model outputs with river discharge measurements. This will evidently open up new challenges on modeling concepts and parameterization procedures.

The scope of this thesis was on lowland temperate areas, where groundwater is mainly recharged through diffuse recharge and discharges to surface water networks. Although some concepts could be used on other environments, this can be limited by the difference in hydrological settings. Groundwater recharge calculations have been performed under the assumption of 1D flow within the unsaturated zone. While this seems to be a reasonable assumption for flat land with shallow groundwater, this can be questionable in other systems, where 2 and 3D processes above the water table are important. Concerning groundwater – surface water interactions, our conductance expression has been derived only to represent

connected surface water body (i.e. no unsaturated zone between surface water body and groundwater). However, below some rivers (depending on hydrological settings and riverbed properties), an unsaturated zone can develop (disconnected river or in a transitional state). In these conditions, surface water is infiltrating to groundwater and can be the main source of groundwater recharge (Brunner et al., 2011, 2009; Wöhling et al., 2018). Simulating groundwater – surface water interactions using a conductance approach with the current conceptualization in such conditions is also problematic (Brunner et al., 2010). Further research would be needed to develop an adequate approach for the estimation of aquifer groundwater – surface water conductance in disconnected (or in a transitional state) river, taking into account unsaturated flow processes.

References

Abbott, M.B., Bathurst, J.C., Cunge, J.A., O'Connell, P.E., Rasmussen, J., 1986a. An introduction to the European Hydrological System—Systeme Hydrologique Europeen,"SHE", 2: Structure of a physically-based, distributed modelling system. J. Hydrol. 87, 61–77.

Abbott, M.B., Bathurst, J.C., Cunge, J.A., O'Connell, P.E., Rasmussen, J., 1986b. An introduction to the European Hydrological System—Systeme Hydrologique Europeen,"SHE", 1: History and philosophy of a physically-based, distributed modelling system. J. Hydrol. 87, 45–59.

Aerts, R., Bakker, C., De Caluwe, H., 1992. Root turnover as determinant of the cycling of C, N, and P in a dry heathland ecosystem. Biogeochemistry 15, 175–190.

Allen, R.G., 2009. REF-ET: Reference Evapotranspiration Calculation Software for FAO and ASCE standardized Equations. University of Idaho.

Allen, R.G., Pereira, L.S., Raes, D., Smith Rome, M., 1998. Crop evapotranspiration-Guidelines for computing crop water requirements-FAO Irrigation and drainage paper 56. Fao 300, D05109.

Anderson, E.I., 2005. Modeling groundwater–surface water interactions using the Dupuit approximation. Adv. Water Resour. 28, 315–327. https://doi.org/https://doi.org/10.1016/j.advwatres.2004.11.007

Anderson, E.I., 2003a. An analytical solution representing groundwater–surface water interaction. Water Resour. Res. 39. https://doi.org/doi:10.1029/2002WR001536

Anderson, E.I., 2003b. The effective resistance to vertical flow in Dupuit models. Adv. Water Resour. 26, 513–523. https://doi.org/https://doi.org/10.1016/S0309-1708(03)00002-2

Anderson, M.G., Burt, T.P., 1978. The role of topography in controlling throughflow generation. Earth Surf. Process. 3, 331–344. https://doi.org/10.1002/esp.3290030402

Anderson, S.P., von Blanckenburg, F., White, A.F., 2007. Physical and chemical controls on the critical zone. Elements 3, 315–319.

Anibas, C., Tolche, A.D., Ghysels, G., Nossent, J., Schneidewind, U., Huysmans, M., Batelaan, O., 2018. Delineation of spatial-temporal patterns of groundwater/surface-water interaction along a river reach (Aa River, Belgium) with transient thermal modeling. Hydrogeol. J. 26, 819–835. https://doi.org/10.1007/s10040-017-1695-9

Arnold, J.G., Moriasi, D.N., Gassman, P.W., Abbaspour, K.C., White, M.J., Srinivasan, R., Santhi, C., Harmel, R.D., Van Griensven, A., Van Liew, M.W., 2012. SWAT: Model use, calibration, and validation. Trans. ASABE 55, 1491–1508.

Aroca, R., Porcel, R., Ruiz-Lozano, J.M., 2011. Regulation of root water uptake under abiotic stress conditions. J. Exp. Bot. 63, 43–57. https://doi.org/10.1093/jxb/err266

Aufdenkampe, A.K., Mayorga, E., Raymond, P.A., Melack, J.M., Doney, S.C., Alin, S.R., Aalto,

R.E., Yoo, K., 2011. Riverine coupling of biogeochemical cycles between land, oceans, and atmosphere. Front. Ecol. Environ. 9, 53–60. https://doi.org/10.1890/100014

Austin, A.T., Yahdjian, L., Stark, J.M., Belnap, J., Porporato, A., Norton, U., Ravetta, D.A., Schaeffer, S.M., 2004. Water pulses and biogeochemical cycles in arid and semiarid ecosystems. Oecologia 141, 221–235. https://doi.org/10.1007/s00442-004-1519-1

Bailey, R.T., Wible, T.C., Arabi, M., Records, R.M., Ditty, J., 2016. Assessing regional-scale spatio-temporal patterns of groundwater–surface water interactions using a coupled SWAT-MODFLOW model. Hydrol. Process. 30, 4420–4433. https://doi.org/doi:10.1002/hyp.10933

Baird, K.J., Stromberg, J.C., Maddock, T., 2005. Linking riparian dynamics and groundwater: an ecohydrologic approach to modeling groundwater and riparian vegetation. Environ. Manage. 36, 551–564.

Banta, E.R., 2000. MODFLOW-2000: The US Geological Survey Modular Ground-water Model--documentation of Packages for Simulating Evapotranspiration with a Segmented Function (ETS1) and Drains with Return Flow (DRT1). US Department of the Interior, US Geological Survey.

Barton, R.R., 1994. Metamodeling: a state of the art review, in: Proceedings of Winter Simulation Conference. IEEE, pp. 237–244.

Batelaan, O., De Smedt, F., 2007. GIS-based recharge estimation by coupling surface-subsurface water balances. J. Hydrol. 337, 337–355.

Batelaan, O., De Smedt, F., 2001. WetSpass: a flexible, GIS based, distributed recharge methodology for regional groundwater modelling. IAHS Publ. 11–18.

Batelaan, O., De Smedt, F., Triest, L., 2003. Regional groundwater discharge: phreatophyte mapping, groundwater modelling and impact analysis of land-use change. J. Hydrol. 275, 86–108.

Bauer, P., Thabeng, G., Stauffer, F., Kinzelbach, W., 2004. Estimation of the evapotranspiration rate from diurnal groundwater level fluctuations in the Okavango Delta, Botswana. J. Hydrol. 288, 344–355. https://doi.org/https://doi.org/10.1016/j.jhydrol.2003.10.011

Bayani, C.M., Zlotnik, V., 2003. Three-dimensional model of modern channel bend deposits. Water Resour. Res. 39. https://doi.org/doi:10.1029/2002WR001383

Bear, J., Cheng, A.H.-D., 2010. Modeling groundwater flow and contaminant transport. Springer Science & Business Media.

Beegum, S., Šimůnek, J., Szymkiewicz, A., Sudheer, K.P., Nambi, I.M., 2018. Updating the Coupling Algorithm between HYDRUS and MODFLOW in the HYDRUS Package for MODFLOW. Vadose Zo. J. 17.

Bencala, K.E., 1984. Interactions of solutes and streambed sediment: 2. A dynamic analysis of coupled hydrologic and chemical processes that determine solute transport. Water Resour. Res. 20, 1804–1814.

Beven, K., 2001. How far can we go in distributed hydrological modelling? Hydrol. Earth Syst. Sci. Discuss. 5, 1–12.

Beven, K., Calver, A., Morris, E.M., 1987. The Institute of Hydrology distributed model.

Beven, K., Germann, P., 2013. Macropores and water flow in soils revisited. Water Resour. Res. 49, 3071–3092.

Beven, K., Germann, P., 1982. Macropores and water flow in soils. Water Resour. Res. 18, 1311–1325.

Beven, K.J., 1990. A discussion of distributed hydrological modelling, in: Distributed Hydrological Modelling. Springer, pp. 255–278.

Bond, B.J., Jones, J.A., Moore, G., Phillips, N., Post, D., McDonnell, J.J., 2002. The zone of vegetation influence on baseflow revealed by diel patterns of streamflow and vegetation water use in a headwater basin. Hydrol. Process. 16, 1671–1677.

Boulton, A.J., Datry, T., Kasahara, T., Mutz, M., Stanford, J.A., 2010. Ecology and management of the hyporheic zone: stream–groundwater interactions of running waters and their floodplains. J. North Am. Benthol. Soc. 29, 26–40. https://doi.org/10.1899/08-017.1

Brantley, S.L., Goldhaber, M.B., Ragnarsdottir, K.V., 2007. Crossing disciplines and scales to understand the critical zone. Elements 3, 307–314.

Bresler, E., 1987. Application of a conceptual model to irrigation water requirement and salt tolerance of crops. Soil Sci. Soc. Am. J. 51, 788–793.

Breuer, L., Eckhardt, K., Frede, H.-G., 2003. Plant parameter values for models in temperate climates. Ecol. Modell. 169, 237–293.

Brouyère, S., Batlle-Aguilar, J., Goderniaux, P., Dassargues, A., 2008. A new tracer technique for monitoring groundwater fluxes: The Finite Volume Point Dilution Method. J. Contam. Hydrol. 95, 121–140.

Brunner, P., Cook, P.G., Simmons, C.T., 2011. Disconnected Surface Water and Groundwater: From Theory to Practice. Groundwater 49, 460–467. https://doi.org/10.1111/j.1745-6584.2010.00752.x

Brunner, P., Cook, P.G., Simmons, C.T., 2009. Hydrogeologic controls on disconnection between surface water and groundwater. Water Resour. Res. 45. https://doi.org/10.1029/2008wr006953

Brunner, P., Simmons, C.T., Cook, P.G., Therrien, R., 2010. Modeling Surface Water-Groundwater Interaction with MODFLOW: Some Considerations. Groundwater 48, 174–180. https://doi.org/10.1111/j.1745-6584.2009.00644.x

Cai, G., Vanderborght, J., Couvreur, V., Mboh, C.M., Vereecken, H., 2018a. Parameterization of Root Water Uptake Models Considering Dynamic Root Distributions and Water Uptake Compensation. Vadose Zo. J. 17. https://doi.org/10.2136/vzj2016.12.0125

Cai, G., Vanderborght, J., Langensiepen, M., Schnepf, A., Hüging, H., Vereecken, H., 2018b. Root growth, water uptake, and sap flow of winter wheat in response to different soil water conditions. Hydrol. Earth Syst. Sci. 22, 2449–2470. https://doi.org/10.5194/hess-22-2449-2018

Caldwell, M.M., Dawson, T.E., Richards, J.H., 1998. Hydraulic lift: consequences of water efflux

from the roots of plants. Oecologia 113, 151–161.

Camporese, M., Paniconi, C., Putti, M., Orlandini, S., 2010. Surface-subsurface flow modeling with path-based runoff routing, boundary condition-based coupling, and assimilation of multisource observation data. Water Resour. Res. 46. https://doi.org/doi:10.1029/2008WR007536

Cape, J.N., Brown, A.H.F., Robertson, S.M.C., Howson, G., Paterson, I.S., 1991. Interspecies comparisons of throughfall and stemflow at three sites in northern Britain. For. Ecol. Manage. 46, 165–177. https://doi.org/https://doi.org/10.1016/0378-1127(91)90229-O

Carsel, R.F., Parrish, R.S., 1988. Developing joint probability distributions of soil water retention characteristics. Water Resour. Res. 24, 755–769. https://doi.org/doi:10.1029/WR024i005p00755

Čermák, J., Kučera, J., Bauerle, W.L., Phillips, N., Hinckley, T.M., 2007. Tree water storage and its diurnal dynamics related to sap flow and changes in stem volume in old-growth Douglas-fir trees. Tree Physiol. 27, 181–198.

Chorover, J., Kretzschmar, R., Garcia-Pichel, F., Sparks, D.L., 2007. Soil biogeochemical processes within the critical zone. Elements 3, 321–326.

Christensen, N.S., Wood, A.W., Voisin, N., Lettenmaier, D.P., Palmer, R.N., 2004. The Effects of Climate Change on the Hydrology and Water Resources of the Colorado River Basin. Clim. Change 62, 337–363. https://doi.org/10.1023/B:CLIM.0000013684.13621.1f

Clarke, R., Lawrence, A., Foster, S.S.D., 1996. Groundwater: a threatened resource. United Nations Environment Programme.

Coelho, E.F., Or, D., 1999. Root distribution and water uptake patterns of corn under surface and subsurface drip irrigation. Plant Soil 206, 123–136.

Cool, W., Vermariën, E., Wacquier, W., Perko, J., 2013. The long-term safety and performance analyses of the surface disposal facility for the Belgian category A waste at Dessel, in: ASME 2013 15th International Conference on Environmental Remediation and Radioactive Waste Management. American Society of Mechanical Engineers Digital Collection.

Cousquer, Y., Alexandre, P., Nicolas, F., Célestine, D., Alain, D., 2017. Estimating River Conductance from Prior Information to Improve Surface-Subsurface Model Calibration. Groundwater 55, 408–418. https://doi.org/doi:10.1111/gwat.12492

Cousquer, Y., Pryet, A., Atteia, O., Ferré, T.P.A., Delbart, C., Valois, R., Dupuy, A., 2018. Developing a particle tracking surrogate model to improve inversion of ground water – Surface water models. J. Hydrol. 558, 356–365. https://doi.org/https://doi.org/10.1016/j.jhydrol.2018.01.043

Crosbie, R.S., Scanlon, B.R., Mpelasoka, F.S., Reedy, R.C., Gates, J.B., Zhang, L., 2013. Potential climate change effects on groundwater recharge in the High Plains Aquifer, USA. Water Resour. Res. 49, 3936–3951.

Crutzen, P.J., 2006. The “anthropocene,” in: Earth System Science in the Anthropocene. Springer, pp. 13–18.

Dams, J., Dujardin, J., Reggers, R., Bashir, I., Canters, F., Batelaan, O., 2013. Mapping impervious surface change from remote sensing for hydrological modeling. J. Hydrol. 485, 84–95.

Dams, J., Salvadore, E., Van Daele, T., Ntegeka, V., Willems, P., Batelaan, O., 2012. Spatio-temporal impact of climate change on the groundwater system. Hydrol. Earth Syst. Sci. 16, 1517–1531.

Dams, J., Woldeamlak, S.T., Batelaan, O., 2008. Predicting land-use change and its impact on the groundwater system of the Kleine Nete catchment, Belgium. Hydrol. Earth Syst. Sci. 12, 1369–1385. https://doi.org/10.5194/hess-12-1369-2008

Davie, T., Quinn, N.W., 2002. Fundamentals of hydrology. Routledge.

Davis, S., De Wiest, J.M., 1966. Hydrogeology. Vol. 2. New-York.

de Graaf, I.E.M., van Beek, R.L.P.H., Gleeson, T., Moosdorf, N., Schmitz, O., Sutanudjaja, E.H., Bierkens, M.F.P., 2017. A global-scale two-layer transient groundwater model: Development and application to groundwater depletion. Adv. Water Resour. 102, 53–67. https://doi.org/https://doi.org/10.1016/j.advwatres.2017.01.011

De Lange, W.J., 1999. A Cauchy boundary condition for the lumped interaction between an arbitrary number of surface waters and a regional aquifer. J. Hydrol. 226, 250–261.

Deutscher, J., Kupec, P., Dundek, P., Holík, L., Machala, M., Urban, J., 2016. Diurnal dynamics of streamflow in an upland forested micro-watershed during short precipitation-free periods is altered by tree sap flow. Hydrol. Process. 30, 2042–2049. https://doi.org/10.1002/hyp.10771

Di Ciacca, A., Leterme, B., Laloy, E., Jacques, D., Vanderborght, J., 2019. Scale-dependent parameterization of groundwater–surface water interactions in a regional hydrogeological model. J. Hydrol. 576, 494–507. https://doi.org/https://doi.org/10.1016/j.jhydrol.2019.06.072

Diersch, H.-J.G., 2013. FEFLOW: finite element modeling of flow, mass and heat transport in porous and fractured media. Springer Science & Business Media.

Doble, R.C., Crosbie, R.S., 2017. Current and emerging methods for catchment-scale modelling of recharge and evapotranspiration from shallow groundwater. Hydrogeol. J. 25, 3–23.

Doble, R.C., Pickett, T., Crosbie, R.S., Morgan, L.K., Turnadge, C., Davies, P.J., 2017. Emulation of recharge and evapotranspiration processes in shallow groundwater systems. J. Hydrol. 555, 894–908. https://doi.org/https://doi.org/10.1016/j.jhydrol.2017.10.065

Durner, W., 1994. Hydraulic conductivity estimation for soils with heterogeneous pore structure. Water Resour. Res. 30, 211–223.

Durner, W., Priesack, E., Vogel, H.-J., Zurmühl, T., van Genuchten, M.T., 1999. Determination of parameters for flexible hydraulic functions by inverse modeling, in: Proc. Int. Workshop on Characterization and Measurement of the Hydraulic Properties of Unsaturated Porous Media. University of California CA, Riverside. pp. 817–829.

Ernst, L.F., 1962. Grondwaterstromingen in de verzadigde zone en hun berekening bij aanwezigheid van horizontale evenwijdige open leidingen. Centrum voor

Landbouwpublikaties en Landbouwdocumentatie.

Fahle, M., Dietrich, O., 2014. Estimation of evapotranspiration using diurnal groundwater level fluctuations: Comparison of different approaches with groundwater lysimeter data. Water Resour. Res. 50, 273–286.

Fan, J., Ostergaard, K.T., Guyot, A., Fujiwara, S., Lockington, D.A., 2016. Estimating groundwater evapotranspiration by a subtropical pine plantation using diurnal water table fluctuations: Implications from night-time water use. J. Hydrol. 542, 679–685. https://doi.org/https://doi.org/10.1016/j.jhydrol.2016.09.040

Fatichi, S., Vivoni, E.R., Ogden, F.L., Ivanov, V.Y., Mirus, B., Gochis, D., Downer, C.W., Camporese, M., Davison, J.H., Ebel, B., Jones, N., Kim, J., Mascaro, G., Niswonger, R., Restrepo, P., Rigon, R., Shen, C., Sulis, M., Tarboton, D., 2016. An overview of current applications, challenges, and future trends in distributed process-based models in hydrology. J. Hydrol. https://doi.org/10.1016/j.jhydrol.2016.03.026

Feddes, R.A., Kowalik, P.J., Zaradny, H., 1978. Simulation of field water use and crop yield. Centre for Agricultural Publishing and Documentation.

Fleckenstein, J.H., Krause, S., Hannah, D.M., Boano, F., 2010. Groundwater-surface water interactions: New methods and models to improve understanding of processes and dynamics. Adv. Water Resour. 33, 1291–1295.

Foglia, L., Mehl, S.W., Hill, M.C., Burlando, P., 2013. Evaluating model structure adequacy: The case of the Maggia Valley groundwater system, southern Switzerland. Water Resour. Res. 49, 260–282. https://doi.org/doi:10.1029/2011WR011779

Fraser, C.E., McIntyre, N., Jackson, B.M., Wheater, H.S., 2013. Upscaling hydrological processes and land management change impacts using a metamodeling procedure. Water Resour. Res. 49, 5817–5833. https://doi.org/10.1002/wrcr.20432

Freeze, R.A., Harlan, R.L., 1969. Blueprint for a physically-based, digitally-simulated hydrologic response model. J. Hydrol. 9, 237–258. https://doi.org/https://doi.org/10.1016/0022-1694(69)90020-1

Gale, M.R., Grigal, D.F., 1987. Vertical root distributions of northern tree species in relation to successional status. Can. J. For. Res. 17, 829–834.

Galleguillos, M., Jacob, F., Prévot, L., Faúndez, C., Bsaibes, A., 2017. Estimation of actual evapotranspiration over a rainfed vineyard using a 1-D water transfer model: A case study within a Mediterranean watershed. Agric. Water Manag. 184, 67–76. https://doi.org/https://doi.org/10.1016/j.agwat.2017.01.006

Gedeon, M., 2008. Neogene Aquifer Model. External report SCK-CEN-ER-48. Mol, Belgium.

Gedeon, M., Wemaere, I., 2003. Updated Regional Hydrogeological Model for the Mol Site (The North-Eastern Belgium Model). External Report of the Belgian Nuclear Research Centre SCK CEN.

Ghazavi, G., Thomas, Z., Hamon, Y., Marie, J.-C., Corson, M., Merot, P., 2008. Hedgerow impacts on soil-water transfer due to rainfall interception and root-water uptake. Hydrol. Process. An Int. J. 22, 4723–4735.

Ghysels, G., Benoit, S., Awol, H., Jensen, E.P., Debele Tolche, A., Anibas, C., Huysmans, M., 2018. Characterization of meter-scale spatial variability of riverbed hydraulic conductivity in a lowland river (Aa River, Belgium). J. Hydrol. 559, 1013–1027. https://doi.org/https://doi.org/10.1016/j.jhydrol.2018.03.002

Ghysels, G., Mutua, S., Veliz, G.B., Huysmans, M., 2019. A modified approach for modelling river–aquifer interaction of gaining rivers in MODFLOW, including riverbed heterogeneity and river bank seepage TT - Une approche modifiée de la modélisation par MODFLOW de l'interaction rivière–aquifère dans le cas des r. Hydrogeol. J. 27, 1851–1863. https://doi.org/http://dx.doi.org/10.1007/s10040-019-01941-0

Gnatowski, T., Szatyłowicz, J., Brandyk, T., Kechavarzi, C., 2010. Hydraulic properties of fen peat soils in Poland. Geoderma 154, 188–195. https://doi.org/https://doi.org/10.1016/j.geoderma.2009.02.021

González-Pinzón, R., Ward, A.S., Hatch, C.E., Wlostowski, A.N., Singha, K., Gooseff, M.N., Haggerty, R., Harvey, J.W., Cirpka, O.A., Brock, J.T., 2015. A field comparison of multiple techniques to quantify groundwater–surface-water interactions. Freshw. Sci. 34, 139–160. https://doi.org/10.1086/679738

Gou, S., Miller, G.R., Saville, C., Maxwell, R.M., Ferguson, I.M., 2018. Simulating groundwater uptake and hydraulic redistribution by phreatophytes in a high-resolution, coupled subsurface-land surface model. Adv. Water Resour. https://doi.org/https://doi.org/10.1016/j.advwatres.2018.08.008

Granier, A., Breda, N., Biron, P., Villette, S., 1999. A lumped water balance model to evaluate duration and intensity of drought constraints in forest stands. Ecol. Modell. 116, 269–283.

Gribovszki, Z., Kalicz, P., Szilágyi, J., Kucsara, M., 2008. Riparian zone evapotranspiration estimation from diurnal groundwater level fluctuations. J. Hydrol. 349, 6–17. https://doi.org/https://doi.org/10.1016/j.jhydrol.2007.10.049

Gribovszki, Z., Szilágyi, J., Kalicz, P., 2010. Diurnal fluctuations in shallow groundwater levels and streamflow rates and their interpretation – A review. J. Hydrol. 385, 371–383. https://doi.org/https://doi.org/10.1016/j.jhydrol.2010.02.001

Haitjema, H., Kelson, V., de Lange, W., 2001. Selecting MODFLOW Cell Sizes for Accurate Flow Fields. Groundwater 39, 931–938. https://doi.org/doi:10.1111/j.1745-6584.2001.tb02481.x

Hall, R.L., 1985. Further interception studies of heather using a wet-surface weighing lysimeter system. J. Hydrol. 81, 193–210.

Harbaugh, A.W., 2005. MODFLOW-2005, the U.S. Geological Survey modular ground-water model -- the Ground-Water Flow Process. U.S. Geological Survey Techniques and Methods 6-A16.

Harbaugh, A.W., Banta, E.R., Hill, M.C., McDonald, M.G., Geological, S., 2000. MODFLOW-2000, The U.S. Geological Survey Modular Ground-Water Model - User Guide to Modularization Concepts and the Ground-Water Flow Process, Open-File Report.

Healy, R.W., 2010. Estimating groundwater recharge. Cambridge University Press.

Heijmans, M.M.P.D., Mauquoy, D., Van Geel, B., Berendse, F., 2008. Long-term effects of climate change on vegetation and carbon dynamics in peat bogs. J. Veg. Sci. 19, 307–320.

Hildebrandt, A., Guillamón, M., Lacorte, S., Tauler, R., Barceló, D., 2008. Impact of pesticides used in agriculture and vineyards to surface and groundwater quality (North Spain). Water Res. 42, 3315–3326.

Hooghoudt, S.B., 1940. Bijdrage tot de kennis van enige natuurkundige grootheden van de grond. Versl. van Landbouwkd. Onderz. 46, 515–707.

Hunt, R.J., Feinstein, D.T., Pint, C.D., Anderson, M.P., 2006. The importance of diverse data types to calibrate a watershed model of the Trout Lake Basin, Northern Wisconsin, USA. J. Hydrol. 321, 286–296.

Jackson, C.R., 1992. Hillslope infiltration and lateral downslope unsaturated flow. Water Resour. Res. 28, 2533–2539.

Jacques, D., Leterme, B., Beerten, K., Schneider, S., Finke, P., Mallants, D., 2010. Long-term evolution of the multi-layer cover: project near surface disposal of category a waste at Dessel. NIROND-TR Rep. Ser. 2010.

Jacques, D., Mallants, D., Leterme, B., 2011. Modelling potential and actual evapotranspiration and drainage at the nuclear zone Mol-Dessel, NIROND-TR.

Jacques, D., Wang, L., Martens, E., Mallants, D., 2008. Time dependence of the geochemical boundary conditions for the cementitious engineered barriers of the Belgian surface disposal facility, NIRAS-MP5 DATA-LT (NF) Version.

Jasechko, S., Sharp, Z.D., Gibson, J.J., Birks, S.J., Yi, Y., Fawcett, P.J., 2013. Terrestrial water fluxes dominated by transpiration. Nature 496, 347.

Javaux, M., Couvreur, V., Vanderborght, J., Vereecken, H., 2013. Root Water Uptake: From Three-Dimensional Biophysical Processes to Macroscopic Modeling Approaches. Vadose Zo. J. 12. https://doi.org/10.2136/vzj2013.02.0042

Jin, R., Chen, W., Simpson, T.W., 2001. Comparative studies of metamodelling techniques under multiple modelling criteria. Struct. Multidiscip. Optim. 23, 1–13. https://doi.org/10.1007/s00158-001-0160-4

Kalbus, E., Reinstorf, F., Schirmer, M., 2006. Measuring methods for groundwater? surface water interactions: a review. Hydrol. Earth Syst. Sci. Discuss. 10, 873–887.

Kim, N.W., Chung, I.M., Won, Y.S., Arnold, J.G., 2008. Development and application of the integrated SWAT–MODFLOW model. J. Hydrol. 356, 1–16.

Kløve, B., Ala-aho, P., Bertrand, G., Boukalova, Z., Ertürk, A., Goldscheider, N., Ilmonen, J., Karakaya, N., Kupfersberger, H., Kvœrner, J., Lundberg, A., Mileusnić, M., Moszczynska, A., Muotka, T., Preda, E., Rossi, P., Siergieiev, D., Šimek, J., Wachniew, P., Angheluta, V., Widerlund, A., 2011. Groundwater dependent ecosystems. Part I: Hydroecological status and trends. Environ. Sci. Policy 14, 770–781. https://doi.org/https://doi.org/10.1016/j.envsci.2011.04.002

Kollet, S.J., Maxwell, R.M., 2006. Integrated surface–groundwater flow modeling: A free-surface overland flow boundary condition in a parallel groundwater flow model. Adv.

Water Resour. 29, 945–958.

Kollet, S.J., Zlotnik, V.A., 2007. Evaluation of the streambed leakage concept in analytical models using data from three pumping tests. Hydrogeol. J. 15, 1051–1062. https://doi.org/10.1007/s10040-006-0156-7

Kollet, S.J., Zlotnik, V.A., 2003. Stream depletion predictions using pumping test data from a heterogeneous stream–aquifer system (a case study from the Great Plains, USA). J. Hydrol. 281, 96–114. https://doi.org/https://doi.org/10.1016/S0022-1694(03)00203-8

Krause, S., Jacobs, J., Bronstert, A., 2007. Modelling the impacts of land-use and drainage density on the water balance of a lowland–floodplain landscape in northeast Germany. Ecol. Modell. 200, 475–492. https://doi.org/https://doi.org/10.1016/j.ecolmodel.2006.08.015

Kroes, J.G., Van Dam, J.C., Groenendijk, P., Hendriks, R.F.A., Jacobs, C.M.J., 2008. SWAP version 3.2: Theory description and user manual. Alterra Wageningen, The Netherlands.

Kuffour, B.N.O., Engdahl, N.B., Woodward, C.S., Condon, L.E., Kollet, S., Maxwell, R.M., 2019. Simulating Coupled Surface-Subsurface Flows with ParFlow v3.5.0: Capabilities, applications, and ongoing developmentof an open-source, massively parallel, integrated hydrologic model. Geosci. Model Dev. Discuss. 2019, 1–66. https://doi.org/10.5194/gmd-2019-190

Laloy, E., Vrugt, J.A., 2012. High-dimensional posterior exploration of hydrologic models using multiple-try DREAM (ZS) and high-performance computing. Water Resour. Res. https://doi.org/10.1029/2011WR010608

Lam, Q.D., Schmalz, B., Fohrer, N., 2012. Assessing the spatial and temporal variations of water quality in lowland areas, Northern Germany. J. Hydrol. 438–439, 137–147. https://doi.org/https://doi.org/10.1016/j.jhydrol.2012.03.011

Lambin, E.F., Geist, H.J., 2008. Land-use and land-cover change: local processes and global impacts. Springer Science & Business Media.

Lange, B., Lüscher, P., Germann, P., 2009. Significance of tree roots for preferential infiltration in stagnic soils. Hydrol. Earth Syst. Sci. 13, 1809–1821.

Langevin, C.D., Hughes, J.D., Banta, E.R., Niswonger, R.G., Panday, S., Provost, A.M., 2017. Documentation for the MODFLOW 6 groundwater flow model. US Geological Survey.

Lautz, L.K., 2008. Estimating groundwater evapotranspiration rates using diurnal water-table fluctuations in a semi-arid riparian zone. Hydrogeol. J. 16, 483–497.

Lawrence, D.M., Slingo, J.M., 2004. An annual cycle of vegetation in a GCM. Part I: implementation and impact on evaporation. Clim. Dyn. 22, 87–105.

Le Lay, H., Thomas, Z., Rouault, F., Pichelin, P., Moatar, F., 2019. Characterization of Diffuse Groundwater Inflows into Stream Water (Part II: Quantifying Groundwater Inflows by Coupling FO-DTS and Vertical Flow Velocities). Water 11, 2430.

Leterme, B., Gedeon, M., Jacques, D., 2013. Groundwater Recharge Modeling of the Nete Catchment (Belgium) Using the HYDRUS-1D–MODFLOW Package, in: Proceedings of the 4th International Conference HYDRUS Software Applications to Subsurface Flow and

Contaminant Transport Problems, Prague, Czech Republic.

Leterme, B., Mallants, D., 2012. Simulation of evapotranspiration and groundwater recharge in the Nete catchment accounting for different land cover types and for present and future climate conditions, SCK•CEN Reports. SCK•CEN - Studiecentrum voor Kernenergie/Centre d'Etude de l'Energie Nucléaire.

Leterme, B., Mallants, D., Jacques, D., 2012. Sensitivity of groundwater recharge using climatic analogues and HYDRUS-1D. Hydrol. Earth Syst. Sci. 16, 2485–2497. https://doi.org/10.5194/hess-16-2485-2012

Leuschner, C., 2001. Changes in Forest Ecosystem Function with Succession in the Lüneburger Heide, in: ECOLOGICAL STUDIES, 2000 - Springer Science and Media. pp. 517–568. https://doi.org/10.1007/978-3-662-04504-6_29

Lewis, S.L., Maslin, M.A., 2015. Defining the anthropocene. Nature 519, 171–180.

Li, Q., Qi, J., Xing, Z., Li, S., Jiang, Y., Danielescu, S., Zhu, H., Wei, X., Meng, F.R., 2014. An approach for assessing impact of land use and biophysical conditions across landscape on recharge rate and nitrogen loading of groundwater. Agric. Ecosyst. Environ. 196. https://doi.org/10.1016/j.agee.2014.06.028

Liu, Y.B., De Smedt, F., 2004. WetSpa extension, a GIS-based hydrologic model for flood prediction and watershed management. Vrije Univ. Brussel, Belgium 1–108.

Loheide, S.P., 2008. A method for estimating subdaily evapotranspiration of shallow groundwater using diurnal water table fluctuations. Ecohydrol. 1, 59–66. https://doi.org/10.1002/eco.7

Loheide, S.P., Butler, J.J., Gorelick, S.M., 2005. Estimation of groundwater consumption by phreatophytes using diurnal water table fluctuations: A saturated-unsaturated flow assessment. Water ressources Res. 41. https://doi.org/10.1029/2005wr003942

Lv, M., Hao, Z., Liu, Z., Yu, Z., 2013. Conditions for lateral downslope unsaturated flow and effects of slope angle on soil moisture movement. J. Hydrol. 486, 321–333. https://doi.org/https://doi.org/10.1016/j.jhydrol.2013.02.013

Mallants, D., Volckaert, G., Marivoet, J., Neerdael, B., 2000. Disposal of flow-level radioactive waste in Belgium: A safety analysis for inorganic chemotoxic elements.

Mallants, D., Wang, L., Weetjens, E., Cool, W., 2008. Evaluating Chemical Toxicity of Surface Disposal of LILW-SL in Belgium. MRS Proc. 1107, 689. https://doi.org/10.1557/PROC-1107-689

Mamer, E.A., Lowry, C.S., 2013. Locating and quantifying spatially distributed groundwater/surface water interactions using temperature signals with paired fiber-optic cables. Water Resour. Res. 49, 7670–7680. https://doi.org/10.1002/2013WR014235

Marchionni, V., Guyot, A., Tapper, N., Walker, J.P., Daly, E., 2019. Water balance and tree water use dynamics in remnant urban reserves. J. Hydrol. 575, 343–353. https://doi.org/https://doi.org/10.1016/j.jhydrol.2019.05.022

Markewitz, D., Devine, S., Davidson, E.A., Brando, P., Nepstad, D.C., 2010. Soil moisture

depletion under simulated drought in the Amazon: impacts on deep root uptake. New Phytol. 187, 592–607. https://doi.org/10.1111/j.1469-8137.2010.03391.x

Mati, B.M., Mutie, S., Gadain, H., Home, P., Mtalo, F., 2008. Impacts of land-use/cover changes on the hydrology of the transboundary Mara River, Kenya/Tanzania. Lakes Reserv. Sci. Policy Manag. Sustain. Use 13, 169–177. https://doi.org/10.1111/j.1440-1770.2008.00367.x

Maxwell, R.M., Condon, L.E., Kollet, S.J., 2015. A high-resolution simulation of groundwater and surface water over most of the continental US with the integrated hydrologic model ParFlow v3. Geosci. Model Dev. 8, 923–937. https://doi.org/10.5194/gmd-8-923-2015

Maxwell, R.M., Kollet, S.J., 2008. Interdependence of groundwater dynamics and land-energy feedbacks under climate change. Nat. Geosci. 1, 665–669.

Maxwell, R.M., Kollet, S.J., Smith, S.G., Woodward, C.S., Falgout, R.D., Ferguson, I.M., Baldwin, C., Bosl, W.J., Hornung, R., Ashby, S., 2009. ParFlow user's manual. Int. Gr. Water Model. Cent. Rep. GWMI 1, 129.

Maxwell, R.M., Miller, N.L., 2005. Development of a coupled land surface and groundwater model. J. Hydrometeorol. 6, 233–247.

Maxwell, R.M., Putti, M., Meyerhoff, S., Delfs, J.O., Ferguson, I.M., Ivanov, V., Kim, J., Kolditz, O., Kollet, S.J., Kumar, M., Lopez, S., Niu, J., Paniconi, C., Park, Y.J., Phanikumar, M.S., Shen, C., Sudicky, E.A., Sulis, M., 2014. Surface-subsurface model intercomparison: A first set of benchmark results to diagnose integrated hydrology and feedbacks. Water Resour. Res. 50. https://doi.org/10.1002/2013WR013725

McDonald, M.G., Harbaugh, A.W., 2003. The history of MODFLOW. Groundwater 41, 280–283.

McDonald, M.G., Harbaugh, A.W., 1988. A modular three-dimensional finite-difference ground-water flow model. US Geological Survey Reston, VA.

McLaughlin, D.L., Cohen, M.J., 2011. Thermal artifacts in measurements of fine-scale water level variation. Water Resour. Res. 47. https://doi.org/10.1029/2010wr010288

Mehl, S., Hill, M.C., 2010. Grid-size dependence of Cauchy boundary conditions used to simulate stream–aquifer interactions. Adv. Water Resour. 33, 430–442. https://doi.org/https://doi.org/10.1016/j.advwatres.2010.01.008

Meinzer, O.E., 1927. Plants as indicators of ground water. US Govt. print. off.

Meiresonne, L., Sampson, D.A., Kowalski, A.S., Janssens, I.A., Nadezhdina, N., Cermák, J., Van Slycken, J., Ceulemans, R., 2003. Water flux estimates from a Belgian Scots pine stand: a comparison of different approaches. J. Hydrol. 270, 230–252. https://doi.org/https://doi.org/10.1016/S0022-1694(02)00284-6

Meyus, Y., 1998. Sub-regional simulation of the groundwater flow in the Neogene aquifer at the Mol site. SCK• CEN, Mol.

Meyus, Y., Adyns, D., Woldeamlak, S., Batalaan, O., De Smedt Brussel België, F. %J V.U.B., 2004. Opbouw van een Vlaams Grondwatervoedingsmodel. Deelrapport 2: Totaal VGM-karteergebied en Vlaanderen.

Miller, G.R., Chen, X., Rubin, Y., Ma, S., Baldocchi, D.D., 2010. Groundwater uptake by woody vegetation in a semiarid oak savanna. Water Resour. Res. 46.

Morel-Seytoux, H.J., Miller, C.D., Mehl, S., Miracapillo, C., 2018. Achilles' heel of integrated hydrologic models: The stream-aquifer flow exchange, and proposed alternative. J. Hydrol. 564, 900–908. https://doi.org/https://doi.org/10.1016/j.jhydrol.2018.07.010

Morel-Seytoux, H.J., Miller, C.D., Miracapillo, C., Mehl, S., 2017. River Seepage Conductance in Large-Scale Regional Studies. Groundwater 55, 399–407. https://doi.org/doi:10.1111/gwat.12491

Morel-Seytoux, H.J., 2009. The Turning Factor in the Estimation of Stream-Aquifer Seepage. Groundwater 47, 205–212.

Morel-Seytoux, H.J., Steffen, M., Kyle, M., 2014. Factors Influencing the Stream-Aquifer Flow Exchange Coefficient. Groundwater 52, 775–781. https://doi.org/doi:10.1111/gwat.12112

Mould, D.J., Frahm, E., Salzmann, T., Miegel, K., Acreman, M.C., 2010. Evaluating the use of diurnal groundwater fluctuations for estimating evapotranspiration in wetland environments: case studies in southeast England and northeast Germany. Ecohydrology 3, 294–305. https://doi.org/10.1002/eco.108

Mualem, Y. %J W. resources research, 1976. A new model for predicting the hydraulic conductivity of unsaturated porous media. Water Resour. Res. 12, 513–522.

Mulla, D.J., McBratney, A.B., 2002. Soil spatial variability. Soil Phys. companion 343–373.

Nace, R.L., 1967. Are we running out of water? US Geological Survey.

Nachabe, M., Shah, N., Ross, M., Vomacka, J., 2005. Evapotranspiration of Two Vegetation Covers in a Shallow Water Table Environment. Soil Sci. Soc. Am. J. 69, 492–499. https://doi.org/10.2136/sssaj2005.0492

Naumburg, E., Mata-gonzalez, R., Hunter, R.G., Mclendon, T., Martin, D.W., 2005. Phreatophytic Vegetation and Groundwater Fluctuations: A Review of Current Research and Application of Ecosystem Response Modeling with an Emphasis on Great Basin Vegetation. Environ. Manage. 35, 726–740. https://doi.org/10.1007/s00267-004-0194-7

Neitsch, S.L., Arnold, J.G., Kiniry, J.R., Williams, J.R., 2011. Soil and water assessment tool theoretical documentation version 2009. Texas Water Resources Institute.

Nimah, M.N., Hanks, R.J., 1973a. Model for estimating soil water, plant, and atmospheric interrelations: I. Description and sensitivity. Soil Sci. Soc. Am. J. 37, 522–527.

Nimah, M.N., Hanks, R.J., 1973b. Model for estimating soil water, plant, and atmospheric interrelations: II. Field test of model. Soil Sci. Soc. Am. J. 37, 528–532.

Niswonger, R.G., Prudic, D.E., Regan, R.S., 2006. Documentation of the Unsaturated-Zone Flow (UZF1) package for modeling unsaturated flow between the land surface and the water table with MODFLOW-2005, Techniques and Methods 6-A19. USGS, Denver, CO.

Or, D., Lehmann, P., Shahraeeni, E., Shokri, N., 2013. Advances in Soil Evaporation Physics—A Review. Vadose Zo. J. 12. https://doi.org/10.2136/vzj2012.0163

Orellana, F., Verma, P., Loheide II, S.P., Daly, E., 2012. Monitoring and modeling water-vegetation interactions in groundwater-dependent ecosystems. Rev. Geophys. 50. https://doi.org/10.1029/2011rg000383

Pauw, P.S., Van der Zee, S., Leijnse, A., Delsman, J.R., De Louw, P.G.B., De Lange, W.J., Oude Essink, G.H.P., 2015. Low-Resolution Modeling of Dense Drainage Networks in Confining Layers. Groundwater 53, 771–781.

Phillips, N.G., Ryan, M.G., Bond, B.J., McDowell, N.G., Hinckley, T.M., Čermák, J., 2003. Reliance on stored water increases with tree size in three species in the Pacific Northwest. Tree Physiol. 23, 237–245.

Prickett, T.A., Lonnquist, C.G., 1971. Selected digital computer techniques for groundwater resource evaluation, Bulletin (Illinois State Water Survey) no. 55.

Pumo, D., Tamea, S., Noto, L.V., Miralles-Wilhem, F., Rodriguez-Iturbe, I., 2010. Modeling belowground water table fluctuations in the Everglades. Water Resour. Res. 46. https://doi.org/10.1029/2009wr008911

Rassam, D.W., Pagendam, D.E., Hunter, H.M., 2008. Conceptualisation and application of models for groundwater–surface water interactions and nitrate attenuation potential in riparian zones. Environ. Model. Softw. 23, 859–875. https://doi.org/https://doi.org/10.1016/j.envsoft.2007.11.003

Refsgaard, J C, 1996. Terminology, Modelling Protocol And Classification of Hydrological Model Codes, in: Abbott, M.B., Refsgaard, Jens Christian (Eds.), Distributed Hydrological Modelling. Springer Netherlands, Dordrecht, pp. 17–39. https://doi.org/10.1007/978-94-009-0257-2_2

Renger, M., Strebel, O., Wessolek, G., Duynisveld, W.H.M., 1986. Evapotranspiration and groundwater recharge – A case study for different climate, crop patterns, soil properties and groundwater depth conditions -. Zeitschrift für Pflanzenernährung und Bodenkd. 149, 371–381. https://doi.org/10.1002/jpln.19861490403

Richards, J.H., Caldwell, M.M., 1987. Hydraulic lift: substantial nocturnal water transport between soil layers by Artemisia tridentata roots. Oecologia 73, 486–489.

Ritzema, H.P., 1994. Drainage principles and applications. International Institute for Land Reclamation and Improvement (ILRI).

Roberts, J., 1976. A study of root distribution and growth in a Pinus sylvestris L.(Scots pine) plantation in East Anglia. Plant Soil 44, 607–621.

Robinson, T.W., 1958. Phreatophytes. US Government Printing Office.

Rosenberry, D.O., 2008. A seepage meter designed for use in flowing water. J. Hydrol. 359, 118–130.

Rosenberry, D.O., Duque, C., Lee, D.R., 2020. History and evolution of seepage meters for quantifying flow between groundwater and surface water: Part 1–Freshwater settings. Earth-Science Rev. 103167.

Rushton, B. %J J.J. of the A.W.R.A., 1996. HYDROLOGIC BUDGET FOR A FRESHWATER MARSH IN FLORIDA 1. JAWRA J. Am. Water Resour. Assoc. 32, 13–21.

Rushton, K., 2007. Representation in regional models of saturated river–aquifer interaction for gaining/losing rivers. J. Hydrol. 334, 262–281. https://doi.org/https://doi.org/10.1016/j.jhydrol.2006.10.008

Salama, R.B., Bartle, G.A., Farrington, P., 1994. Water use of plantation Eucalyptus camaldulensis estimated by groundwater hydrograph separation techniques and heat pulse method. J. Hydrol. 156, 163–180.

Scanlon, B.R., Reedy, R.C., Stonestrom, D.A., Prudic, D.E., Dennehy, K.F., 2005. Impact of land use and land cover change on groundwater recharge and quality in the southwestern US. Glob. Chang. Biol. 11, 1577–1593.

Schaap, M.G., Leij, F.J., Van Genuchten, M.T., 2001. Rosetta: A computer program for estimating soil hydraulic parameters with hierarchical pedotransfer functions. J. Hydrol. 251, 163–176.

Schimel, D.S., Kittel, T.G.F., Parton, W.J., 1991. Terrestrial biogeochemical cycles: global interactions with the atmosphere and hydrology. Tellus A 43, 188–203. https://doi.org/10.1034/j.1600-0870.1991.00017.x

Schmalz, B., Springer, P., Fohrer, N., 2009. Variability of water quality in a riparian wetland with interacting shallow groundwater and surface water. J. Plant Nutr. Soil Sci. 172, 757–768. https://doi.org/10.1002/jpln.200800268

Schneider, S., Jacques, D., Mallants, D., 2013. Inverse modelling with a genetic algorithm to derive hydraulic properties of a multi-layered forest soil. Soil Res. 51, 372–389.

Schwartz, M.O., 2020. Groundwater contamination associated with a potential nuclear waste repository at Yucca Mountain, USA. Bull. Eng. Geol. Environ. 79, 1125–1136.

Scibek, J., Allen, D.M., Cannon, A.J., Whitfield, P.H., 2007. Groundwater–surface water interaction under scenarios of climate change using a high-resolution transient groundwater model. J. Hydrol. 333, 165–181. https://doi.org/10.1016/J.JHYDROL.2006.08.005

Seo, H.S., Simunek, J., Poeter, E.P., 2007. Documentation of the HYDRUS Package for MODFLOW-2000, the U.S. Geological Survey Modular Ground-Water Model, IGWMC-International Ground Water Modeling Center.

Shah, N., Nachabe, M., Ross, M., 2007. Extinction Depth and Evapotranspiration from Ground Water under Selected Land Covers. Groundwater 45, 329–338. https://doi.org/10.1111/j.1745-6584.2007.00302.x

Shiklomanov, I.A., Rodda, J.C., 2004. World water resources at the beginning of the twenty-first century. Cambridge University Press.

Siebert, S., Burke, J., Faures, J.M., Frenken, K., Hoogeveen, J., Döll, P., Portmann, F.T., 2010. Groundwater use for irrigation – a global inventory. Hydrol. Earth Syst. Sci. 14, 1863–1880. https://doi.org/10.5194/hess-14-1863-2010

Simunek, J., Hopmans, J.W., 2009. Modeling compensated root water and nutrient uptake. Ecol. Modell. 220, 505–521.

Simunek, J., Sejna, M., Van Genuchten, M.T., 2018. New features of version 3 of the HYDRUS

(2D/3D) computer software package. J. Hydrol. Hydromechanics 66, 133–142.

Simunek, J., Van Genuchten, M.T., Sejna, M., 2005. The HYDRUS-1D software package for simulating the movement of water, heat, and multiple solutes in variably saturated media, version 3.0, HYDRUS software series 1. Dep. Environ. Sci. Univ. Calif. Riverside, Riverside Ed.

Simunek, J., Van Genuchten, M.T., Šejna version, M., 2012. The HYDRUS software package for simulating the two-and three-dimensional movement of water, heat, and multiple solutes in variably-saturated porous media, Technical manual.

Simunek, van Genuchten, M.T., 2008. Modeling nonequilibrium flow and transport processes using HYDRUS. Vadose Zo. J. 7, 782–797.

Simunek, van Genuchten, M.T., Šejna, M., 2008. Development and Applications of the HYDRUS and STANMOD Software Packages and Related Codes. Vadose Zo. J. https://doi.org/10.2136/vzj2007.0077

Smerdon, B.D., 2017. A synopsis of climate change effects on groundwater recharge. J. Hydrol. https://doi.org/https://doi.org/10.1016/j.jhydrol.2017.09.047

Sophocleous, M., 2002. Interactions between groundwater and surface water: the state of the science. Hydrogeol. J. 10, 52–67.

Spalding, R.F., Exner, M.E., 1993. Occurrence of nitrate in groundwater—a review. J. Environ. Qual. 22, 392–402.

Spencer, S.A., van Meerveld, H.J., 2016. Double funnelling in a mature coastal British Columbia forest: spatial patterns of stemflow after infiltration. Hydrol. Process. 30, 4185–4201. https://doi.org/https://doi.org/10.1002/hyp.10936

Staudinger, M., Stoelzle, M., Cochand, F., Seibert, J., Weiler, M., Hunkeler, D., 2019. Your work is my boundary condition! Challenges and approaches for a closer collaboration between hydrologists and hydrogeologists. J. Hydrol. https://doi.org/https://doi.org/10.1016/j.jhydrol.2019.01.058

Stegen, J.C., Fredrickson, J.K., Wilkins, M.J., Konopka, A.E., Nelson, W.C., Arntzen, E. V, Chrisler, W.B., Chu, R.K., Danczak, R.E., Fansler, S.J., 2016. Groundwater–surface water mixing shifts ecological assembly processes and stimulates organic carbon turnover. Nat. Commun. 7, 11237.

Szilagyi, J., Zlotnik, V.A., Jozsa, J., 2013. Net recharge vs. depth to groundwater relationship in the Platte River Valley of Nebraska, United States. Groundwater 51, 945–951.

Taylor, R.G., Scanlon, B., Döll, P., Rodell, M., van Beek, R., Wada, Y., Longuevergne, L., Leblanc, M., Famiglietti, J.S., Edmunds, M., Konikow, L., Green, T.R., Chen, J., Taniguchi, M., Bierkens, M.F.P., MacDonald, A., Fan, Y., Maxwell, R.M., Yechieli, Y., Gurdak, J.J., Allen, D.M., Shamsudduha, M., Hiscock, K., Yeh, P.J.-F., Holman, I., Treidel, H., 2013. Ground water and climate change. Nat. Clim. Chang. 3. https://doi.org/10.1038/nclimate1744

Therrien, R., Sudicky, E.A., 2006. HydroGeoSphere A three-dimensional numerical model describing fullyintegrated subsurface and overland flow and solute transport. User Guide 218p.

Thomas, Z., Ghazavi, R., Merot, P., Granier, A., 2012. Modelling and observation of hedgerow transpiration effect on water balance components at the hillslope scale in Brittany. Hydrol. Process. 26, 4001–4014.

Thoms, R.B., Johnson, R.L., Healy, R.W., 2006. User's guide to the Variably Saturated Flow (VSF) Process for MODFLOW, U.S. Geological Survey Techniques and Methods 6-A18.

Todd, D.K., Mays, L.W., 2005. Groundwater hydrology, Wiley.

Todini, E., 2007. Hydrological catchment modelling: past, present and future. Hydrol. Earth Syst. Sci.

Twarakavi, N.K.C., Šimůnek, J., Seo, S., 2008. Evaluating Interactions between Groundwater and Vadose Zone Using the HYDRUS-Based Flow Package for MODFLOW. Vadose Zo. J. 7, 757. https://doi.org/10.2136/vzj2007.0082

van Beers, W.F.J., 1976. Computing drain spacings. Bull. Int. Inst. L. Reclam. Improv. 15.

van Dam, J.C., Groenendijk, P., Hendriks, R.F.A., Kroes, J.G., 2008. Advances of Modeling Water Flow in Variably Saturated Soils with SWAP. Vadose Zo. J. 7, 640. https://doi.org/10.2136/vzj2007.0060

van Genuchten, M.T., 1980. A Closed-form Equation for Predicting the Hydraulic Conductivity of Unsaturated Soils. Soil Sci. Soc. Am. J. https://doi.org/10.2136/sssaj1980.03615995004400050002x

Van Orshoven, J., Maes, J., Vereecken, H., Feyen, J., Dudal, R., 1988. A structured database of Belgian soil profile data. Pedol. Bull. van Belgische Bodemkd. Ver. 38, 191–206.

Vandersteen, K., Gedeon, M., Beerten, K., 2014. A synthesis of hydraulic conductivity measurements of the subsurface in Northeastern Belgium. Geol. Belgica.

Vereecken, H., Huisman, J.A., Pachepsky, Y., Montzka, C., Van Der Kruk, J., Bogena, H., Weihermüller, L., Herbst, M., Martinez, G., Vanderborght, J., 2014. On the spatio-temporal dynamics of soil moisture at the field scale. J. Hydrol. 516, 76–96.

Vereecken, H., Kasteel, R., Vanderborght, J., Harter, T., 2007. Upscaling hydraulic properties and soil water flow processes in heterogeneous soils. Vadose Zo. J. 6, 1–28.

Verstraeten, W.W., Muys, B., Feyen, J., Veroustraete, F., Minnaert, M., Meiresonne, L., De Schrijver, A., 2005. Comparative analysis of the actual evapotranspiration of Flemish forest and cropland, using the soil water balance model WAVE. Hydrol. Earth Syst. Sci. 9, 225–241. https://doi.org/10.5194/hess-9-225-2005

Vincke, C., Thiry, Y., 2008. Water table is a relevant source for water uptake by a Scots pine (Pinus sylvestris L.) stand: Evidences from continuous evapotranspiration and water table monitoring. Agric. For. Meteorol. 148, 1419–1432. https://doi.org/http://dx.doi.org/10.1016/j.agrformet.2008.04.009

Vrugt, J.A., 2016. Markov chain Monte Carlo simulation using the DREAM software package: Theory, concepts, and MATLAB implementation. Environ. Model. Softw. https://doi.org/10.1016/j.envsoft.2015.08.013

Wang, Z.-M., Batelaan, O., De Smedt, F., 1996. A distributed model for water and energy

transfer between soil, plants and atmosphere (WetSpa). Phys. Chem. Earth 21, 189–193.

White, W.N., 1932. A method of estimating ground-water supplies based on discharge by plants and evaporation from soil: Results of investigations in Escalante Valley, Utah. US Government Printing Office.

Wöhling, T., Gosses, M.J., Wilson, S.R., Davidson, P., 2018. Quantifying River-Groundwater Interactions of New Zealand's Gravel-Bed Rivers: The Wairau Plain. Groundwater 56, 647–666.

Yashi, D.K., Suzuki, K., Nomura, M., 1990. Diurnal fluctuation in stream flow and in specific electric conductance during drought periods. J. Hydrol. 115, 105–114. https://doi.org/https://doi.org/10.1016/0022-1694(90)90200-H

Zhang, L., Dawes, W., 1998. An integrated energy and water balance model, in: CSIRO Land and Water Technical Report.

Zhang, P., Yuan, G., Shao, M., Yi, X., Du, T., 2016. Performance of the White method for estimating groundwater evapotranspiration under conditions of deep and fluctuating groundwater. Hydrol. Process. 30, 106–118. https://doi.org/10.1002/hyp.10552

Zomlot, Z., Verbeiren, B., Huysmans, M., Batelaan, O., 2015. Spatial distribution of groundwater recharge and base flow: Assessment of controlling factors. J. Hydrol. Reg. Stud. 4, 349–368.

Appendices

Appendix A: Supplementary material for Chapter II

Aquifer resistance metamodel

This section shows the intermediate steps between Equation 6 and 7.

$$h_{GW}{}^2(x) = -\frac{R}{K_{\text{hor}}}x^2 + \frac{RL}{K_{\text{hor}}}x + h_{\text{SW}}{}^2$$

Equation 6

$$h^2{}_{\text{GW,mean}}(x) = \frac{1}{x}\int_0^x -\frac{R}{K_{\text{hor}}}x^2 + \frac{RL}{K_{\text{hor}}}x + h_{\text{SW}}{}^2$$

$$h^2{}_{\text{GW,mean}}(x) = \frac{1}{x}\left(-\frac{R}{3K_{\text{hor}}}x^3 + \frac{RL}{2K_{\text{hor}}}x^2 + h_{\text{SW}}{}^2 x\right)$$

$$h^2{}_{\text{GW,mean}}(x) = -\frac{R}{3K_{\text{hor}}}x^2 + \frac{RL}{2K_{\text{hor}}}x + h_{\text{SW}}{}^2$$

Equation 7

$$h^2{}_{\text{GW,mean}}(x) = -\frac{q_{\text{2D,GW-SW}}}{3K_{\text{hor}}L}x^2 + \frac{q_{\text{2D,GW-SW}}}{2K_{\text{hor}}}x + h_{\text{SW}}{}^2$$

$$h^2{}_{\text{GW,mean}}(x) = q_{\text{2D,GW-SW}}\left(-\frac{x^2}{3K_{\text{hor}}L} + \frac{x}{2K_{\text{hor}}}\right) + h_{\text{SW}}{}^2$$

$$q_{\text{2D,GW-SW}}\left(-\frac{x^2}{3K_{\text{hor}}L} + \frac{x}{2K_{\text{hor}}}\right) = h^2{}_{\text{GW,mean}}(x) - h_{\text{SW}}{}^2$$

$$q_{\text{2D,GW-SW}} = \frac{h^2{}_{\text{GW,mean}}(x) - h_{\text{SW}}{}^2}{-\frac{x^2}{3K_{\text{hor}}L} + \frac{x}{2K_{\text{hor}}}}$$

$$q_{\text{2D,GW-SW}} = \frac{h_{\text{GW,mean}}(x) + h_{\text{sw}}}{\frac{x}{2K_{\text{hor}}} - \frac{x^2}{3K_{\text{hor}}L}}\left(h_{\text{GW,mean}}(x) - h_{\text{SW}}\right)$$

Equation 8

Results

This section presents, in a first sub-section, the same figures than in the section II.5.2 but including the two approaches Mehl_01 and Mehl_02 and, in a second sub-section, the tables with all the results of the evaluation of the 3D hydrogeological models.

Figures including Mehl_01 and Mehl_02 approaches

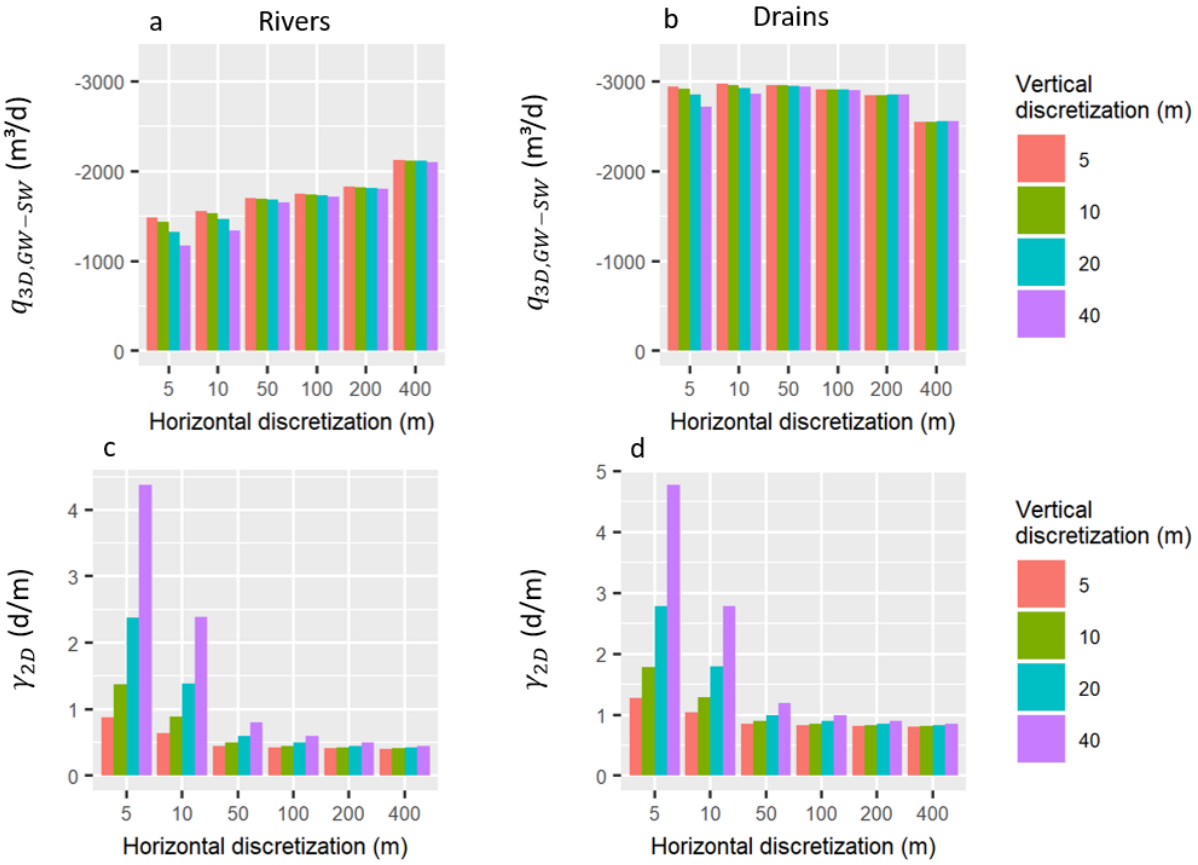

Total net rivers – groundwater (a) and ditch drains – groundwater (b) fluxes ($q_{3D,GW-SW}$) in all the upscaled models considering the Mehl 01 resistance and the associated mean 2D resistances (γ_{2D}), c and d respectively

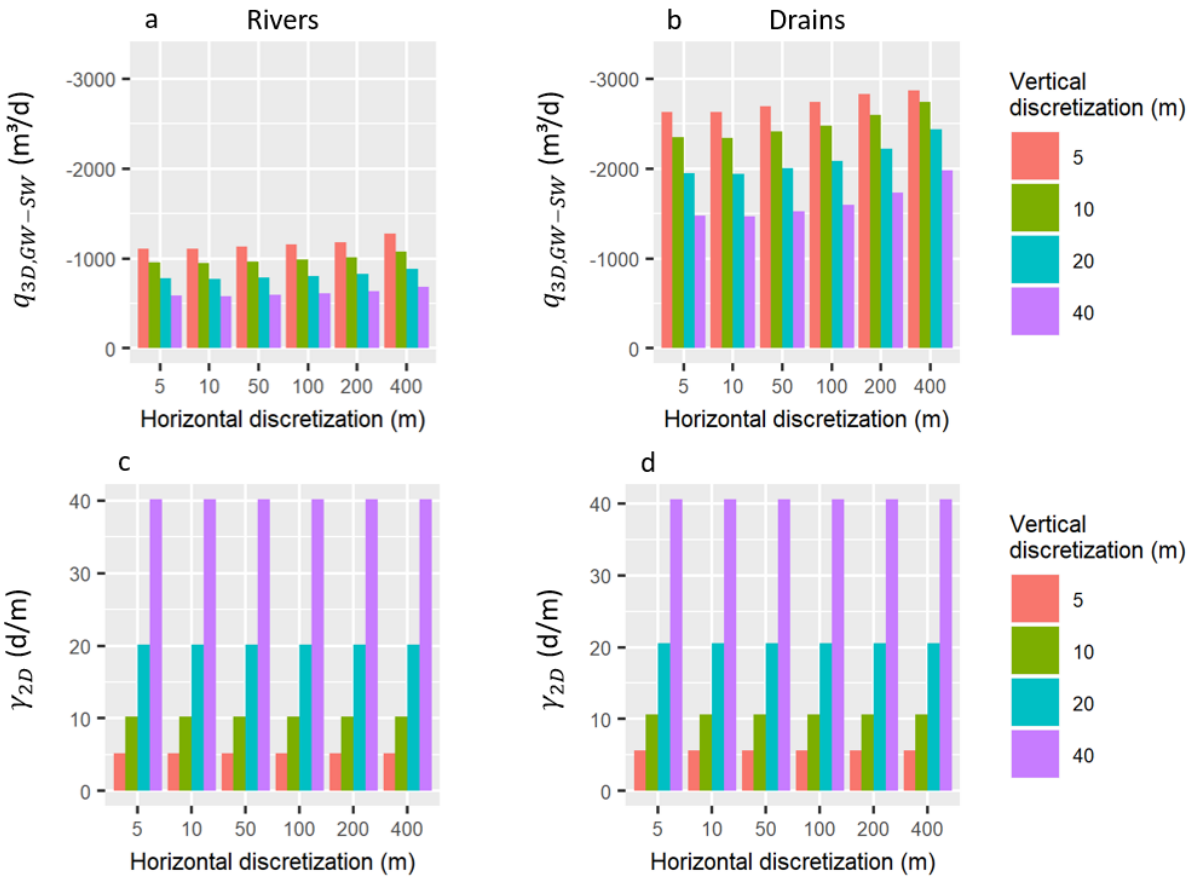

Total net rivers – groundwater (a) and ditch drains – groundwater (b) fluxes ($q_{3D,GW-SW}$) in all the upscaled models considering the Mehl 02 resistance and the associated mean 2D resistances (γ_{2D}), c and d respectively

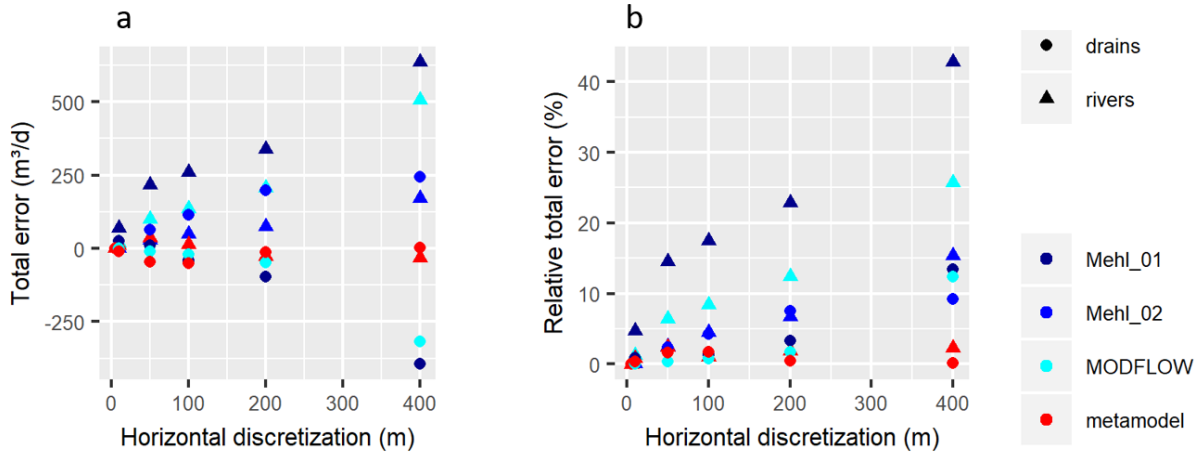

Absolute (a) and relative (b) errors of GW – SW total fluxes for the horizontal upscaling study for the models of 5 m vertical discretization

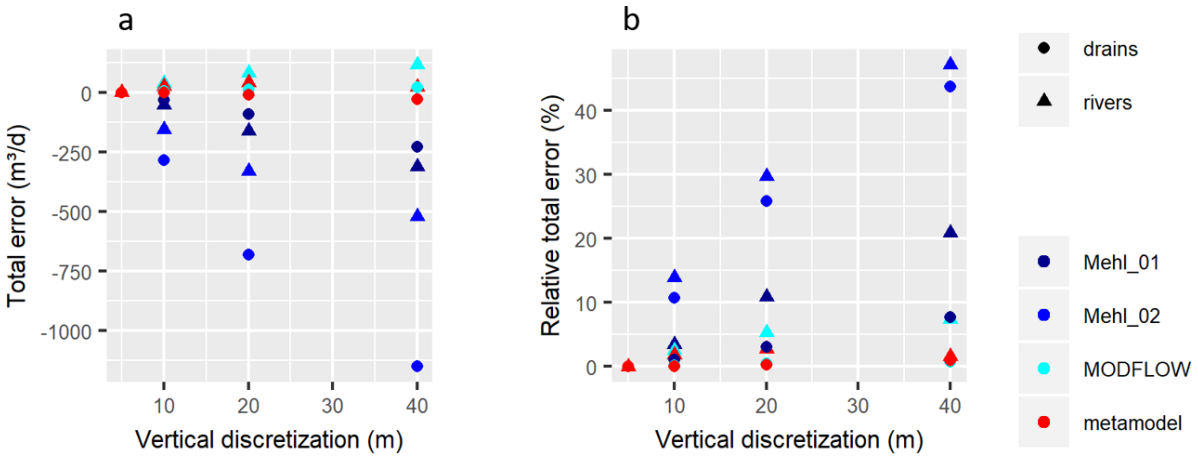

Absolute (a) and relative (b) errors of GW − SW total fluxes for the vertical upscaling study for the models of 5 m horizontal discretization

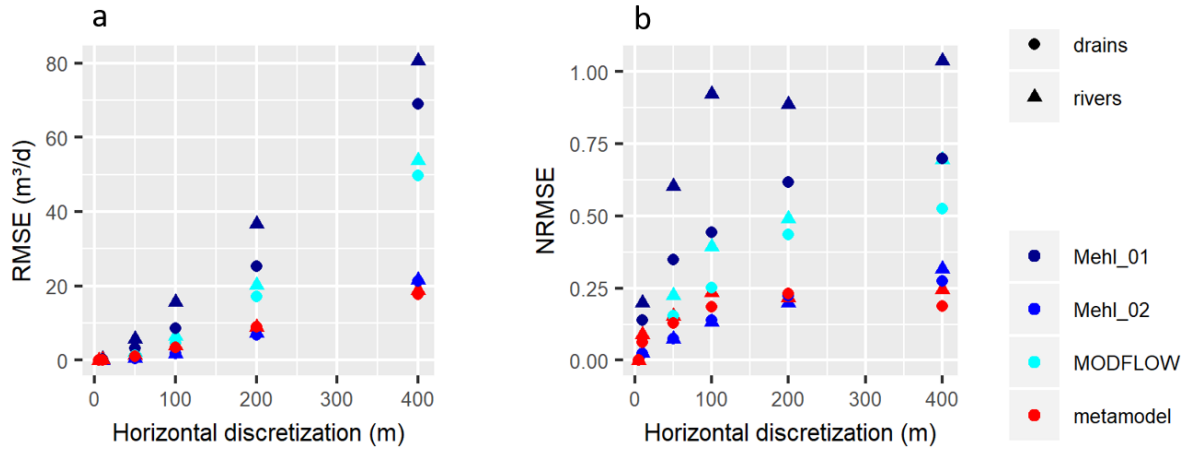

RMSE (a) and NRMSE (b) of GW − SW fluxes per cell for the horizontal upscaling for the models of 5 m vertical discretization

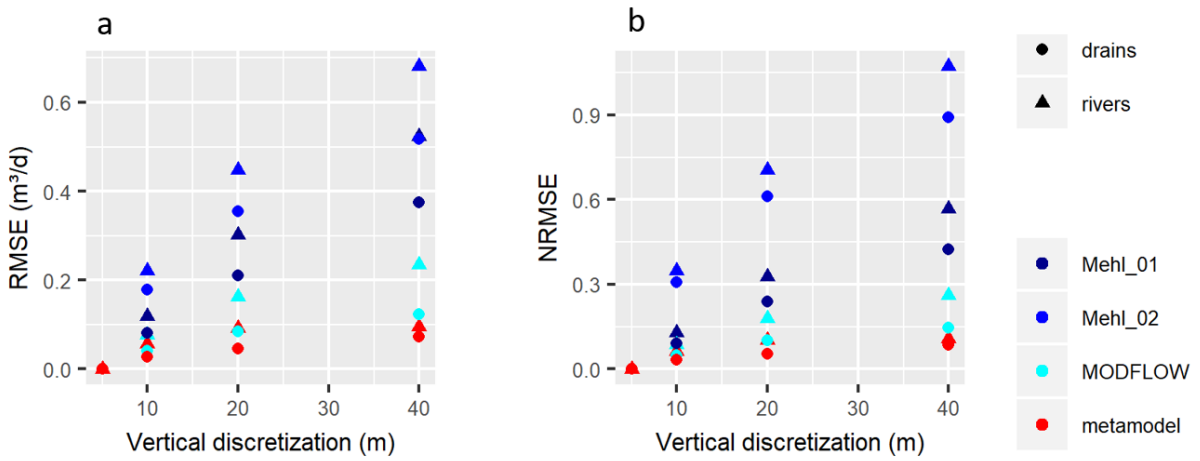

RMSE (a) and NRMSE (b) of GW − SW fluxes per cell for the vertical upscaling for the models of 5 m horizontal discretization

Tables 3D hydrogeological model upscaling study

Note that in the following tables, the rows are referring to the different horizontal discretization sizes and the columns to the vertical discretization sizes.

Total error

All the errors are expressed in m³/d.

Absolute errors of GW − SW total fluxes of the horizontal and vertical upscaling

MODFLOW								
	Rivers		**5**	**10**	**50**	**100**	**200**	**400**
		5	0.0	18.2	99.8	135.0	206.9	506.6
		10	38.7	47.0	107.9	138.7	208.5	506.9
		20	81.0	84.5	121.4	145.1	211.1	507.4
		40	117.0	120.1	138.4	153.9	214.6	507.9
	Drains		**5**	**10**	**50**	**100**	**200**	**400**
		5	0.0	−1.0	−9.1	−21.4	−47.7	−317.1
		10	6.3	4.6	−9.0	−21.9	−48.2	−317.1
		20	14.1	11.4	−8.6	−22.8	−48.8	−317.0
		40	21.1	19.0	−7.7	−24.2	−49.7	−316.8
Metamodel								

	Rivers		5	10	50	100	200	400
		5	0.0	11.4	35.9	14.7	−27.2	−33.5
		10	26.5	27.5	32.7	9.3	−33.2	−39.4
		20	41.3	37.7	24.1	−1.9	−44.7	−50.8
		40	23.2	19.6	−0.3	−24.3	−66.1	−72.1
	Drains		5	10	50	100	200	400
		5	0.0	−9.4	−46.9	−50.4	−13.3	2.8
		10	−1.3	−10.6	−46.2	−47.9	−9.3	7.8
		20	−8.6	−16.5	−44.9	−42.8	−1.8	17.3
		40	−29.2	−31.9	−41.6	−34.7	10.9	34.7
Mehl_01								
	Rivers		5	10	50	100	200	400
		5	0.0	69.5	216.2	260.5	339.4	636.3
		10	−51.5	48.8	210.7	256.4	336.2	633.8
		20	−161.9	−14.1	198.6	247.9	329.5	628.3
		40	−310.5	−143.7	166.9	228.7	315.3	617.8
	Drains		5	10	50	100	200	400
		5	0.0	24.8	10.2	−39.7	−97.3	−395.0
		10	−31.1	8.9	9.5	−39.3	−96.1	−393.6
		20	−90.7	−23.4	5.8	−39.1	−93.8	−390.8
		40	−226.9	−82.8	−5.9	−40.2	−89.8	−385.8
Mehl_02								
	Rivers		5	10	50	100	200	400
		5	0.0	1.0	28.0	49.9	74.5	169.9
		10	−154.1	−156.5	−139.1	−120.6	−98.2	−28.9
		20	−328.9	−332.8	−318.5	−301.7	−276.7	−220.7
		40	−521.8	−526.2	−513.4	−497.9	−471.2	−421.6

	Drains		5	10	50	100	200	400
		5	0.0	0.4	63.6	113.6	197.6	243.7
		10	−283.7	−290.6	−220.3	−151.9	−31.7	111.9
		20	−679.8	−692.1	−623.7	−548.1	−408.0	−189.0
		40	−1150.4	−1164.7	−1104.9	−1034.5	−896.8	−645.4

Total relative error

All the relative errors are expressed as percentage.

Relative errors of GW − SW total fluxes of the horizontal and vertical upscaling

MODFLOW								
	Rivers		**5**	**10**	**50**	**100**	**200**	**400**
		5	0.0	1.2	6.4	8.5	12.4	25.8
		10	2.6	3.1	6.9	8.7	12.5	25.8
		20	5.3	5.5	7.7	9.0	12.6	25.8
		40	7.4	7.6	8.7	9.5	12.8	25.8
	Drains		**5**	**10**	**50**	**100**	**200**	**400**
		5	0.0	0.0	0.3	0.7	1.7	12.4
		10	0.2	0.2	0.3	0.8	1.7	12.4
		20	0.5	0.4	0.3	0.8	1.7	12.4
		40	0.7	0.7	0.3	0.8	1.8	12.4
Metamodel								
	Rivers		**5**	**10**	**50**	**100**	**200**	**400**
		5	0.0	0.8	2.4	1.0	1.9	2.3
		10	1.8	1.8	2.2	0.6	2.3	2.8
		20	2.8	2.5	1.6	0.1	3.2	3.6
		40	1.6	1.3	0.0	1.7	4.7	5.2
	Drains		**5**	**10**	**50**	**100**	**200**	**400**
		5	0.0	0.3	1.7	1.8	0.5	0.1

		10	0.0	0.4	1.6	1.7	0.3	0.3
		20	0.3	0.6	1.6	1.5	0.1	0.6
		40	1.0	1.1	1.5	1.2	0.4	1.2
Mehl_01								
	Rivers		**5**	**10**	**50**	**100**	**200**	**400**
		5	0.0	4.7	14.5	17.5	22.8	42.8
		10	3.5	3.3	14.2	17.3	22.6	42.6
		20	10.9	0.9	13.4	16.7	22.2	42.3
		40	20.9	9.7	11.2	15.4	21.2	41.6
	Drains		**5**	**10**	**50**	**100**	**200**	**400**
		5	0.0	0.8	0.3	1.3	3.3	13.4
		10	1.1	0.3	0.3	1.3	3.3	13.4
		20	3.1	0.8	0.2	1.3	3.2	13.3
		40	7.7	2.8	0.2	1.4	3.0	13.1
Mehl_02								
	Rivers	5	**5**	**10**	**50**	**100**	**200**	**400**
		5	0.0	0.1	2.5	4.5	6.7	15.3
		10	13.9	14.1	12.6	10.9	8.9	2.6
		20	29.7	30.1	28.8	27.3	25.0	19.9
		40	47.1	47.5	46.4	45.0	42.6	38.1
	Drains		**5**	**10**	**50**	**100**	**200**	**400**
		5	0.0	0.0	2.4	4.3	7.5	9.3
		10	10.8	11.0	8.4	5.8	1.2	4.3
		20	25.8	26.3	23.7	20.8	15.5	7.2
		40	43.7	44.3	42.0	39.3	34.1	24.5

RMSE

All RMSE are expressed in m^3/d.

RMSE of GW − SW fluxes per cell of the horizontal and vertical upscaling

MODFLOW								
	Rivers		**5**	**10**	**50**	**100**	**200**	**400**
		5	0.0	0.2	2.0	6.6	20.2	53.7
		10	0.1	0.2	2.1	6.6	20.3	53.7
		20	0.2	0.3	2.3	6.6	20.3	53.8
		40	0.2	0.5	2.5	6.7	20.4	53.8
	Drains		**5**	**10**	**50**	**100**	**200**	**400**
		5	0.0	0.1	1.4	4.7	17.1	49.8
		10	0.0	0.1	1.4	4.7	17.1	49.8
		20	0.1	0.2	1.4	4.7	17.1	49.8
		40	0.1	0.2	1.5	4.7	17.0	49.7
Metamodel								
	Rivers		**5**	**10**	**50**	**100**	**200**	**400**
		5	0.0	0.2	1.4	3.9	8.9	18.8
		10	0.1	0.2	1.3	3.7	8.7	19.0
		20	0.1	0.2	1.1	3.4	8.6	19.4
		40	0.1	0.2	1.2	3.6	9.1	20.6
	Drains		**5**	**10**	**50**	**100**	**200**	**400**
		5	0.0	0.1	1.1	3.4	9.1	17.7
		10	0.0	0.1	1.1	3.3	9.0	17.9
		20	0.0	0.1	0.9	3.2	8.9	18.1
		40	0.1	0.2	0.9	3.2	8.9	18.8
Mehl_01								
	Rivers		**5**	**10**	**50**	**100**	**200**	**400**
		5	0.0	0.4	5.7	15.7	36.7	80.6
		10	0.1	0.2	5.3	15.0	36.2	80.0
		20	0.3	0.2	4.6	13.9	35.2	79.0

		40	0.5	0.6	3.4	11.9	33.4	76.9
	Drains		**5**	**10**	**50**	**100**	**200**	**400**
		5	0.0	0.2	3.2	8.7	25.3	69.0
		10	0.1	0.1	3.0	8.5	25.1	68.7
		20	0.2	0.1	2.7	8.1	24.7	68.2
		40	0.4	0.4	2.1	7.3	23.9	67.2
Mehl_02								
	Rivers		**5**	**10**	**50**	**100**	**200**	**400**
		5	0.0	0.0	0.5	1.8	7.4	21.6
		10	0.2	0.5	2.1	3.6	6.7	7.7
		20	0.4	0.9	4.5	8.3	16.0	23.0
		40	0.7	1.4	7.0	13.3	26.9	45.0
	Drains		**5**	**10**	**50**	**100**	**200**	**400**
		5	0.0	0.0	0.5	1.9	6.9	21.3
		10	0.2	0.4	1.7	3.5	5.9	14.8
		20	0.4	0.7	3.6	7.4	13.6	25.0
		40	0.5	1.0	5.3	11.2	22.3	44.4

NRMSE

All NRMSE are expressed as decimal fraction.

NRMSE of GW − SW fluxes per cell of the horizontal and vertical upscaling

MODFLOW								
	Rivers		5	10	50	100	200	400
		5	0.0	0.1	0.2	0.4	0.5	0.7
		10	0.1	0.1	0.2	0.4	0.5	0.7
		20	0.2	0.2	0.2	0.4	0.5	0.7

		40	0.3	0.2	0.3	0.4	0.5	0.7
	Drains		5	10	50	100	200	400
		5	0.0	0.1	0.2	0.3	0.4	0.5
		10	0.0	0.1	0.2	0.3	0.4	0.5
		20	0.1	0.1	0.2	0.3	0.4	0.5
		40	0.1	0.1	0.2	0.3	0.4	0.5
Metamodel								
	Rivers		5	10	50	100	200	400
		5	0.0	0.1	0.2	0.2	0.2	0.2
		10	0.1	0.1	0.1	0.2	0.2	0.2
		20	0.1	0.1	0.1	0.2	0.2	0.3
		40	0.1	0.1	0.1	0.2	0.2	0.3
	Drains		5	10	50	100	200	400
		5	0.0	0.1	0.1	0.2	0.2	0.2
		10	0.0	0.1	0.1	0.2	0.2	0.2
		20	0.1	0.1	0.1	0.2	0.2	0.2
		40	0.1	0.1	0.1	0.2	0.2	0.2
Mehl_01								
	Rivers		5	10	50	100	200	400
		5	0.0	0.2	0.6	0.9	0.9	1.0
		10	0.1	0.1	0.6	0.9	0.9	1.0
		20	0.3	0.1	0.5	0.8	0.9	1.0
		40	0.6	0.3	0.4	0.7	0.8	1.0
	Drains		5	10	50	100	200	400
		5	0.0	0.1	0.3	0.4	0.6	0.7
		10	0.1	0.1	0.3	0.4	0.6	0.7
		20	0.2	0.1	0.3	0.4	0.6	0.7

		40	0.4	0.2	0.2	0.4	0.6	0.7
Mehl_02								
	Rivers		5	10	50	100	200	400
		5	0.0	0.0	0.1	0.1	0.2	0.3
		10	0.3	0.4	0.3	0.3	0.2	0.1
		20	0.7	0.7	0.7	0.6	0.4	0.3
		40	1.1	1.1	1.0	1.0	0.7	0.7
	Drains		5	10	50	100	200	400
		5	0.0	0.0	0.1	0.1	0.2	0.3
		10	0.3	0.3	0.3	0.2	0.2	0.2
		20	0.6	0.6	0.6	0.5	0.4	0.3
		40	0.9	0.9	0.8	0.8	0.7	0.6

Appendix B: Supplementary material for Chapter III

Materials and methods

Site C

Site C was instrumented with a pressure sensor of the same type as used on site A. The vegetation cover consists of mosses with a very shallow root system (0-10 cm) and the groundwater table remains relatively deep all over the year (> 1.5 m). Therefore, no connection between the roots and the groundwater (which could otherwise cause diurnal groundwater level fluctuations) is expected and measurement at this site will verify whether diurnal fluctuations are absent in the measurement after temperature correction.

Laboratory tests

In addition to the field measurements, two laboratory tests were performed to assess the possible bias induced by the temperature correction on the measured water pressure. The two tests were conducted in the same way. Three water pressure sensors were disposed at the bottom of a bucket filled with tap water. The amplitude of the temperature diurnal fluctuations was different between the two tests.

The first test (referred to as 01) was performed from the 29th of May until the 2nd of June 2019. The amplitude of the associated temperature diurnal fluctuations ranged from 5 to 10 °C. The second test (referred to as 02) was performed from the 21st until the 23rd of June 2019 in a better isolated laboratory. The amplitude of the associated temperature diurnal fluctuations ranged from 0.5 to 1.5 °C.

Data processing

Data processing steps are similar to those described in the manuscript (i.e. atmospheric pressure correction, detrending).

Results

Site C

Piezometric time series

Figure A shows the rainfall data and piezometric measurements for the summer 2016. The datum is set to the sensor level which is 2.85 m deep. This time series is not discussed in detail as these data are only used to assess the reliability of site A diurnal fluctuations measurements.

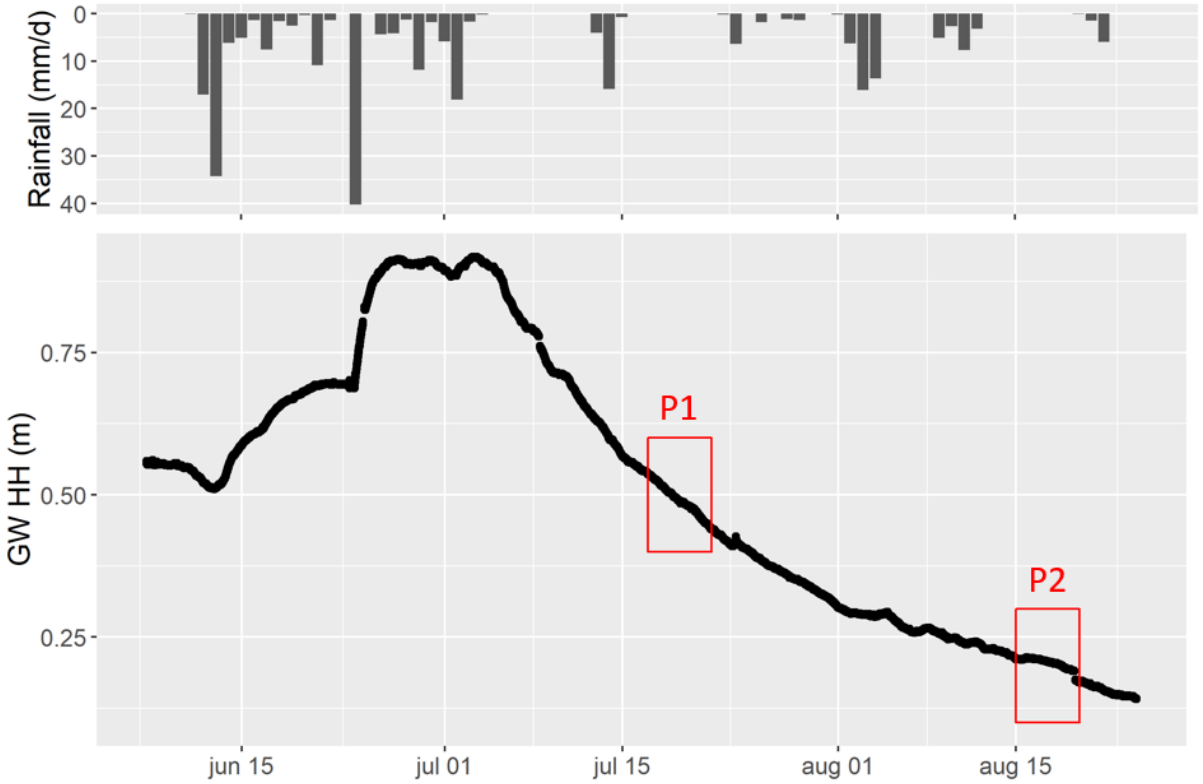

Figure A: Piezometric (GW HH) time series for the summer 2016 measured on site C and rainfall measured at the Herentals weather station

Zoom on P1 and P2

Figure B shows the measured groundwater levels and the extracted diurnal fluctuations after removing the trend using daily moving averages of groundwater level and temperature for the P1 and P2 periods.

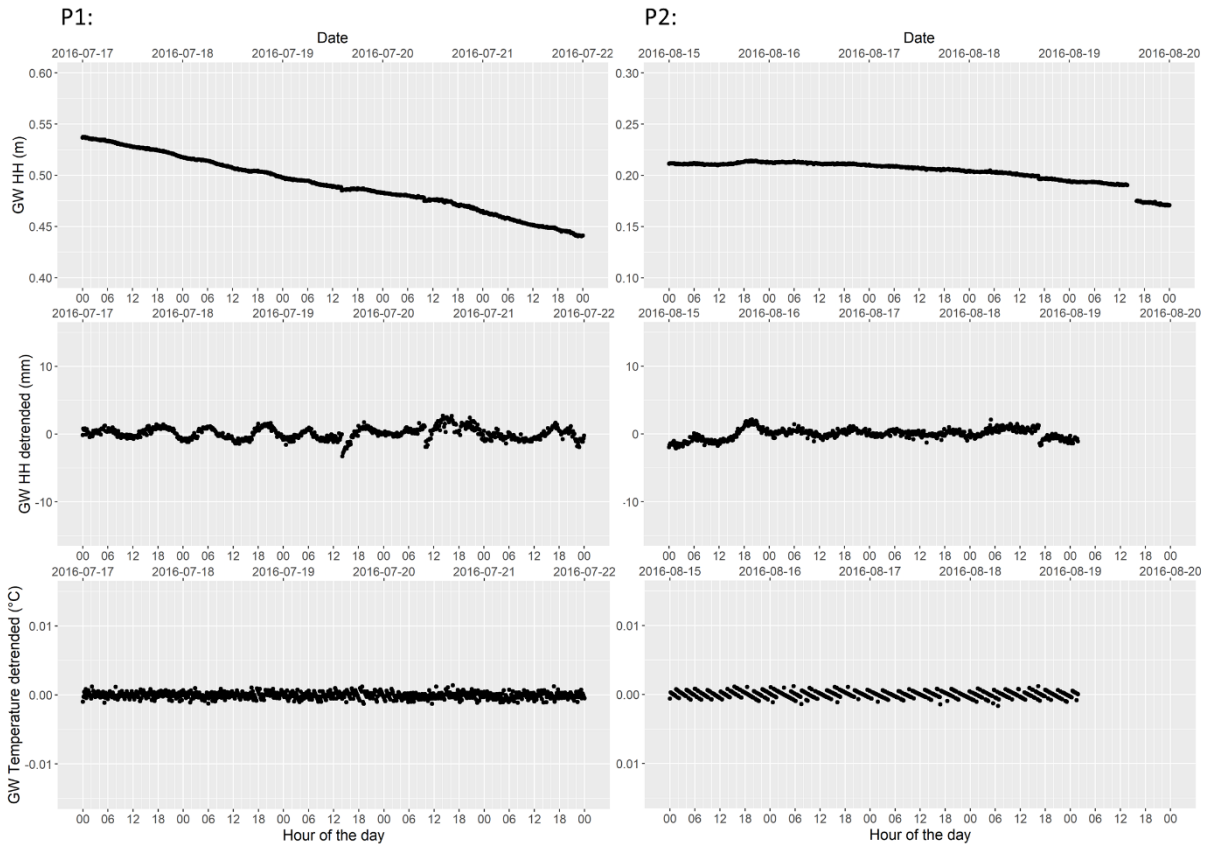

Figure B: Groundwater level (GW HH) measured (first row) and extracted diurnal fluctuations of the groundwater level (second row) and temperature (third row) for the P1 (left) and P2 (right) period at site C

No diurnal fluctuations can be seen neither in groundwater levels nor temperatures data. Some kind of periodic signal is present, but it does not have a 24 hours wavelength.

Laboratory tests

Only the amplitude of the diurnal fluctuations is discussed in this part.

The diurnal fluctuations of water level and temperature are shown in Figure C. During the laboratory test 01, amplitudes of the diurnal fluctuations are in the range of 3 to 6 mm for the water level and 5 to 10 °C for the temperature. During the laboratory test 02, amplitudes of the diurnal fluctuations were in the range of 0 to 2 mm for the water level and 0.5 to 1.5 °C for the temperature.

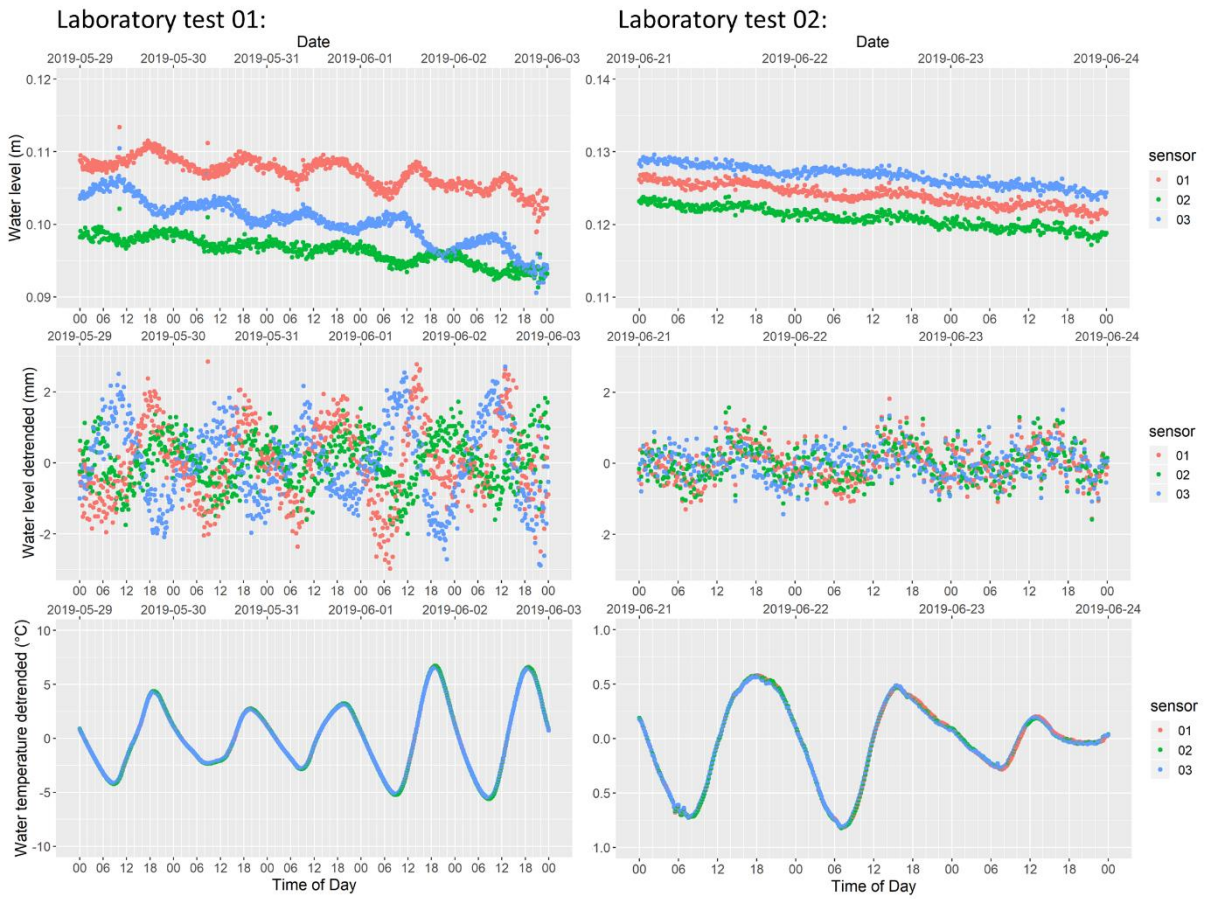

Figure C: Water level measured (first row) and extracted diurnal fluctuations of the water level (second row) and temperature (third row) for the laboratory test 01 (left) and 02 (right)

It can be seen further that while all sensors measure the same temperature, the error in pressure differs from one sensor to the other. Sensor 01 and 02 show a positive correlation between temperature and pressure error while sensor 03 shows a negative correlation. The amplitudes of the pressure artefacts present some minor differences between sensors but remain in the same order of magnitude.

Discussion

Sensors reliability to measure groundwater level diurnal fluctuations

The amplitude of the diurnal water level and temperature fluctuations observed in the field time series are summarized in Table A for the P1 period and in Table B for the P2 period. The Table C summarized the amplitude of the diurnal fluctuations observed in the laboratory tests.

Table A: Summary of diurnal fluctuation amplitude observed in the field time series for the P1 period

Field, P1	**Groundwater level (mm)**	**Groundwater temperature (°C)**
Site A, woods	15-30	0.01
Site A, grass	5	0.015
Site B	10	0.005
Site C	0	0

Table B: Summary of diurnal fluctuation amplitude observed in the field time series for the P2 period

Field, P2	**Groundwater level (mm)**	**Groundwater temperature (°C)**
Site A, woods	5-10	0.01
Site A, grass	2.5-5	0.01
Site B	10	0.005
Site C	0	0

Table C: Summary of diurnal fluctuation amplitude observed in the laboratory tests

Laboratory test	**Water level (mm)**	**Water temperature (°C)**
Test 01	3-6	5-10
Test 02	0-2	0.5-1.5

The field data of the three monitoring sites show water level diurnal fluctuations on the sites where they were expected (sites A and B) and not on the site where they were not (site C and to less extent site A grassland). This suggests that the observed groundwater level diurnal fluctuations are not measurement artefacts.

The laboratory tests show that diurnal temperature fluctuations superior to 0.5 °C induce a bias in the water level measurements and that, for temperature fluctuation amplitudes of 1.5 °C, the water level fluctuation amplitudes are around 2 mm. The temperature fluctuations are much smaller in the field measurements (≤ 0.1 °C) and the groundwater level fluctuations are bigger (> 2.5 mm).

Therefore, it can be concluded that even though the water pressure sensors show a bias linked to temperature correction, this does not affect significantly our observations of the diurnal groundwater level fluctuations.

Another potential concern is that the atmospheric pressure data used to correct the water level measurements could also be biased by their temperature correction. However, if that would be the case, the measurements performed on site C would also show diurnal fluctuations as groundwater level measurements from all field sites are corrected with the same atmospheric pressure data set.

Appendix C: Supplementary material for Chapter IV

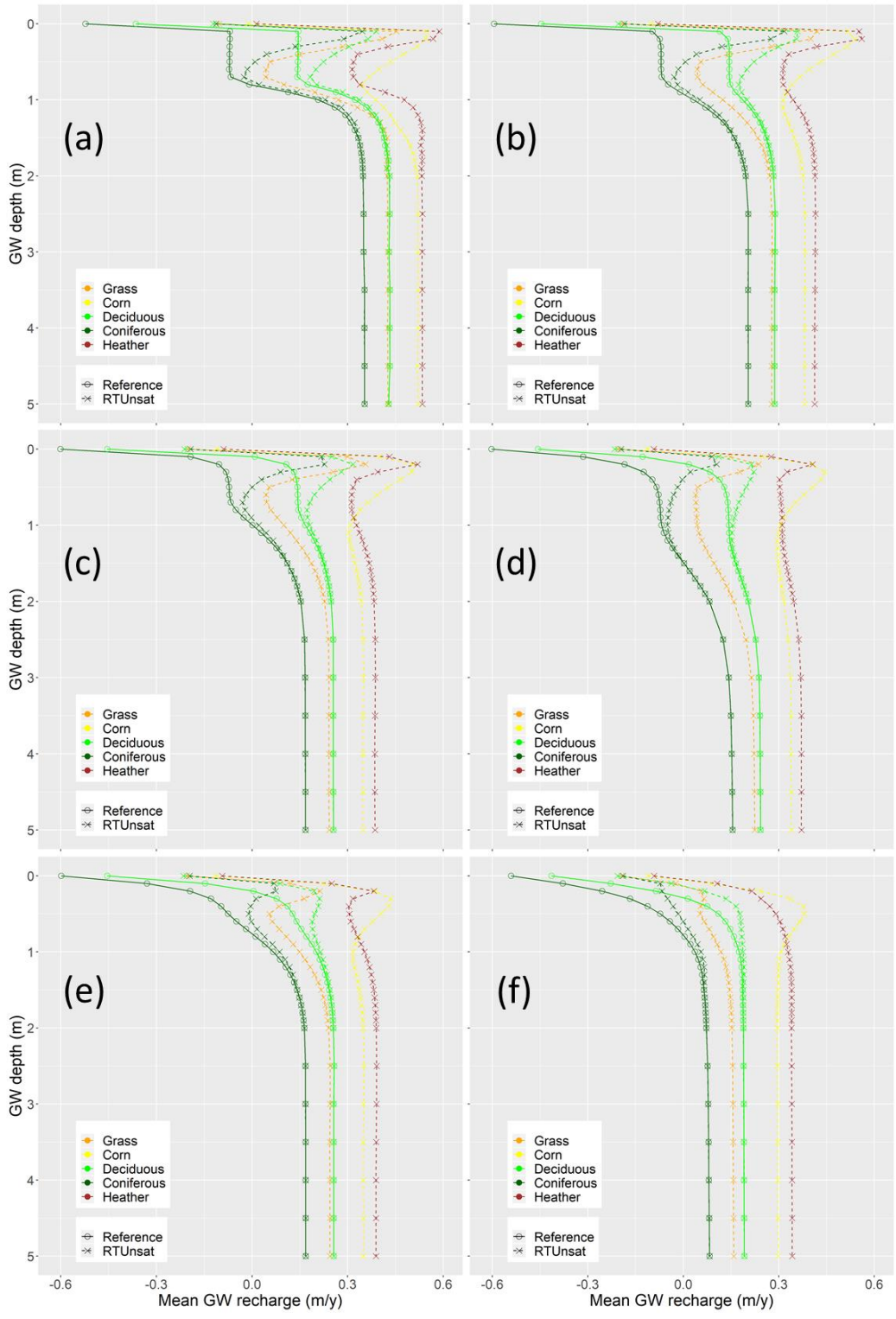

Figure A: Groundwater recharge as a function of groundwater depth simulated for dune (a), loamy sand (b), light sandy-loam (c), sandy-loam (d), clay (e) and peat (f) soils with different vegetation covers. Fluxes are presented for simulations considering tree water uptake from the saturated zone (Reference) and excluding it (RTUnsat). Circles indicate the HYDRUS simulations outputs and lines the linear interpolation.

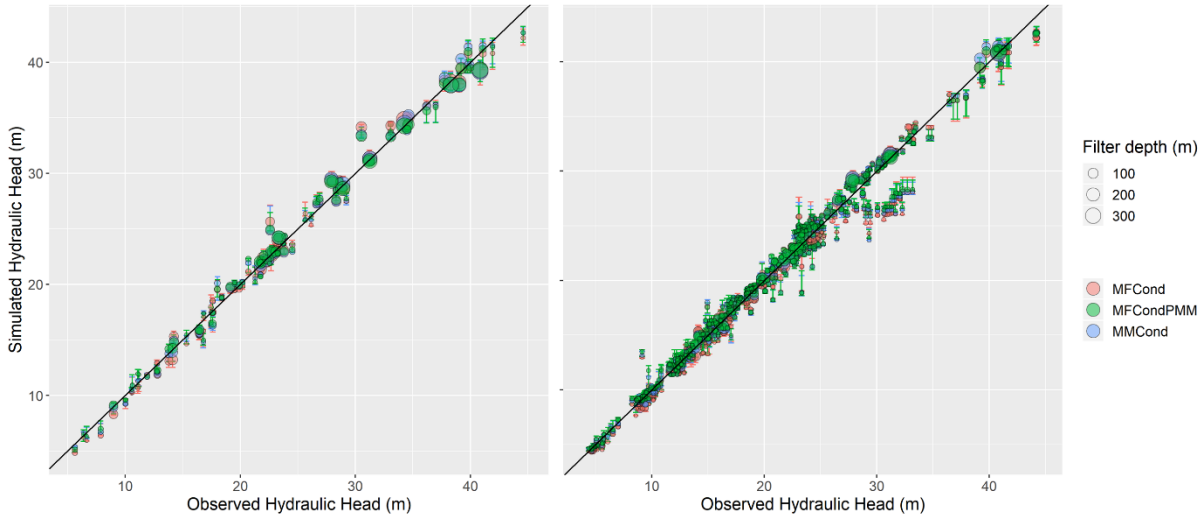

Figure B: Comparison between observed and simulated piezometric heads. Circles indicate simulations using MAP set or parameters and error bars represent 95 % confidence intervals. MFCond simulations use a calibrated homogenous 1D river conductance value obtained without prior information, MFCondPMM simulations use a calibrated homogenous 1D river conductance value obtained with prior information from the metamodel and MMCond simulations consider spatial variability of the river conductance due to aquifer properties calculated with the metamodel.

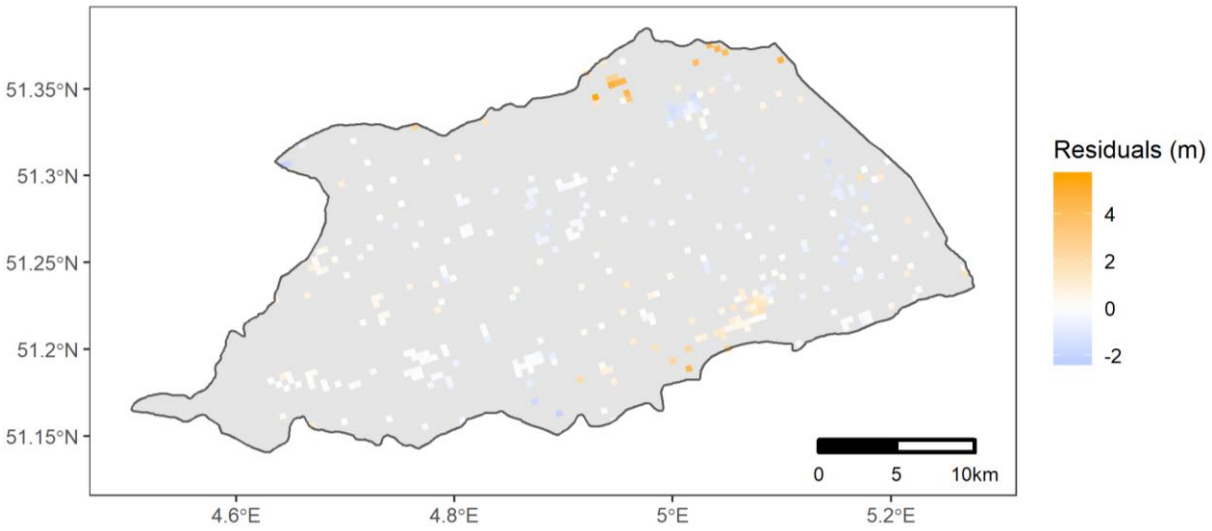

Figure C: Map of residuals per cell (average observed value – average simulated value) obtained using the MMCond model (spatially variable river conductance calculated with the metamodel) with the MAP set of parameters

List of publications and communications

Articles in international peer-reviewed journals

- Di Ciacca, A., Leterme, B., Laloy, E., Jacques, D., Vanderborght, J., 2019. Scale-dependent parameterization of groundwater–surface water interactions in a regional hydrogeological model. J. Hydrol. 576. https://doi.org/10.1016/j.jhydrol.2019.06.072

Communications at international conferences

- Drain discharge monitoring to estimate plot scale groundwater recharge, *Antoine Di Ciacca, Bertrand Leterme, Diederik Jacques & Jan Vanderborght,* EGU General assembly 2016, Vienna, Austria, 17–22 April 2016, poster presentation

- Parameterization of small water courses conductance in hydrogeological models based on field scale virtual experiments, *Antoine Di Ciacca, Bertrand Leterme, Eric Laloy, Diederik Jacques, Jan Vanderborght,* poster, EGU General assembly 2018, Vienna, Austria, 7–12 April 2019, poster presentation

- Scale-dependent parameterization of aquifer conductance to simulate groundwater - surface water interactions in regional hydrogeological models, *Antoine Di Ciacca, Bertrand Leterme, Eric Laloy, Diederik Jacques, Jan Vanderborght,* ISMC conference 2018, Wageningen, Netherlands, 5–7 November 2019, oral presentation

- Scale-dependent parameterization of groundwater − surface water interactions in a regional hydrogeological model, *Antoine Di Ciacca, Bertrand Leterme, Eric Laloy, Diederik Jacques, Jan Vanderborght,* MODFLOW and More conference 2019, Golden, Colorado, USA, 2–5 June 2019, poster presentation

Internal seminars at the KU Leuven

- Model abstraction for groundwater flow towards drainage network in a lowland temperate catchment, 3 November 2017

- Groundwater recharge modelling on a heterogeneous vegetation covered plot, 10 May 2019

Communications at SCK CEN Day of the PhDs

- Spatially distributed recharge in groundwater model: bridging the gap between soil profile and catchment scale, October 2016

- Virtual experiments to investigate groundwater flow towards drainage network in the Kleine Nete catchment, April 2017

- Scale-dependent parameterization of aquifer conductance to simulate groundwater – surface water interactions in regional hydrogeological models, September 2018

- Unraveling the link between diurnal groundwater fluctuations and root water uptake from the groundwater using HYDRUS-3D simulations, October 2019